Title

The Interaction of Valve Dysfunction and Left Ventricular Assist Device Support on Intraventricular Flow Dynamics

Author

Vu, Vi

Publication Date

2020

Peer reviewed|Thesis/dissertation

UNIVERSITY OF CALIFORNIA SAN DEIGO

SAN DIEGO STATE UNIVERSITY

The Interaction of Valve Dysfunction and Left Ventricular Assist Device Support on Intraventricular Flow Dynamics

A Dissertation submitted in partial satisfaction of the

requirements for the degree

Doctor of Philosophy

in

Engineering Science (Mechanical and Aerospace)

by

Vi Vu

Committee in charge

San Diego State University

Professor Karen May-Newman, Co-Chair
Professor Peiman Naseradinmousavi

University of California San Diego

Professor Juan Carlos del Álamo, Co-Chair
Professor Andrew M. Kahn
Professor Juan C. Lasheras
Professor John T. Watson

2020

The Dissertation of Vi Vu is approved and it is acceptable in quality and form for the publication on microfilm and electronically:

Co-Chair

Co-Chair

University of California San Diego

San Diego State University

2020

DEDICATION

This dissertation is dedicated to my parents, Vũ Văn Vũ, M.D., Ph.D. and Phạm Thị Hải. Without them, I would not be here.

EPIGRAPH

The brick walls are there for a reason. The brick walls are not there to keep us out, the brick walls are there to give us a chance to show how badly we want something. Because the brick walls are there to stop the people who don't want it badly enough.

Randy Pausch, computer scientist

If you're not stubborn, you'll give up on experiments too soon. And if you're not flexible, you'll pound your head against the wall and you won't see a different solution to a problem you're trying to solve.

Jeff Bezos, businessman

Don't be nervous. Work calmly, joyously, recklessly on whatever is in hand

Henry Millar, writer

TABLE OF CONTENTS

LIST OF FIGURES

LIST OF TABLES

ACKOWLEDGMENTS

First of all, I want to give my deepest gratitude to my advisor, Professor Karen May-Newman. She has been a remarkable mentor who inspired me to pursue a doctoral degree. Her tremendous commitment and immense knowledge have guided me through the completion of this study. It has been an enriching experience to have her as my mentor for the past years.

I want to genuinely thank all the members of my doctoral committee for their time and support. A special thanks to Professor Juan C. del Álamo, co-chair of the committee, for his insightful suggestion and impartment of knowledge.

I want to extend special thanks to Pablo Aguiló Ph.D., and Lorenzo Rossini, Ph.D. who have written several programs to use in the data analysis.

Thanks to all the members of the Cardiovascular Bioengineering Lab, present and past, for making the last 5 years more enjoyable: Claudine, Julie, Ricardo, Sanjya, Nick, Frances, Jacob, Shelby, and Kavya.

Lastly, I am forever grateful to my family for their unconditional love and support.

Chapter 2, in full, is in an early prepared stage for publication. The co-authors are Frances Lagarda, Karen May-Newman. The working title of this paper is "Aortic Insufficiency During LVAD Support: Feature, Mechanisms, Clinical Options." The dissertation author is the primary author of this paper.

Chapter 3, in full, is in an early prepared stage for publication. The co-author is Karen May-Newman. The working title of this paper is "The Effect of Aortic Insufficiency on Left Ventricular Flow in the HeartMate II LVAD Supported Heart." The dissertation author is the primary author of this paper.

Chapter 4, in full, is in an early prepared stage for publication. The co-author is Karen May-Newman. The working title of this paper is "The Effect of Aortic Insufficiency on Left

Ventricular Flow in the HeartMate 3 LVAD Supported Heart". The dissertation author is the primary author of this paper.

Chapter 5, in full, is in an early prepared stage for publication. The co-authors are Lorenzo Rossini, Pablo Martinez-Legazpi, Juan C. del Álamo, and Karen May-Newman. The working title of this paper is "The Effect of Mitral Valve Prostheses Design and Orientation on Left Ventricular Flow during LVAD support." The dissertation author is the primary author of this paper.

VITA

2010 Bachelor of Science, Bioengineering, University of California San Diego

2012 Teaching and Research Assistant, San Diego State University

2014 Master of Science, Bioengineering, San Diego State University

2014 Research and Development Engineer at Next Orthosurgical Inc.

2015 Teaching and Research Assistant, San Diego State University

2020 Doctor of Philosophy in Engineering Science (Mechanical and Aerospace Engineering), University of California San Diego and San Diego State University, Joint Doctoral Program

PUBLICATIONS

M.S.

1. May-Newman K., Y. K. Wong, R. Adamson, P. Hoagland, **V. Vu**, W. Dembitsky, "Thromboembolism is linked to intraventricular flow stasis in a patient supported with a left ventricle assist device," *ASAIO Journal* 59(4):452-455, 2013.

2. May-Newman, K., B. Herold and **V. Vu**, "Modeling the link between left ventricular flow and thromboembolic risk using Lagrangian Coherent Structures" *Fluids* 2016, 1(4), 38.

Ph.D.

3. Rossini, L., P. Martinez-Legazpi, **V. Vu**, L. Fernandez-Friera, C. Perez del Villar, S. Rodriguez-Lopez, Y. Benito, M. Borja, D. Pastor-Escuredo, R. Yotti, M. Iedesma-Carbayo, A. Kahn, B. Ibanez, F. Fernandez-Aviles, K. May-Newman, J. Bermejo, J.C. del Alamo. "A clinical method for mapping and quantifying blood stasis in the left ventricle," *J. Biomechanics 2016 Jul 26 49(11):2152-61.*

4. **Vu, V**., L. Rossini, J. Campos, R. Montes, V. Ramesh, J. Moon, C. Reider, B. Herold, P. Martinez-Legazpi, J. Bermejo, J.C. del Alamo, and K. May-Newman. "Mitral valve prosthesis design affects hemodynamic stasis and shear in the dilated left ventricle," *Annals of Biomedical Engineering*, 2019 Feb; 47(5):1265-1280.

5. **Vu, V**. and K. May-Newman. "Bileaflet prosthesis design and orientation affect fluid shear, residence time and thrombus formation," *Journal of Cardiac and Vascular Anesthesia,* 2019 Oct;33(10):2870-2872

6. **Vu, V**. and K. May-Newman. “Mitral valve orientation affects vortex formation and turbulence in the left ventricle,” *Journal of Cardiac and Vascular Anesthesia,* 2019 Nov;33(11):3211-3213

7. May-Newman, K., R. Montes, J. Campos, N. Marquez-Maya, **V. Vu**, E. Zebrowski, T. Motomura, and R. Benkowski. “Reducing regional flow stasis and improving intraventricular transport with a tipless inflow cannula design: An in vitro flow visualization study using the EVAHEART LVAD,” *Artificial Organs*, 2019 Sep;43(9):834-848.

8. Rossini, L, O. Braun, M. Brambatti, Y. Benito, A. Mizeracki, M. Miramontes, Cathleen Nguyen, P. Martinez-Legazpi, S. Almeida, **V. Vu**, K. May-Newman, J. Bermejo, E. Adler, A. Kahn and J. C. del Álamo. “Intraventricular flow patterns in patients treated with left ventricular assist devices”, *ASAIO*, accepted 2020.

9. Ortiz, S, **V. Vu**, R. Montes, A. Sparks, and K. May-Newman. “The effect of the LVAD artificial pulse feature on the intraventricular flow filed an *in vitro* flow visualization study using HeartMate3 LVAD”, submitted.

10. Tanaka, Y., **V. Vu**, I. Fischer, T. Nakajima, K. May-Newman, A. Itoh. “Is the severity of aortic insufficiency with left ventricular assist device underestimated in traditional echocardiographic evaluation? A mock loop study”, submitted.

ABSTRACT OF THE DISSERTATION

The Interaction of Valve Dysfunction and Left Ventricular Assist Device Support on Intraventricular Flow Dynamics

by

Vi Vu

Doctor of Philosophy in Engineering Sciences (Mechanical and Aerospace Engineering)

University of California San Diego, 2020

San Diego State University, 2020

Professor Karen May-Newman, Co-Chair

Professor Juan Carlos del Álamo, Co-Chair

Healthy heart valves act as gateways to ensure unidirectional blood flow inside the normal heart. Dysfunctional valves compromise cardiac output and disrupt the intraventricular flow pattern, resulting in a degeneration of cardiac function. In the presence of a left ventricular assist device (LVAD), valvular dysfunction can significantly affect patient outcomes. As LVAD implants

become more common, the duration of LVAD support routinely exceeds several years. Flow-related complications such as stroke, thromboembolism, and valve dysfunction worsen, indicating that subtleties of flow architecture are increasingly important. The LVAD patient population is challenging to study as numbers are few, and many have co-morbidities. Furthermore, flow measurement in LVAD patients relies on Doppler echocardiography, which does not produce high-quality velocity measurements. To overcome these challenges, a mock circulatory loop was developed to mimic the hemodynamics of end-stage heart failure (HF) and study the flow interaction of heart valve dysfunction and LVAD support.

Aortic insufficiency (AI) is a serious complication in >20% of LVAD patients within one year post-implant. Pre-existing mild AI is often untreated but can rapidly progress to significant AI that requires repair. Hemodynamics and intraventricular flow were measured for three levels of LVAD support combined with three levels of AI severity in the mock loop. LVAD support worsened regurgitant flow for all AI levels, creating a recirculating flow in the ascending aorta. Conventional indices were not sensitive to these increases, but our results suggest alternative indices such as aortic valve net flow and energy dissipation rate may be more effective for AI assessment in LVAD patients. Dysfunctional mitral valves are also common in advanced HF patients and may be repaired or replaced by mechanical or bioprosthetic valves. Each design produces a unique inflow pattern that affects LV vortex formation and residence time. When combined with LVAD support, the best flow conditions were observed with the bioprosthesis.

Valve dysfunction, whether aortic or mitral, disrupts the intraventricular flow and contributes to declining heart function. When combined with the mechanical alterations imposed by a LVAD, the flow interactions become of great clinical importance for assessing the progression and associated risk of thrombus, stroke, and AI.

Chapter 1

Background and Significance

1.1 Introduction

Cardiovascular disease is the leading cause of death in the United States (US) and is responsible for more than 17.6 million annual deaths worldwide[1]. 9.3% of deaths are attributed to heart failure (HF), which causes by myocardial injury induced cardiac remodeling (such as ischemic, inflammatory, high blood pressure, etc.) or other underlying diseases[1,2]. HF afflicts 5.8 million Americans, with 700k new cases diagnosed annually. By 2030, the prevalence of HF is predicted to increase significantly and affects more than 8 million Americans[3,4]. One-year HF mortality rate is approximately 22% and can exceed 50% in severe cases[3,5,6]. The cost of HF to the US health care system is expected to reach $70 billion US dollars by 2030, a 127% increase from 2012 expenditures[4].

The classic “gold standard” treatment for severe HF patients is heart transplant (HTx) but has limited donor availability and restricted eligibility. Annually only 1500 organs are suitable for transplant worldwide, while in the US alone, 4000 patients are added on the wait-list, and 10% will die before receiving HTx. Within the last decade, the number of available donors has decreased while the need for HTx has almost double[1,7–11]. Moreover, HTx survival rate decreases by 10% with higher donor age and receiver comorbidity[12]. The alternative treatment is left ventricular assist device (LVAD) implant, which has become increasingly prevalent.

1.2 Left Ventricular Assist Devices

In 1654, the National Heart, Lung, and Blood Institute in the US began the "Artificial Heart Program," providing funding for the development of long term mechanical circulatory support systems (MCS). The first pneumatically driven LVAD was implanted in 1966, and the first total

artificial heart (TAH) was implanted in 1969[13,14]. Due to very high complication rates, the TAH was implanted in only 1% of cases; MCS then became a favorable alternative and underwent a rapid rate of technology development[11,15–18]. The LVAD is a mechanical pump, which is surgically connected to the left ventricle (LV) and the aorta[19,20]. The timing of the LVAD implant is crucial to exploit its full benefits. Eligible candidates may suffer from worsened outcomes due to HF's prolonged tissue damage if the LVAD is received too late[11].

The LVAD can be implanted as long term support (bridge to recovery (BTR), and bridge to transplantation (BTT)), or as permanent support (destination therapy (DT)). In a small number of BTR cases, patients typically had shorter HF history, thus allowed sufficient cardiac recovery, LVAD weaning and removal[21–24]. The outcome of patients after pump explant, however, cannot be predicted accurately; in fact, less than 20% of LVAD patients were successfully weaned off while maintaining stable cardiac functions[2,25].

In the BTT group, patients tend to have nonreversible LV failure, high mortality risk and are awaiting for HTx. In this group, LVAD provides temporary relief and support until the patient receives a transplant. For patients considered unsuitable for HTx, LVADs are implanted for the remainder of their life (DT). Since 2006, approximately 2500 new patients have received LVAD implants annually, with DT increasing from 15% to 46% at the present[1]. Compared to optimal medical management, LVAD costs five times more ($360k vs. $62k), but patients also gain five times higher quality-adjusted life years[11,26]. Between 2005-2011, continuous flow (cf) LVADs replaced the pulsatile pump design. The cost of LVAD-related hospitalization increased by 21%, but the in-hospital mortality and average hospital stay decreased significantly[27,28]. Currently, one- and two-year survival rates of HTx patients is 88% and 82%, in comparison to 74% and 61% patients with cf HeartMate II (HM2), respectively[29]. The one-year total cost for LVAD implantation and patient care is also higher than HTx patients[30,31].

1.2.1 Axial And Centrifugal Continuous-Flow LVADs

The 1st generation of LVADs were pulsatile pumps, which operated similarly to the heart. This generation of pumps, such as Berlin Heart EXCOR, Thoratec PVAD, and VE, etc., consisted of a pneumatically or electrically driven membrane with bioprosthetic valves (BP) as gateways at the inflow and outflow conduits[11]. The pump was designed with open-loop control as the fixed motor speed was set by the physician, adjusted to the individual native cardiac function. The HeartMate XVE (HM VE) (Thoratec Corp./Abbott) was first approved by the US Food and Drug Administration (FDA) in December 2001 as BTT, and later in April 2003 as DT[8,32]. The pump design included a pusher plate driven by an electric motor with percutaneous power and control circuit, titanium alloy housing with two chambers (one with textured blood path, and one with a motor); that operated in either fixed or automatic mode. The textured blood-contacting surface and BP features helped to minimize the thrombosis risk, and patients often were prescribed with minimal or no anticoagulant[33]. Compared to the no-treatment group, HM VE had fewer complications and a higher 1-year survival rate[21]. Compared to optimal medical therapy, the pump had double the number of adverse events but provided better cardiac recovery, higher quality of life, and higher survival rate[8,34].

HeartMate XVE **HeartMate II** **HeartMate 3** **HeartWare**

Figure 1.1: Pulsatile left ventricular assist device (LVAD) (HeartMate XVE), continuous axial flow LVAD (HeartMate II), and continuous centrifugal flow LVAD (HeartMate 3 and HeartWare).

Serious complications (such as infection, bleeding, and thromboembolic event, etc.), and suboptimal pump design and operation mode are the limitations of the 1st LVAD generation. Because of its large size and multiple moving parts, pulsatile pumps were less durable and more prone to mechanical failure, including degradation of the membrane and artificial valves[11,32]. The new generation of LVAD is a continuous pump, with compact size, less moving parts, and provides a better patient outcome[1,27,35]. Axial flow with blood wash bearing (HM2, MicroMed DeBakey), and centrifugal flow with magnetic levitation (HeartMate 3 (HM3), HeartWare (HW)) are two common types of cf pumps[35]. The cf LVAD is surgically implanted via bilateral thoracotomy without full sternotomy or extensive tissue dissection[36,37]. Between 2012-2016, the rate of axial pump implant was 60% higher than the centrifugal pump; but since 2017, they are approximately the same[35].

1.2.1.1 Axial Continuous Flow LVAD

The FDA approved the HM2 for BTT in 2008 and DT in 2010[38,39]. The HM2 is implanted in more than 26000 patients worldwide and is one of the most common LVADs in the US (Abbott data as of May 10, 2018, on file. SJM-HM-1016-0032(3)). The improvements from the HM VE design provided better durability, patient outcomes, and fewer adverse effects. HM2 designs consist of an impeller inside a metal case, moving blood through a mechanical bearing, and five years minimum reliability[40]. HM2 was proven clinically to be superior to HM VE and optimal therapy. Twelve and eighteen-month survival rate of HM2 patients is 85% and 79%, respectively, in comparison to 90% and 88% in HTx patients[29]. At two years of support, approximately 50% of HM2 patients are alive and free of major adverse events[29,38,41]. However, due to the high shear rate from the contact between the mechanical bearing and blood, HM2 causes serious bleeding complications in the capillary bed[38]. High thrombosis incidences of 8% at three months LVAD support were reported in HM2. However, this rate seemed to decrease since 2014, attributing to the improvement of post-implantation anticoagulation management[42,43].

1.2.1.2 Centrifugal Continuous-Flow LVAD

The HM3, approved by the FDA as BTT and DT in 2017, is the newest generation of cf HM with more than 4500 implants worldwide[44]. While still classified as a cf pump, the HM3 incorporates an artificial pulse (AP) signal, which is a short speed change occurring every 2 seconds (s), as an effort to create additional pulsatility and limit the hemorrhagic and thrombotic problems[11]. With no mechanical bearing, HM3 transports blood through a wide flow gap (10-20 times larger than standard bearings) using magnetically levitated bearing and thereby minimizes the shear and compressive force imposing on the blood cells[45,46]. This pump has 3000-9000 rotations per minute (rpm) operation range and can provide up to 10 L/min cardiac support. Moreover, the AP occurs asynchronously with the heart contraction, thus inducing a fluctuation in flow and pressure and helps to minimize the stasis flow region inside the pump and LV[47]. Recent clinical trials reported similar survival outcomes (83% and 46% at 1 and 5 years respectively), functional status, quality of life, and infection rate between HM2 and HM3[35,44]. The hemocompatibility performance of HM3 is more enhanced by lower shear stress exposure to blood cells, lower hemolysis complications (such as gastrointestinal bleeding, hemorrhagic stroke, and epistaxis, etc.), and fewer incidents of pump thrombosis or replacement[44,47].

HW is another common cf centrifugal LVAD. With a compact size, HW can be used in biventricular implant, pediatric, or in small adults. The pump also can fit entirely inside the pericardium, eliminating the need for upper abdominal pocket dissection. With at least ten years of durability and up to 10 L/min flow output, HW was approved by the FDA for DT in 2017[11,48,49].

1.2.2 Left Ventricular Unloading And Myocardial Recovery

By unloading the LV, increasing cardiac output (CO), and end-organ perfusion, LVADs alleviate HF symptoms and improve patient outcomes[2,8]. The pump also plays a significant role in myocardial reverse remodeling by reducing LV pressure (LVP) and stress on the ventricular wall, improving contractility and regression of myocyte hypertrophy[50,51]. Almost immediately after

LVAD implantation, the diastolic and systolic function improves substantially, leading to higher EF, smaller LV and LA size, and a thicker interventricular septum. Moreover, previous studies found signs of myocyte recovery from the decrease of wavy band fiber, contraction band necrosis on cardiac tissue, and lower neurohormones and cytokines levels[2,52,53]. The LV mass does not return to its normal range, suggesting the lack of atrophic remodeling process[54–56]. While the clinical evidence indicates that LVADs improve LV structure and function, damage to cardiac tissues appears to be irreversible, and the remodeled state only establishes a new normalized structure[2,34]. Both pulsatile and cf LVADs lead to LV chamber reduction. Nevertheless, they have differential unloading effects due to their design and control, as summarized in table 1 below[57].

Table 1.1: The difference in the unloading effect of pulsatile and continuous LVAD adapting from Bartoli et al. 2010

Continuous LVAD	**Pulsatile LVAD**
• Altering LV peak systolic pressure, aortic systolic/diastolic pressure	• Maintaining a normal profile
• During high support, increasing transaortic pressure and keeps aortic valve permanently closed	• Maintaining a normal pressure range.
• Reducing cardiac metabolic demands significantly	• A similar but smaller effect

1.2.3 Alteration Of Left Ventricular Flow During LVAD Support

Depending on the contractility of the native heart, the implanted LVAD produces little or no AV opening (AVO), which significantly changes the LV flow patterns[58,59]. Many improvements in pump design and surgical techniques were made to optimize the interaction between the LVAD and LV blood flow. In a healthy heart, the aortic valve (AV) opens and closes at each heartbeat. Blood passes through the mitral valve (MV) and enters LV from the atrium during the diastolic filling phase. Then, during the systolic ejecting period, blood got ejected to the aorta through the AV. At mid-systole, the AV starts to close, and subsequently experience diastolic phase pressure on the leaflets at complete closure[60]. The presence of LVAD drastically alters the LV flow pattern,

redistributing stress, and pressure on the LV wall, AV, and aorta[61,62]. By drawing blood from the apex and directing it into the ascending aorta, the LVAD decreases LVP, prolonging the diastolic phase and reducing the AVO area and duration. During low LVAD support, the heart contracts and opens the AV during systole, and blood is transported through AV and the pump to the aorta. During high levels of LVAD support, the AV is continuously closed and chronically exposed to high transaortic pressure (TVP). The higher strain imposed on the leaflet tissue likely induces abnormal valvular remodeling (in particular fibrosis, myocardial wall stiffening, etc.)[63–65].

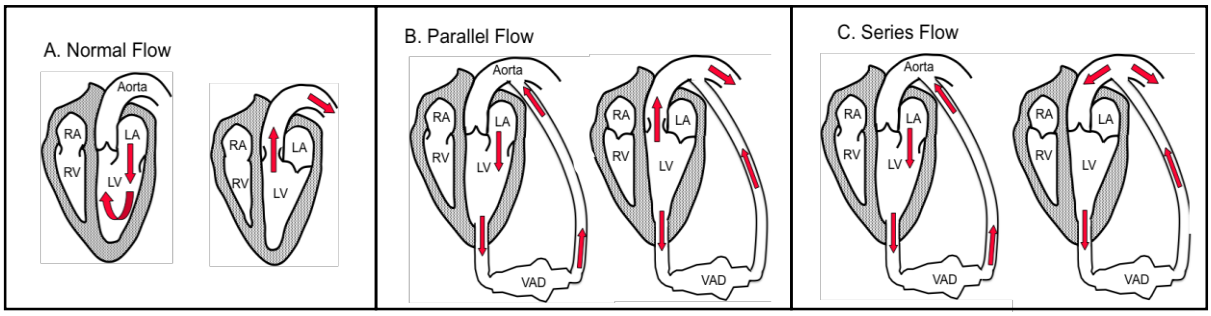

Figure 1.2: Blood flow alterations during LVAD support, (A) Pre-LVAD implantation; (B) During low LVAD support, a small portion of flow exists through the aortic valve; (C) During high LVAD support, all flow passes through the LVAD.

1.2.4 The Effect Of HearMate3 Artificial Pulse Feature

The HM3 with an AP feature introduces a small speed change every 2s, intending to improve the LV flow and pulsatility. A recently submitted work examined the impact of AP on hemodynamics and flow structure in the LV chamber[66]. In the absence of cardiac contraction (CSoff), the pressure, flow, and pulsatility index (PI) were recorded for both HM2 and HM3 using an in-house mock cardiovascular loop, as described previously[59,66]. The HM2's hemodynamics were steady, while HM3's signals oscillated every 2s (0.5 Hz frequency) as the result of AP (Figure 1.3). The cyclic variations of the HM2 were less than 2% of the mean values. For HM3, pressure variations were less than 15% and decreased at higher pump speed, while the variations of flow (LVAD and AV) and pulsatility index (PI) were higher. A well-defined vortex ring was captured at

the beginning of the AP using particle image velocimetry technique. It then migrated toward the LV apex and dissipated around 500 milliseconds (ms) (Figure 1.4)

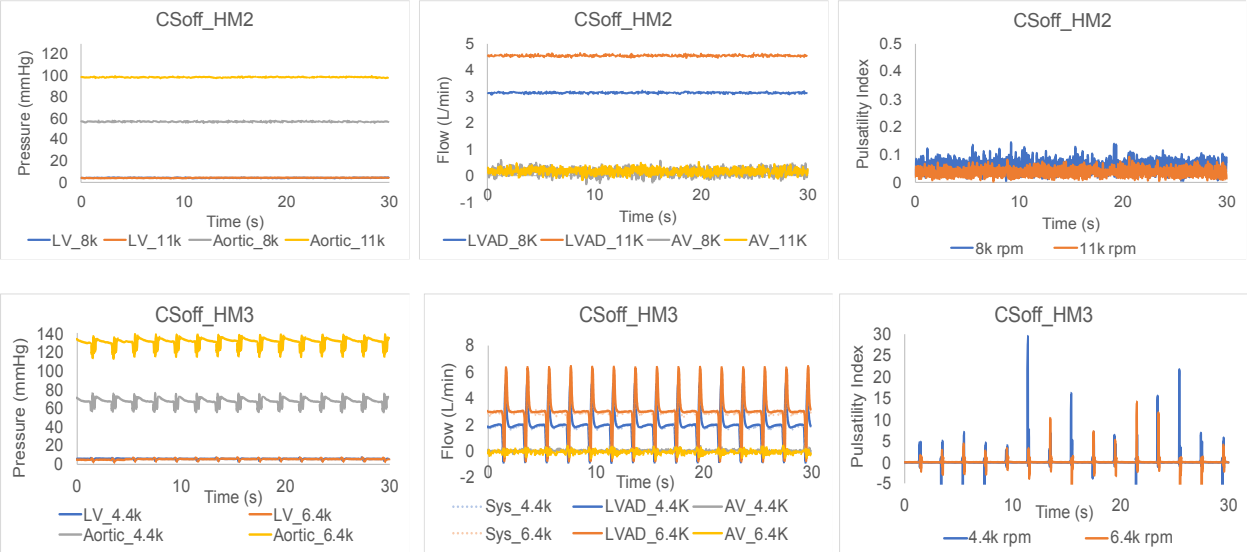

Figure 1.3: Cyclic variation of the left ventricle (LV) and aortic pressures, LVAD and aortic valve flow, and pulsatility index during low and high HeartMate II (HM2) and HeartMate 3 (HM3) supports (without native heart function).

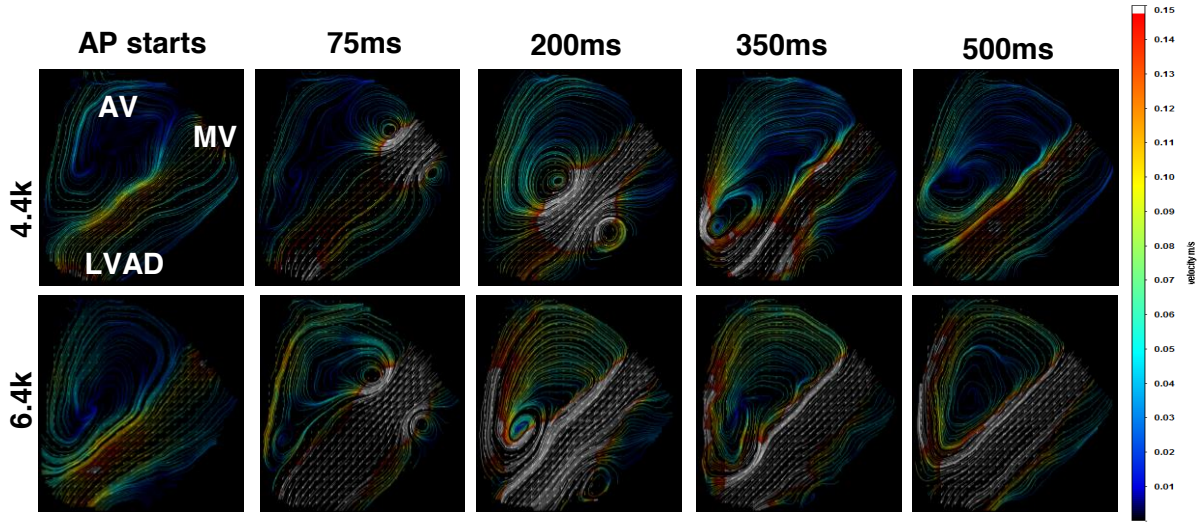

Figure 1.4: Velocity field images at different speeds of HeatMate 3 LVAD in the absence of cardiac contraction (mitral valve (MV), aortic valve (AV), and LVAD inlet (LVAD)).

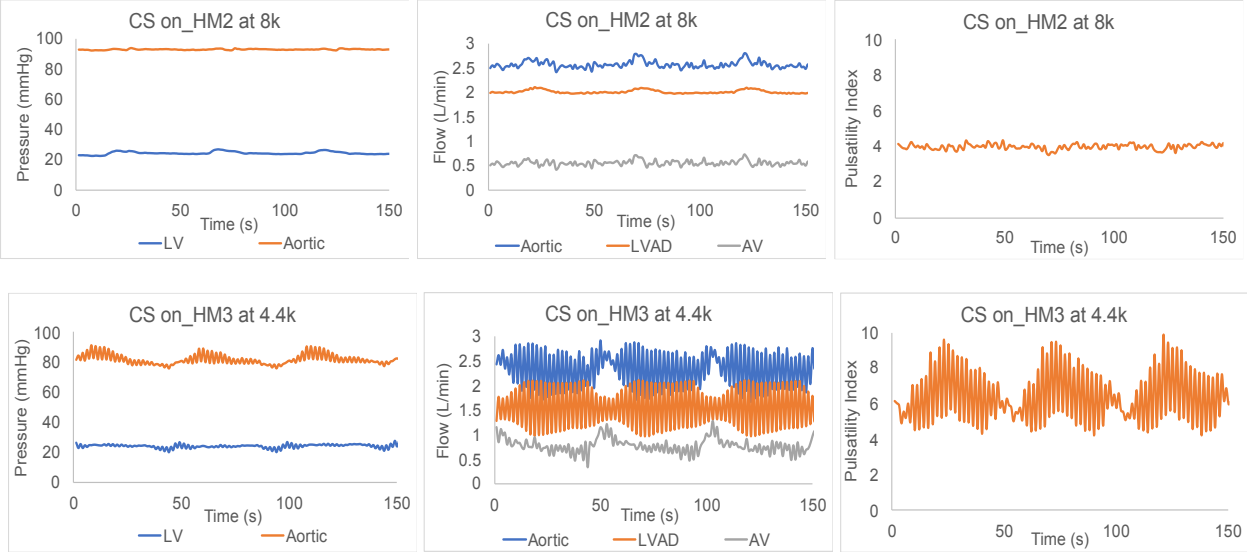

Figure 1.5: Cyclic variation (1 Hz frequency) of the left ventricle (LV) and aortic pressures, LVAD and aortic valve flow, and pulsatility index during HeartMate 3 (HM3) support with native heart function (CS on).

Table 1.2: Average and standard deviation (Ave ± SD) at 1Hz frequency during HeartMate 3 (HM3) support with native heart function. (Left ventricle pressure (LVP), aortic pressure (AoP), systemic flow (Qsys), LVAD flow (Q_{LVAD}), aortic valve flow (Q_{AV}), pulsatility index)

Parameters	**HM2 8k rpm**	**HM3 4.4k rpm**
LVP (mmHg)	24.18 ± 1.05	24.13 ± 1.28
AoP (mmHg)	92.87 ± 0.33	82.13 ± 3.89
Q_{sys} (L/min)	2.56 ± 0.07	2.34 ± 0.41
Q_{LVAD} (L/min)	2.01 ± 0.04	1.57 ± 0.45
Q_{AV} (L/min)	0.55 ± 0.05	0.77 ± 0.16
PI	4.00 ± 0.15	6.34 ± 1.59

On the other hand, when the cardiac function was present (60 beats/minute), its pulsatility interaction with AP produced a new pattern varying every 50 s (Figure 1.5 bottom). While the beat-to-beat LVP variations during HM2 and HM3 low support conditions were comparable, the AP introduced more substantial fluctuation in AoP (0.4% vs. 4.7%). Moreover, significant variation at 17-29% from the average values were observed in the flow and PI waveforms during HM3 support (Table 1.2). The HM3 AV flow had a wider range, 0.33-1.15 L/min, resulting from the

alternative constructive and destructive interference of the couple of AP and cardiac contraction. Overall, AP increased PI and AV flow, which potentially enhanced flow mixing and AVO.

1.2.5 Patients Outcomes And Complications

1.2.5.1 Mechanical Circulatory Support Trials

The Randomized Evaluation of Mechanical Assistance of the Treatment of Congestive HF (REMATCH) trial (1998-2001) compared the outcome of HM VE to optimal medical management, resulting in the FDA approval of HM VE as DT[8]. The trial reported that while LVAD doubled the risk of severe adverse events (e.g., sepsis, bleeding, neurologic dysfunction, etc.), it improved patient life expectancy. At 1 and 2 years, LVAD patients had 24% and 16% higher survival rate. Mortality was primarily attributed to sepsis and device failure in the LVAD group, while caused by the progression of HF in the optimal therapy group[8]. Patients were continuously followed for two additional years after the trial ended. Some improvements in survival rate and adverse events during this period suggested patient outcomes could be improved with better post-LVAD management[67]. A retrospective review of 39 BTT patients reported that the majority continued to have dilated LV post-implant, especially those in NYHA class IV, suggesting that HM VE did not administer any significant myocardial recovery[68].

To overcome some complications in the 1st generation pulsatile LVAD, 2nd and 3rd generations cf LVAD were developed. HM2, continuous axial LVAD, was approved as BTT in 2008 and DT in 2010. The 1- and 2-year survival rate of HM2 was respectively at 74% and 61%. Moreover, more than 50% of patients are alive and free of severe adverse events (e.g., stroke, infection, pump thrombosis, etc.) at two years[29,38,39,41]. The two most recent LVAD clinical trials are the ENDURANCE and MOMENTUM 3 to evaluate the performance of the 3rd generation centrifugal LVAD. The ENDURANCE trial compared HW performance with HM2 in patients who were older and ineligible for HTx. After the two-year endpoint, both LVAD groups had a similar survival rate. HW, while having fewer device failures due to pump thrombosis, had three times

higher stroke rate than HM2[49,69]. Due to the comparable outcomes with HM2, HW was approved for DT in 2017, and patients were required to monitor their blood pressure at home upon hospital discharge. The MOMENTUM 3 multicenter trial examined HM3 performance, reporting very similar mortality and infection, as well as patient functional status and quality of life compared to HM2. HM3, however, demonstrated better hemocompatibility, with a reduction in stroke, major bleeding or gastrointestinal bleeding incidences, cardiac and ventricular arrhythmias, hospital stay, readmission rate, and pump replacement due to thrombosis. Moreover, at 1 and 2 years, the percentage of HM3 patients' survival without disabling stroke was 9% and 15% higher than those with HM2, respectively[44,49].

1.2.5.2 Axial And Centrifugal Continuous-Flow LVAD's Adverse Events

The INTERMACS 2019 reported that the average cf LVAD support duration was 1.7 years, with a similar survival rate in axial and centrifugal cf LVAD (around 83% and 46% at 1 and 5 years)[35]. The percentage of LVAD implants designated as DT was increased by 30% from 2006 to 2014, and 95% of implants are cf pumps currently[70,71]. In both axial and centrifugal LVAD designs, the leading causes of death are similar, including neurologic dysfunction, multisystem organ failure, infection, and stroke (ischemic or hemorrhagic)[35]. Moreover, the risk of readmission due to severe adverse events increases as patients stay longer in LVAD support[35].

Some recurrent adverse events are implant-site infections, gastrointestinal bleeding, stroke, and pump thrombosis occurring at the rate of 25%, 25%, 14%, 10% respectively for axial, and 28%, 20%, 20%, and 1% for centrifugal pump respectively at 1-year post implants[35,44]. Many efforts have been made in peri- and post-implant management and design improvements to minimize driveline infection rate[72]. The next generation of LVAD will focus on wireless pump recharging development to eliminate the driveline component[73]. Separately, pump thrombosis is categorized as an intrinsic failure (consequences of suboptimal pump design and operation method), patient-related failure (due to distinctive patient physiological response), and therapy-

related failure (a result of deficient post-LVAD management). LVAD patients are often prescribed anticoagulation, such as warfarin and aspirin, to minimize the risk of thrombosis[37]. Patients who required pump exchange due to thrombosis are more likely to have similar recurrent incidences and higher mortality rates [43].

Although both axial and centrifugal designs have a similar mortality rate over time, the centrifugal pump has better hemocompatibility, with less GI or significant bleeding, and pump thrombosis. The HM2 axial pump, generating a high shear rate from blood contacting the mechanical bearing, yielded a higher rate of pump thrombosis and hemocompatibility-related impacts[43,74,75]. During the first three months of implantation, adverse events (especially GI bleeding) are very common and have the most significant impact on patient survival[44,71,76]. Moreover, the risk of mortality is higher for those with renal dysfunction, right ventricle (RV) failure, early multisystem organ failure, or needed pump exchange due to thrombosis[71]. RV failure typically occurs in 13-40% of LVAD patients[77]. Since the pump relies on RV proper function for preloading, RV failure can lead to severe morbidity (such as systemic hypoperfusion, multisystem failure, and low quality of life, etc.) and mortality consequences[78–81].

Another common but less well-understood complication is aortic insufficiency (AI), in which AV does not close completely. Thus it induces a backward flow from the aorta back to the LV. During LVAD support, significant AI creates a substantial LVAD-LV regurgitant flow loop, which negatively affects cardiac recovery, lowers CO, and induces end-organ hypoperfusion[82,83]. Moderate-severe AI is found in more than 50% of patients at 18 months LVAD support and can be de novo or progress from pre-existing trace/mild AI conditions[83–88]. The following section will examine the valvular mechanics in normal and LVAD-support hearts to understand the pump effect on the mitral and aortic valve.

1.3 Valvular Mechanics

1.3.1 In Normal Heart

During the cardiac cycle, human heart valves change their shapes and size in response to their surrounding hemodynamics[89]. This mechanism helps to facilitate the leaflet function and reduces the effect of flexural stress on the valve surface[90]. An average heart valve opens and closes more than three billion times in a lifetime, and experiences various stress and strain types (e.g., tensile, compressive, stretching, and bending)[90,91]. During diastole, the AV leaflets are under cyclic tensile stretch and experience the highest TVP[92,93]. In systole, AV opens, and its leaflets experience bending and unidirectional shear along the ventricular surface[94]. The valve starts to close at the end of the systole deceleration phase, with the minimum reverse flow[90,95]. During late systole, the difference in TVP develops a fluid boundary layer and forms small vortices in the sinus, helping to facilitate leaflets closing. Although the TVP difference is sufficient in closing the AV, vortices presence makes this process more efficient[90,96].

The AV leaflets are thin, membranous folds of trilaminar tissue that typically experienced 10% of cyclic stretch during diastole[97,98]. This stretch modulates the biosynthetic activity and maintains the optimal valvular operation. Higher cyclic stretch can upregulate the valvular collagen synthesis, resulting in the alteration of the matrix structure and damage the valve structure[99–101]. The valvular endothelial cells (VECs) form monolayers, covering both sides of the valve. They are, however, regulated independently according to each side's differentiated hemodynamics, and very responsive to the local shear changes[90,102–104]. The VECs are arranged perpendicular to the blood flow direction to provide pressure-load bearing during valve closure[104,105].

The heart valve is composed of three layers: fibrosa, spongiosa, and ventricularis. The fibrosa layer faces the aorta side, containing a majority of type 1 collagen fibers; this layer bears load by providing structural stiffness and tensile strength, as well as supports smooth opening and closing of the valve[106–108]. The ventricularis layer faces the LV chamber and is composed of

a dense collagen and elastin fibers networks, providing elasticity[98,108]. The shear stress experienced by the fibrosa surface is oscillated between -8 to 10 dynes/cm^2, while the ventricularis experiences peak shear stress of 80 dynes/cm[104]. Finally, the spongiosa layer, covering 60-70% cusp thickness, is a central core rich in glycosaminoglycans (GAGs)[109]. This layer serves as lubrication and shock absorber for the fibrosa and ventricularis, allowing them to deform with respect to each other during valve opening and closing[98,108].

Valvular endothelial cells (VECs) line the blood-contacting surfaces of the ventricular and aortic side of the valve in a smooth monolayer[103,109]. The VECs play a key role in maintaining homeostasis and regulating the metabolic and inflammatory processes[110]. Valvular interstitial cells (VICs) are the most abundant cell type and found in all three layers of the valve. VICs are crucial to valve function and are responsible for the extracellular matrix maintenance and repair[108,111]. They are a heterogeneous fibroblast population that transition between phenotypes and contain 1-5% smooth muscle cells and myofibroblasts[103,112,113]. Moreover, the VICs can initiate valvular remodeling and pathologies to alter cellular stiffness in response to abnormal stress[114].

1.3.2 During LVAD Support

Typically, the cf LVAD reduces AVO area and duration, subsequently initiates valvular dysfunctions (e.g., commissural fusion and valvular incompetence[64,115]. In an animal study with axial cf Micromed DeBakey LVAD, during high LVAD support, TVP increased, and AVO time decreased significantly in both healthy and diseased hearts. The aortic root alteration and leaflet coaptation were noted immediately after the LVAD implanted[115]. In an *in-vitro* study using the cardiac simulator, the Micromed DeBakey LVAD decreased the AVO area and duration by 50% and 20%, respectively. The average strain on the valve leaflets was also significantly elevated due to the increase in minimum strain during systole[64].

By keeping the AV closed for an extended time, LVAD support imposed a prolonged circumferential and radial tensile stress/strain on the valve leaflet and likely promoted soft tissue remodeling[62,64,116–118]. Some researchers have theorized that the increase in bending stress would induce the calcification process by initiating cellular mechanobiological response, while others suspect the lack of nutrients of the VECs and VICs during the extended stretch state have accelerated pathological remodeling[91,98].

1.4 Mitral Valve Dysfunction

The mitral valve (MV) opens during diastole when left atrium (LA) pressure accedes LVP, and blood flows into the LV. Left ventricular relaxation induces the initial filling phase, allowing incoming flow to reach its peak velocity. As the flow gradually decelerated, the MV begins to close. During late diastole, the left atrium contraction produces a 2nd incoming flow but at a lower speed[119]. MV diseases are common in advanced HF patients, who often require surgical corrections to repair or replace the MV. The 5-year mortality rate of HF patients post-MV replacement is 30%[120]. In comparison to MV repair, valve replacement had a higher rate of thromboembolic events, infective endocarditis, etc., and a 30% mortality rate at five years[120–122]. Interestingly, in patients with double valve diseases (AV and MV), there are no differences in valve-related complications in either management methods[122,123]. In some cases, patients' pre-existing conditions seemed to be the significant determinants of their outcomes and survival[122].

Bioprosthesis (BP), bi-leaflet (BL), single-leaflet (tilting-disk (TD)), etc. are different kinds of MV prostheses (MVP), which each have a distinct interaction with the incoming blood flow during diastole[124]. Presently, each valve type is linked with different complications, e.g., higher thromboembolic risk in TD, a higher bleeding complication in BL, and a higher rate of deterioration and stenosis in BP[125,126]. Moreover, in a normal patient, MR can occur after MV replacement and increase the risk of HF[127,128]. In a small clinical study of pulsatile LVAD patients, similar survival rates, and thromboembolism incidences were reported between the MVP and native heart valve

groups[129]. Additional studies are needed to assess the effects of continuous-flow LVAD support in patients with MVP.

1.5 Aortic Insufficiency

Aortic insufficiency (AI), affecting approximately 0.5% general population and 2% elders (75 years or older), is responsible for 4% of AV disease deaths[130,131]. Commonly, AI is caused by annular dilation or leaflet lengthening and occurs in a small percentage of HF patients[132,133]. While during LVAD support, AI is a consequence of valvular dysfunction, induced by the mechanobiological response due to the alteration of the surrounding hemodynamics. The increasing of tensile stress and strain on the AV leaflet when LVAD was operating caused valvular remodeling and resulted in commissural fusion and AI[94]. Many cases of AV leaflet fusion and AI are reported in patients upon LVAD implantations[82,88,134,135]. The leaflets did not have large scale remodeling, just some pathological remodeling on the ventricularis layers (such as fibrosis, loss of endothelium, and commissural fusion, etc.)[94]. De novo AI is irreversible, time-dependent, and worsens with more extended LVAD support[83,136–138]. In patients with pre-existing AI conditions, LVAD further aggravates AI severity, thence reducing end-organ perfusion and worsening HF[83,86,137,139,140]. AI progresses to moderate-severe in 50% of LVAD patients after six months of implantation, which then requires corrective surgeries (e.g., AV repair, replacement, closure, or urgent transplant)[138,141,142]. Moreover, during LVAD support, AI occurs during both diastole and systole, so the traditionally used echocardiographic indices (to assess AI) would underestimate its impact and severity in this particular condition[138,143].

1.6 Objective and Chapter Outlines

The presence of LVAD alters the normal intraventricular flow patterns and pressure distributions. Previous research efforts were made to characterize the LV flow during LVAD support; still, there is incomprehension regarding the flow dynamics in LVAD supported heart at

the presence of pre-existing AI or MVP. This work presented summaries of *in-vitro* testing of LV flow during HM2 and HM3 supports using an in-house cardiac simulator. Under matching hemodynamics conditions, AI at various severity and different MVP orientations and types were tested. The results were then assessed and compared with clinical studies to understand and correlate the change in hemodynamics and flow patterns to potential patient outcomes. Followings are the chapter summaries:

- Chapter 2 is a review of previous literature on AI development during LVAD supports. This chapter gives an overview of AI timeline and consequence in LVAD patient, following by a short discussion on different indices to assess AI. The mechanism, clinical options, and treatment outcomes of AI are also reported
- Chapter 3 describes the effect of pre-existing AI on intraventricular flow during HM2 supports. Testable and reversible 3D-printed stents were used to induce mild, moderate, and severe AI in a mock circulatory loop. Hemodynamics and 2D vortical flow structures were recorded during low, medium, and high LVAD support. It was hypothesized that higher LVAD support would further worsen AI by reducing LVP and AVO. AI indices were calculated and compared with the published data. The result helps to explain the progression of pre-existing AI during LVAD support.
- Chapter 4 describes the effect of pre-existing AI on intraventricular flow during HM3 supports and compares with chapter 3 results. With a similar method, as described in Chapter 3, different AI severities were tested under low, medium, and high HM3 support. Calculated AI indices were used to quantify the impact of HM3 to AI progression in comparison to HM2.
- Chapter 5 describes the effect of MVP designs and orientations on intraventricular flow during HM2 supports. Three different types of MVP were tested in different orientations using a mock circulatory loop, under HM2 support. The results were used to determine the associated risk between the altered flow pattern and thromboembolic events.

- Chapter 6 presents a summary of the conclusion from each chapter and discuss the limitations and future directions.

Chapter 2

Aortic Insufficiency During LVAD Support: Features, Mechanisms and Clinical Options

2.1 Introduction

Since heart transplant is limited in donor availability and restricted eligibility, left ventricular assist devices (LVAD) have become an increasingly popular alternative treatment for end-stage heart failure (HF) patients[1,10]. One and two-year transplant survival rates are 88% and 82%, in comparison to 83% and 73% in the LVAD group[29,35]. The total cost for pump implant and patient care in one year is significantly higher (37% to 116%)[30,31]. The average length of LVAD support is 1.7 years, but the range can go up to 10 years[35,144]. Currently, the axial continuous-flow (cf) HeartMate II (HM2), centrifugal cf HM3 (Abbott), and HeartWare (Medtronic) are commonly used. The HM2 design consists of an impeller insider a metal case, which moves blood through a mechanical bearing, while HM3 and HeartWare transports blood through a wide flow gap using magnetically bearing to minimize shear and compressive force[11,40]

Serious complications are more likely to occur with an extended length of LVAD support, many of which related to the blood-device compatibility[35,44,145]. The most common causes of mortality in LVAD patients are neurologic (19%) and multisystem organ dysfunction (15%)[35]. Despite having similar rates of survival and common adverse event (e.g., implant-site infections, gastrointestinal bleeding, and stroke) at 1-year post implants, HM3 was found to have better hemocompatibility than HM2, subsequently fewer cases of hemolysis and pump thrombosis/replacement[35,44].

Another common but less well-understood complication of LVAD support is aortic insufficiency (AI). AI occurs when the aortic valve (AV) does not close completely, allowing backward flow into the LV. Significant AI during LVAD support creates a substantial LVAD-LV

regurgitant flow loop, which negatively affects cardiac recovery, and causes lower cardiac output (CO) and end-organ hypoperfusion[82,83]. Additionally, the regurgitant flow loop causes blood to be exposed to longer resident time and higher shear stress, which might pose a high risk of hemolysis and subendocardial ischemia[63,146–148].

Moderate-severe AI is found in more than 50% of patients at 1.5 years LVAD support and can be *de novo* or progress from pre-existing AI conditions[83–88,136–138,140,149]. AI developed as early as at six months post-implant, and freedom from significant AI decreases as LVAD support duration increases[83,149]. In pre-existing AI cases, the severity tended to increase post-LVAD implant (10% increase in severity every 18 months)[83,86,136,139]. Particularly, cf LVAD is associated with higher AI prevalence and severity than pulsatile pump[83,136,137,139,150].

Transthoracic echocardiography (TTE) is used to evaluate AI severity based on the recommendation of the American Society of Echocardiography (ASE) in normal patients[151]. AI classification as Mild, Moderate, or Severe is graded according to three major parameters[151]:

(1) Structural parameters, such as LV size, AV, and aortic root structures,

(2) Doppler parameters, such as inflow jet area, density, and contour, and

(3) Quantitative parameters, such as vena contracta width, regurgitant volume and fraction, and effective regurgitant.

The goals for AI management are treating the symptoms, lowering long term consequences, and improving patients' outcomes[152]. Patients with mild-moderate AI and normal size aortic root, or asymptomatic severe AI and regular LV size/function are usually managed with vasodilators[153,154]. Although many debate the drug effectiveness in delaying AV repair or replacement[152,155,156]. Meanwhile, patients with symptomatic severe AI, asymptomatic severe AI, and systolic dysfunction/LV dilation are required surgical management[157–159]. Mild-moderate AI is often corrected at the time of LVAD implantation, especially in long-term supported patients, or those with larger body size, blood type O, and large body surface area-indexed aortic root[138,160,161]. AV replacement or repair are two surgical options to correct AI. Valvular replacement is more

durable but poses a higher risk of thromboembolism[162]. Alternatively, repairing allows the preservation of original tissue and precludes the need for anticoagulation[163].

The AV is a thin tissue structure with three leaflets that attach to the aortic root wall in a u-shaped pattern in a roughly symmetric arrangement. Each leaflet forms a pocket with the corresponding sinus, which plays an important role in the fluid mechanics of the AV[92,164]. The AV leaflets close at the orifice center, in the middle between the sinotubular and aortoventricular junctions, forming a functional aortic annulus[165]. When the leaflets are closed, the free margins press together to form the coaptation area, and the leaflet belly stretches in opposition to the pressure load. The leaflets are essentially slack when open, although the ejecting blood imparts shear stress to the leaflet surface. The leaflets relax when they open in systole, reducing the stretch as blood flows over the ventricular surface into the aorta.

Different than LVAD-induced AI, regurgitant lesion develops and progresses in a normal heart over a longer time course[166]. AI is caused by aortic root enlargement or leaflet degeneration (results of congenital or generative diseases)[167,168]. Typically AI is divided into three classifications depending on the lesion mechanisms, such as leaflet perforation, prolapse, or restriction[169]. In any case, the presence of the regurgitant jet during diastole decreases systemic perfusion, and creates LV flow turbulence, potentially inducing LV dysfunction and congestive HF[86,152,170–172]. Mild AI is relatively asymptomatic, while severe AI reduces exercise tolerance and causes pulmonary edema[152]. Moreover, significant AI increases the rate of morbidity (myocardial hypertrophy, hypotension, cardiogenic shock, and right HF) and mortality[152,173].

During LVAD support, AI might occur during systole or throughout the entire cardiac cycle (CC), while normal AI typically occurs during diastole[143]. The presence of LVAD induced larger regurgitant flow, resulting in lower CO, higher preload, and impacting LV recovery[63,88,137,162,174]. An increase in LVAD flow while systemic flow dropped or relatively unchanged is the sign of AI presence or worsening[174,175]. Using a mock circulatory loop, Garcia et al. reported LVAD and systemic flow ratio greater than 1 in the presence of AI, indicating more flow bypassing the LVAD

than attributing to the systemic circulation[174]. In an animal study, Iizuka et al. reported that in severe AI cases increasing pump speed increased regurgitant flow without contributing to the total systemic flow[175].

Moreover, LVAD patient with concurrent AI is associated with higher readmission rate and adverse events (mitral (MR) and tricuspid regurgitation, hemolysis, worsening of right ventricle function, etc.)[82,137,138,140,176]. Temporarily, LVAD speed can be increased to compensate for flow loss; but extendedly, it would further damage AV and worsen AI[138,162,175]. The current American Heart Association classification of progressive mild-moderate AI includes criteria that don't apply to end-stage HF patients, including normal LV size and function[157]. Instead, these patients typically have dilated LV volume and depressed systolic function, which raises a question if the current AI classification is applicable to this particular group. The goal of this review paper is to evaluate AI development with LVAD support compared with natural occurring AI and present the features, mechanisms, and links to clinical treatment options.

2.2 Features of AI in the LVAD Supported Heart

The rapid progression of AI in LVAD patients suggests an alternative mechanism from no-LVAD AI. The reduction of AV opening (AVO) is suspected inducing AV leaflet borders fusion (commissural fusion), thus causes *de novo* AI. This mechanism is time-dependent, irreversible, and worsens with extended LVAD support[83,137,138]. The commissural fusion incidences in patients with required-venting LVAD (allowing periodic AVO) was ten times lower than non-venting pump[135]. The duration and frequency of AVO decreased in all patients under LVAD supported[63]. Mudd et al. reported 44% of patients had closed AV within the 1st month of implant, and more than 50% at six months[86]. Subsequently, AI development has been associated with the prevalence of no- or limited-AVO[83,86,139].

In 2000-2006, AV fusion was observed in 50-67% of patients implanted with pulsatile LVAD, and somewhat correlated with AI development[82,88,134,135]. Distinct from a rheumatic induced

lesion, the LVAD-induced fused leaflets appeared macroscopically normal. The deposition of disorganized collagen fibers and dense collagen appeared adjacent to the ventricular face, while the fusion migrating from the valve annulus toward the center prevented the leaflets from closing completely and producing AI. The extended LVAD support resulted in the loss of valvular laminar elastin structure and extensive leaflet fusion[94]. As the cf LVAD was clinically approved and used instead of the pulsatile pump, higher occurrences of AI were reported. After one year of HM2 support, 25-83% of patients developed mild to worse AI[83,86,138,177]. Mudd et al. were one of the first groups who reported the association between commissural fusion and AI in HM2 patients: 89% developed commissural fusion after one year post-implants, and 50% had mild AI, and 33% had moderate AI[86].

While long-term LVAD support and low ejection fraction were found to be independent predictors of *de novo* AI development[84,138–140,149,178,179], clinical studies have reported multiple factors associated with the worsening of pre-existing tracel AI in post-LVAD support. Patient-related factors included pre-existing valvular dysfunction, old age, and abnormal cardiac function. Pre-existing valvular dysfunctions include uncorrected mild AI[161,180], mild-worse MR[140], large body surface area-index aortic roots[161,180]; large aortic sinus diameters[83,84,136,138,139,161,176,181–183], or degenerative remodeling of the aortic root (thinning wall, smooth muscle cell apoptosis, fragmentation of elastic fiber)[86,136,150,184,185]. Older patients had a high risk of age-related valve degeneration and decreased aorta elasticity[84,136,138,139,176,181–183,186,187]. The abnormal cardiac function included low LV diastolic and systolic volumes, and diastolic filling abnormality[83]. LVAD related factors included reduction of AVO area and duration, high LVAD speed, and type of LVAD[41,83,84,136,138–140,176,181–183]. The high rate of progressive AI in cf LVAD patietns was the suspected consequence of low pulsatility flow, which potentially induces larger regurgitant flow and a higher rate of valvular remodeling[40,176,178,188,189].

2.2.1. Changes of Clinical AI Indices in LVAD Supported Heart

Diagnosis of AI severity and treatment strategy is largely informed by the long history of AV repair and replacement in the absence of LVAD support. Presently, many centers continue to use the American Society of Echocardiography guidelines, intending for patients with normal cardiac physiology and pulsatility, to evaluate and monitor AI progression in LVAD patients (as summarized in table 2.1)[190]. When applying to LVAD patients, experts suggested to note for the presence of AI during the whole cardiac cycle, change in left and right's ventricle size, and emphasized on the change of vena contracta width and the jet width/LVOT width ratio parameter[193,194]. In HF pre-LVAD patients, severe reduction of LV stroke volume, low systemic pressure, and high LV diastolic pressure resulted in low AI velocities and regurgitant volume (RV), which ultimately causes difficulty in AI assessment and underestimation of AI severity[194].

Table 2.1: Clinical qualitative and quantitative parameter for grading AI[190]

Parameter		Mild AI	Moderate AI	Severe AI
Qualitative	Structural parameters LA size/ Aortic leaflet	Normal/ Normal or abnormal	Normal or dilated/ Normal or abnormal	Usually dilated/ abnormal
	Doppler parameters Jet width in LVOT Jet density/ deceleration rate	Small Incomplete/ Slow	Intermediate Dense/ Medium	Large Dense/ Steep
	Diastolic flow reversal in descending aorta	Brief early diastolic reversal	Intermediate	Prominent holo-diastolic reversal
Quantitative	Vena Contracta width (cm)	< 0.3	0.3-0.6	> 0.6
	Jet width/ LVOT width (%)	< 25	25-45 46-64	≥ 65
	Jet CSA/ LVOT CSA (%)	< 5	5-20 21-59	≥ 60
	R Vol (ml/ beat)	< 30	30-44 45-59	≥ 60
	RF (%)	< 30	30-39 40-49	≥ 50
	EROA (cm^2)	< 0.10	0.01-0.19 0.20-0.29	≥ 0.30

On the other hand, LVAD support produced a larger, more persisted regurgitant jet and larger vena contracta[138,190]. Therefore, the traditional TTE indices and rationale are not translatable to LVAD patient physiology and would underestimate AI severity[191,192]. These indices were found to underestimate AI severity in 33% cf LVAD patients and fail to distinguish the morbidity and mortality difference in mild-moderate and moderate-severe AI groups[190]. The RF, which is the ratio between the RV and total systemic flow (Q_{sys}), is also an unreliable index. In the native heart, the RV increases while Q_{sys} decreases, which results in higher RF as AI worsens. When an LVAD is present, both RV and Q_{sys} increase (in some cases, Q_{sys} increases more significantly); as a result, RF stays the same or decreases, indicates a false conclusion of improved AI.

Currently Proposed Indices to Assess AI in LVAD Supported Heart

Clinicians have proposed several new indices to grade AI severity in the LVAD-assisted heart. The diastolic flow acceleration and the ratio between systolic and diastolic peak velocity of the LVAD outflow cannula (S/D ratio) are suggested by Grinstein et al. They reported these two indices are highly correlated with RF and pulmonary capillary wedge pressure. Since the flow passing through LVAD outflow cannula is directly proportional to the LV preload, and inverse proportional to the ascending aorta afterload, the diastolic acceleration is expected to increase while the S/D ratio decrease as AI increases in severity. After testing in a small group of patients with different AI severity (n=57), Grinstein et al. reported that the diastolic flow acceleration and S/D ratio were more accurate in predict future HF admissions, the need for AV intervention, urgent transplantation, and mortality than vena contracta and other echo indices[190,195]. The early diastolic phase slope (EDPS) calculated from LVAD flow was another new proposed index. In a study of 30 patients, Imamura et al. reported EDPS value higher or equal to (>=) -17.6 L/min/sec is an indication for significant AI (RF >30%) and suggested this index as an indicator for the presence and progression of significant AI[196].

Table 2.2 summarizes three different published indices experimental data from a mock circulatory loop. In the experimental data, the S/D ratio decreased as AI worsens and at higher LVAD support, in agreement with the published result. Especially in the case of mild AI, at substantial LVAD support, the S/D ratio indicated moderate/severe AI regurgitation. The diastolic acceleration increased as AI worsened but decreased at higher LVAD speeds, unlike the published result. The EDPS index increased as AI worsened as well as with increased LVAD support, but was insufficient to reach -17.6 for which would classify the AI as moderate/severe. The newer indices calculated from the experimental study exhibited agreement with the published data, except for the diastolic acceleration index, which suggests this index is not sensitive with a significant change in LVAD support.

Table 2.2: Proposed indices to assess AI in LVAD supported heart

	Published Data*		Experimental data**			
	Trace/Mild AI	Moderate/ Severe AI	Mild AI		Moderate AI	
			Low LVAD	High LVAD	Low LVAD	High LVAD
S/D ratio	6.0	2.6	3.80	1.87	2.59	1.81
Diastolic acceleration cm/s^2	35.7	68.7	10.22	4.3	14.23	8.91
EDPS L/min/sec		>= -17.6	-24.04	-18.54	-22.46	-17.71

*Published data are obtained from[190,195,196]

** In vitro experimental data obtained using the cardiac simulator, a similar method described in the previous publication[59]. Mild and moderate AI models were created using a 3D printed stent [197], with RF ~ 20% and 40% for mild and moderate AI conditions, respectively, without LVAD support. Heartmate II (Abbott, US) was used, and test at two different LVAD support level: low (8k rpm) and high (11k rpm) supports.

2.3 Mechanism of AI in the LVAD Supported Heart

2.3.1 Biomechanics: Altered LV Flow Paths

In a normal heart, the AV opens and closes at each heartbeat. Blood passes through the mitral valve (MV) and enters LV from the atrium during the diastolic filling, then ejects to the aorta

through AV during the systolic ejecting phase. At mid-systole, AV starts to close, and subsequently experience diastolic phase pressure on its leaflets at complete closure (Figure 2.1A)[60]. The presence of the LVAD modifies the LV flow pattern, alters the magnitude and phase duration of myocardial stress and strain on the AV and aorta[61–63]. By drawing blood from the apex and directing it to the aorta, LVAD decreases LV pressure (LVP) and load, thus promoting the LV reverse remodeling process. Consequently, the transaortic pressure (TVP) increased, thus effectively prolonging diastole and reducing the AVO area and duration. During low LVAD support, the heart contracts and opens the AV during systole, blood is transported through the AV and the LVAD into the aorta. During high LVAD support, the reduced LVP keeps the AV hemodynamically closed throughout the entire cardiac cycle (Figure 2.1B). This exposes the AV tissue to high aortic pressure and continuous high tensile strain[64]. Additionally, the LVAD deliveries flow directly to the aortic root, lowering aortic flow pulsatility, and altering the flow profiles at the aorta[63,174,198,199].

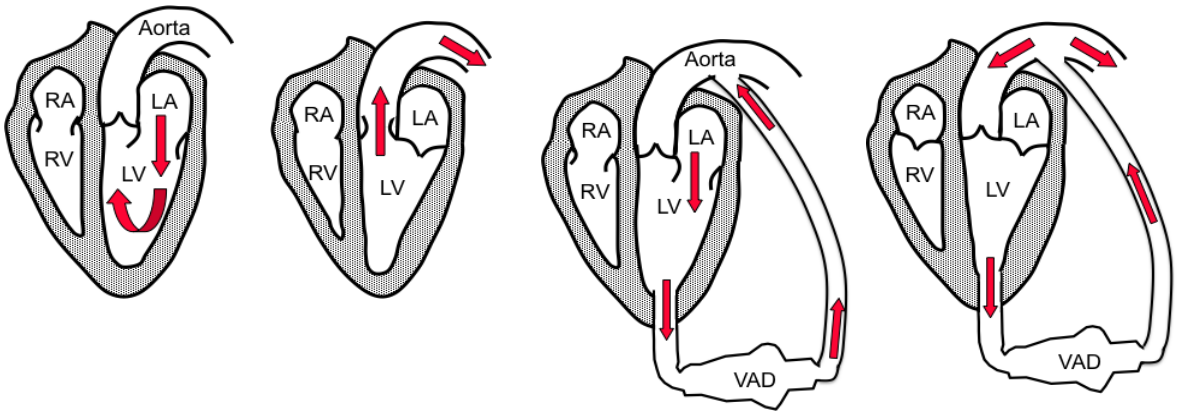

Figure 2.1 [A] Blood flow normally exits the LV through the AV, and [B] LVAD support alters this path, diverting flow through the LVAD and eliminating AV opening

LVAD presences increased circumferential and radial tensile stress and strain on the AV leaflet[64,116]. Since stress cannot be directly measured in valvular tissue, the change in stress

was estimated from strain measurement[116]. The minimum systolic strain on AV leaflets was found to increase significantly during cf LVAD support using a mock circulatory loop. Moreover, prolonged diastole keeps the leaflet in a closed position, subsequently increased the duration of leaflet stretching[64]. Continuously closed AV was clinically linked to commissural fusion and AI development in LVAD patients[86,94,134,135,200].

2.3.2 Remodeling: Mechanobiological Response

During the cardiac cycle, the normal AV experiences pulsatile pressure and various stress and strain types such as tensile, compressive, stretching, and bending[90]. When the AV closes during diastole, its leaflets stretch against the TVP and experience bending stretch from the aorta side and tensile stretch from the LV side. During systole, the AV leaflets experience a small amount of tensile stress caused by the unidirectional pulsatile shear stress of blood flow at the ventricular side, and the bending stress and oscillatory shear stress on the aortic side[201]. The valve surfaces are lined with a monolayer of the valvular endothelial cells (VECs), which are sensitive to shear stress. In response to any changes in the surrounding shear stress, VECs initiate mechanotransduction pathways (biological response from external mechanical stimuli), which can lead to structural changes in vessel walls[108,202].

The ventricularis (an elastin layer on the ventricular side of AV), regularly exposed to laminar blood flow with high velocity and shear stress, have higher expression of many cytokines inhibiting fibrosis and calcification formation, therefore is relatively disease protected[203]. On the other hand, the fibrosa (the dense collagen layer on the aortic side), experiences turbulent flow with low velocity and shear stress (due to the presence of sinus vortices at the aortic root) and is more prone to local lesions[108,204,205]. The increased expression of bone morphogenetic protein 4 (BMP-4) and decreased expression of osteoprotegerin, C-type natriuretic peptide (CNP), chordin, and other biochemical markers in the fibrosa layer make it more susceptible to disease[103]. The VECs on the fibrosa side have higher expression of genes associated with bone formation and

lower calcification inhibiting genes, and their transcriptional profiles have higher expression of endothelial adhesion molecules during altered hemodynamics[203,206]. The valvular interstitial cells (VICs), the most prevalent cell type in AV, are more sensitive to pathological stress. During elevated stress, the VICs increase the expression of remodeling enzymes, pro-inflammatory proteins, and pathological markers, which can lead to fibrosis and calcification[167,168,207–209].

LVAD extends the duration and magnitude of stress on AV leaflets. Previous studies have found that high cyclic stretch and low, oscillatory shear stress affects the AV biosynthetic activity, leading to pathological matrix remodeling[167,168,207,210,211]. An in vitro study on porcine AV reported that at in comparison to 10% physiological stretch, higher pathological stretch (15-20%) altered the expression and activity of the proteolytic enzymes, increased cell proliferation, and apoptosis, thereby initiating a cascade of events leading to valvular degeneration and disease progression[168]. The altered biomechanics in the presence of LVAD could initiate a remodeling response in VICs and VECs, which results in fibrosis, contracture, and ultimately AI.

While the pathological molecular pathway of AI initiation and progression during LVAD support is not yet understood, it likely involves features similar to those in valvular diseases such as inflammation, VIC differentiation, and matrix remodeling. Inflammation from altered pressure or flow can allow VIC division into myofibroblasts, which deposit extracellular matrix components (ECM) and are associated with valvular fibrosis progression. This process involves the production of transforming growth factor 1 (TGF-β) and BMPs[103]. Elevated levels of TGF-β initiates myofibroblast differentiation, which triggers an increase in collagen synthesis and cellular contractility and is shown by α-smooth muscle actin protein expression (α-SMA)[212–214]. The VIC phenotypic changes result from microenvironmental stimuli, elevating valvular stiffness and tensile stretch, and lead to disease progression[101,214,215].

2.3.3. Other Possible Mechanisms

In HeartMate VE (pulsatile LVAD) patients, only local AV abnormalities were observed, e.g., loss of endothelium, presence of fibrosis, and dense collagen, instead of large scale remodeling. The pathological structures were spanned from the valvular annulus toward the center, pulling the valve open and initiating AI development[94]. In cf LVAD patients, different observations were made. Martina et al. suspected commissural fusion was a consequence of the disappearance of the endothelial layer between leaflet boundaries when the valve stayed permanently in a closed state[200]. While another noted the thickening of the leaflet, consequences of the extension of fibrous tissue, loss of elastic layer, or leaflet folding, prevented the AV from closing properly and caused AI[216].

2.4 Clinical Options

2.4.1 Recommendation about Surgical Intervention

Pre-existing moderate-worse AI grade is repaired at the time of LVAD implant[162]. Depending on patients' underlying pathology, LVAD support duration, and INTERMAC classification, different repairing techniques would be used to maintain the native AV structure and function, minimize potential adverse events, and allow the possibility of LV recovery (as summarized in figure 2.2)[138,160]. Partial stitch or polytetrafluoroethylene patch is commonly used to repair mild-moderate AI, while AV closure or replacement is used for moderate-severe AI[22,138,145,217–219]. Without any repairing procedure, pre-existing mild AI patients were three times more likely to develop significant AI post-LVAD implant[161]. Moreover, in the long term, those patients experienced worse complications, such as higher RV dysfunction, significant AI, mitral, and tricuspid regurgitant[180]. The following section will discuss several conventional AV correction methods.

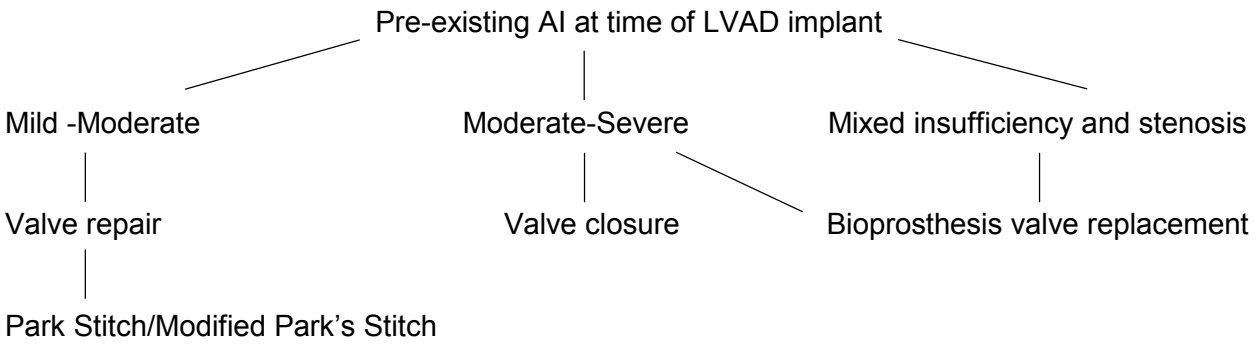

Figure 2.2 Summary of the current treatment guidelines for pre-existing AI at the time of LVAD implant[63,138,162,179].

Partial Closure Central Park Stitch

Park stitch is the single, pledgeted 4-0 Prolene suture placing at the central portion of the AV leaflets[219]. It is considered a simple, durable, and effective method to correct mild-moderate AI provided that the original tissue is sufficiently thick and has enough tensile strength to hold the sutures. In the case of a regular/thin and fragile leaflet structure, this method may lead to leaflet tearing and recurring AI. While allowing partial opening and forward flow through AV, Park stitch method still has some limitations such as potential AI recurrence, risk of stenosis development/progression, and suture detachability (in cases of valve deterioration, or tear at coaptation points). Moreover, Park stitch is not a suitable treatment for severe AI, or bridge-to-recovery patients (who need to maintain the original AV's structure and function)[162,219,220]. Park stitch's patient must be monitored carefully during LVAD speed regulation and ramp testing to avoid stitch rupture from sudden AV opening[162]. The effectiveness and durability of this method during pulsatile and cf LVAD support up to 2 years were reported[138,219–221]. One clinical study found that Park stitch method significantly prevented AI progression in pre-existing moderate-worse AI patients, and did not affect patient survival rate[221]. In another study, there was a similar AI prevalence at 1-year post LVAD support for those with correct AV and normal AV. Moreover, approximately 40% of patients undergoing this procedure had some degree of AV opening[138].

Modified Park Stitch

Modified Park stitch method is recommended for mild-moderate AI in which the valvular leaflets are relatively regular or thin. This technique consists of stitches securing pledgets with each commissural at the center of AV for reinforcement. Since the repair is not centrally localized instead of distributes across the leaflets, this method can prevent sutures tearing while allowing partial AV opening and forward flow[220]. This method had similar limitations as Park stitch, as discussed above[162]. Compared to other correction methods, AV repairs (central AV closure by Park and modified Park stitches) have debatable durability. At 4-6 months post-LVAD follow up, approximately 20% moderate-worse AI recurrence rate occurred in some centers[160,222], while other groups report a much lower recurrence rate (0-7%)[138,220,221].

Complete Valve Closure

Complete AV closure is recommended for patients with moderate-serve AI or degenerative AV, such as leaflets prolapse or mal-coaptation[162]. This procedure performed using three felt strips suturing the valve leaflet, anchoring the aortic wall at the commissures; in some cases, a patch can be sewed directly to cover the valve annulus or cusp. If the patient has bioprosthesis (BP) AV, the BP would be removed, and a pericardial patch is used to close the outflow tract[145,218]. It is a relatively fast procedure with long term durability (no AV deterioration or recurrent AI), no long term emboli complication. Still, some limitations exist, such as no forward flow, no systemic flow in case of pump failure, high risk of thrombosis, limiting the possibility of myocardial recovery or device weaning off[145,160,162]. There are mixed findings regarding the survival rate for patients with AV closure: Adamson et al. reported a higher survival rate in comparison to the intact AV group, while Robertson et al. reported this group had higher unexplained deaths and death incidences from device failure[145,160].

AV Replacement

AV can be replaced with BP and mechanical heart valve in patients with mixed stenosis and insufficient or calcific pathology. This method offers some advantages such as the possibility of myocardial recovery and pump removal, complete AV opening allowing higher exercise tolerance, etc. On the other hand, its limitations include long and complicated procedures, high risk of thrombosis (even with the use of anticoagulation), potential valvular fusion, or stenosis in porcine BP valve[63,87,162,174,220,223–227].

2.4.2. Outcomes of Different AI Correction Methods

Previously, Adamson et al. had reported that post-LVAD patients with AV closures had a higher 1- and 3-year survival rate and less valvular compromising related adverse events (such as retrograde flow or embolization) in comparison to those with intact AV[145]. However, recent studies reported the opposite trend. At one year, patients with AV repair or no-intervention had the highest survival rate (roughly 80%), followed by AV replacement (72%) and AV closure (64%)[160,161]. In terms of durability, the valvular repair was ranked last with the highest AI recurrent rate at approximately 20%, following by 10%, 9%, and 5% in patients with no-intervention, AV replacement, and closure, respectively. Interesting, causes of death, re-hospitalization, stroke, or right heart failure incidences were found similar in all groups[160].

2 4.3. Other Options

Regardless of which procedures were used previously to correct AI, the LVAD support level needs to be optimized, AV structure and operation (open/close), and the progression of AI, should be monitored regularly with routine echoes measurements[228]. The current guidelines for AI management in post-LVAD patients are summarized in figure 2.3. While decreasing LVAD speed reduces the TVP and AI severity, it also increases LV filling pressure and worsens end-organ perfusion[179]. Optimization of LVAD speed was generally defined as the lowest possible

level of LVAD support that maintains adequate CO and oxygen, eliminates moderate/worse mitral regurgitant, and allows AVO[138]. Intermittent AVO during LVAD support was found to reduce the risk of AI development, improve LV systolic function and EF (especially in patients with preoperative short HF duration)[83,136–138,176].

When no trace of AI is present, patients should still be monitored carefully to ensure LVAD operating at the right speed and no AI development[138]. If mild AI is detected, optimization of LVAD speed, allowing partial or intermittent AV opening, could prevent the progression of AI. In the case of significant AI, speed optimization, however, might cause inadequate CO and worsen HF symptom[138,162]. Instead, when symptomatic AI is present post-LVAD, higher speed should be set to improve CO. If the patient's AI and HF symptoms worsen with no changes in hemodynamics, AV repair, replacement, or closure procedure will be required. 5-10% of LVAD patients would need AI-correction surgery after three years or longer post-implant[138].

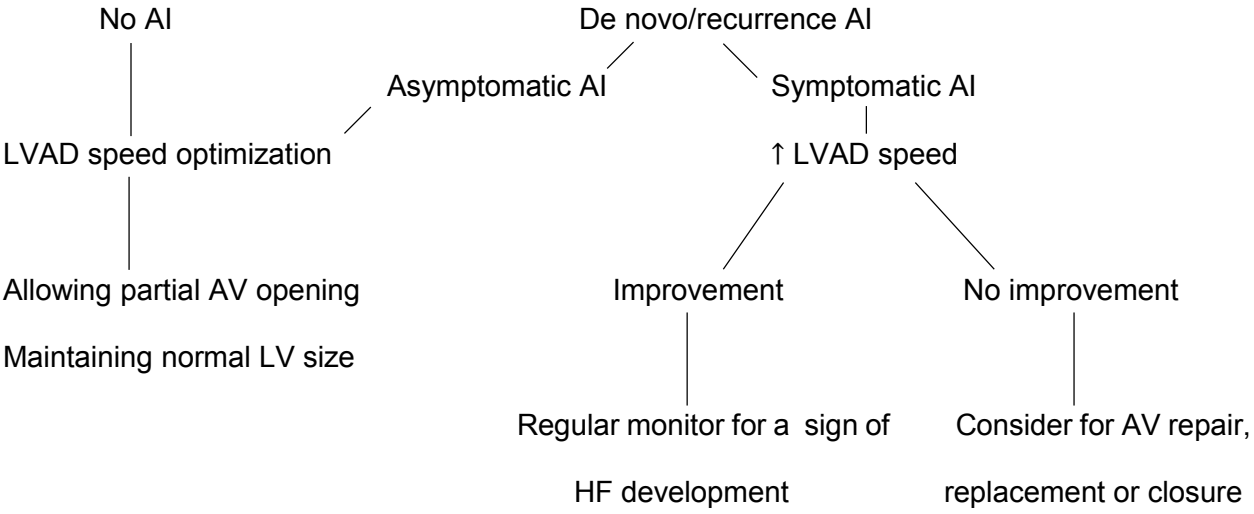

Figure 2.3 Summary of the current post-LVAD management guidelines[138,179]

2.5 Conclusion

This chapter gave a literature review on the AI features, mechanism, and clinical options during LVAD support. AI is a common complication, affecting morbidity and mortality in LVAD

patients. While the mechanism of *de novo* AI development is unknown, it was linked to commissural fusion, lack of AVO, and alteration of valvular tissue mechanics. Pre-existing AI also worsens in post-LVAD, interfering with the pump benefits. Chapters 3 and 4 will investigate the effect of HM2 and HM3 to intraventricular flow in the presence of pre-existing AI.

2.6 Acknowledgements

This chapter, in full, is in an early prepared stage for publication. The co-authors are Frances Lagarda, Karen May-Newman. The dissertation author is the primary author of this paper.

Chapter 3

The Effect of Aortic Insufficiency on Left Ventricular Flow in The HeartMate II LVAD Supported Heart

3.1 Background

Left ventricular assist device (LVAD) support increases systemic blood flow and improves the end-organ functions in heart failure (HF) patients. The LVAD provides intermediate support for Bridge-to-Transplant patients while waiting for suitable heart donors, as well as long-term support for Destination Therapy patients who are ineligible for transplant[67,229]. In most HF patients, the pumps facilitate consistent cardiac output (CO) improvements[230–232]. In a small number of cases, the patient's heart recovers sufficiently to be weaned off of the device. However, the majority of LVAD patients remain on the device permanently[233–238].

The aortic valve (AV) leaflets contain a dense network of highly aligned collagen fibers orientated along the circumferential direction in the outer layer[239]. As a result, the stress-strain response along this direction is stiffer compared to the transverse radial direction[116]. Aortic insufficiency (AI) is the inability of AV to close during diastole, which allows blood to leak back into the left ventricle (LV) (Figure 3.1A). In LVAD-related lesion, AI resulted from the alternation of aortic root geometry or valvular leaflets and developed within a few months of pump implant[152]. Previous studies reported strong associations between LVAD-induced AI with decreasing in AV opening frequency and development of commissural fusion[83,86,94,115,134,135,139,143].

The short term outcome of patients with pre-existing/uncorrected Mild AI at the time of LVAD implant is similar to those with normal AV. However, in the long term, those patients developed worse complications (e.g., HF dysfunction, greater incidence of Moderate-Severe AI, mitral regurgitation (MR), etc.)[180]. Significant (Moderate-Severe) AI is found in more than 50% of

LVAD patients at 18 months support and can arise *de novo* or progress from pre-existing Trace/Mild AI conditions[83–88]. The *de novo* AI, associating with AV commissural fusion, is irreversible, time-dependent, and progresses with extended LVAD support[83,86,88,136–138]. In the first 1.5 years post-implantation, the rate of Moderate-Severe *de novo* AI diagnoses doubles every six months; and the risk of AI is approximately 65% at three years post-implant[83,149]. Pre-existing AI tends to worsen post-LVAD implantation[83,86,136,139]. At two years of continuous-flow (cf) LVAD support, AI (regardless of classifications) did not affect patient survival rate, excepted for those with pre-existing right ventricle dysfunction[84,137,138,176,180–182].

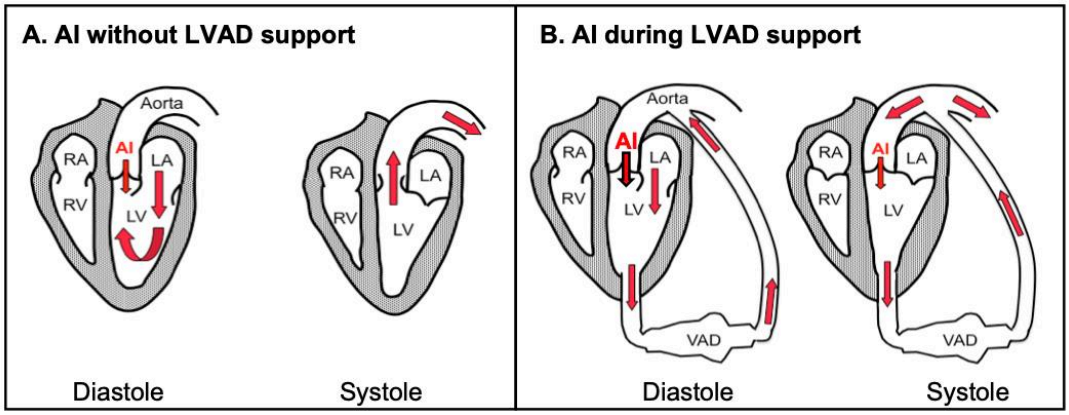

Figure 3.1: Schematic of AI (A) without and (B) with LVAD support.

AI regurgitant jet decreases systemic perfusion and alters the LV flow pattern, ultimately inducing LV dysfunction and exacerbating HF[171,172,240,241]. Significant AI can lead to higher patient readmission rates, end-organ hypoperfusion, and worsening right ventricle hypokinesis[82,83,137,138,140,176,180]. During LVAD support, the regurgitant flow loop (Figure 3.1B) extends the time-history of shear stress exposure of the blood, increasing hemolysis and thromboembolism. In this condition, the pump needs to run at a higher speed to achieve adequate CO, which increases wear on the device. The AV dysfunction interferes with cardiac recovery and pump weaning in “Bridge-to-Recovery” patients[83], and limit patient’s exercise capacity and quality

of life[242]. The goal of this project is to (i) evaluate the LV fluid mechanics during AI, and (ii) quantify indices associated with hydrodynamic efficiency and vortex development during the HeartMate II (HM2) LVAD (Abbott, IL) support.

3.2 Method

3.2.1 Experimental Setup

Experimental studies were performed with the San Diego State University (SDSU) mock circulatory loop, which mimics the cardiac hemodynamics[59,174]. The customized transparent model of the dilated LV was fabricated from platinum-cured silicone rubber based on idealized geometry. The inflow cannula was connected to a HM2, and the outflow graft was replaced with 16mm-diameter Tygon tubing and connected to the ascending aorta. The assembly was immersed in a water-filled tank and connected to the systemic circulation, based on the Windkessel design(Figure 3.2 (Left))[59]. A linear displacement piston pump (controlled by LabView) imposed cyclic pressure to the LV, producing the fluid displacement with the E- wave and A-wave, and systole. The circulating fluid, supplied through the left atrial chamber, was a viscosity-match blood analog containing 40% glycerol and deionized water (3.72 cP at 20°C) neutrally buoyant fluorescent particles (20 mm, PMMA-RhB) for flow quantification. Pressure and flow transducers were used to record LV pressure (LVP), aortic root pressure (AoP), systemic flow rate (Q_{sys}), and LVAD flow rate (Q_{LVAD}) at 200Hz. Porcine bioprosthetic valves, 26-mm Medtronic Mosaic, and 25-mm Medtronic 305 Cinch were placed in the AV and MV positions, respectively.

AI was created with small 3-D printed stents with thin walls to minimize the effect of transvalvular pressure differences during systole (Figure 3.2 (Right, bottom)[197]. The stent was inserted into the AV to prevent complete valve closure and to induce a regurgitant jet without obstructing the forward flow. The stent openings had regurgitant orifice areas of 3, 10, 15 mm^2

which generated regurgitation fractions of 19% (mild AI), 29% (mild-moderate AI), and 41% (moderate-severe AI) respectively[151,157]. These three models are classified as Mild, Moderate, and Severe for short.

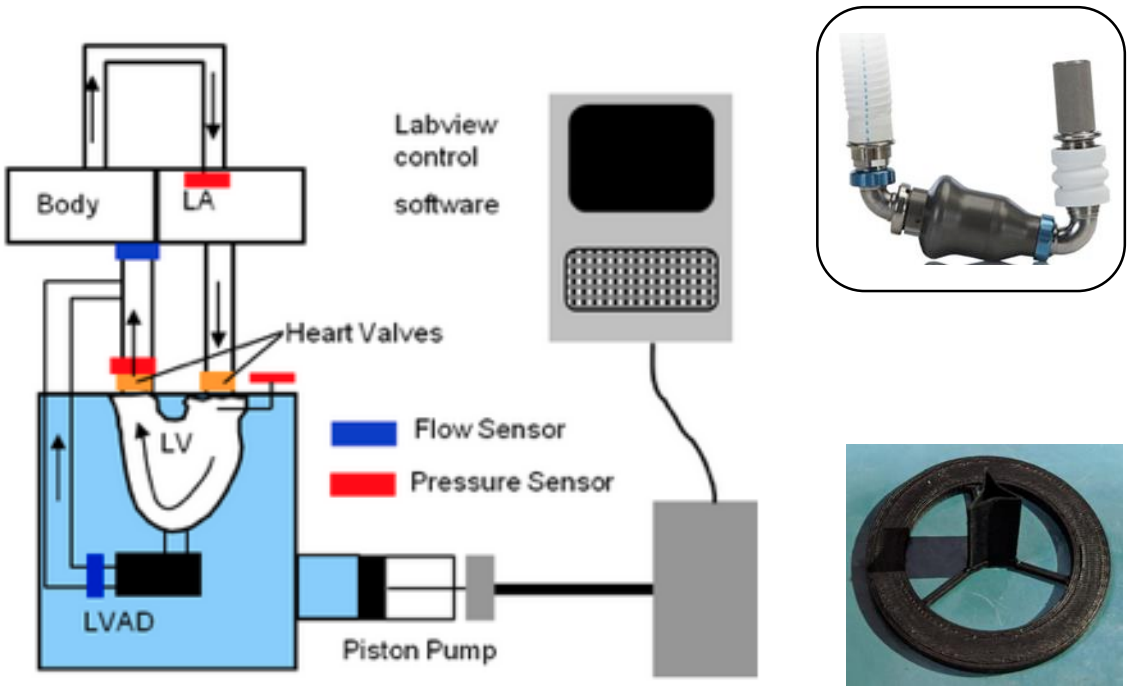

Figure 3.2: (Left) The mock circulatory loop; (Right, top) HeartMate II; (Right, bottom) AI stent.

The systemic resistance was adjusted to achieve the hemodynamics of Class IV New York Heart Association dilated cardiomyopathy (DCM). In particular, a mean aortic pressure (AoP) of 60 ± 5 mmHg, CO of 2.0 ± 0.5 L/min, and end-diastolic volume (EDV) of 180 mL were obtained[170]. In the pre-LVAD condition, the LVAD conduit is clamped, and the HM2 is off (LVAD-off). For the post-LVAD conditions (LVAD on), three different HM2 speeds were tested noth with (CS on) and without (CS off) native cardiac function. These levels were defined as Low, Medium, and High LVAD support and corresponded to 8k, 9.4k, and 11k rotations per minute (rpm). Each stent was then incorporated into the AV, and the same conditions repeated.

The velocity fields, measuring using Digital Particle Image Velocity (PIV), were captured by a thin (1-2 mm) laser light sheet positioned at the LV mid-plane (Figure 3.3)[243]. The LaVision Imager Intense high-resolution camera recorded 12-bit digital images with a time interval of 700-2000 μs. A sufficient spatial resolution (14 pixels/mm) was achieved by using 32 x 32 pixels interrogation windows on 1376 x 1040 pixels field. Triggered image pairs were acquired at 40 Hz for each condition, and 50 image sets were collected and phases-average for each time points[59]. Each CC lasts 0.95s and contains 39 frames.

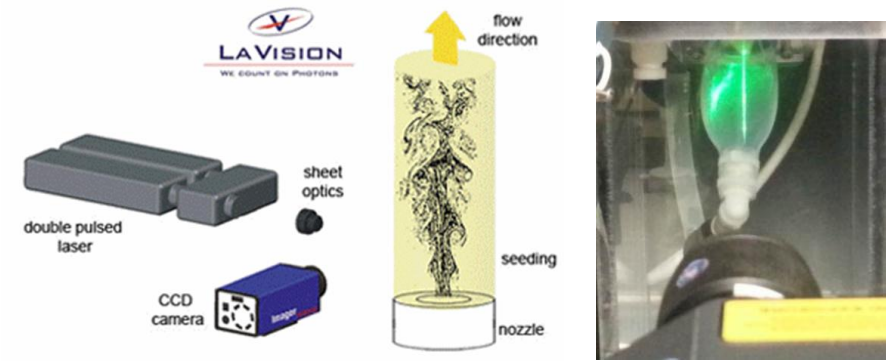

Figure 3.3: PIV.

3.2.2 Data Analysis

Hemodynamic analysis

Sixty cycles of pressure and flow for each condition were analyzed and computed the average, maximum, and minimum values (Figure 3.4). The flow waveforms were integrated to calculate stroke volume (SV). The LVP waveforms were used to define the duration of systole and diastole. Other parameters were derived from the hemodynamics data, as described below.

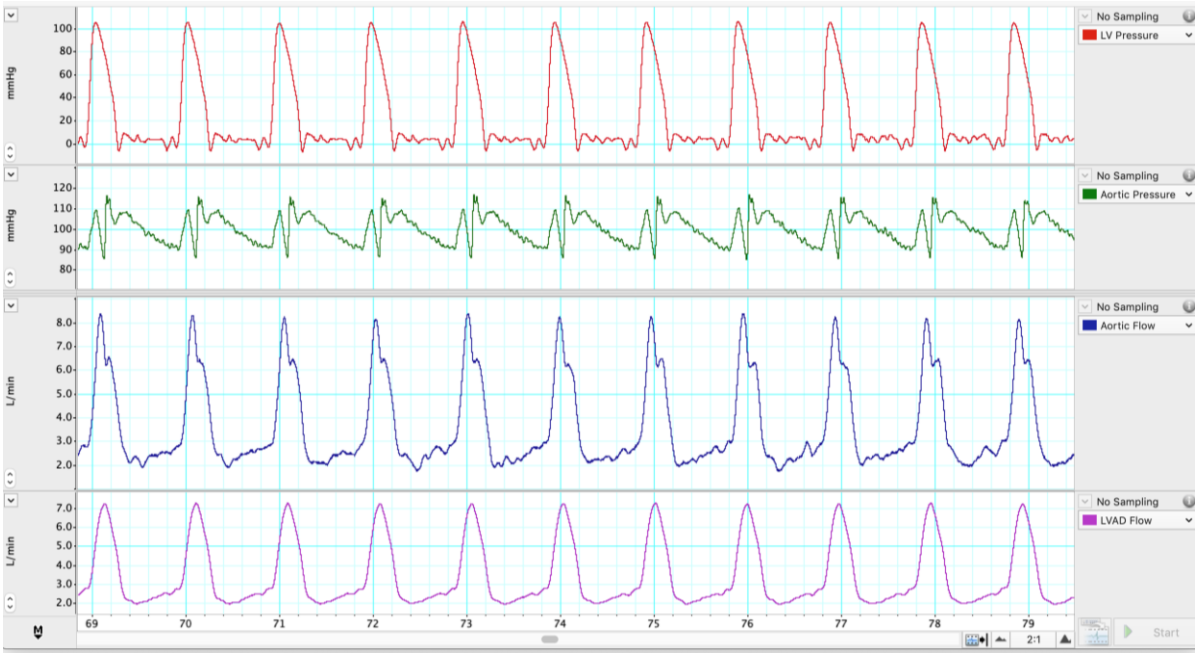

Figure 3.4: Pressure and flow curves from Lab Chart.

Transaortic pressure (TVP):

$$TVP(t) = AoP(t) - LVP(t) \quad \text{(Equation 3.1)}$$

Flow-through AV (Q_{AV}):

$$Q_{AV}(t) = Q_{sys}(t) - Q_{LVAD}(t) \quad \text{(Equation 3.2)}$$

(positive Q_{AV}: forward flow, and negative Q_{AV}: backward flow through AV)

Flow ratio (Q_{ratio}):

$$Q_{ratio} = \frac{\bar{Q}_{LVAD}}{\bar{Q}_{sys}} \quad \text{(Equation 3.3)}$$

Pulsatility index (PI):

$$PI = \frac{Q_{sys}\,max - Q_{sys}\,min}{Q_{sys}} \quad \text{(Equation 3.4)}$$

Net flow through AV (NF):

$$NF = \frac{\bar{Q}_{AV}}{\bar{Q}_{sys}} \times 100\% \quad \text{(Equation 3.5)}$$

Forward LV ejection fraction (LVEF)[244]:

$$\text{Forward LVEF} = \frac{\overline{SV}_{sys}}{LV_{EDV}} \times 100\% \qquad \text{(Equation 3.6)}$$

($\overline{SV}_{sys}$: average systemic stroke volume, LV_{EDV}: left ventricle end-diastolic volume)

S/D ratio[190]:

$$\text{S/D ratio} = \frac{LVAD_{\text{peak systolic velocity}}}{LVAD_{\text{peak diastolic velocity}}} \qquad \text{(Equation 3.7)}$$

AV opening (AVO) time (second) was estimated from the transvalvular signal as shown below

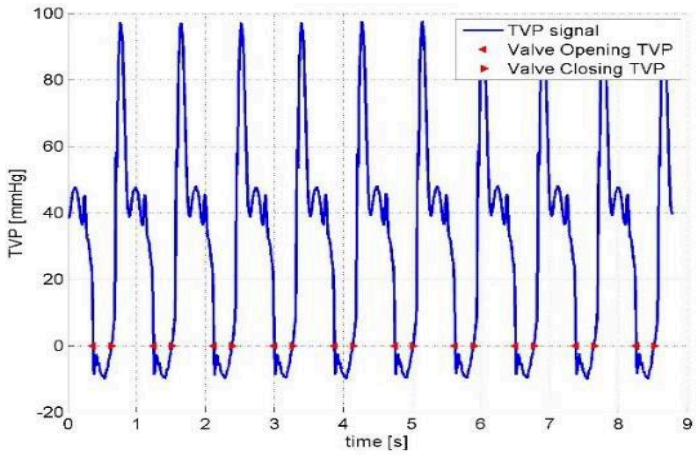

Figure 3.5: Aortic valve transvalvular pressure is used to estimate AV opening time

Diastolic acceleration (A_{dia})[190] and early diastolic phase slope (EDPS)[196] were estimated from the LVAD velocity and flow, as shown in figure 3.6:

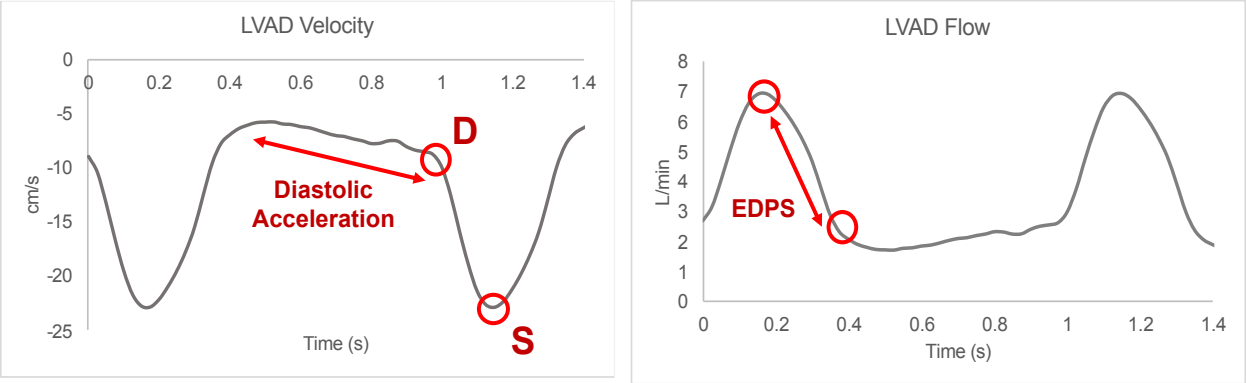

Figure 3.6: Estimation of diastolic acceleration and early diastolic phase slope (EDPS) from LVAD velocity and flow.

LV vortical flow tracking and analysis

Vortex structures were determined from the vorticity of the measured velocity field, applying the Q criterion to identify the vortex boundaries, as previously described[245]. The vortex ring is visible in the 2-dimensional mid-plane as two counter-rotating vortices: clockwise (CW) and counterclockwise (CCW) (Figure 3.7). The temporal waveforms for the radius, position, circulation, and in-plane kinetic energy (KE) were obtained over the full CC for both CW and CCW vortices[124,245].

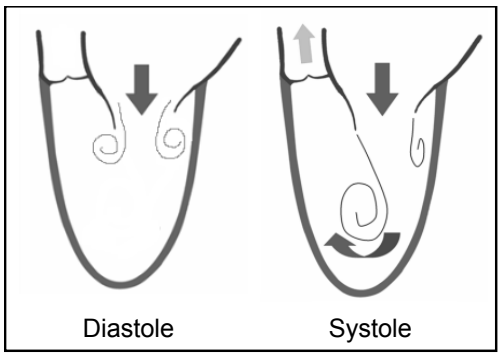

Figure 3.7: Vortex clockwise and counterclockwise features.

Region of interest analysis

The average regional velocity of the backward/forward flow through the AV and flow entering the pump was obtained from user-defined areas of interest (ROI) near the AV, MV, and LVAD inlet (Figure 3.8 (Left)).

An in-house MATLAB program was developed to characterize the regurgitant jet (RJ) from the PIV velocity images using a velocity threshold of 0.15 m/s (Figure 3.7 (Right)). The RJ area, vena contracta, lengths, and average velocity of the RJ over the full CC were determined.

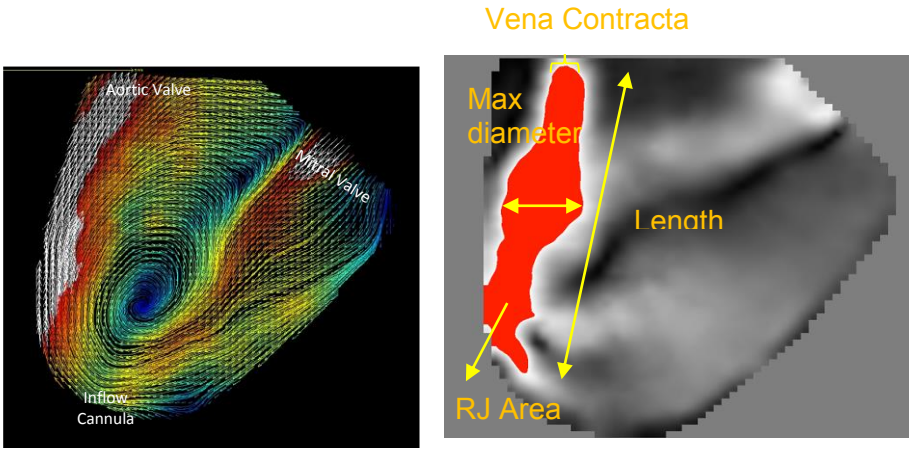

Figure 3.8: (Left) ROI analysis and (Right) RJ analysis.

Energy Dissipation Rate

Energy dissipation rate (EDR) was computed from the recorded velocity fields as defined in equation 8[197]

$$\mathrm{EDR} = \mu \left[\left(\frac{\partial u}{\partial x}\right)^2 + \left(\frac{\partial v}{\partial y}\right)^2 + 0.5\left(\frac{\partial u}{\partial y} + \frac{\partial v}{\partial x}\right)^2 \right] \qquad \text{(Equation 3.8)}$$

where μ is the fluid viscosity, u and v are the velocity components in the x and y directions, respectively.

Residence Time Analysis

Blood residence time (T_R) was calculated from the modified advection equation, as described in detail in our previous publications[124,246]. The equation was integrated in time for 20 CC, which ensured convergence to a periodic solution.

Estimation of quantitative clinical parameters for grading AI

Vena contracta width (cm) is estimated from the regurgitant jet analysis as discussed earlier

Jet width/LVOT width (%):

$$\frac{\text{Jet width}}{\text{LVOT width}} = \frac{\text{jet}_{\text{max diameter}}}{\text{LVOT}_{\text{width}}} \qquad \text{(Equation 3.9)}$$

where LOVT (LV outflow tract) width is estimated from the PIV velocity image and approximately 26mm.

Jet CSA/LVOT CSA (%):

$$\frac{\text{Jet CSA}}{\text{LVOT CSA}} = \frac{\pi * \left(\frac{\text{jet}_{\text{max diameter}}}{2}\right)^2}{\pi * \left(\frac{\text{LVOT}_{\text{width}}}{2}\right)^2} = \frac{\text{RJ}_{\text{max diameter}}{}^2}{\text{LVOT}_{\text{width}}{}^2} \quad \text{(Equation 3.10)}$$

where CSA (cross-sectional area) (estimated value, assuming CSA has circular shape)

Regurgitant volume (RegV) (mL/beat) is estimated from negative stroke volume of AV

Regurgitant fraction (RF):

$$\text{RF} = \frac{\text{Total}_{\overline{\text{SV}}}\text{ baseline} - \text{Total}_{\overline{\text{SV}}}\text{AI}}{\text{Total}_{\overline{\text{SV}}}\text{baseline}} \quad \text{(Equation 3.11)}$$

Effective regurgitant orifice area (EROA) (cm^2):

$$\text{EROA} = \frac{\text{RegV}}{\int \text{jet}_{\text{average velocity}}} \quad \text{(Equation 3.12)}$$

Statistical Analysis

The hemodynamics properties (LVP, AoP, Q_{sys}, Q_{AV}, Q_{LVAD}, and Q_{ratio}), vortex properties, and regurgitant jet properties were tested for normality using the Shapiro-Wilk test. A Kruskal-Wallis one-way ANOVA test was used to assess the statistical significance of each group. Significance was achieved for $p \leq 0.01$.

3.3 Result

Aortic Insufficiency during LVAD Support in the Absence of Cardiac Contraction

In the absence of native cardiac function (CS off), AoP, TVP, and Q_{sys} increased as LVAD speed increased, yet LVP remained low across different AI conditions (Table 3.1A). Q_{sys} progressively decreased, while Q_{LVAD} and Q ratio increased as AI became more severe. Substantial flow entering the pump without contributing to the systemic circulation resulted in a Q ratio larger than one, an indication of regurgitant flow loop. Without the cardiac contraction to

generate pressure and open the AV, the AV hemodynamically closed, allowing only backward (negative) flow. Higher LVAD supports increased backward flow through the AV by 20-80% in comparison to the lowest LVAD support, especially in the Mild AI case (Table 3.1A).

The velocity field maps of Figure 3.9 illustrate the pattern of series flow through the LV during CS off conditions, with all flow exiting the LV through the LVAD. The HM2 continuously pulled fluid toward the apex, resulting in two incoming jets from the MV and AV entering the LV. The interaction between the mitral and AI inflow jets created turbulence, CW and CCW vortices that did not normally occur (Table 3.1B). The RJ appeared along the LVOT. As AI severity increased, the larger RJ collided with the septal walls, generating higher CW circulation and KE. In contrast, the CCW vortices formed near the LV free-wall, and increased in size with increased LVAD speeds. The persistent AI jets grew in size with AI severity and LVAD speed (Table 3.1C). At higher LVAD speeds, the RJ areas and maximum diameters increased significantly, especially for Mild AI conditions (200-500%). In each AI group, the velocity increased only slightly with AI, and the Vena Contracta width (VC) (minimum RJ diameter captured near the AV) was similar. The Average ROI velocity across the AV and inflow cannula, as shown in Figure 3.10, followed the same pattern: velocity increased with increased LVAD speed and more severe AI.

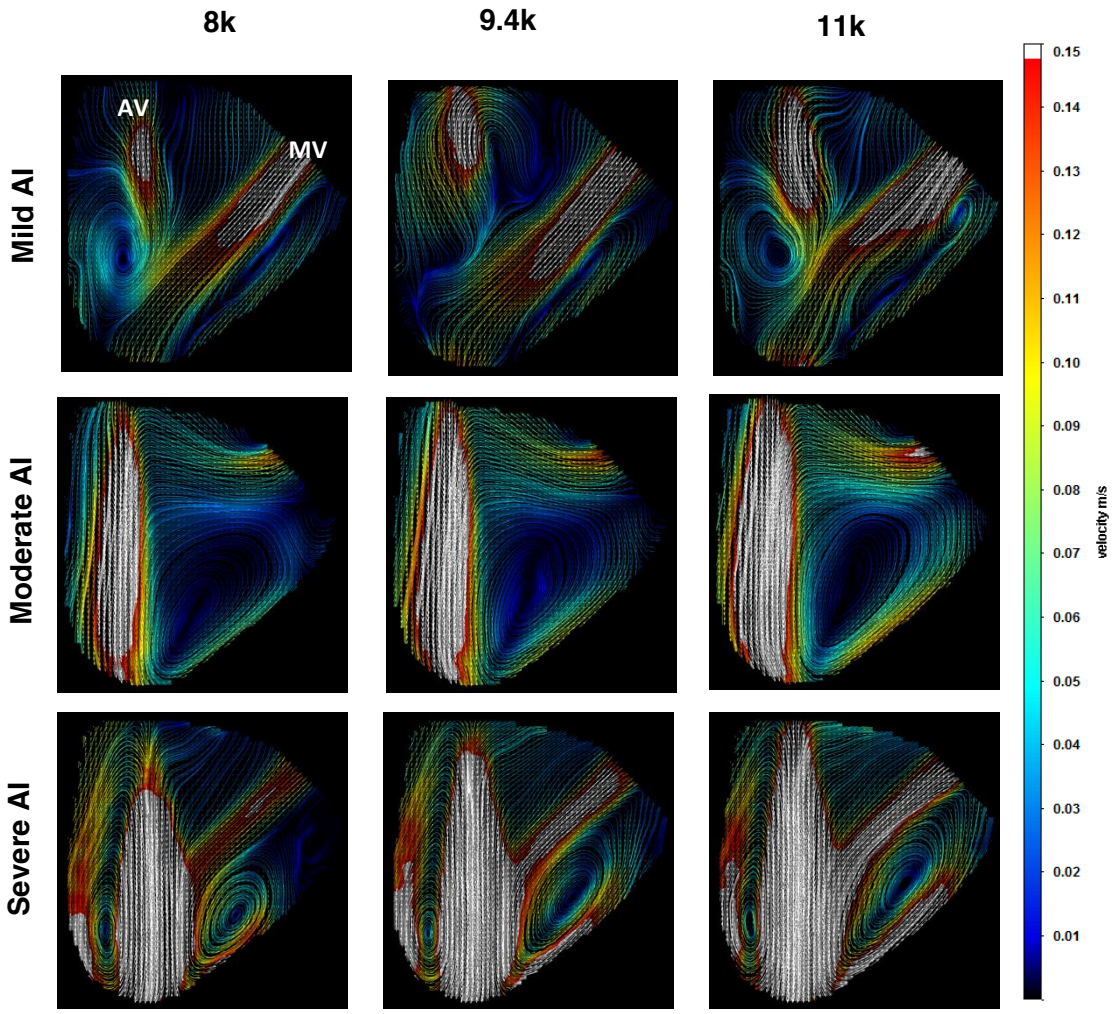

Figure 3.9: Velocity Field Images of Mild, Moderate, and Severe AI conditions for CS off conditions (Aortic valve (AV), mitral valve (MV)).

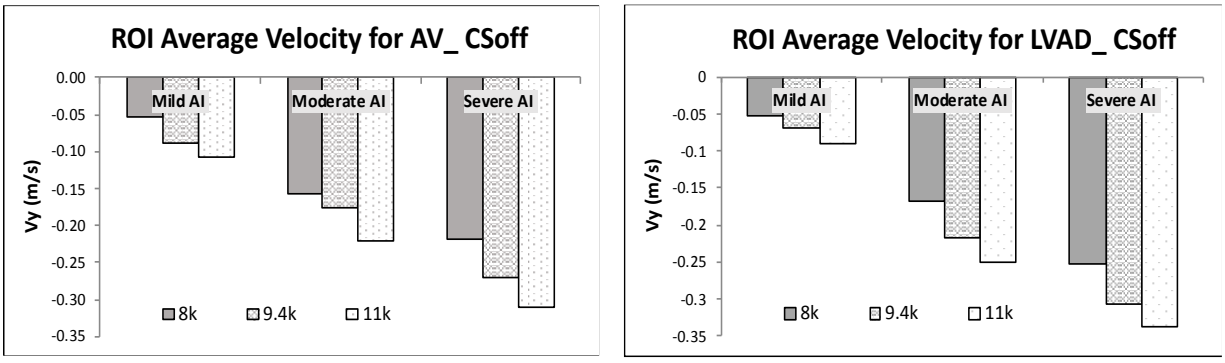

Figure 3.10: Average velocity across the aortic valve and LVAD inflow cannula for the CS off conditions at different AI classifications.

Table 3.1: Average values of [A] Hemodynamics, [B] Intraventricular vortex properties, and [C] Regurgitant jet properties of Mild, Moderate and Severe aortic insufficiency (AI) conditions in the absence of native cardiac function (CS Off)
(†, ‡ Statistical significance ($p<0.01$) for different LVAD speeds and AI conditions, respectively)

Parameters	Mild AI			Moderate AI			Severe AI		
	8k	**9.4k**	**11k**	**8k**	**9.4k**	**11k**	**8k**	**9.4k**	**11k**
LVP (mmHg)	4.94	4.17	3.97	4.50	4.27	4.13	2.47	1.86	2.10
AoP (mmHg) † ‡	73.52	95.24	125.78	70.42	92.32	121.54	70.57	91.22	120.37
TVP (mmHg) † ‡	68.59	91.06	121.81	65.93	88.05	117.42	68.10	89.36	118.27
Q_{sys} *(L/min)* † ‡	1.65	1.98	2.37	1.59	1.92	2.32	1.31	1.60	1.93
Q_{LVAD} *(L/min)* † ‡	1.86	2.26	2.74	2.24	2.69	3.23	2.27	2.76	3.33
Q_{AV} *(L/min)*	-0.20	-0.28	-0.37	-0.65	-0.78	-0.91	-0.97	-1.17	-1.40
Q ratio	1.12	1.14	1.16	1.41	1.40	1.39	1.74	1.73	1.72
PI	0.25	0.21	0.21	0.42	0.30	0.33	0.46	0.32	0.31

[A] Hemodynamic result (LVP (LV pressure), AoP (Aortic pressure), Q_{sys} (total systemic flow), Q_{LVAD} (LVAD flow), Q_{AV} (flow through aortic valve), Q_{ratio} (Flow ratio), PI (Aortic pulsatility index))

Parameters		Mild AI			Moderate AI			Severe AI		
		8k	**9.4k**	**11k**	**9.4k**	**11k**	**11k**	**8k**	**9.4k**	**11k**
Circulation ($x10^{-3}$ m^2/s)	*CW*	5.55	0.00	3.36	10.44	2.74	3.08	13.77	17.48	25.07
	CCW	-4.48	-4.70	-2.95	-21.55	-26.79	-34.23	-11.18	-19.54	-24.64
Kinetic Energy (mJ/m)	*CW*	0.14	0.00	0.04	0.77	0.11	0.14	1.01	1.64	2.52
	CCW	0.09	0.10	0.13	1.14	1.64	2.57	0.42	1.09	1.77
Radius (cm)	*CW*	0.77	N/A	0.43	0.46	0.31	0.29	0.62	0.60	0.57
	CCW	0.67	0.61	0.33	0.98	1.04	1.11	0.81	1.16	1.18
Aspect Ratio	*CW*	3.44	N/A	1.51	2.49	1.44	1.40	3.36	1.16	3.47
	CCW	5.38	5.23	1.25	1.67	1.58	1.33	1.65	1.19	1.32
Vortex symmetry CW:CCW		1.14	N/A	1.30	0.46	0.30	0.26	0.77	0.51	0.48

[B] Intraventricular vortex properties (Clockwise (CW), and counter-clockwise (CCW))

Table 3.1: (cont.)

Parameters	Mild AI			Moderate AI			Severe AI		
	8k	**9.4k**	**11k**	**8k**	**9.4k**	**11k**	**8k**	**9.4k**	**11k**
Area (cm^2) † ‡	0.29	0.73	1.48	3.27	4.37	5.45	6.10	7.22	8.49
Max Diameter (cm) † ‡	0.36	0.73	0.97	0.85	1.09	1.21	1.58	1.70	1.82
Vena Contracta Width (cm) † ‡	0.24	0.24	0.24	0.36	0.36	0.36	0.61	0.61	0.61
Length (cm) † ‡	1.09	1.70	2.42	5.70	6.06	6.30	4.85	5.70	6.30
Velocity (m/s) † ‡	0.17	0.18	0.19	0.39	0.40	0.43	0.32	0.34	0.37
Peak velocity (m/s) † ‡	0.19	0.23	0.27	0.57	0.60	0.64	0.56	0.65	0.74

[C] Regurgitant jet properties

Aortic Insufficiency before LVAD implantation (Pre-LVAD)

Native heart function (CS on) without LVAD support produced a 17% EF, 1.9 L/min CO at 63 bpm heart rate at BL condition. For all pre-LVAD conditions, the average of LVP, AoP, and TVP was similar, but systemic flow was reduced by 20%, 30%, and 41% for the Mild, Moderate, and Severe AI, respectively. As AI severity increased, the AVO time, NF, forward LVEF, and diastolic SV decreased (Table 3.2A, B). The velocity field maps (Figure 3.11) illustrate four cardiac cycle events: early diastole peak-E, mid-diastole, atrial contraction peak-A, and mid-systole. In all conditions, the E-wave vortex pattern reflects the incoming mitral jet, which forms a vortex ring with larger CW and smaller CCW vortex. The CW vortex grows in size while the CCW vortex dissipates rather quickly due to its interaction with the free-wall. This pattern helps to direct flow toward the LVOT during late-diastole, and through the AV during systole. In AI conditions, the RJs appear during isovolumic relaxation, before MV opening, then continues to grow before disappearing by the start of systole. The interaction between the RJ and the incoming MV jet produces collision in the LV. Severe AI increases CW and CCW circulation and KE, significantly higher than BL. As AI progresses, a larger CCW vortex is formed, resulting in reduced vortex symmetry (Table 3.2B).

The ROI was plotted for the full CC, starting from diastole at t = 0, the A-wave occurred at t = 0.525 s, and systole started at t=0.65 s (Figure 3.12A). For the AV ROI, positive and negative values denote forward flow to the aorta or backward flow to the LV, respectively. In the BL condition, maximum forward flow occurred during systole (~0.15m/s). In the presence of AI, backward diastolic flow occurred with a maximum velocity of -0.14, -0.17, and -0.35 m/s for Mild, Moderate, and Severe AI levels. Increased AI severity effectively prolongs diastole and shortens systole, extending the time of backward flow and increasing regurgitant volume. For the MV ROI, the negative value denotes incoming LV flow. Each graph displays two peaks representing the E- and A-waves. The BL condition has the maximum peak E and A velocity. As AI severity increases, peak E velocity increases while peak A velocity decreases.

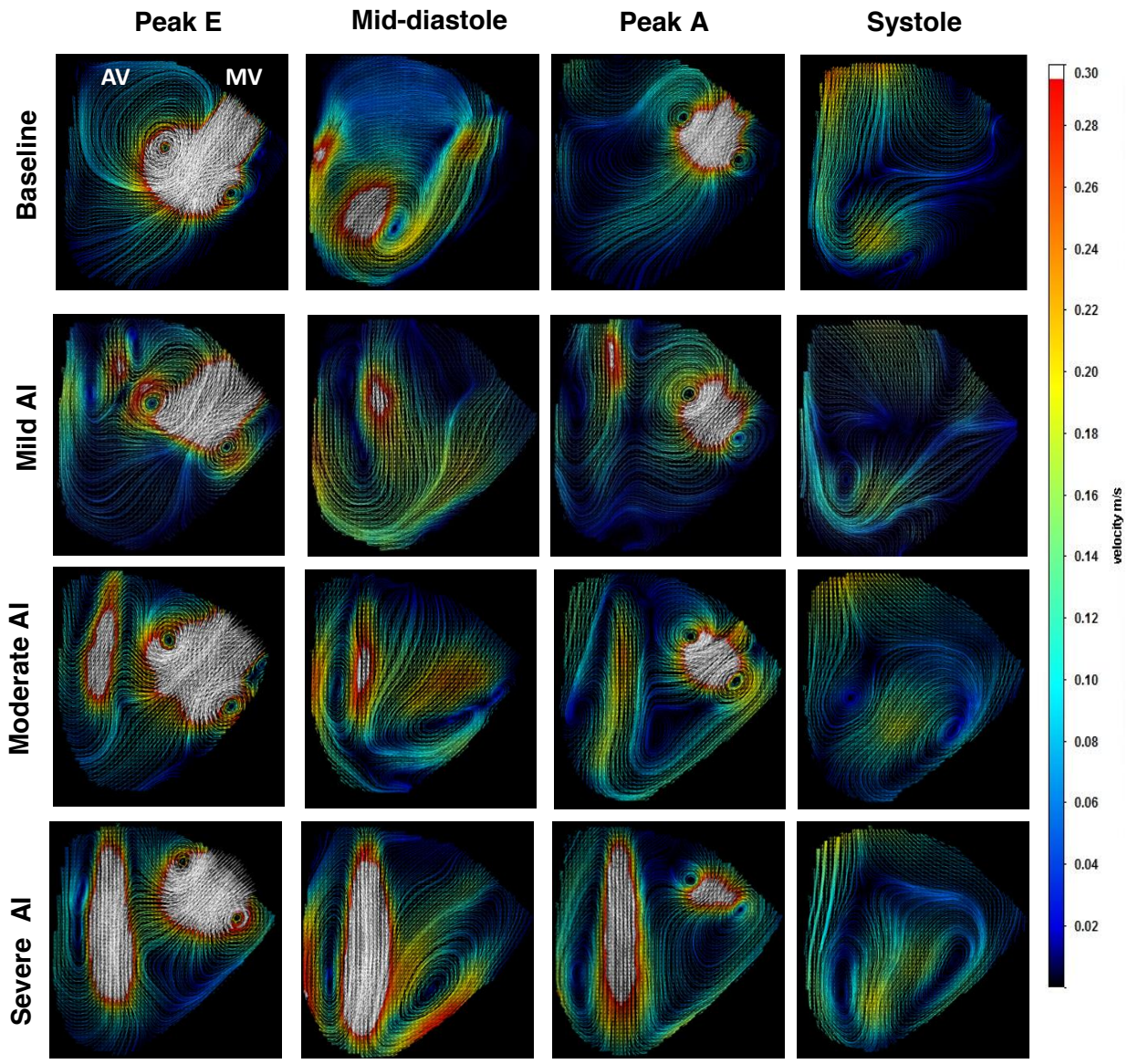

Figure 3.11: Velocity Field Images of Baseline and Mild, Moderate and Severe AI conditions for pre-LVAD conditions in the presence of native cardiac function (Aortic valve (AV), mitral valve (MV)).

Table 3.2: [A] Hemodynamic result, [B] Stroke volume, [C] Intraventricular vortex properties, and [D] Regurgitant jet properties (mean ± standard error) of Baseline (normal valve), Mild, Moderate and Severe aortic insufficiency (AI) conditions in the presence of native cardiac function (CS On) without LVAD support (Pre-LVAD) († Statistical significance ($p<0.01$) for different tested conditions).

Parameters	**Baseline**	**Mild AI**	**Moderate AI**	**Severe AI**
LVP (mmHg)	20.21 ± 0.22	20.02 ± 0.23	24.68 ± 0.24	20.11 ± 0.22
AoP (mmHg)	64.99 ± 0.13	61.29 ± 0.11	63.58 ± 0.11	62.15 ± 0.13
TVP (mmHg)	44.78	41.27	38.89	42.05
Q_{sys} *(L/min)* †	1.90 ± 0.03	1.53 ± 0.03	1.34 ± 0.03	1.12 ± 0.03
PI	10.14	10.95	13.03	17.16
RF (%)	0	19	29	41
NF (%)	99.64	80.49	70.68	59.56
Forward LVEF (%)	17.05	13.92	12.30	10.12
AVO time (s)	0.25	0.23	0.20	0.18

[A] Hemodynamic result (LVP (LV pressure), AoP (Aortic pressure), Q_{sys} (total systemic flow), Q_{LVAD} (LVAD flow), Q_{AV} (flow through aortic valve), Q_{ratio} (Flow ratio), PI (Aortic pulsatility index), RF (regurgitant fraction), NF (net flow through AV), LVEF (left ventricle ejection fraction, AVO (aortic valve opening) time.

Stroke volume	**Baseline**	**Mild AI**	**Moderate AI**	**Severe AI**
Diastole (mL)	-0.03 ± 0.36	-1.96 ± 0.27	-7.50 ± 0.23	-10.26 ± 0.20
Systole (mL)	30.71 ± 0.22	27.55 ± 0.19	29.64 ± 0.13	30.17 ± 0.25

[B] Stroke volume during diastole and systole

Parameters		**Baseline**	**Mild AI**	**Moderate AI**	**Severe AI**
Circulation $(x10^{-3}\ m^2/s)$	*CW* †	8.93 ± 0.91	8.04 ± 0.49	7.69 ± 0.69	17.36 ± 1.46
	CCW †	-3.97 ± 0.71	-4.02 ± 0.71	-5.54 ± 0.81	-13.47 ± 1.26
Total Kinetic Energy (mJ/m) †		0.97 ± 0.26	0.61 ± 0.11	0.73 ± 0.14	2.06 ± 0.28
Kinetic Energy (mJ/m)	*CW* †	0.59 ± 0.14	0.36 ± 0.05	0.39 ± 0.06	1.20 ± 0.14
	CCW †	0.38 ± 0.12	0.25 ± 0.06	0.35 ± 0.08	0.86 ± 0.17
Radius (cm)	*CW* †	0.44 ± 0.03	0.45 ± 0.02	0.48 ± 0.03	0.56 ± 0.02
	CCW †	0.29 ± 0.02	0.31 ± 0.01	0.60 ± 0.05	0.72 ± 0.05
Aspect Ratio	*CW* †	1.84 ± 0.12	1.92 ± 0.11	2.38 ± 0.20	2.78 ± 0.20
	CCW †	1.40 ± 0.04	1.51 ± 0.07	2.13 ± 0.12	2.06 ± 0.12
Vortex symmetry CW:CCW †		1.64 ± 0.12	1.46 ± 0.10	0.97 ± 0.11	0.90 ± 0.06

[C] Intraventricular vortex properties (Clockwise (CW), and counter-clockwise (CCW))
(In the case which had multiple CW and CCW vortices occurrences: total CW and CCW vortex circulation and kinetic energy, radius/aspect ratio/vortex symmetry of the main (largest) CW and CCW vortex were reported).

Table 3.2: (cont.)

Parameters	Mild AI	Moderate AI	Severe AI
Area (cm^2) †	1.86 ± 0.17	2.60± 0.14	6.21 ± 0.36
Max Diameter (cm) †	0.93 ± 0.04	1.09 ± 0.04	1.42 ± 0.04
Vena Contracta Width (cm) †	0.27 ± 0.01	0.35 ± 0.01	0.55 ± 0.01
Length (cm) †	2.75 ± 0.20	3.60 ± 0.14	5.55 ± 0.28
Velocity (m/s) †	0.20 ± 0.00	0.21 ± 0.00	0.29 ± 0.01
Peak velocity (m/s) †	0.31 ± 0.01	0.32 ± 0.01	0.55 ± 0.03

[C] Regurgitant jet properties

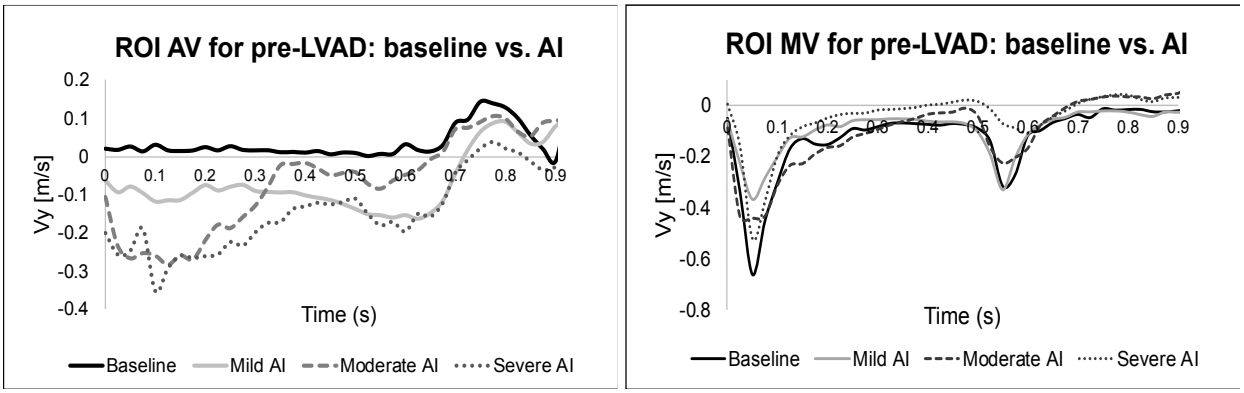

[A]

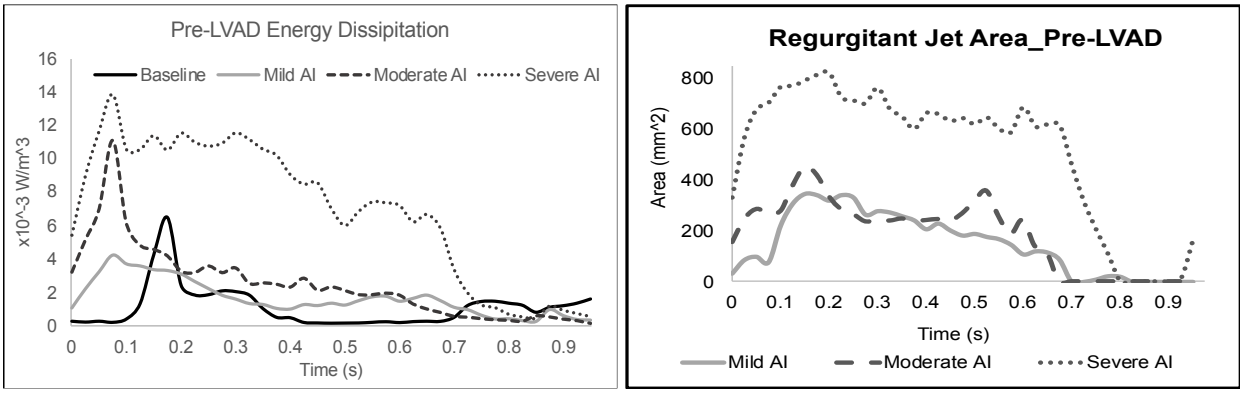

[B] [C]

Figure 3.12: Time-varying during one cardiac cycle of [A] Average velocity across the aortic valve and mitral valves, [B] Energy dissipation rate and [C] Regurgitant jet area for all pre-LVAD conditions(Diastole starts at t = 0, the 2nd filling phase occurs at t = 0.525 s and the systole starts at t = 0.65 for baseline condition).

The time series plots of EDR and RJ area during the CC are shown in Figure 3.12B and C, respectively. Average EDR was lowest in the BL condition and increased significantly by 144%,

227%, and 620% for Mild, Moderate, and Severe AI, respectively. EDR remained high during diastole for Severe AI, but decreased more rapidly in Mild and Moderate AI cases. During systole, the AV opens and allows forward flow, leading to the disappearance of EDR. The RJ area evolution followed similar patterns, featuring jet growth during diastole and dissipation during systole. The severe AI jet persisted the longest, which is consistent with AV ROI results. The properties of RJ is shown in table 3.2C.

Baseline vs. Mild Aortic Insufficiency during LVAD support

During BL conditions, LVAD support increased the AoP, TVP, and Q_{sys}, while LVP was kept approximately constant (Table 3.3). The increasing Q_{sys} resulted from a combination of LVAD flow and reduced AV flow. The effect of LVAD support on the flow patterns of LV has been studied previously by our lab with other LVAD models. The HM2 LVAD produces a similar behavior in our mock loop. Parallel flow (positive Q_{AV} and Q ratio <1), during which a significant portion of LV flow is ejected through the AV, was observed when the LVAD was operated at low and medium speeds (8k and 9.4k rpm). Series flow ($Q_{AV} \approx 0$ and Q ratio ≈ 1), during which the AV is hemodynamically closed and all flow exits through the pump, was observed when the LVAD was operated at high speed (11k rpm). For the Mild AI conditions, Q_{sys} and forward LVEF decreased by 9-24%, while Q_{LVAD} decreased by 3.5-7.4% compared to BL conditions at the same LVAD support level. During low LVAD support, the Q_{AV} and NF are positive. Increasing LVAD speeds resulted in backward Q_{AV}, negative NF, and lower AVO time.

The addition of LVAD support increases CW circulation, KE, and vortex symmetry in BL condition (Table 3.4A). The circulation and trajectories for CW and CCW vortices during the CC, beginning with the MV opening, following by early and late diastolic filling, and concluding at end-systole (Figure 3.14A). The pre-LVAD condition shows the CW vortex formed, following a straight trajectory toward the apex during the E-filling phase, then moving up toward the base. A weaker

jet arrived with the A-wave, joined the main CW vortex, and strengthened its circulation. The CW vortex then moved toward the LVOT by the onset of systole. The CCW vortices appeared at early E- and A- wave filling phases, but decayed quickly due to confinement by the LV free wall. During LVAD support at 9.4k rpm, the mitral jet got pulled toward the LV apex by the pump, still a similar pattern was observed. Vortex circulation increased, but the CW vortex dissipated much faster when LVAD presence.

For Mild AI, similar circulation and KE average to the BL conditions were recorded for all levels of LVAD supports (Table 3.4B). The presence of AI interfered with the mitral inflow, causing multiple vortices to form (Figure 3.13 and 3.14B). Before LVAD support, the primary vortices evolved similarly to the BL condition, except that the CW and CCW vortex circulations at peak E were lower. During the E-filling phase, secondary (2°) CW and CCW appeared with the incoming RJ. The 2° CW vortex dissipated quickly due to confinement by the septal wall, while the 2° CCW vortex moved toward the LV center and collided with the main CW vortex. Consequently, the interaction between these two vortices prevented the main CW from rolling up and moving toward the base. During the A-wave filling phase, the 2° CCW vortex appeared again merging with the primary CW vortex, and all flow structure move toward the AV by the onset of systole. The presence of the LVAD created a larger RJ, as well as larger 2° CW and CCW vortices. The 2° CW vortex persisted longer with increased LVAD support. During LVAD support at 9.4k rpm, the primary CW vortex rolled from the LV apex and collided with the RJ's vortices at the LV center at the end of diastole. High LVAD speed produced stronger and more persisted RJ's vortices that traveled toward the apex before merging with the primary CW vortex.

Average ROI velocities were shown in Figure 3.15A (negative velocity indicated incoming velocities toward the LV or the LVAD inlet). As LVAD speed increased, the average velocities increased by 13-18%, 34-67%, and 56-92% for the AV, MV, and LVAD inflow ROI, respectively. Moreover, the presence of LVAD increased EDR by 40-46% and RJ area 75-101% from the pre-

LVAD condition (Figure 3.15C, D). The average RJ properties of mild AI are reported in table 3.5A. Higher LVAD speed resulted in larger jet area and length and prolonged diastole consistent with ROI result in Figure 3.15B.

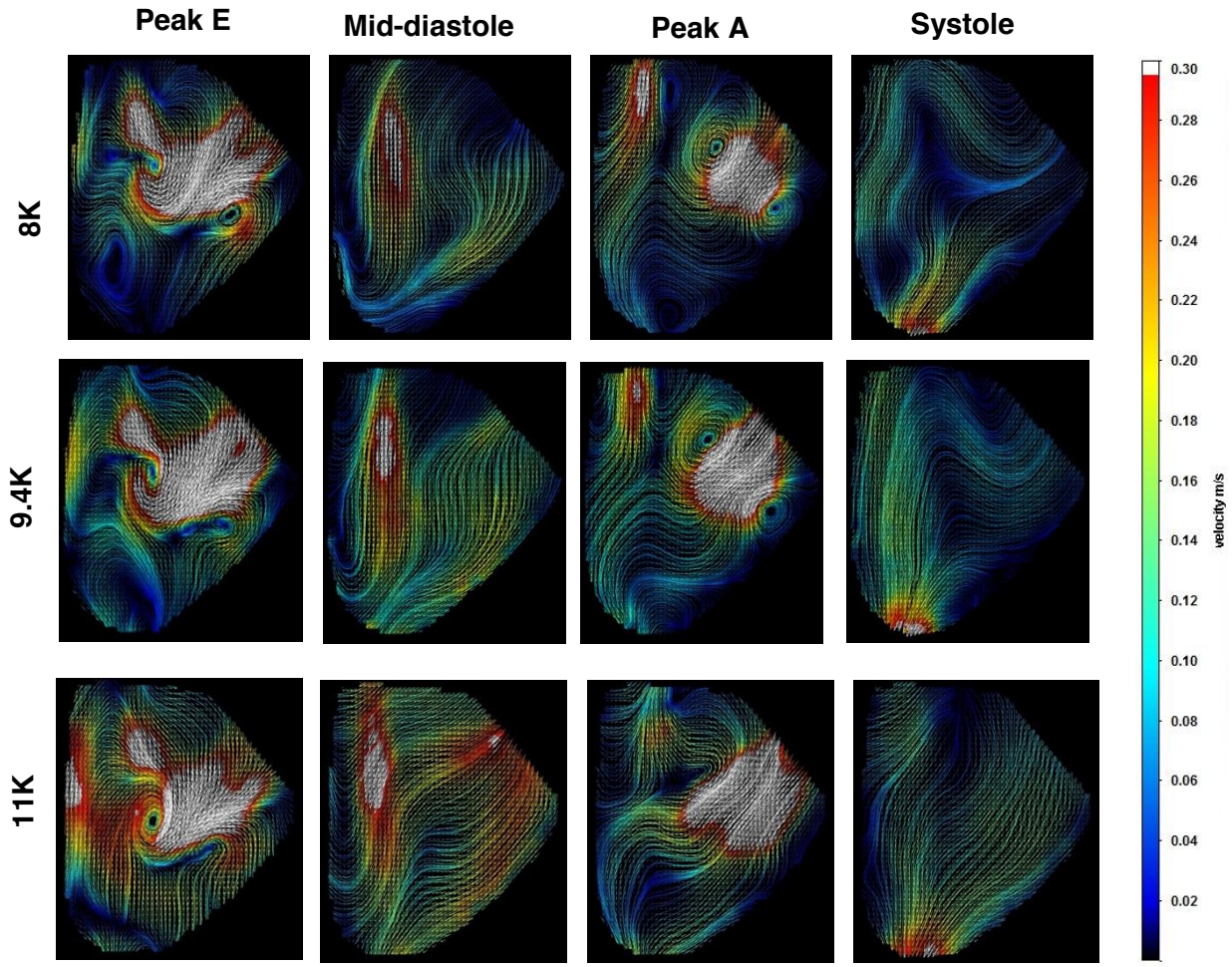

Figure 3.13: Velocity Field Images of Mild AI during the different levels of HeartMate II supports.

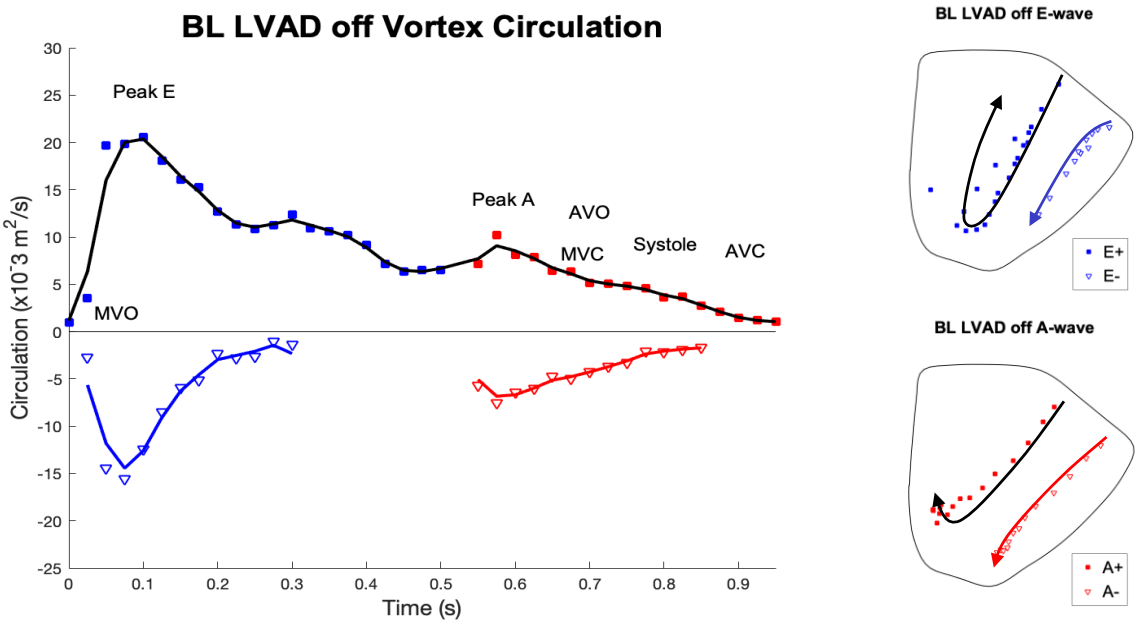

[A] Baseline conditions

Figure 3.14: (Left) Time-varying (positive) clockwise (CW) and (negative) counterclockwise (CCW) vortex circulation are shown for [A] Baseline and [B] Mild AI conditions. (Middle, Right) Vortex core trajectories as the result of the E-wave and A-wave inflow contributions are shown: the trajectories' symbols and lines are corresponded to the circulation plot (symbol indicates the merging to vortices). (Diastole starts at t = 0, the 2nd filling phase occurs at t = 0.525 s, and the systole starts at t = 0.65 for baseline condition). (Blue symbols denote E wave vortices, red symbols denote A wave and systolic vortices; square symbols denote main CW vortices, circle symbols denote secondary CW vortices, down-triangle symbols denote main CCW vortices, up-triangle symbols denote secondary CCW vortices; blue lines and red lines denote vortices that appear and dissipate during E wave and A wave respectively, black lines denote vortices that perpetuate the entire cardiac cycle (MVO = mitral valve opens, MVC = mitral valve closes, AoVO = aortic valve opens, AoVC = aortic valve closes).

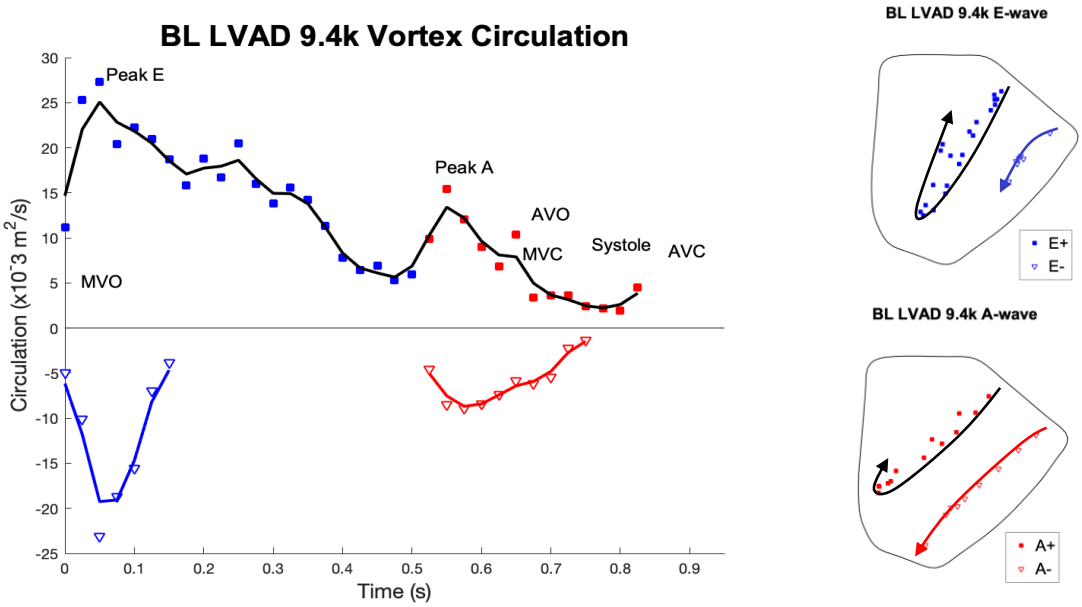

[A] Baseline conditions

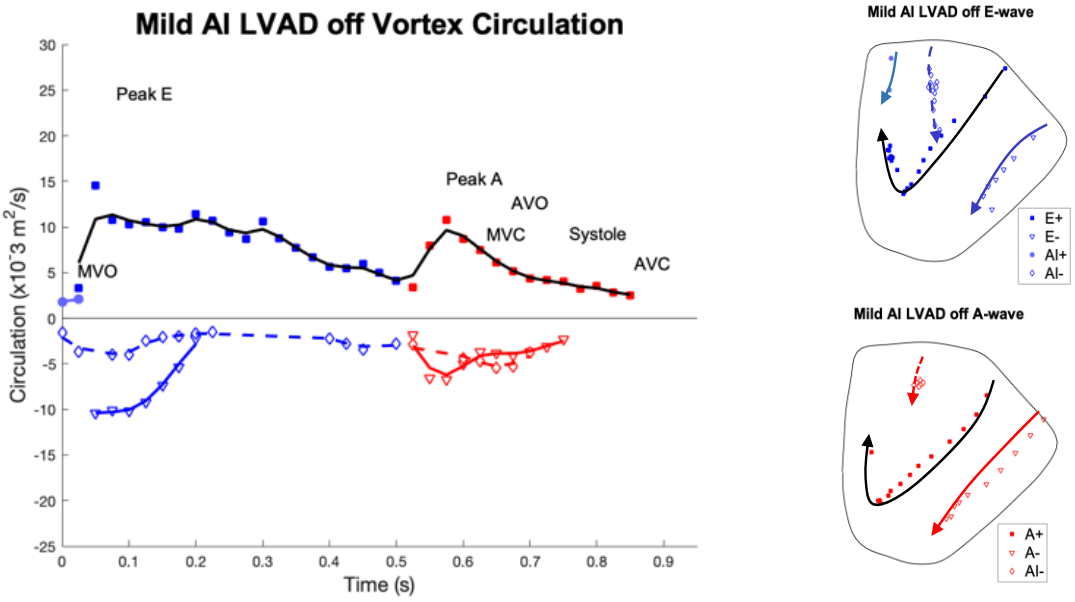

[B] Mild AI conditions

Figure 3.14: Vortex Circulation and Trajectories (cont.)

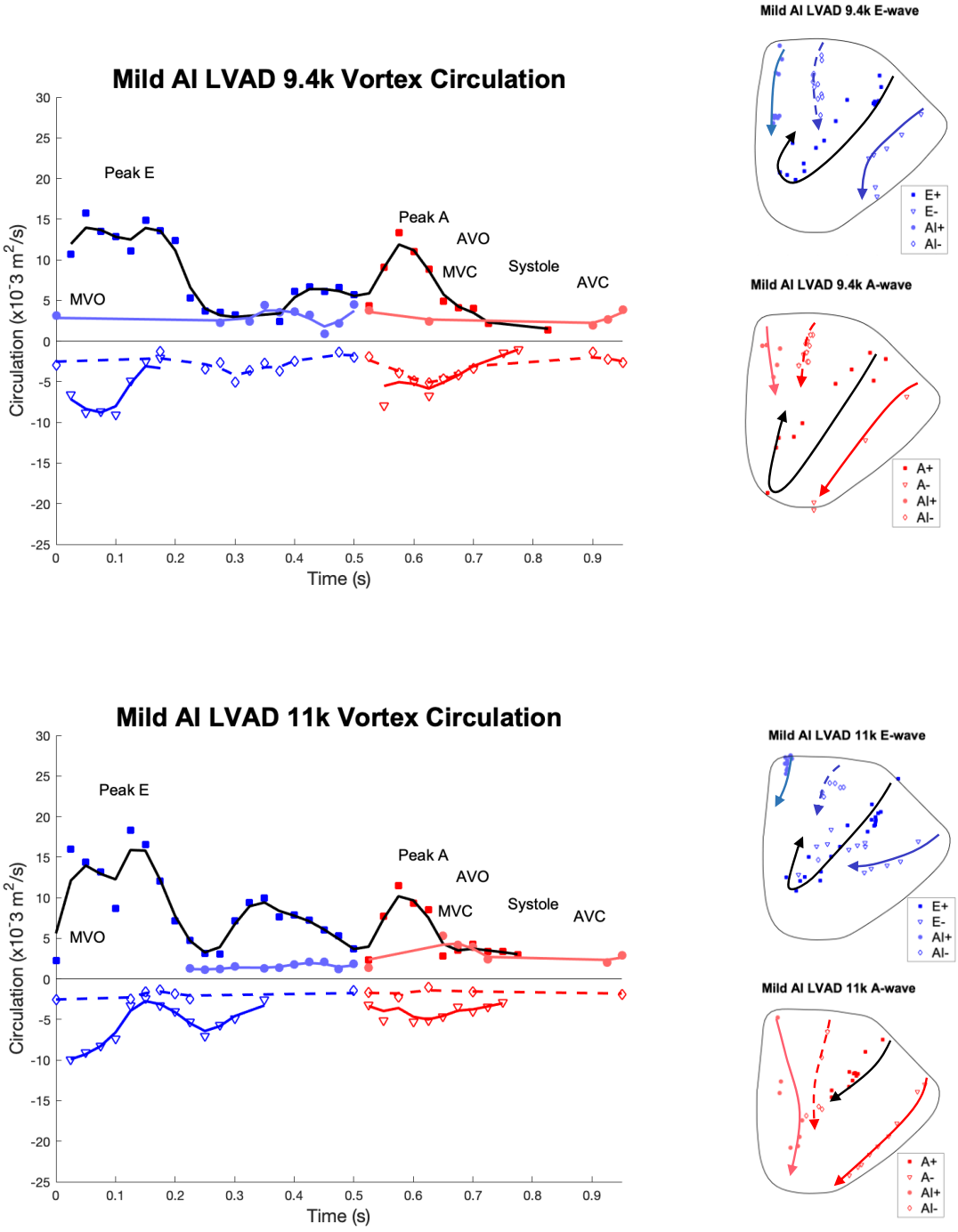

[B] Mild AI conditions

Figure 3.14: Vortex Circulation and Trajectories (cont.)

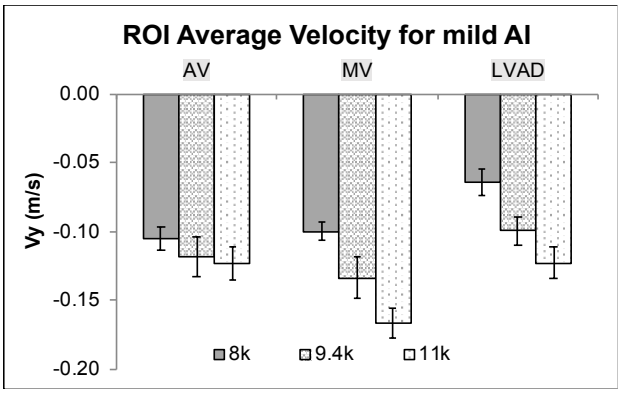

[A]

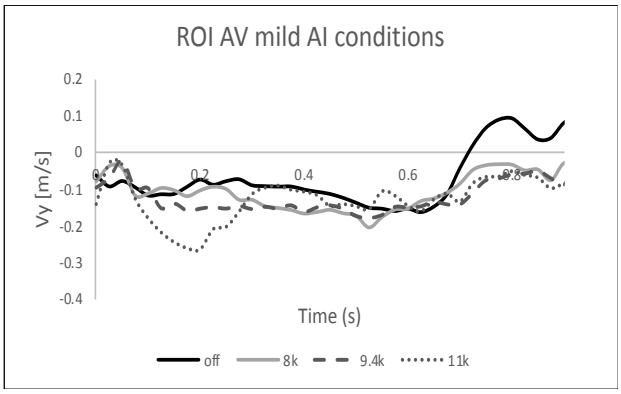

[B]

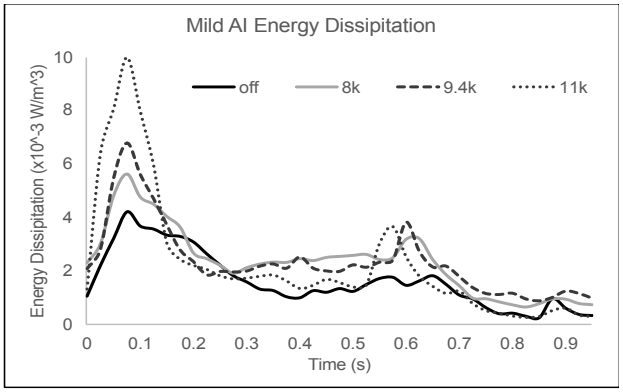

[C]

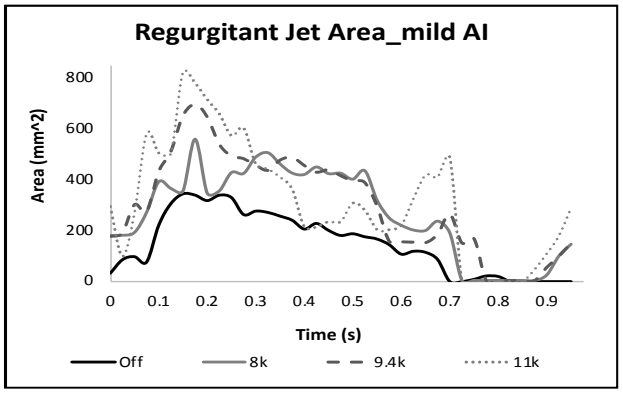

[D]

Figure 3.15: [A] Average velocity in the region of interest at aortic valve (AV), mitral valve, and LVAD. Time-varying during one cardiac cycle of [B] Average velocity at the AV, [C] Energy dissipation rate, and [D] Regurgitant jet area for mild AI conditions. (Diastole starts at t = 0, the 2nd filling phase occurs at t = 0.525 s, and the systole starts at t = 0.65 for baseline condition).

Table 3.3: Hemodynamics result (mean ± standard error) of Baseline (normal valve), Mild, Moderate, and Severe aortic insufficiency (AI) conditions in the presence of native cardiac function (CS on). († Statistical significance ($p<0.01$) for different tested conditions). (LVP (LV pressure), AoP (Aortic pressure), Q_{sys} (total systemic flow), Q_{LVAD} (LVAD flow), Q_{AV} (flow through aortic valve), Q_{ratio} (Flow ratio), PI (Aortic pulsatility index), RF (regurgitant fraction), NF (net flow through AV), LVEF (left ventricle ejection fraction), S/D ratio (ratio between systolic and diastolic peak LVAD velocity), A_{dia} (diastolic acceleration), EDPS (early diastolic phase slope), rpm (rotations per minute), AVO (aortic valve opening))

8k rpm Parameters	**Baseline**	**Mild AI**	**Moderate AI**	**Severe AI**
LVP (mmHg)	24.59 ± 0.25	21.40 ± 0.25	25.41 ± 0.27	14.80 ± 0.26
AoP (mmHg)	93.12 ± 0.09	92.78 ± 0.07	89.91 ± 0.09	92.56 ± 0.09
TVP (mmHg)	68.53	71.39	64.50	77.75
Q_{sys} *(L/min)* †	2.58 ± 0.02	1.97 ± 0.02	1.88 ± 0.02	1.45 ± 0.02
Q_{LVAD} *(L/min)*	2.01 ± 0.01	1.86 ± 0.01	2.03 ± 0.01	2.03 ± 0.01
Q_{AV} *(L/min)* †	0.57	0.11	-0.15	-0.58
Q ratio	0.78	0.95	1.08	1.40
PI	4.21	4.73	6.94	8.53
NF (%)	22.26	4.09	-5.78	-22.40
Forward LVEF (%)	22.93	17.85	17.04	12.76
S/D ratio		3.80	2.59	2.34
A_{dia} *(cm/s^2)*		10.22	14.23	13.85
EDPS (L/min/sec)		-24.04	-22.46	-20.60
AVO time (sec)	0.19	0.16	0.16	0.15

[A] Low LVAD speed

9.4k rpm Parameters	**Baseline**	**Mild AI**	**Moderate AI**	**Severe AI**
LVP (mmHg)	23.99 ± 0.25	18.06 ± 0.24	25.14 ± 0.28	27.40 ± 0.27
AoP (mmHg)	100.29 ± 0.05	99.80 ± 0.04	101.75 ± 0.06	101.26 ± 0.06
TVP (mmHg)	76.30	81.74	76.61	73.86
Q_{sys} *(L/min)* †	3.61 ± 0.01	3.11 ± 0.01	2.74 ± 0.02	2.35 ± 0.02
Q_{LVAD} *(L/min)*	3.43 ± 0.01	3.26 ± 0.01	3.26 ± 0.01	3.35 ± 0.01
Q_{AV} *(L/min)* †	0.17	-0.15	-0.52	-1.00
Q ratio †	0.95	1.05	1.19	1.42
PI	1.92	1.93	3.50	3.95
NF (%)	4.81	-4.11	-14.29	-27.65
Forward LVEF (%)	32.57	28.11	24.85	21.27
S/D ratio		2.61	2.06	1.82
A_{dia} *(cm/s^2)*		6.86	13.37	13.62
EDPS (L/min/sec)		-21.41	-20.20	-18.33
AVO time (sec)	0.14	0.13	0.13	0.13

[B] Medium LVAD speed

Table 3.3: (cont.)

11k rpm Parameters	Baseline	Mild AI	Moderate AI	Severe AI
LVP (mmHg)	21.26 ± 0.22	15.53 ± 0.22	21.93 ± 0.26	20.08 ± 0.25
AoP (mmHg)	110.12 ± 0.03	108.15 ± 0.03	109.41 ± 0.04	109.72 ± 0.04
TVP (mmHg)	88.86	92.62	87.48	89.65
Q_{sys} *(L/min)* †	5.02 ± 0.01	4.59 ± 0.01	4.11 ± 0.02	3.68 ± 0.01
Q_{LVAD} *(L/min)*	4.96 ± 0.01	4.79 ± 0.01	4.85 ± 0.01	4.89 ± 0.01
Q_{AV} *(L/min)* †	0.05	-0.20	-0.73	-1.21
Q ratio †	0.99	1.04	1.18	1.33
PI	1.04	1.18	1.72	1.83
NF (%)	1.02	-4.02	-14.62	-24.05
Forward LVEF (%)	45.19	41.47	37.31	33.25
S/D ratio		1.87	1.81	1.80
A_{dia} *(cm/s^2)*		4.30	8.91	6.85
EDPS (L/min/sec)		-18.54	-17.71	-15.98
AVO time (sec)	0	0	0	0

[C] High LVAD speed

LVAD support worsens AI severity

At the same LVAD speed, the LVP, AoP, and TVP were relatively unchanged across all groups (Table 3.3). For the Moderate and Severe AI groups, Q_{sys} and forward LVEF reduced by 18-27% and 26-44%, while Q_{LVAD} was relatively similar in comparison to BL conditions at the same LVAD speed. Backward flow through the AV and negative NF was observed in all post-LVAD conditions and increased with LVAD speed. Q ratio > 1 followed a similar pattern and indicated the presence of regurgitant flow loops. The S/D ratio and AVO time decreased, while the A_{dia} and EDPS increased as AI became more severe at the same LVAD speed. However, at the same AI classification, increasing LVAD speed resulted in lower diastolic acceleration. Vortex properties of different AI classification are provided in Tables 3.4B, C, D. As AI worsened, vortex circulation and KE increased, and the CCW vortex became more dominant, particularly in severe AI cases (vortex symmetry < 1). For the same AI condition, increasing LV speed also increased circulation and KE.

Table 3.4: Intraventricular vortex properties (mean ± standard error) of Baseline (normal valve), Mild, Moderate, and Severe aortic insufficiency (AI) conditions in the presence of native cardiac function (CS on) (Clockwise (CW), and counterclockwise (CCW)). († Statistical significance ($p<0.01$) for different LVAD speeds).(In the case which had multiple CW and CCW vortices occurrences: total CW and CCW vortex circulation and kinetic energy, radius/aspect ratio/vortex symmetry of the primary (largest) CW and CCW vortex were reported).

Baseline Parameters		**8k**	**9.4k**	**11k**
Circulation ($x10^{-3}$ m^2/s)	*CW*	11.30 ± 1.13	11.50 ± 1.25	13.81 ± 1.49
	CCW †	-3.78 ± 0.67	-4.41 ± 0.85	-6.20 ± 0.72
Total Kinetic Energy (mJ/m) †		1.22 ± 0.29	1.40 ± 0.34	1.82 ± 0.42
Kinetic Energy (mJ/m)	*CW*	0.81 ± 0.18	0.87 ± 0.19	1.13 ± 0.25
	CCW †	0.41 ± 0.12	0.53 ± 0.17	0.53 ± 0.23
Radius (cm)	*CW*	0.68 ± 0.05	0.65 ± 0.04	0.70 ± 0.19
	CCW †	0.35 ± 0.03	0.40 ± 0.05	0.38 ± 0.03
Aspect Ratio	*CW* †	1.89 ± 0.11	2.05 ± 0.14	2.11 ± 0.12
	CCW †	1.87 ± 0.17	2.24 ± 0.24	2.12 ± 0.22
Vortex symmetry CW:CCW †		2.04 ± 0.17	2.15 ± 0.24	1.99 ± 0.16

[A] Baseline conditions during different LVAD speeds

Mild AI Parameters		**8k**	**9.4k**	**11k**
Circulation ($x10^{-3}$ m^2/s)	*CW* †	6.21 ± 0.68	7.16 ± 0.76	8.17 ± 0.88
	CCW †	-6.56 ± 0.56	-5.30 ± 0.60	-4.11 ± 0.48
Total Kinetic Energy (mJ/m) †		0.71 ± 0.10	0.74 ± 0.11	0.85 ± 0.11
Kinetic Energy (mJ/m)	*CW* †	0.38 ± 0.06	0.45 ± 0.07	0.58 ± 0.08
	CCW †	0.34 ± 0.04	0.29 ± 0.04	0.27 ± 0.04
Radius (cm)	*CW* †	0.40 ± 0.03	0.49 ± 0.04	0.60 ± 0.05
	CCW †	0.49 ± 0.05	0.44 ± 0.05	0.40 ± 0.04
Aspect Ratio	*CW* †	1.91 ±0.16	2.04 ± 0.19	2.28 ± 0.23
	CCW	1.66 ± 0.14	2.11 ± 0.20	1.97 ± 0.21
Vortex symmetry CW:CCW		1.16 ± 0.12	1.29 ± 0.15	1.90 ± 0.26

[B] Mild AI conditions during different LVAD speeds

Moderate AI Parameters		**8k**	**9.4k**	**11k**
Circulation ($x10^{-3}$ m^2/s)	*CW*	10.33 ± 1.05	10.04 ± 1.05	9.10 ± 1.25
	CCW	-6.53 ± 0.82	-6.87 ± 0.86	-9.30 ± 0.83
Total Kinetic Energy (mJ/m)		1.09 ± 0.18	1.25 ± 0.22	1.46 ± 0.26
Kinetic Energy (mJ/m)	*CW*	0.70 ± 0.10	0.73 ± 0.11	0.80 ± 0.15
	CCW †	0.39 ± 0.09	0.53 ± 0.12	0.65 ± 0.12
Radius (cm)	*CW* †	0.42 ± 0.02	0.44 ± 0.03	0.35 ± 0.02
	CCW	0.54 ± 0.05	0.64 ± 0.08	0.60 ± 0.06
Aspect Ratio	*CW* †	2.36 ± 0.16	2.71 ± 0.21	2.07 ± 0.14
	CCW	2.19 ± 0.16	2.12 ± 0.14	2.17 ± 0.20
Vortex symmetry CW:CCW		0.87 ± 0.06	0.84 ± 0.07	0.86 ± 0.11

[C] Moderate AI conditions during different LVAD speeds

Table 3.4: (cont.)

Severe AI Parameters		**8k**	**9.4k**	**11k**
Circulation ($x10^{-3}$ m^2/s)	*CW* †	18.44 ± 1.48	18.50 ± 1.59	15.67 ± 1.36
	CCW †	-18.47 ± 1.58	-20.09 ± 1.75	-22.20 ± 1.43
Total Kinetic Energy (mJ/m) †		3.08 ± 0.38	3.54 ± 0.45	3.83 ± 0.40
Kinetic Energy (mJ/m)	*CW* †	1.58 ± 0.18	1.66 ± 0.21	1.74 ± 0.20
	CCW †	1.50 ± 0.22	1.88 ± 0.26	2.09 ± 0.19
Radius (cm)	*CW* †	0.53 ± 0.03	0.49 ± 0.03	0.46 ± 0.02
	CCW †	0.77 ± 0.06	0.71 ± 0.05	0.77 ± 0.04
Aspect Ratio	*CW* †	3.03 ± 0.21	2.93 ± 0.21	2.47 ± 0.16
	CCW †	1.79 ± 0.13	2.10 ± 0.13	2.08 ± 0.11
Vortex symmetry CW:CCW †		0.82 ± 0.06	0.82 ± 0.08	0.70 ± 0.05

[D] Severe AI conditions during different LVAD speeds

The SV of LVAD, AV, and systemic are shown in table 3.5 and figure 3.16 for different conditions before and during LVAD support. For the BL conditions, the presence of the LVAD increased total SV by increasing flow through LVAD and reducing flow through the AV. As LVAD speed increased from 8k to 11k, both systemic and LVAD SV increased by over 300% during diastole, but only 16% and 56%, respectively, during systole. When AI is present, a similar pattern but with more dramatic changes in systemic and LVAD SV during the diastole were noted. During the filling phase, high LVAD speed increased systemic SV but induced negative AV SV, indicating backward flow through the AV. The backward flow occurred for all AI classification and increased with AI severity. During systole, an increase in LVAD SV was coupled with a decrease in AV SV. For Moderate and Severe AI, backward AV flow occurred during high LVAD support.

The average AV ROI velocity is shown in Figure 3.17A. Positive and negative values denote forward flow to aorta and backward flow to LV, respectively. Increasing LVAD speed decreased forward AV velocity in the BL condition. When AI was present, high LVAD speed and worsening AI increased backward AV velocity. Moreover, larger EDR was observed in conditions with higher LVAD support and AI severity (Figure 3.17B). Higher LVAD support increased the average area, length, and peak velocity of the RJ (Figure 3.17C and Table 3.6). In comparison to

the pre-LVAD condition, RJ areas increased the most in Mild AI cases when LVAD speed changed from 8k to 11k rpm (Table 3.7). Within the same level of LVAD support, the quantitative clinical parameter increases as AI severity increases (Table 3.8).

Table 3.5: Diastole and systole systemic, aortic valve (AV), and LVAD stroke volume (mean ± standard error)

8k Parameters		**Baseline**	**Mild AI**	**Moderate AI**	**Severe AI**
Systemic SV (mL)	Diastole	10.96 ± 0.16	5.36 ± 0.32	-1.12 ± 0.35	-3.70 ± 0.23
	Systole	31.03 ± 0.15	26.71 ± 0.22	30.74 ± 0.14	27.60 ± 0.21
AV SV (mL)	Diastole	1.15 ± 0.14	-2.42 ± 0.21	-9.64 ± 0.31	-13.57 ± 0.13
	Systole	8.21 ± 0.07	4.22 ± 0.05	6.35 ± 0.11	4.66 ± 0.08
LVAD SV (mL)	Diastole	9.82 ± 0.10	7.79 ± 0.18	8.51 ± 0.05	9.87 ± 0.16
	Systole	22.81 ± 0.12	22.49 ± 0.18	24.38 ± 0.06	22.95 ± 0.15
9.4k Parameters					
Systemic SV (mL)	Diastole	27.32 ± 0.21	21.79 ± 0.17	14.87 ± 0.40	9.63 ± 0.31
	Systole	31.32 ± 0.19	28.70 ± 0.19	29.96 ± 0.36	28.31 ± 0.22
AV SV (mL)	Diastole	0.85 ± 0.10	-2.82 ± 0.12	-9.04 ± 0.27	-15.30 ± 0.23
	Systole	1.95 ± 0.04	0.37 ± 0.04	0.76 ± 0.10	-0.93 ± 0.06
LVAD SV (mL)	Diastole	26.47 ± 0.19	24.61 ± 0.21	23.91 ± 0.27	24.93 ± 0.20
	Systole	29.37 ± 0.17	28.33 ± 0.21	29.20 ± 0.26	29.25 ± 0.19
11k Parameters					
Systemic SV (mL)	Diastole	45.52 ± 0.25	40.39 ± 0.24	32.06 ± 0.16	28.14 ± 0.22
	Systole	35.82 ± 0.15	34.15 ± 0.16	34.61 ± 0.20	31.62 ± 0.18
AV SV (mL)	Diastole	0.44 ± 0.13	-3.11 ± 0.09	-9.99 ± 0.14	-15.39 ± 0.09
	Systole	0.31 ± 0.04	-0.24 ± 0.03	-2.15 ± 0.06	-4.16 ± 0.04
LVAD SV (mL)	Diastole	45.08 ± 0.16	43.51 ± 0.16	42.05 ± 0.17	43.53 ± 0.19
	Systole	35.51 ± 0.14	34.39 ± 0.17	36.75 ± 0.16	35.78 ± 0.17

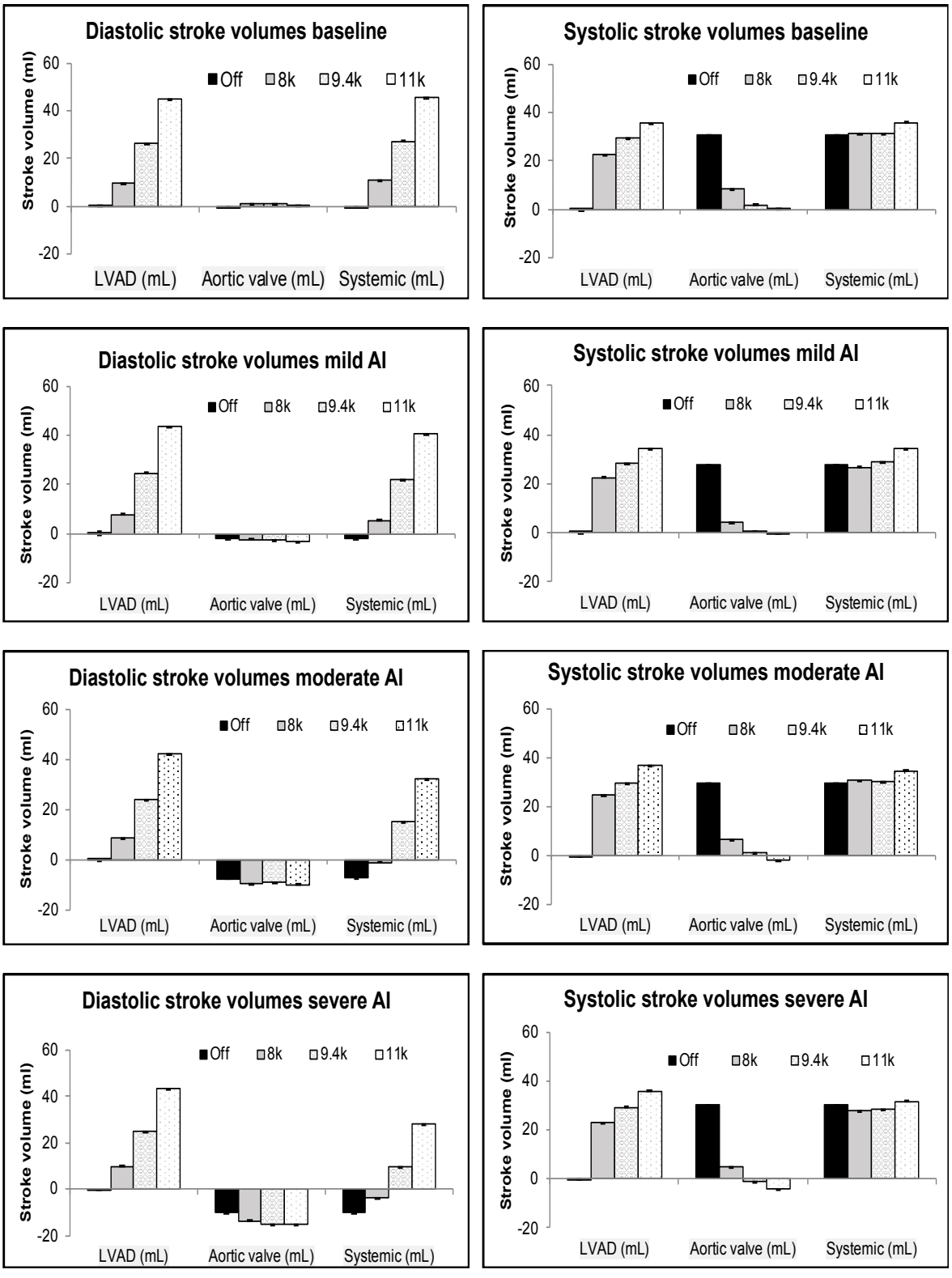

Figure 3.16: Stroke volume during diastole and systole for Baseline, Mild, Moderate, and Severe AI conditions.

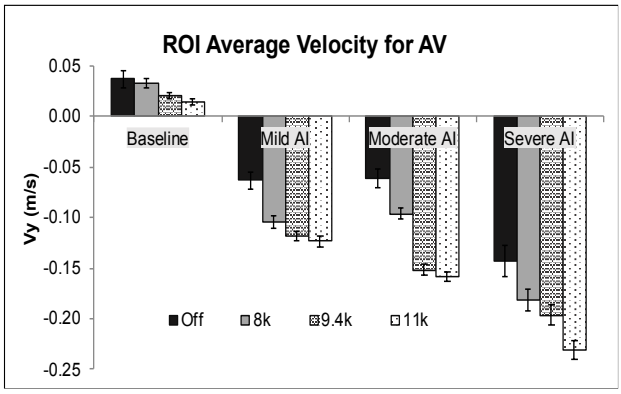

[A]

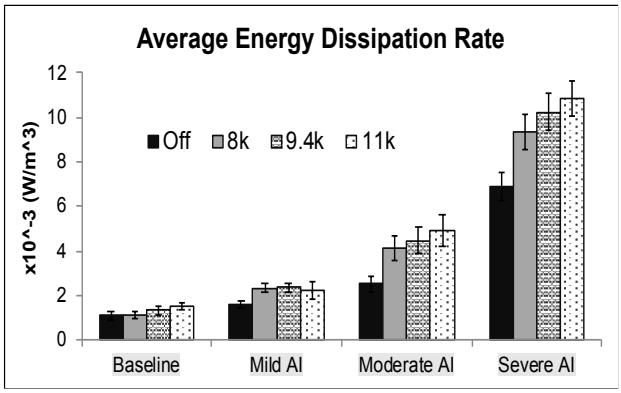

[B]

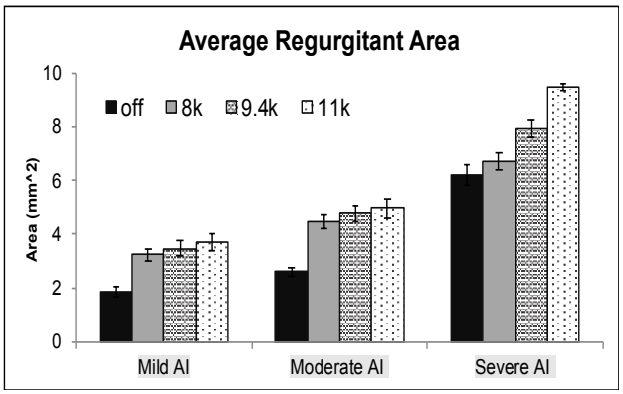

[C]

Figure 3.17: [A] Average velocity in the region of interest at the aortic valve, [B] Average energy dissipation rate, and [C] Average regurgitant area for all conditions.

Table 3.6: Regurgitant jet properties (mean ± standard error) of Mild, Moderate, and Severe aortic insufficiency (AI) conditions in the presence of native cardiac function (CS on). († Statistical significance ($p<0.01$) for different LVAD speeds).

Mild AI	**8k**	**9.4k**	**11k**
Area (cm^2) †	3.23 ± 0.21	3.47 ± 0.28	3.74 ± 0.33
Max Diameter (cm) †	1.31 ± 0.05	1.31 ± 0.06	1.35 ± 0.05
Vena Contracta Width (cm) †	0.34 ± 0.02	0.35 ± 0.01	0.36 ± 0.01
Length (cm) †	3.55 ± 0.16	3.87 ± 0.21	3.89 ± 0.25
Velocity (m/s) †	0.22 ± 0.00	0.21 ± 0.00	0.20 ± 0.00
Peak velocity (m/s) †	0.37 ± 0.01	0.36 ± 0.01	0.32 ± 0.01

[A] Mild AI conditions during different LVAD speeds

Moderate AI	**8k**	**9.4k**	**11k**
Area (cm^2) †	4.47 ± 0.25	4.78 ± 0.28	4.98 ± 0.36
Max Diameter (cm) †	1.22 ± 0.05	1.22 ± 0.05	1.44 ± 0.05
Vena Contracta Width (cm) †	0.38 ± 0.01	0.38 ± 0.01	0.39 ± 0.01
Length (cm) †	4.85 ± 0.20	5.16 ± 0.19	5.58 ± 0.12
Velocity (m/s) †	0.24 ± 0.01	0.24 ± 0.01	0.24 ± 0.01
Peak velocity (m/s) †	0.40 ± 0.02	0.42 ± 0.02	0.41 ± 0.03

[B] Moderate AI conditions during different LVAD speed

Severe AI	**8k**	**9.4k**	**11k**
Area (cm^2) †	6.72 ± 0.32	7.93 ± 0.29	9.48 ± 0.13
Max Diameter (cm) †	1.42 ± 0.03	1.72 ± 0.05	2.04 ± 0.04
Vena Contracta Width (cm) †	0.58 ± 0.02	0.57 ± 0.01	0.60 ± 0.02
Length (cm) †	6.02 ± 0.26	6.26 ± 0.17	6.72 ± 0.02
Velocity (m/s) †	0.34 ± 0.01	0.33 ± 0.01	0.35 ± 0.01
Peak velocity (m/s) †	0.61 ± 0.02	0.67 ± 0.02	0.70 ± 0.02

[C] Severe AI conditions during different LVAD speeds

Table 3.7: Percentage change of average RJ area in Mild and Severe AI.

Average RJ area	*% changes from Pre-LVAD to*		*% changes from 8k to 11k rpm*
	8k rpm	*11k rpm*	
Mild AI	74	101	16
Severe AI	8	53	41

Table 3.8: Quantitative clinical parameters for grading AI

Mild AI	*VC width (cm)*	*Jet width/ LVOT width (%)*	*Jet CSA/ LVOT CSA (%)*	*Regurgitant Volume (mL/beat)*	*Regurgitant fraction (%)*	*EROA (cm^2)*
Off	0.27	36	13	1.96	18	0.13
8k	0.34	50	25	2.42	28	0.14
9.4k	0.35	50	25	2.82	16	0.16
11k	0.36	52	27	3.36	9	0.21
Moderate AI						
Off	0.35	42	28	7.5	28	0.54
8k	0.38	42	33	9.64	35	0.56
9.4k	0.38	47	33	9.04	31	0.53
11k	0.39	55	31	12.14	21	0.68
Severe AI						
Off	0.55	55	30	10.26	41	0.62
8k	0.58	55	30	13.57	80	0.69
9.4k	0.57	66	44	16.24	53	0.78
11k	0.60	78	62	19.55	36	0.85

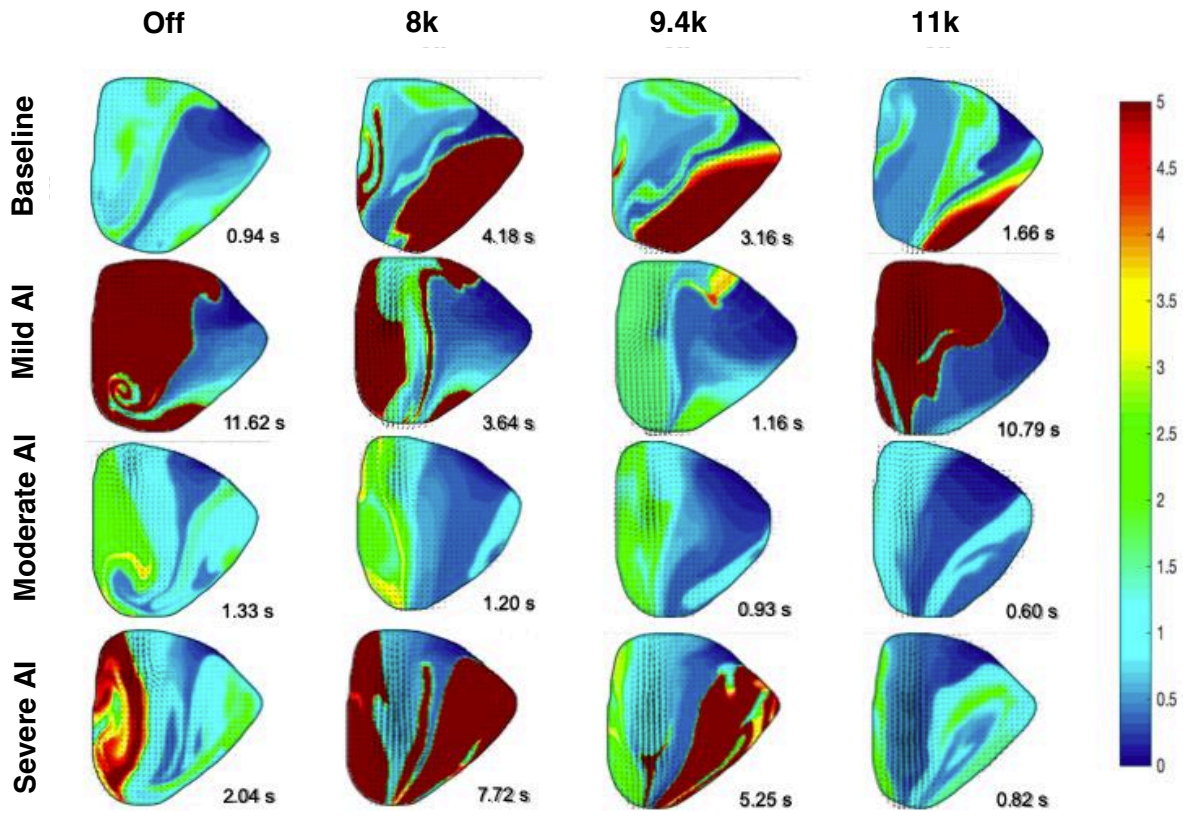

Figure 3.18: Left ventricle maps of residence time (T_R) calculated for the midplane area over 20 cycles of integration are shown for all conditions.

Table 3.9**:** Residence time (T_R) summary after 20 cardiac cycles of Baseline (normal valve), Mild, Moderate, and Severe aortic insufficiency (AI) conditions.

Parameter		*Average T_R (s)*	*% T_R area > 2CC (%)*	*Average T_R of area > 2CC (s)*
Baseline	*Off*	0.94	3.31	2.1
	8k	4.18	44.56	7.02
	9.4k	3.16	38.67	5.21
	11k	1.67	21.32	3.32
Mild AI	*Off*	11.62	67.01	16.25
	8k	3.64	36.24	8.1
	9.4k	1.16	7.01	2.86
	11k	10.79	57.84	17.87
Moderate AI	*Off*	1.33	26.19	2.35
	8k	1.2	23.23	2.57
	9.4k	0.93	13.09	2.07
	11k	0.6	N/A	N/A
Severe AI	*Off*	2.04	33.6	2.9
	8k	7.72	63.14	11.61
	9.4k	5.25	46.05	9.72
	11k	0.82	5.44	2.16

T_R maps varied notably among different conditions (Figure 3.18 and Table 3.9). For the Pre-LVAD conditions, the BL case exhibited the lowest T_R and residual region of 3% (T_R > 2 cycles) followed by Moderate, Severe, and Mild AI. Small residual regions in BL located near the MV base and LV free-wall, while in AI cases, they formed along the LVOT. After LVAD implantation, the T_R and residual regions varied depended on LVAD speeds. The presence of LVAD increased the average T_R in BL and Severe AI conditions, but T_R gradually decreased as LVAD support increased. On the other hand, Moderate AI experienced lower T_R during LVAD support. Mild AI cases exhibited a similar pattern except during high LVAD speed. During low and medium LVAD speed, Moderate AI had the lowest T_R, followed by Mild AI, BL, and Severe AI. While the residual flow regions in Moderate and Mild AI localized along the LVOT, they spread out along the free-wall in BL and Severe AI cases. During high LVAD speed, Moderate and Severe

AI had the lowest T_R, followed by BL and Mild AI. Moderate AI has no residual flow region, while more than half Mild AI mild-plane area contained flow > 2 seconds.

3.4 Discussion

This study presents the side-by-side comparison of normal AV versus AI models under the dilated heart failure model's hemodynamics during axial continuous flow HM2 support. Characterization of the hemodynamics, intraventricular flow filed, and residence time enable validation with clinical results.

Traditional Clinical AI Indices Applied to LVAD patients

Table 3.10: Quantitative parameters for grading AI in normal and LVAD patients[162,190,192,196].

	Parameters	***Mild***	***Moderate***		***Severe***
			Mild-Moderate	*Moderate-Severe*	
Pre-LVAD	*Vena Contracta width (cm)*	< 0.3	0.3-0.6		> 0.6
	Jet width/ LVOT width (%)	< 25	25-45	46-64	≥ 65
	Jet CSA/ LVOT CSA (%)	< 5	5-20	21-59	≥ 60
	RVol (mL/beat)	< 30	30-44	40-49	≥ 60
	Regurgitant fraction (%)	< 30	30-39	40-49	≥ 50
	EROA (cm^2)	< 10	0.01-0.19	0.20-0.29	≥ 0.30
Post-LVAD	*S/D ratio*	↓ as AI worsens			
	A_{dia} *(cm/s^2)*	↑ as AI worsens			
	EDPS (L/min/sec)	≥ -17.6 indicates Moderate-Severe AI			

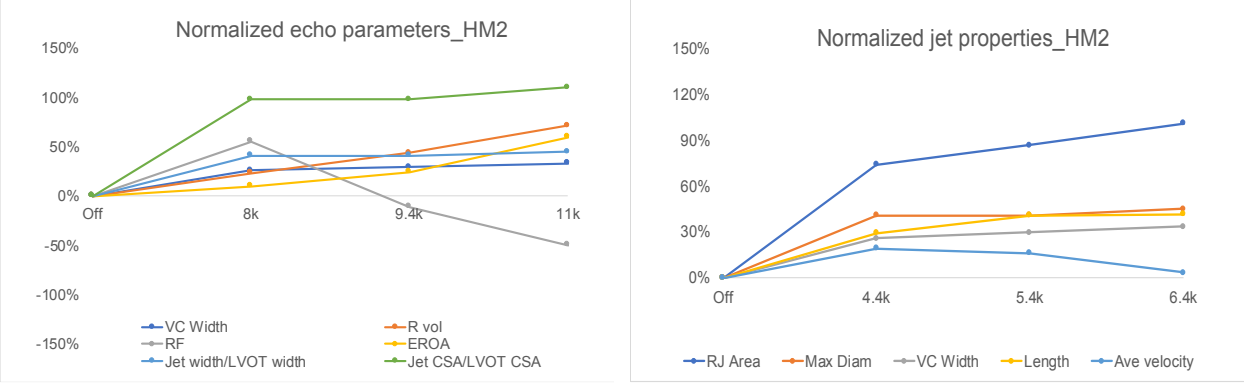

Figure 3.19: Percentage change of different AI indices from pre-LVAD

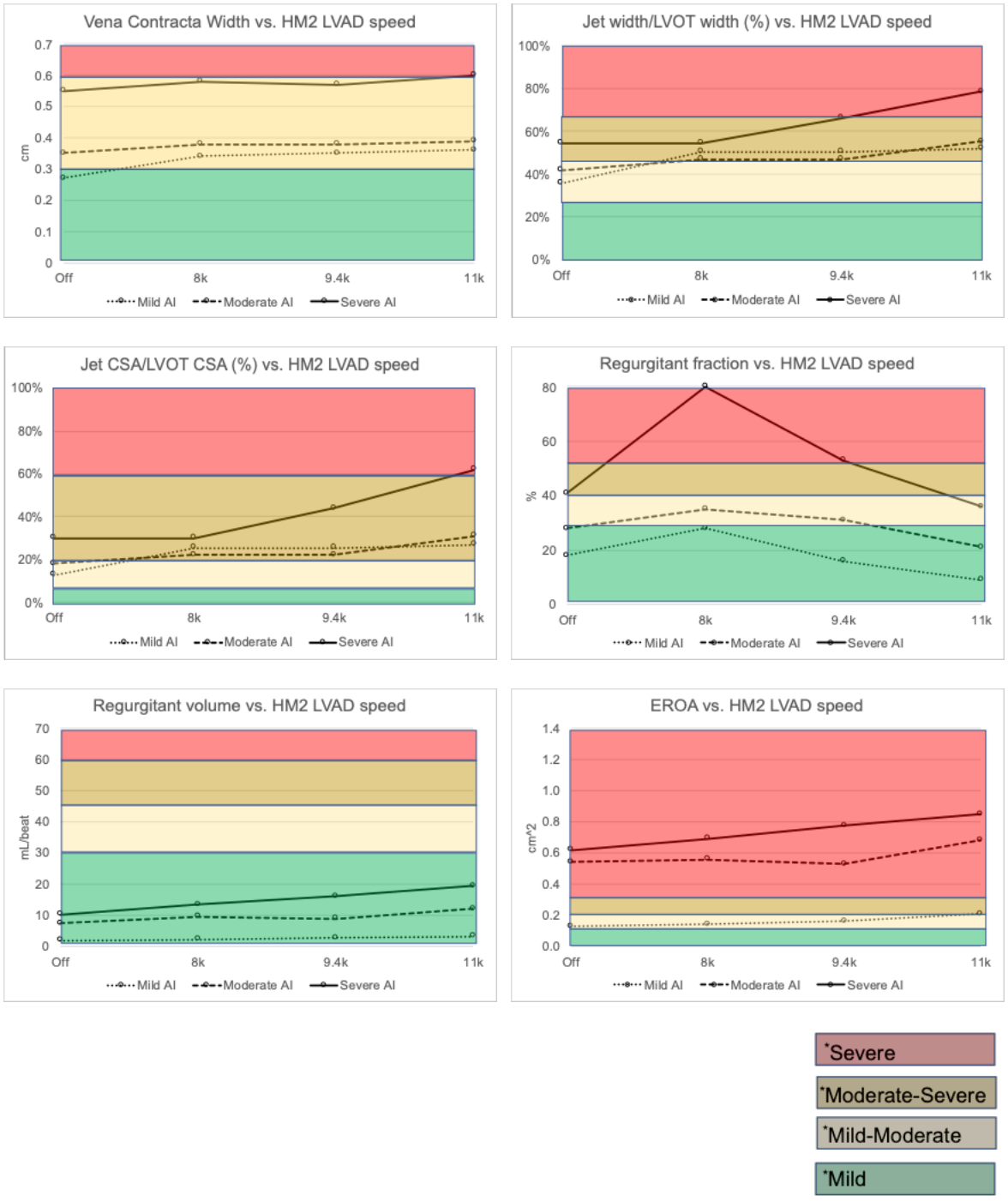

Figure 3.20: Sensitivity of echo quantitative parameters as a function of LVAD speed

The American Society of Echocardiography guidelines is typically used to evaluate and classify AI[192]. Table 3.10 summarizes the quantitative Transthoracic echocardiography indices

used to clinically grade AI in non-LVAD patients[162,192], and the new proposed indices for LVAD patients[190,196]. Figure 3.19 showed the normalized changes of different parameters as a function of LVAD speed. Due to the unloading effect of the LVAD, which increases the systemic flow and decreases LV pressure, the RF and EROA decreased. The jet CSA/LVOT CSA had the highest percentage of changes (Figure 3.19 left). For the jet properties, the RJ area changed significantly, 48-68% higher than the VC width (Figure 3.19 right). The normalized changes of different echo parameters of all tested conditions were shown in Figure 3.20. AI severity was classified according to the current AHA standard, where green is mild AI, yellow and brown is moderate AI, and red is severe AI[151]. The RegV underestimated AI severity in all cases, while RF suggested improving AI with high LVAD support, contradicting other parameters.

For the proposed parameter in post-LVAD support, Grinstein et al. have reported that the flow passing through LVAD outflow cannula is directly proportional to the LV load and inversely proportional to the ascending aorta afterload. Thus, the A_{dia} is expected to increase while the S/D ratio decrease with AI severity[190]. The presence of significant AI (RF >30%) was reported to associate with EDPS value higher or equal to (≥) -17.6[196].

The Pre-LVAD AI classifications of this *in-vitro* study were established following clinical grading[162,192]. The RF, a commonly used index, is defined as the ratio between RegV and Q_{sys}. During LVAD support, Q_{sys} increased more significantly in comparison to RegV; thereby, the RF would reduce and give a false conclusion of improved AI. In addition, the VC width was consistent with published values but did not change with LVAD support.

The proposed post-LVAD indices were calculated from the *in-vitro* results compared favorably to published data (Table 3.11). As the AI severity progresses, the S/D ratio and A_{dia} patterns demonstrated worsening of AI, while the EDPS value did not. As LVAD speed increased from 8k to 11k for each of AI groups, A_{dia} indicated AI improvement, disagreeing with the S/D ratio and EDPS. These results indicate that these indices (at least the EDPS) might not be sensitive

enough to quantify AI severity during LVAD support. These proposed indices were validated using a small group of patients from only one center, which could be lack statistical power to address this gap[190,196]. A larger, multicenter study should be performed with the same protocol to confirm their validity. Moreover, ramp studies with a wide range of LVAD speed are needed to understand the sensitivity of these parameters.

Table 3.11: Post-LVAD AI assessment indices characterized base on AI severity and LVAD speed.

Parameters trends	**AI severity: Mild→ Severe**				**LVAD speed: 8k → 11k rpm**		
	8k	**9.4k**	**11k**		**Mild AI**	**Moderate AI**	**Severe AI**
S/D ratio	↓	↓	↓		↓	↓	↓
A_{dia}	↑	↑	↑		↓	↓	↓
EDPS ≥ -17.6	No	No	Yes		No	Yes	Yes

NF and forward LVEF, calculated from the systemic, AV, and LVAD flow, followed a clear pattern. For the Pre-LVAD conditions, worsening AI would increase backward flow through the AV; therefore, the NF should decrease. The forward LVEF, which was proposed to quantify mitral regurgitation and calculated from systemic SV[244], also decreased when AI becomes more severe. During LVAD support, the NF decreased when AI worsened or when LVAD speed increased (Table 3.12). Forward LVEF increased at higher LVAD support for each AI group, due to the increased systemic SV. Consequently, the forward LVEF may not be sensitive to LVAD speed change, but NF could be used to quantify AI severity during LVAD support.

Table 3.12: Net flow (NF) and forward left ventricle ejection fraction (LVEF) trends during the post-LVAD study.

Parameters trends	**AI severity: Mild→ Severe**				**LVAD speed: 8k → 11k rpm**		
	8k	**9.4k**	**11k**		**Mild AI**	**Moderate AI**	**Severe AI**
NF (%)	↓	↓	↓		↓	↓	↓
Forward LVEF (%)	↓	↓	↓		↑	↑	↑

Alteration of Intraventricular Flow During AI

The pre-LVAD BL flow displays the classic LV vortex ring structure, with CW and CCW vortices, that appears at diastole and travels toward the LV apex before rolling up toward the AV[245,247,248]. The vortex formation enhances early LV filling by preserving fluid momentum[241,247], minimizing blood T_R[249], and energy dissipation by preventing flow collision[248]. Disruption in the flow architecture leads to energy loss and creates regions of stasis[250–252]. Mimicking the hemodynamics of DCM patients, the BL's vortex circulation and KE are higher than healthy models, implying higher energy is required for the heart to maintain CO[245,253,254]. In the post-LVAD BL condition, the vortex increases in circulation and KE, and its CW core stays closer to the LV apex, as reported previously[59,255].

The presence of pre-LVAD AI increased CCW vortex circulation and KE, especially in Severe cases. Moreover, the RJ's interaction with the septum and the mitral inflow jet disrupted the normal vortex formation, creating turbulence in the LV and multiple vortices[254–256]. Di Labbio et al. previously described the intraventricular flow pattern when AI is present. For Mild AI, there was minimal effect on intraventricular flow. As long as the mitral inflow remains the dominant jet, the RJ was less forceful and had a smaller velocity magnitude. As AI severity increased, the RJ grew stronger and pushed the mitral vortex ring closer to the LV free-wall. When AI was severe, the RJ became the dominant inflow jet, which limited the trajectory of the normal vortex ring architecture and created a large CCW vortex circulating inside the LV[256].

The combined disruption of AI and LVAD support produces a complex flow pattern. Interaction between the RJ and the mitral jet produces an oscillating flow inside the LV, with the LVAD pulling flow toward the apex, worsening AI. Furthermore, the LVAD introduces a regurgitant flow loop, impairing LV washout, and exposing flow to higher shear and higher T_R[255]. The results of this study agreed with previous work. As the RJ becomes dominant during high LVAD support or in Severe AI, more turbulence and disruption of normal flow architecture were observed in the LV.

During LVAD support AI Increases Energy Loss

EDR (or energy loss) has been used in previous studies to characterize the inefficiency of flow transport, with higher EDR values associated with increase AI severity[197,256–258]. By decreasing the E- and A-wave peak flow rate and interfering with the mitral inflow, AI hinders the vortex growth and creates turbulence inside the LV[197,257]. Consequently, the disruption of the vortex ring's smooth swirling motion creates regions of very high stress and increases the EDR[258]. The evolution of EDR had its peak near the end of the E-wave, then gradually decreased[256]. Similar observations were made in our study, as EDR increased at higher LVAD speeds.

During LVAD support AI Prolongs The Diastolic Filling Phase

Without LVAD support, AI reduces peak E- and A-wave velocity, increases the EDR, and disrupts the normal trajectories of the mitral CW vortex. The vortex lingers at the LV apex and takes longer to gain enough momentum to move toward the AV. As a result, diastole is prolonged. The effect is amplified during LVAD support as the pump continuously pulls flow toward the apex, increasing AI duration, and RegV. A recently published work reported that at low-medium LVAD support (8.8k), AI duration and RegV increased by 8% and 108% in Mild AI, and by 6% and 23% in Severe AI, respectively. Mild AI exhibited the highest increase in AI duration and Reg rates compared to Moderate and Severe AI. These findings suggested that the commonly used clinical indices (effective regurgitant orifice area, RJ) likely underestimate AI severity in LVAD patients[259].

The Effect of LVAD Support on AI Severity

LVAD support produced the biggest change in RegV in Mild AI and the smallest change in Severe AI[259]. Similarly, in our result, Mild AI produces the most significant RJ area change (Table 3.7) with LVAD support but demonstrated little change with LVAD speed. Severe AI followed the opposite pattern. The result suggested that Mild AI got worse immediately after

LVAD support, but was not affected by high LVAD speed, while Severe AI was more sensitive to LVAD speed change. The result is consistent with the clinical observation that pre-existing Mild AI was significantly associated with the progression to Moderate or Severe AI after LVAD implants[180].

3.5 Limitations

The cardiac simulator was designed for reproducibility as well as flexibility through the use of customized components. The system is an open-loop design with a vented left atrium chamber, based on the Windkessel model and lacks the physiological Frank-Starling response[198]. The mock loop produces pressure and flow waveforms and magnitude within the range of hemodynamics of DCM patients, providing a comparative testbed for examining the effect of AI on patients with LVADs. The mitral valve E- and A-wave was produced by LV expansion using the cardiac simulator's piston pump. The mitral annulus was circular to accommodate the valve housing, which differs from the eccentric anatomical D-shape or saddle shape. For the PIV imaging, the 2-D velocity field lacked out of plane information, which sometimes resulted in losing track of particles that left the imaging plane. We assumed that blood particles enter the mid-plane at the same point in space has the same T_R of the particles currently located at that point. Future study of the flow filed with 3D PIV is required to assess the out of plane velocity component fully.

3.6 Conclusion

Intraventricular flow field indies for Baseline, Mild, Moderate, and Severe AI under matched hemodynamic conditions were measured using a cardiac simulator for three LVAD speeds. The results agree with clinical observations of AI that show worsening with LVAD support, especially during high support levels. Pre-existing AI worsens immediately after LVAD support dues to the alteration in the intraventricular flow field, high energy loss, and more extended diastolic phase. Furthermore, this study suggests that current echocardiographic indices

underestimate the severity of AI in LVAD patients, introducing the need to determine new indices to diagnose and evaluate AI in LVAD patients.

3.7 Acknowledgements

This chapter, in full, is in an early prepared stage for publication. The co-author is Karen May-Newman. The dissertation author is the primary author of this paper.

Chapter 4

The Effect of Aortic Insufficiency on HeartMate 3 Left Ventricular Flow in The LVAD Supported Heart

4.1 Background

The HeartMate 3 (HM3) (Abbott) is a centrifugal, continuous flow (cf) LVAD, which was approved by the FDA in 2017 for bridge-to-transplant and destination therapy[44]. It is a 3rd generation pump with a magnetically levitated bearing designed to transport blood[45]. The pump controller generates an artificial pulse (AP) every 2 seconds, producing a speed change, as shown in Figure 4.1. The AP produces pressure and flows fluctuation intended to minimize stasis and the risk of thrombosis[47]. The HM3 has achieved a similar survival compared to the previous generation (HM2) but has superior hemocompatibility[44,47]. In clinical practice, the LVAD speed is usually set by the physician to permit intermittent aortic valve (AV) opening (AVO). However, in some patients, the heart is too weak to contribute to pumping function, and high LVAD support is needed. In these cases, the AV is hemodynamically prevented from opening, and all blood ejects through the LVAD. Previous studies have demonstrated that LVAD support reduces AVO area and opening duration[64,115,260]. As a consequence, the leaflets experience greater stress and strain[64,116]. Moreover, the reduction in AV flow increases the risk of thromboembolism and is correlated with the development of aortic insufficiency (AI)[83,261]. AI incidences of AI in HM2 patients were well documented and described in chapter 2.

The HM3 with AP increases LV pulsatility and AVO, which potentially affect hemodynamics and LV flow patterns differently than the HM2[58,66]. A previous *in vitro* study demonstrated that the AP provided a small degree of pulsatility and improved blood mixing in the LV. For similar conditions, the HM3 increase AVO duration and total flow by 50% and 3%, respectively[66]. This result supports the clinical findings that the HM3 was clinically superior to the

HM2 LVAD by reducing thromboembolic risk[44,49]. However, it is presently unclear whether HM3 will reduce the risk of AI, and whether the AP would increase LV turbulence by its interaction with the regurgitant jet in pre-existing AI patients. This chapter will try to examine the second question by investigating the effect of HM3 during the different levels of AI severity.

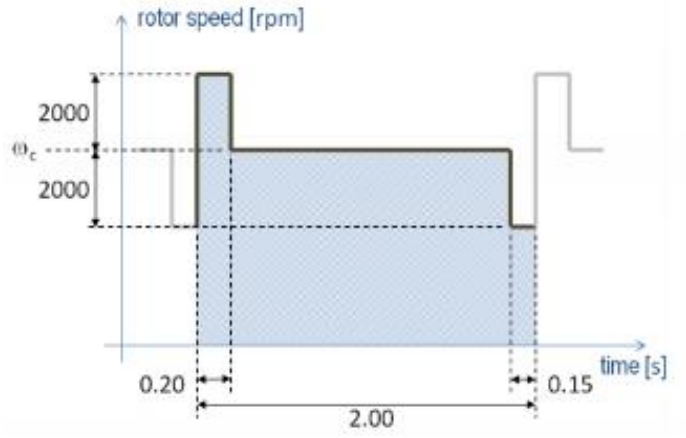

Figure 4.1: Schematic diagram of the artificial pulse (Bourque et al. ASAIO J, 2016)

4.2 Methods

The experimental setup and data analysis are similar to the previous study and are described in detail in Chapter 3, section 2, with the exception that the HM3 was used (Figure 4.2). For the Baseline (BL) (normal valve) LVAD-off condition, the LVAD conduit was clamped, and the HM3 was off. Subsequently, three speeds were tested: 4.4k, 5.4k, and 6.4k rpm for Low, Medium, and High support. Then, three different AI stents were inserted into the AV to induce Mild, Moderate, and Severe AI, and tested for BL and the different LVAD speeds. The AI stents created regurgitation fractions (RF) of 20% (mild AI), 28% (mild-moderate AI), and 45% (moderate-severe AI) and are classified as Mild, Moderate, and Severe AI for the rest of the study description. The velocity fields, measuring using Digital Particle Image Velocity (PIV). Trigger signal was set at the maximum LV pressure (LV) value in each cardiac cycle and delayed by 2 seconds (s) to capture the AP signal.

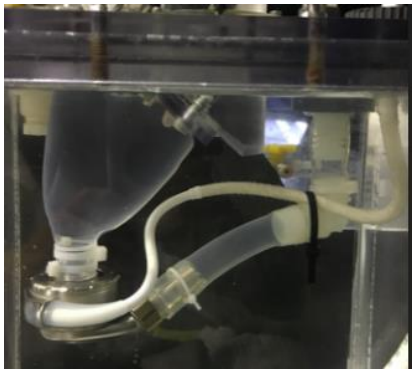

Figure 4.2: A silicone dilated LV model is attached to the HM3 and a Windkessel model of the circulation.

4.3 Result

Aortic Insufficiency during LVAD Support in the Absence of Cardiac Contraction

In the absence of cardiac contraction (CS Off), the HM3 AP repeats every 2 s (0.5 Hz frequency) (Figure 4.3). Overall, the range of LVP and aortic pressure (AoP) were less than 15% and 5% of the mean values. The ranges of flow (systemic, LVAD, and AV) were significantly higher, at 25-50%. In the BL conditions, systemic flow equaled LVAD flow, resulting in zero flow through the AV. During AI, a regurgitant flow loop developed when LVAD flow exceeded systemic flow.

As LVAD speed increased, the AoP, LVP, transaortic pressure (TVP), and systemic flow rate (Q_{sys}) increased, yet LVP remained low across different conditions (Table 4.1A). At the same pump speed, Q_{sys} decreased, while Q_{LVAD} and the Q ratio increased with increasing AI severity. A Q ratio larger than one indicates the presence of a regurgitant flow loop, where more flow passing through the pump without contributing to the systemic circulation. In the Mild, Moderate, and Severe AI, Q_{LVAD} exceeded Q_{sys} by approximately 20%, 60%, and 120%. The AV was hemodynamically closed in the BL conditions, and backward (negative) flow occurred when AI was present. As LVAD speed increased from 4.4k to 6.4k rpm, backward flow through the AV increased from BL by 81%, 64%, and 57% for Mild, Moderate, and Severe AI conditions.

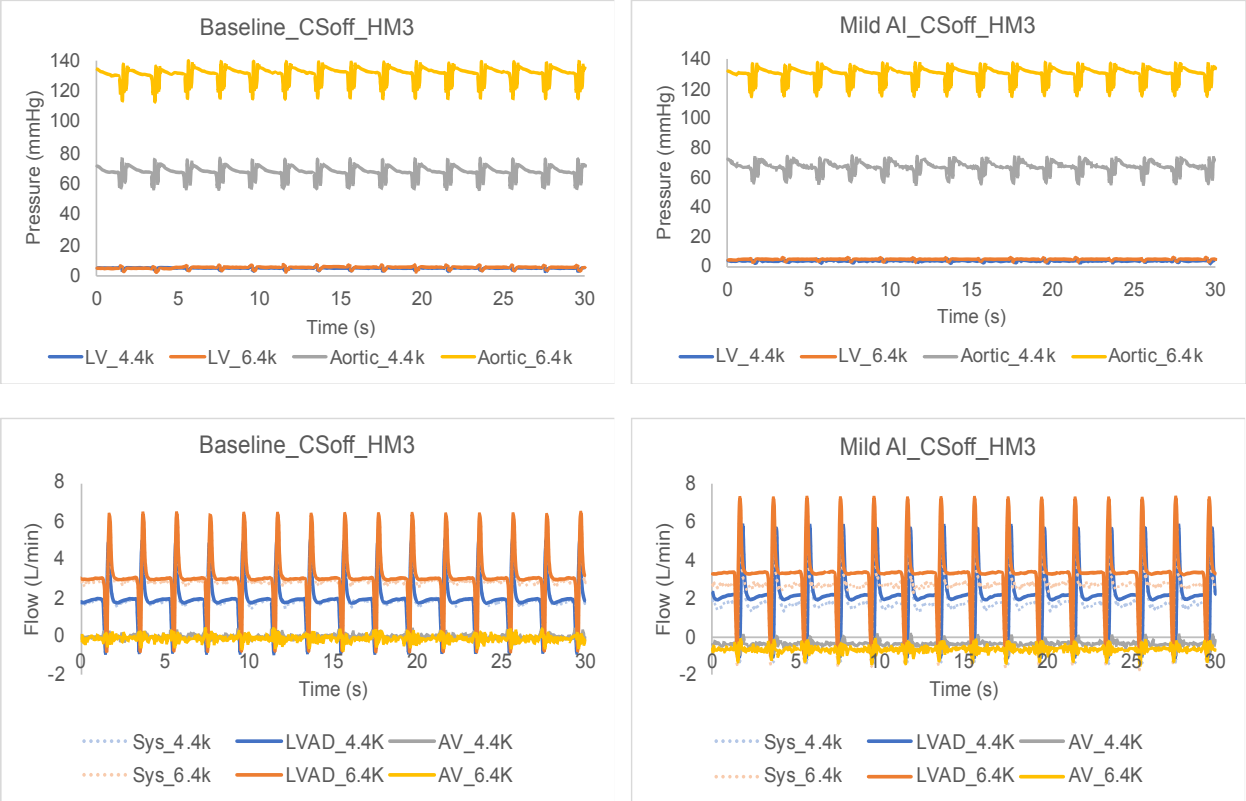

Figure 4.3: Cyclic variations (every 25 milliseconds) of pressures and flow during low (4.4k) and high (6.4k) HeartMate 3 support in the absence of native cardiac function (CSoff) for the normal valve (Baseline) and Mild AI conditions. (Left ventricle (LV), Systemic flow (Sys), aortic valve (AV))

The velocity field maps of Figure 4.4 illustrate the flow pattern generated by the AP for the first 500 milliseconds (ms) at 5.4krpm. A well-defined vortex ring was generated at the beginning of AP, which migrated toward the LV apex and dissipated around 500 ms in the BL condition. When AI was introduced, an additional regurgitant jet entered the LV during filling. Similar vortex rings appeared on the MV side, traveling toward the LV center, then collided with the regurgitant jet (RJ) from the AV. The interaction between these two jets created some persistent clockwise (CW) and counterclockwise (CCW) vortices (Table 3.1B). The RJ was continuously drawn into the LV by the LVAD and grew as AI became more severe. AI severity seemed to have a more substantial impact on the CCW vortex, which increased in circulation, kinetic energy (KE), and size. In the BL conditions, the CW vortex was dominant and almost twice the size of the CCW

vortex, while in AI, this relationship was reversed (Table 4.1C). Similar to the AV backward flow, RJ areas, diameters, and vena contracta width (VC) (minimum jet diameter captured near the AV) increased significantly in Mild AI, followed by Moderate and Severe AI groups when LVAD speed increased from 4.4k to 6.4k rpm. Conversely, the RJ length and average velocity slightly increased (less than 20%).

Table 4.1: Average values (mean ± standard error) of [A] Hemodynamics, [B] Intraventricular vortex properties, [C] Regurgitant jet properties and [D] Residence time (T_R) summary after 20 cardiac cycles of Baseline, Mild, Moderate and Severe aortic insufficiency (AI) conditions in the absence of native cardiac function (CS Off).

Parameter		*LVP (mmHg)* †	*AoP (mmHg)* †	*TVP (mmHg)* †	Q_{sys} *(L/min)* †	Q_{LVAD} *(L/min)* †	Q_{AV} *(L/min)*	*Q ratio*	*PI*
Baseline	**4.4k**	5.39 ± 0.00	67.81 ± 0.03	62.42	1.95 ± 0.01	1.96 ± 0.01	-0.02	1.01	3.15
	5.4k	5.64 ± 0.01	97.05 ± 0.04	91.41	2.45 ± 0.01	2.49 ± 0.01	-0.04	1.02	2.75
	6.4k	5.43 ± 0.01	130.71 ± 0.05	125.28	2.94 ± 0.01	3.03 ± 0.01	-0.10	1.03	2.45

Parameter		*LVP (mmHg)* †	*AoP (mmHg)* †	*TVP (mmHg)* †	Q_{sys} *(L/min)* †	Q_{LVAD} *(L/min)* †	Q_{AV} *(L/min)* †	*Q ratio*	*PI*
Mild AI	**4.4k**	3.79 ± 0.00	67.10 ± 0.01	63.31	1.80 ± 0.00	2.18 ± 0.00	-0.37	1.21	4.09
	5.4k	4.37 ± 0.00	95.30 ± 0.01	90.93	2.27 ± 0.00	2.79 ± 0.00	-0.51	1.23	3.61
	6.4k	4.76 ± 0.00	130.64 ± 0.01	125.88	2.76 ± 0.00	3.43 ± 0.00	-0.67	1.24	3.21

Parameter		*LVP (mmHg)* †	*AoP (mmHg)* †	*TVP (mmHg)* †	Q_{sys} *(L/min)* †	Q_{LVAD} *(L/min)* †	Q_{AV} *(L/min)* †	*Q ratio*	*PI*
Moderate AI	**4.4k**	7.27 ± 0.00	65.85 ± 0.01	58.59	1.65 ± 0.00	2.63 ± 0.00	-0.99	1.6	3.83
	5.4k	7.64 ± 0.00	92.37 ± 0.01	84.73	2.09 ± 0.00	3.37 ± 0.00	-1.29	1.62	3.34
	6.4k	8.47 ± 0.00	123.95 ± 0.01	115.49	2.54 ± 0.00	4.16 ± 0.00	-1.62	1.64	2.94

Parameter		*LVP (mmHg)* †	*AoP (mmHg)* †	*TVP (mmHg)* †	Q_{sys} *(L/min)* †	Q_{LVAD} *(L/min)* †	Q_{AV} *(L/min)* †	*Q ratio*	*PI*
Severe AI	**4.4k**	5.03 ± 0.00	68.75 ± 0.01	63.72	1.12 ± 0.00	2.46 ± 0.00	-1.35	2.21	5.1
	5.4k	4.91 ± 0.00	95.03 ± 0.01	90.12	1.42 ± 0.00	3.15 ± 0.00	-1.73	2.21	4.42
	6.4k	5.09 ± 0.00	128.07 ± 0.01	122.98	1.68 ± 0.00	3.80 ± 0.00	-2.12	2.26	4.08

[A] Hemodynamic result (LVP (LV pressure), AoP (Aortic pressure), Q_{sys} (total systemic flow), Q_{LVAD} (LVAD flow), Q_{AV} (flow through aortic valve), Q_{ratio} (Flow ratio), PI (Aortic pulsatility index)). († Statistical significance ($p<0.01$) for different LVAD speeds).

Table 4.1: (cont.)

Parameter		*Circulation ($x10^{-3}$ m^2/s)*		*Total Kinetic Energy (mJ/m)* †	*Kinetic Energy (mJ/m)*		*Radius (cm)*		*Aspect Ratio*		*Vortex sys* †
		CW †	*CCW* †		*CW* †	*CCW* †	*CW* †	*CCW* †	*CW* †	*CCW* †	
Baseline	**4.4k**	3.81 ± 0.38	-1.14 ± 0.27	0.18 ± 0.03	0.11 ± 0.02	0.07 ± 0.02	0.85 ± 0.05	0.55 ± 0.05	1.58 ± 0.07	2.49 ± 0.22	1.75 ± 0.18
	5.4k	6.16 ± 0.38	-1.66 ± 0.32	0.29 ± 0.04	0.19 ± 0.02	0.10 ± 0.02	0.97 ± 0.04	0.52 ± 0.04	1.85 ± 0.06	2.35 ± 0.17	2.17 ± 0.20
	6.4k	21.29 ± 0.36	-8.13 ± 0.45	2.51 ± 0.13	1.50 ± 0.05	1.01 ± 0.09	1.25 ± 0.02	0.67 ± 0.05	1.87 ± 0.04	2.39 ± 0.17	2.09 ± 0.20

Parameter		*Circulation ($x10^{-3}$ m^2/s)*		*Total Kinetic Energy (mJ/m)* †	*Kinetic Energy (mJ/m)*		*Radius (cm)*		*Aspect Ratio*		*Vortex sys*
		CW †	*CCW* †		*CW* †	*CCW* †	*CW*	*CCW*	*CW*	*CCW*	
Mild AI	**4.4k**	5.37 ± 0.28	-8.03 ± 0.24	0.45 ± 0.02	0.20 ± 0.01	0.25 ± 0.01	0.56 ± 0.03	0.90 ± 0.05	3.68 ± 0.24	1.75 ± 0.13	0.71 ± 0.06
	5.4k	6.93 ± 0.31	-11.09 ± 0.21	0.76 ± 0.02	0.31 ± 0.02	0.45 ± 0.02	0.63 ± 0.04	0.97 ± 0.05	3.88 ± 0.24	1.43 ± 0.04	0.84 ± 0.14
	6.4k	9.05 ± 0.27	-13.57 ± 0.24	1.10 ± 0.03	0.47 ± 0.02	0.64 ± 0.02	0.59 ± 0.04	0.94 ± 0.04	3.55 ± 0.22	1.63 ± 0.06	0.70 ± 0.06

[B] Intraventricular vortex properties (Clockwise (CW), and counter-clockwise (CCW), vortex symmetric CW:CCW (Vortex sys)) (In the case which had multiple CW and CCW vortices occurrences: total CW and CCW vortex circulation and kinetic energy, radius/aspect ratio/vortex symmetry of the main (largest) CW and CCW vortex were reported). († Statistical significance ($p<0.01$) for different LVAD speeds).

Table 4.1: [B] (cont.)

Parameter		Circulation ($x10^{-3}$ m^2/s)		Total Kinetic Energy (mJ/m) †	Kinetic Energy (mJ/m)		Radius (cm)		Aspect Ratio		Vortex sys †
		CW	CCW †		CW †	CCW †	CW	CCW †	CW	CCW	
Moderate AI	**4.4k**	9.80 ± 0.22	-8.60 ± 0.24	0.91 ± 0.02	0.49 ± 0.02	0.42 ± 0.02	0.48 ± 0.01	0.88 ± 0.05	3.37 ± 0.12	1.54 ± 0.09	0.67 ± 0.07
	5.4k	11.60 ± 0.25	-13.57 ± 0.32	1.49 ± 0.04	0.71 ± 0.03	0.78 ± 0.03	0.52 ± 0.02	0.94 ± 0.04	3.47 ± 0.14	1.62 ± 0.13	0.62 ± 0.06
	6.4k	12.66 ± 0.31	-17.55 ± 0.34	2.09 ± 0.04	0.92 ± 0.03	1.17 ± 0.03	0.50 ± 0.01	0.99 ± 0.03	3.34 ± 0.17	1.55 ± 0.09	0.55 ± 0.05

Parameter		Circulation ($x10^{-3}$ m^2/s)		Total Kinetic Energy (mJ/m) †	Kinetic Energy (mJ/m)		Radius (cm)		Aspect Ratio		Vortex sys †
		CW †	CCW †		CW †	CCW †	CW	CCW †	CW	CCW	
Severe AI	**4.4k**	13.16 ± 0.29	-11.55 ± 0.22	1.35 ± 0.03	0.73 ± 0.02	0.62 ± 0.02	0.80 ± 0.04	0.92 ± 0.04	2.89 ± 0.15	1.64 ± 0.06	0.93 ± 0.06
	5.4k	16.53 ± 0.34	-15.22 ± 0.27	2.22 ± 0.05	1.16 ± 0.03	1.06 ± 0.03	0.83 ± 0.04	0.95 ± 0.04	3.26 ± 0.19	1.54 ± 0.04	0.93 ± 0.06
	6.4k	19.06 ± 0.42	-18.81 ± 0.32	3.03 ± 0.06	1.56 ± 0.06	1.48 ± 0.04	0.76 ± 0.04	1.01 ± 0.04	3.29 ± 0.18	1.55 ± 0.07	0.77 ± 0.04

[B] Intraventricular vortex properties (Clockwise (CW), and counter-clockwise (CCW), vortex symmetric CW:CCW (Vortex sys)) (In the case which had multiple CW and CCW vortices occurrences: total CW and CCW vortex circulation and kinetic energy, radius/aspect ratio/vortex symmetry of the main (largest) CW and CCW vortex were reported). († Statistical significance ($p<0.01$) for different LVAD speeds).

Table 4.1: (cont.)

Parameter		*Area (cm^2)* †	*Max Diameter (cm)* †	*Vena Contracta Width (cm)* †	*Length (cm)* †	*Velocity (m/s)* †	*Peak velocity (m/s)* †
Mild AI	**4.4k**	3.25 ± 0.09	1.21 ± 0.02	0.28 ± 0.01	5.11 ± 0.09	0.22 ± 0.00	0.40 ± 0.01
	5.4k	4.75 ± 0.08	1.51 ± 0.02	0.31 ± 0.02	5.81 ± 0.05	0.24 ± 0.00	0.48 ± 0.01
	6.4k	5.87 ± 0.09	1.64 ± 0.02	0.44 ± 0.02	6.04 ± 0.06	0.26 ± 0.00	0.53 ± 0.01

Parameter		*Area (cm^2)* †	*Max Diameter (cm)* †	*Vena Contracta Width (cm)*	*Length (cm)* †	*Velocity (m/s)* †	*Peak velocity (m/s)* †
Moderate AI	**4.4k**	3.88 ± 0.04	1.38 ± 0.02	0.26 ± 0.02	4.76 ± 0.06	0.29 ± 0.00	0.59 ± 0.00
	5.4k	5.20 ± 0.04	1.60 ± 0.01	0.28 ± 0.02	5.36 ± 0.05	0.31 ± 0.00	0.64 ± 0.01
	6.4k	6.36 ± 0.05	1.77 ± 0.02	0.30 ± 0.02	5.74 ± 0.05	0.33 ± 0.00	0.71 ± 0.01

Parameter		*Area (cm^2)* †	*Max Diameter (cm)* †	*Vena Contracta Width (cm)*	*Length (cm)* †	*Velocity (m/s)* †	*Peak velocity (m/s)* †
Severe AI	**4.4k**	5.52 ± 0.04	1.91 ± 0.03	0.28 ± 0.02	5.52 ± 0.04	0.29 ± 0.00	0.58 ± 0.01
	5.4k	7.07 ± 0.05	2.20 ± 0.03	0.34 ± 0.02	5.97 ± 0.05	0.30 ± 0.00	0.70 ± 0.01
	6.4k	7.93 ± 0.06	2.29 ± 0.02	0.33 ± 0.02	6.03 ± 0.06	0.34 ± 0.00	0.79 ± 0.01

[C] Regurgitant jet properties († Statistical significance ($p<0.01$) for different LVAD speeds).

Table 4.1: (cont.)

Parameter		*Average T_R (s)*	*% T_R area > 2CC (%)*	*Average T_R of area > 2CC (s)*
Baseline	**4.4k**	14.77	63.77	21.14
	5.4k	13.19	58.23	19.50
	6.4k	17.83	70.20	19.85
Mild AI	**4.4k**	10.77	24.85	15.56
	5.4k	9.58	28.02	10.89
	6.4k	4.10	41.63	7.30
Moderate AI	**4.4k**	17.16	62.28	21.59
	5.4k	7.57	44.87	16.37
	6.4k	10.46	45.50	22.06
Severe AI	**4.4k**	26.36	83.14	28.56
	5.4k	24.61	81.47	25.26
	6.4k	19.36	71.29	24.30

[D] Residence time (T_R)

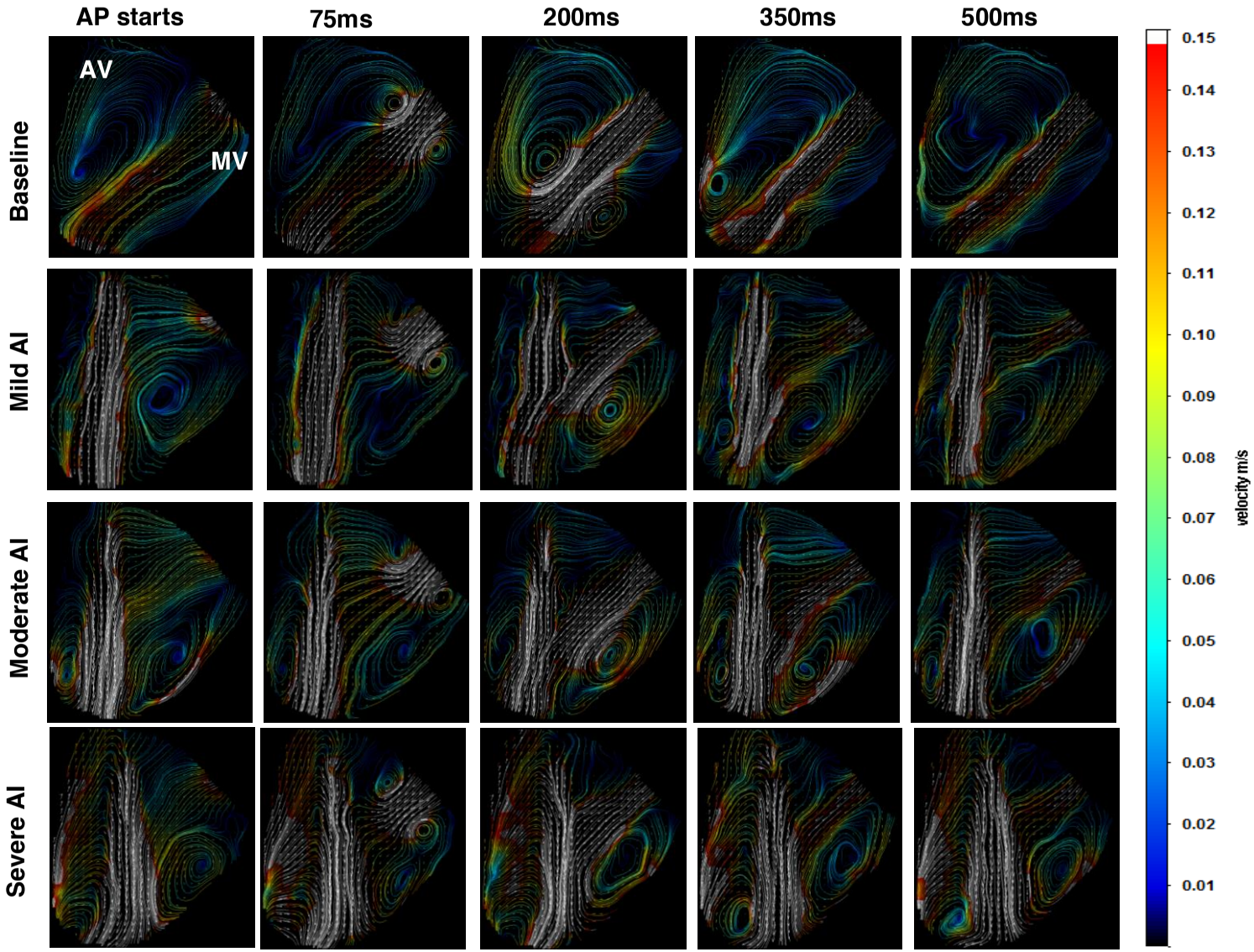

Figure 4.4: Velocity Field Images during 5.4k rpm HM3 support for CS Off conditions (Aortic valve (AV), Mitral valve (MV)

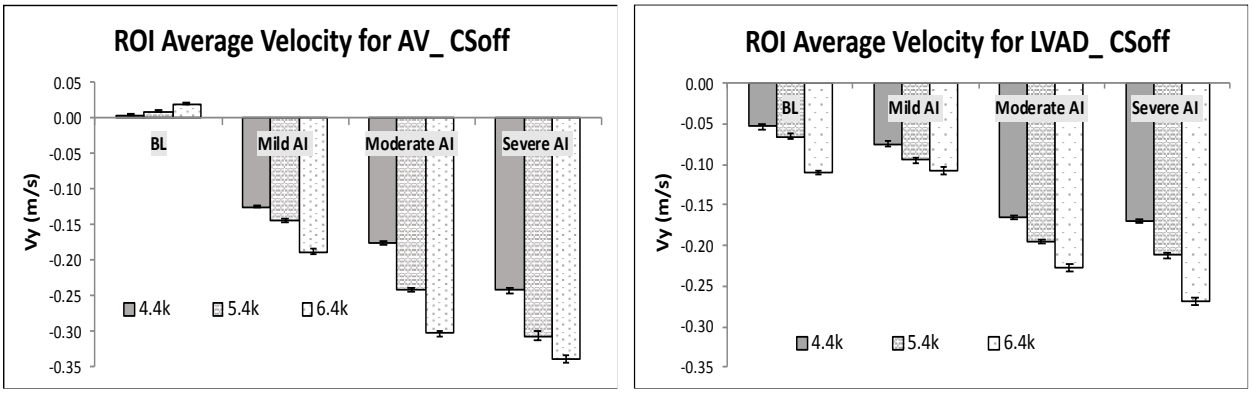

[A]

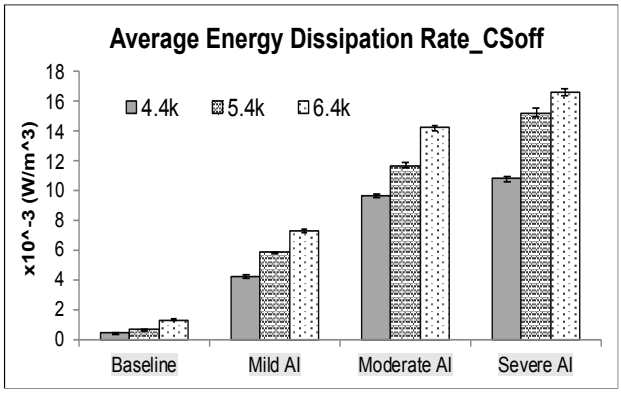

[B]

Figure 4.5: [A] Average velocity across the aortic valve and LVAD inlets and B] Average energy dissipation rate for the CS off conditions at different AI severity levels.

Average ROI velocities across the AV and inflow LVAD cannula are shown in Figure 4.5A. During BL conditions, higher LVAD speed increased forward velocity at the AV. During AI conditions, high pump speed increased backward (negative) velocity at the AV and incoming velocity at the LVAD inlet. The average energy dissipation rate (EDR) remained low in all BL conditions, but increased at higher LVAD speed and more severe AI (Figure 4.5).

Aortic Insufficiency before LVAD implantation (Pre-LVAD)

The simulated native heartbeat (CS on) produced, 2.0 L/min cardiac output (CO), an ejection fraction of 18%, at 63 beats per minute (bpm) for the BL condition. At comparable values of LVP, AoP, and TVP, the Mild, Moderate, and Severe AI reduced the systemic flow by 20%,

27%, and 44,% respectively. As AI severity increased, the AVO time, net flow (NF), LVEF, and diastolic SV decreased while RF increased (Table 4.2A, B). The velocity field maps in Figure 4.6 illustrate four events during the cardiac cycle: diastolic filling at peak E, mid-diastole, peak A, and mid-systolic ejection phase. For the BL condition, the LV vortex pattern reflects the incoming E-wave mitral jet, which forms a vortex ring with a large CW and smaller CCW vortex. The CW vortex grows in size while the CCW vortex dissipates rather quickly due to the LV free-wall's confinement. This pattern helps to direct flow toward the LV outflow tract (LVOT) during late-diastole, and through the AV during systole. The RJ first appear during isovolumic relaxation, before MV opening, then continues to grow before disappearing by the start of systole. The interaction between the RJ and MV incoming jet produces some flow distortion in the LV. As the AI is worsened, circulation and KE increased, and the CW and CCW vortex became elongated (increased aspect ratio). Moreover, the CCW vortex grew in size, competing with the CW vortex to become more dominant (Table 4.2B).

The ROI velocity was plotted for the full CC, starting from diastole at t = 0. The 2nd filling phase (A wave) occurred at t = 0.525 s, and systole began at t=0.65 s for the BL condition (Figure 4.7A). For AV velocity, positive and negative values denote forward flow to aorta and backward flow to LV, respectively. In the BL condition, maximum forward flow occurred during systole (~0.18m/s). In the presence of AI, backward diastolic flow occurred with a maximum velocity of -0.10, -0.23, and -0.29 m/s for Mild, Moderate, and Severe AI classification. Increased AI severity prolonged diastole and shortened systole, especially in Severe AI, when the forward velocity occurred around 0.7 s. For the ROI of MV velocity, the negative value denotes incoming flow to the LV. Each graph contains two peaks representing the E- and A- waves. AI decreased peak E- and A- velocity.

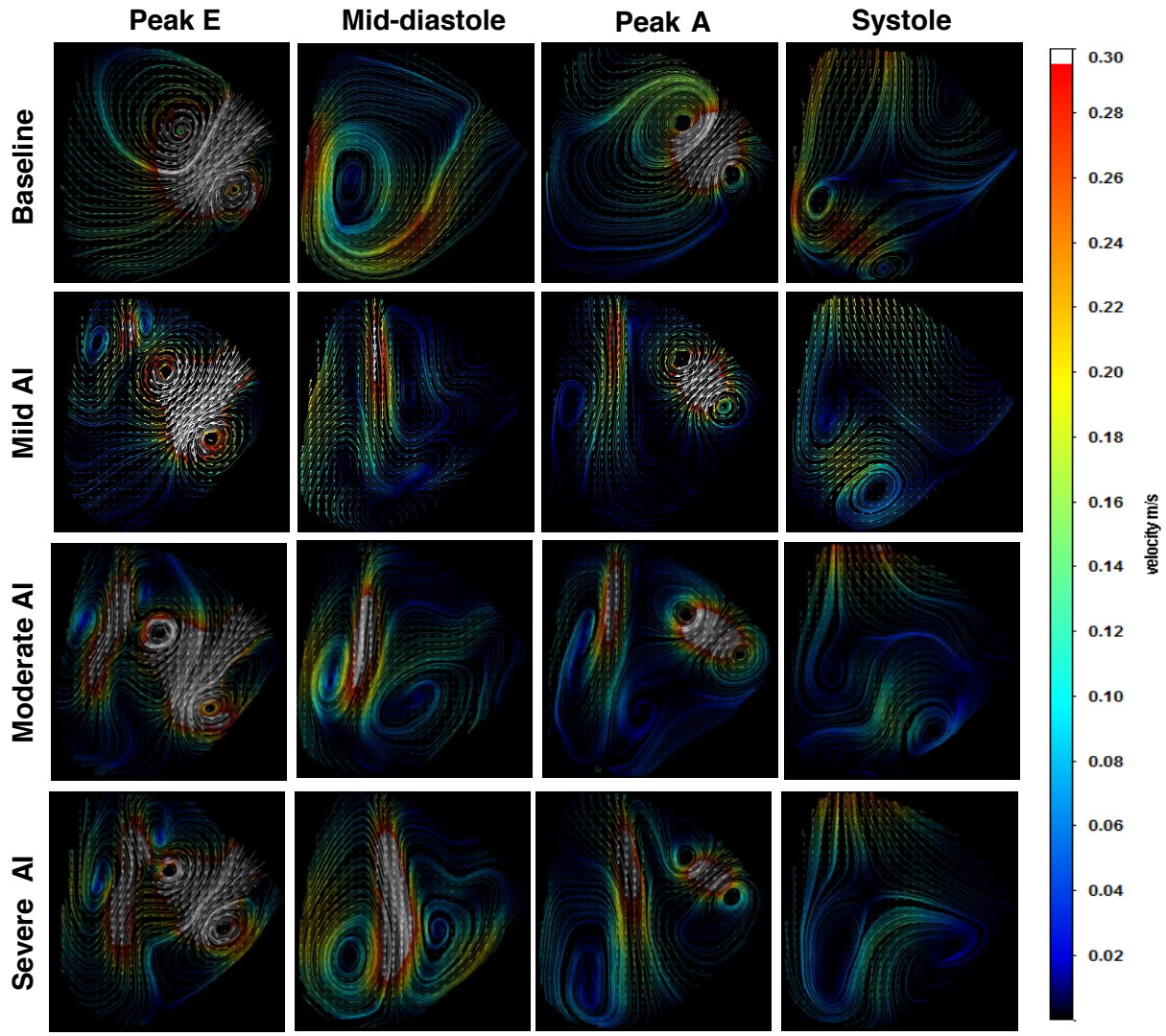

Figure 4.6: Velocity Field Images of Baseline and Mild, Moderate, and Severe AI conditions for pre-LVAD conditions in the presence of native cardiac function.

The EDR and RJ area during the CC are shown in Figures 4.7B and C, respectively. Average EDR was lowest in the BL condition and increased significantly by 144%, 206%, and 232% for Mild, Moderate, and Severe AI, respectively. EDR remained high during diastasis for AI conditions and decreased rapidly at the start of systole. The RJ evolution followed a similar pattern, in which the jet grew during diastole and dissipated in systole. The severe AI jet persisted longer, which is consistent with the ROI AV results. The properties of the RJ are provided in table 3.2C.

Table 4.2: [A] Hemodynamic result, [B] Stroke volume, [C]Intraventricular vortex properties, and [C] Regurgitant jet properties (mean ± standard error) of Baseline (normal valve), Mild, Moderate and Severe aortic insufficiency (AI) conditions in the presence of native cardiac function (CS On) without LVAD support (Pre-LVAD) († Statistical significance ($p<0.01$) for tested conditions).

Parameters	**Baseline**	**Mild AI**	**Moderate AI**	**Severe AI**
LVP (mmHg)	22.97 ± 0. 23	23.16 ± 0.18	29.24 ± 0.13	25.15 ± 0.21
AoP (mmHg) †	61.15 ± 0.17	61.13 ± 0.11	63.06 ± 0.08	64.02 ± 0.13
TVP (mmHg) †	38.18	37.97	33.82	38.87
Q_{sys} *(L/min)* †	1.99 ± 0.03	1.59 ± 0.03	1.44 ± 0.02	1.10 ± 0.03
PI	10.01	13.16	13.74	17.05
RF (%)	0.00	20	28	45
NF (%)	99.93	79.96	72.90	55.90
Forward LVEF (%)	18.03	14.51	13.07	9.86
AVO time (sec)	0.25	0.23	0.20	0.18

[A] Hemodynamic result (LVP (LV pressure), AoP (Aortic pressure), Q_{sys} (total systemic flow), Q_{LVAD} (LVAD flow), Q_{AV} (flow through aortic valve), Q_{ratio} (Flow ratio), PI (Aortic pulsatility index), RF (regurgitant fraction), NF (net flow through AV), LVEF (left ventricle ejection fraction), AVO (aortic valve opening) time.

Stroke volume	**Baseline**	**Mild AI**	**Moderate AI**	**Severe AI**
Diastole (mL)	0.79 ± 0.42	-5.23 ± 0.21	-9.28 ± 0.21	-11.91 ± 0.20
Systole (mL)	31.66 ± 0.27	31.35 ± 0.20	32.81 ± 0.18	29.66 ± 0.25

[B] Stroke volume during diastole and systole

Parameters		**Baseline**	**Mild AI**	**Moderate AI**	**Severe AI**
Circulation $(x10^{-3}\ m^2/s)$	*CW* †	11.69 ± 1.08	6.34 ± 0.66	7.66 ± 0.67	11.11 ± 1.09
	CCW †	-5.29 ± 1.09	-6.87 ± 0.60	-5.68 ± 0.68	-9.06 ± 0.87
Total Kinetic Energy (mJ/m) †		1.65 ± 0.38	0.70 ± 0.15	0.64 ± 0.14	0.98 ± 0.15
Kinetic Energy (mJ/m)	*CW* †	0.89 ± 0.16	0.33 ± 0.07	0.35 ± 0.07	0.57 ± 0.08
	CCW †	0.76 ± 0.22	0.37 ± 0.08	0.29 ± 0.07	0.41 ± 0.07
Radius (cm)	*CW* †	0.63 ± 0.06	0.41 ± 0.04	0.39 ± 0.02	0.69 ± 0.05
	CCW †	0.39 ± 0.03	0.44 ± 0.04	0.60 ± 0.06	0.60 ± 0.04
Aspect Ratio	*CW*	1.42 ± 0.06	1.80 ± 0.15	2.47 ± 0.14	2.18 ± 0.09
	CCW	1.47 ± 0.11	1.93 ± 0.17	1.78 ± 0.19	1.92 ± 0.11
Vortex symmetry CW:CCW †		1.61 ± 0.07	0.93 ± 0.08	0.65 ± 0.08	1.15 ± 0.15

[C] Intraventricular vortex properties (Clockwise (CW), and counter-clockwise (CCW))
(In the case which had multiple CW and CCW vortices occurrences: total CW and CCW vortex circulation and kinetic energy, radius/aspect ratio/vortex symmetry of the main (largest) CW and CCW vortex were reported).

Table 4.2: (cont.)

Parameters	Mild AI	Moderate AI	Severe AI
Area (cm^2) †	1.86 ± 0.18	2.54 ± 0.13	5.28 ± 0.29
Max Diameter (cm) †	0.80 ± 0.05	1.03 ± 0.04	1.59 ± 0.09
Vena Contracta Width (cm) †	0.26 ± 0.01	0.33 ± 0.00	0.49 ± 0.01
Length (cm) †	3.44 ± 0.19	4.03 ± 0.10	5.25 ± 0.13
Velocity (m/s) †	0.23 ± 0.00	0.24 ± 0.00	0.24 ± 0.00
Peak velocity (m/s) †	0.38 ± 0.01	0.41 ± 0.01	0.46 ± 0.01

[D] Regurgitant jet properties

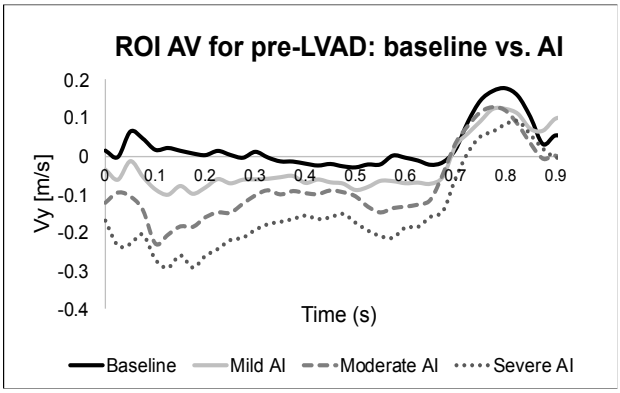

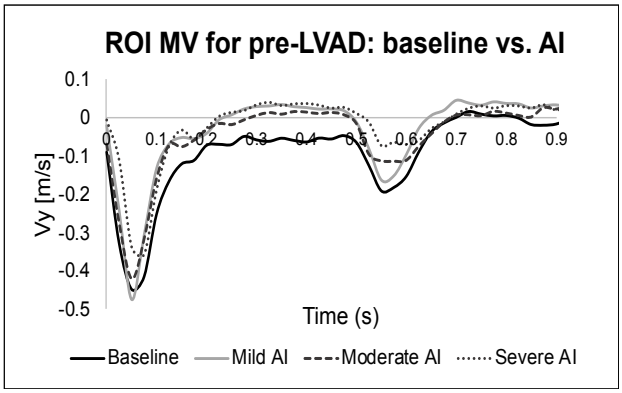

[A]

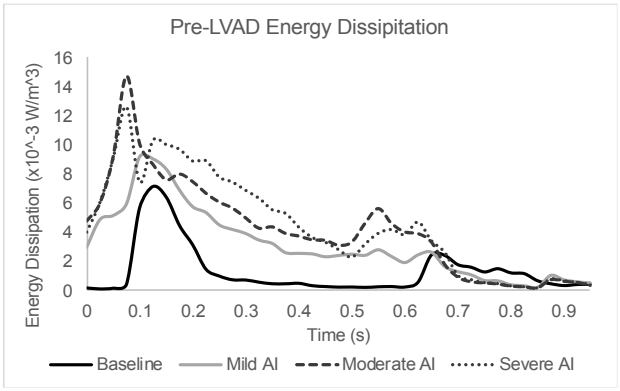

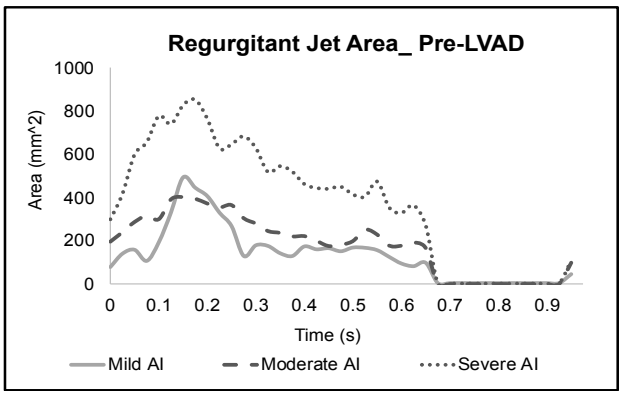

[B] [C]

Figure 4.7: Time-varying during one cardiac cycle of [A] Average velocity across the aortic valve (AV) and mitral valves (MV), [B] Energy dissipation rate and [C] Regurgitant jet area for all pre-LVAD conditions(Diastole starts at t = 0, the 2nd filling phase occurs at t = 0.525 s and the systole starts at t = 0.65 for baseline condition).

Baseline vs. Mild Aortic Insufficiency during LVAD support

In the presence of cardiac contraction (CS On) at 1 Hz frequency (or 60 cycles/minute), the interaction between cardiac contraction and AP waveforms of 4.4k LVAD speed produced a new pattern varying every 50s (Figure 4.8). The beat-to-beat LVP and AoP fluctuations were less than 5.5%, but the flow varied by 9-23%. Notably, the AV flow had the highest variation, ranging from 0.4-1.2 L/min, resulting from the alternative constructive and destructive interference of the AP(0.5 Hz) and cardiac cycle (~1Hz).

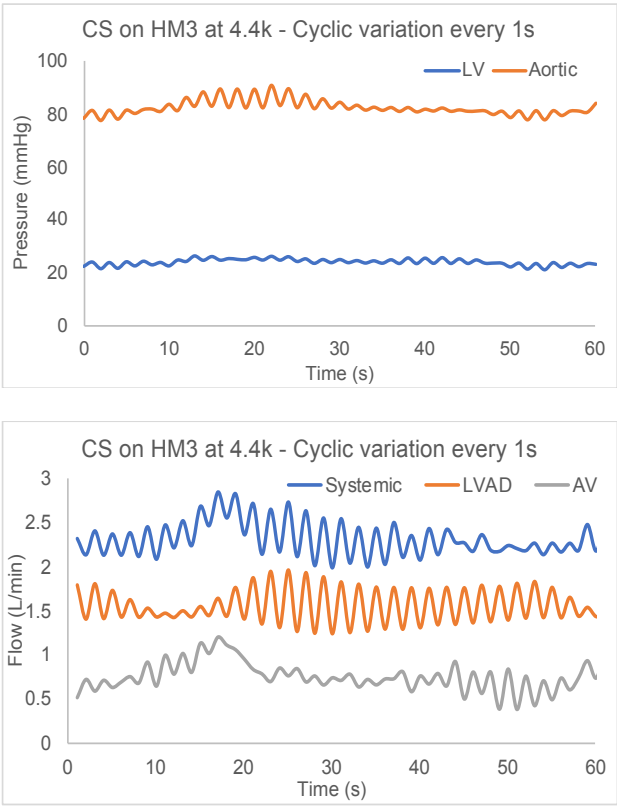

Figure 4.8: Cyclic variations (1 Hz frequency) of the left ventricle (LV) and aortic pressure, systemic, LVAD and aortic valve (AV) flow during HeartMate 3 (HM3) support with native heart function (CS on) for the Baseline condition

For the BL conditions, LVAD support significantly increased AoP, TVP, and Q_{sys}, while maintaining LVP approximately constant (Table 4.3). The increasing Q_{sys} results from a rise in LVAD flow and a reduction in AV flow. Parallel flow (positive Q_{AV} and Q ratio <1), during which a

portion of LV flow is ejected through the AV, was at low and medium LVAD speeds (4.4k and 5.4k rpm). Compared to BL condition at the same LVAD support level, the Q_{sys} and forward LVEF in Mild AI were reduced by 12% or less, while Q_{LVAD} increased 10-16%. At the lower speed, Q_{AV} and NF are positive. Series flow ($Q_{AV} \approx 0$ and Q ratio ≈ 1), when the AV is hemodynamically closed, and all flow exits the LV through the LVAD, was observed for BL at high speed (6.4k rpm). Mild AI increased Q_{LVAD} by 8% while Q_{sys} and forward LVEF were similar. Increasing LVAD speed resulted in backward Q_{AV} and negative net flow (NF), and lower AVO time.

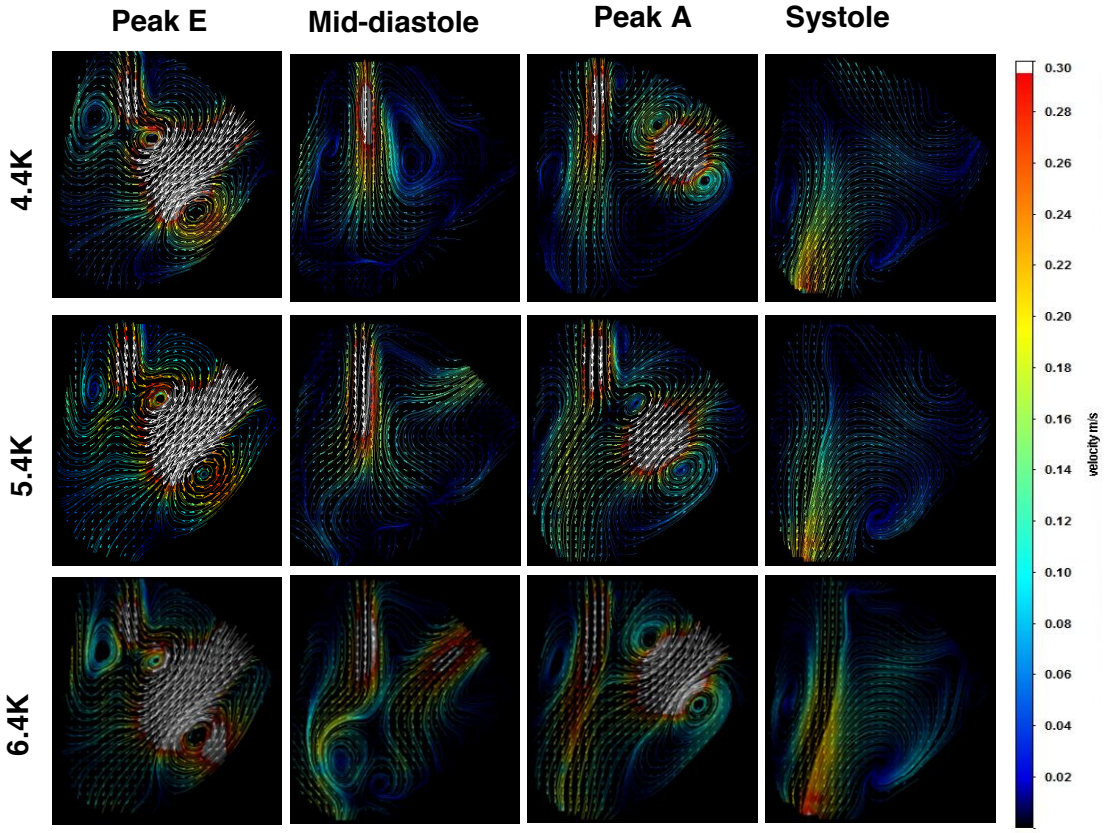

Figure 4.9: Velocity Field Images of Mild AI during different levels of HeartMate 3 supports.

In the BL condition, the presence of LVAD support increases CW and CCW circulation, KE, and vortex symmetry (Table 4.4A). The vortex trajectories for CW and CCW vortices during the CC are shown in Figure 4.10A, beginning with the MV opening, following by early and late

diastolic filling, and concluding at end-systole. For the pre-LVAD conditions, the CW vortex formed and followed a straight trajectory toward the apex during early diastole, then rolled toward the base. A weaker jet arrived with the A-wave, joined, and strengthened vortex circulation. The CW vortex moved toward the LVOT by the onset of systole. The CCW vortices appeared at early E- and A-wave filling, but decayed quickly due to confinement by the LV free wall. During Medium LVAD support, the mitral jet is pulled toward the LV apex, and a similar pattern was observed. The CCW vortex had higher circulation, while the CW vortex decayed at mid-systole.

During Mild AI conditions, vortex circulation, KE, and symmetry also increased during LVAD support (Table 4.4B). The presence of AI interfered with the mitral inflow, causing multiple vortices to form (Figure 4.9 and Figure 4.10B). For Pre-LVAD conditions, the primary vortices evolved similar to the BL condition, but the CW and CCW circulations at peak E and A were reduced. During the E-wave, secondary (2°) CW and CCW vortices appeared from the incoming RJ. The 2° CW vortex dissipated more quickly due to confinement by the septal wall, while the 2° CCW vortex moved toward the LV center and collided with the primary CW vortex. During the A-wave, the 2° CCW vortex appeared again, merged with the main CW vortex, then moved toward the AV by systole. The presence of the LVAD created a larger RJ and subsequently larger 2° CW and CCW vortices. The 2° CW vortex persisted longer as LVAD speed increased. During Medium LVAD support, the main CW vortex rolled up from the LV apex and collided with the RJ vortices at the end-diastole at the LV center. At High LVAD speed, turbulence increased in the LV with the formation of tertiary CW and CCW vortices in early diastole. The primary CCW vortex had the highest circulation and was most persistent, continuously moving flow toward the pump at the LV apex.

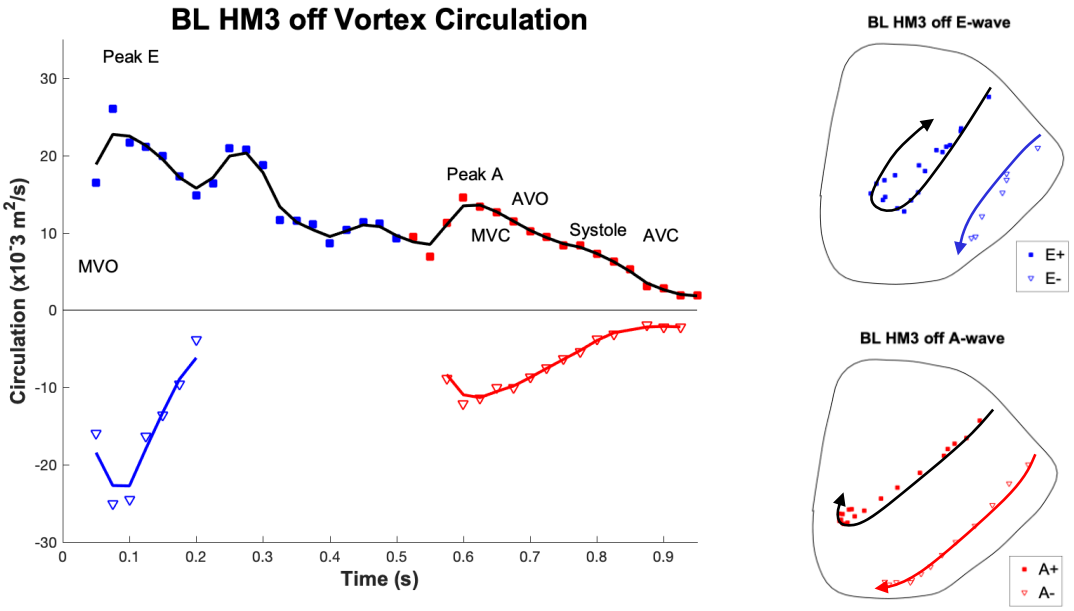

[A] Baseline

Figure 4.10: (Left) Time-varying (positive) clockwise (CW) and (negative) counterclockwise (CCW) vortex circulation are shown for [A] Baseline and [B] Mild AI conditions. (Middle, Right) Vortex core trajectories as the result of the E-wave and A-wave inflow contributions are shown: the trajectories' symbols and lines are corresponded to the circulation plot (symbol indicates the merging to vortices).

(Diastole starts at t = 0, the 2nd filling phase occurs at t = 0.525 s, and the systole starts at t = 0.65 for baseline condition). (Blue symbols denote E wave vortices, red symbols denote A wave and systolic vortices; square symbols denote main CW vortices, circle symbols denote secondary CW vortices, down-triangle symbols denote main CCW vortices, up-triangle symbols denote secondary CCW vortices; blue lines and red lines denote vortices that appear and dissipate during E wave and A wave respectively, black lines denote vortices that perpetuate the entire cardiac cycle (MVO = mitral valve opens, MVC = mitral valve closes, AVO = aortic valve opens, AVC = aortic valve closes).

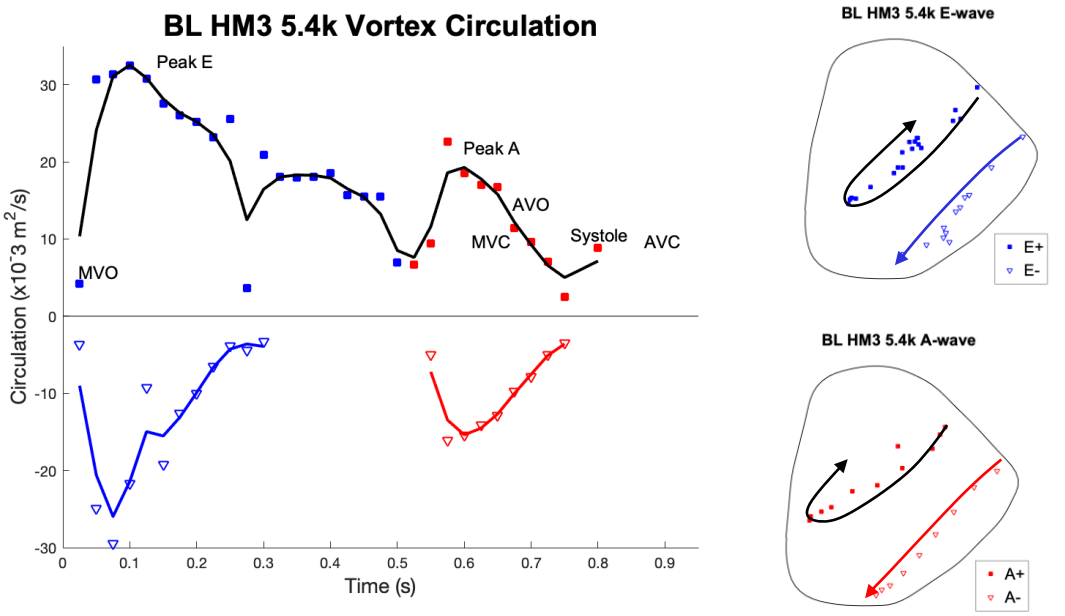

[A] Baseline

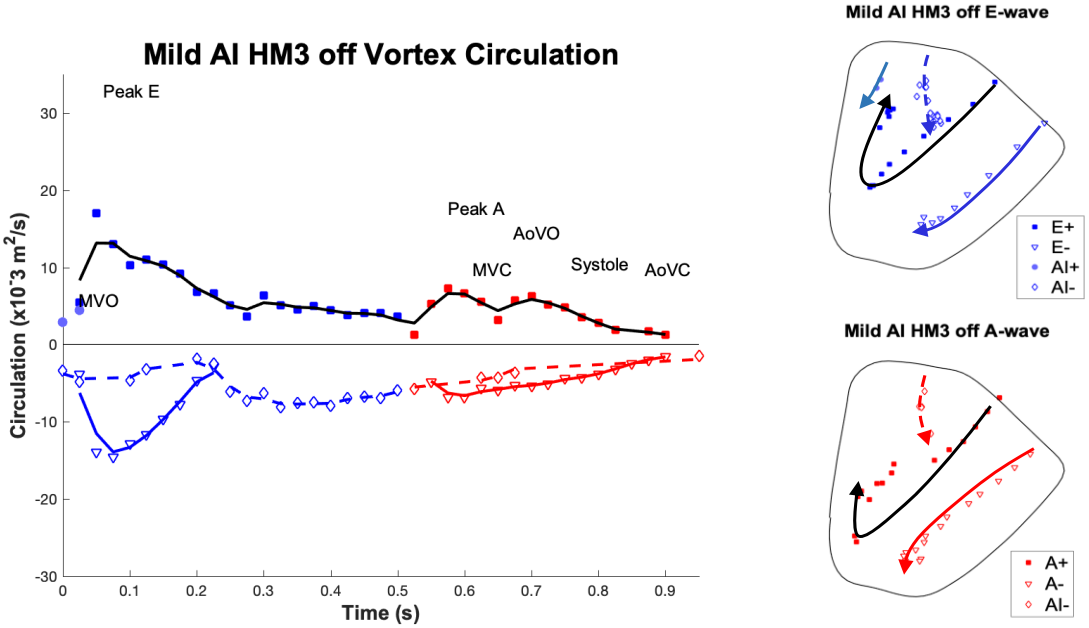

[B] Mild AI

Figure 4.10: Vortex Circulation and Trajectories (cont.)

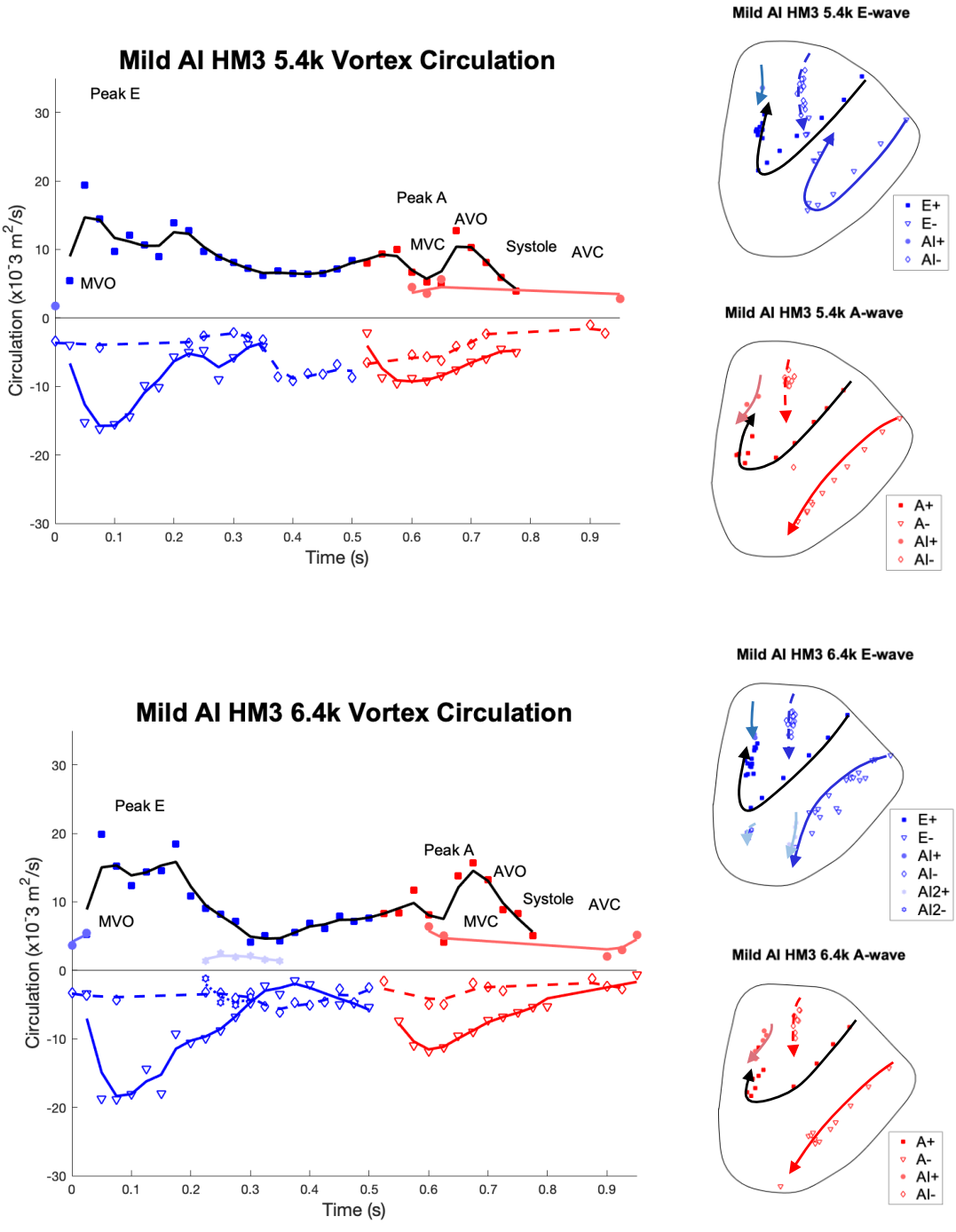

[B] Mild AI

Figure 4.10: Vortex Circulation and Trajectories (cont.)

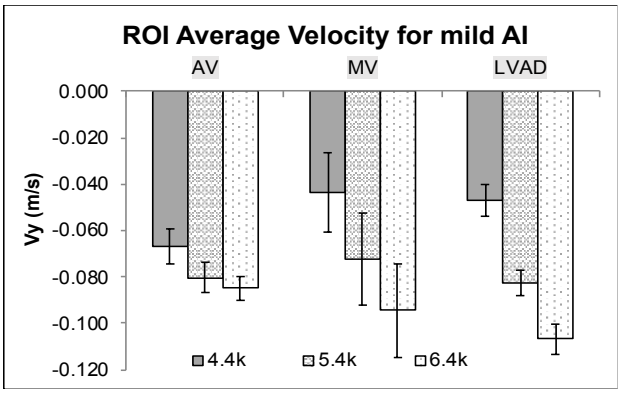

[A]

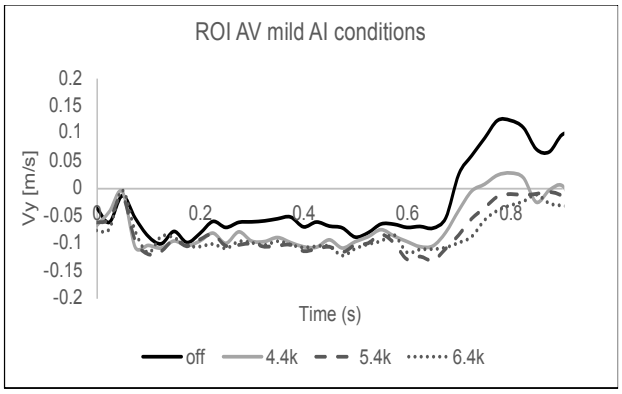

[B]

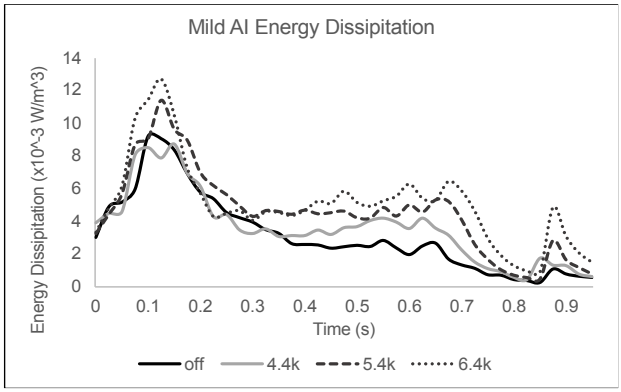

[C]

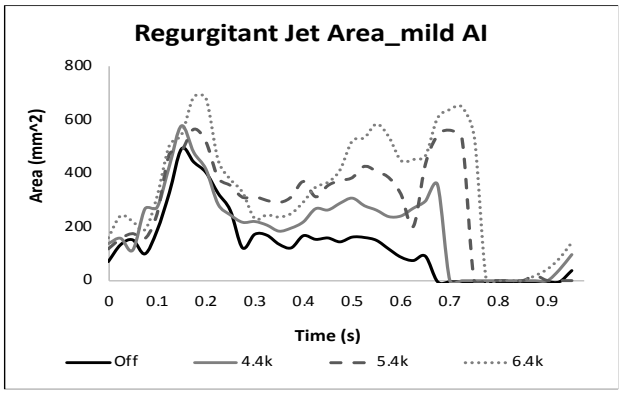

[D]

Figure 4.11: [A] Average velocity in the region of interest at aortic valve (AV), mitral valve, and LVAD. Time-varying during one cardiac cycle of [B] Average velocity at the AV, [C] Energy dissipation rate, and [D] Regurgitant jet area for mild AI conditions. (Diastole starts at t = 0, the 2nd filling phase occurs at t = 0.525 s, and the systole starts at t = 0.65 for baseline condition).

Average ROI velocities are shown in Figure 4.11A (negative velocity indicated incoming velocities toward the LV and toward the LVAD inlet). As LVAD speed increased, the average velocities increased by 20-27%, 66-117%, and 76-128% for the AV, MV, and LVAD inflow ROI, respectively. In addition, the presence of LVAD support increased EDR by 15-61% and RJ area by 41-106% from the pre-LVAD condition (Figure 3.14C, D). Higher LVAD speed resulted in larger RJ dimensions (area, diameter, length) (Table 4.5A). The time-varying plots of ROI AV and RJ area (Figure 4.11B and D) show the prolonged diastolic phase under high LVAD support.

Table 4.3: Hemodynamics result (mean ± standard error) of Baseline (normal valve), Mild, Moderate, and Severe aortic insufficiency (AI) conditions in the presence of native cardiac function (CS on).

(LVP (LV pressure), AoP (Aortic pressure), Q_{sys} (total systemic flow), Q_{LVAD} (LVAD flow), Q_{AV} (flow through aortic valve), Q_{ratio} (Flow ratio), PI (Aortic pulsatility index), RF (regurgitant fraction), NF (net flow through AV), LVEF (left ventricle ejection fraction), S/D ratio (ratio between the systolic and diastolic peak of LVAD velocity), A_{dia} (diastolic acceleration), EDPS (early diastolic phase slope), rpm (rotations per minute), AVO (aortic valve opening) time).
(† Statistical significance ($p<0.01$) for tested conditions).

4.4k rpm Parameters	**Baseline**	**Mild AI**	**Moderate AI**	**Severe AI**
LVP (mmHg)	24.59 ± 0.25	24.54 ± 0.22	31.52 ± 0.15	27.13 ± 0.23
AoP (mmHg)	82.96 ± 0.14	80.71 ± 0.10	87.26 ± 0.07	88.40 ± 0.11
TVP (mmHg)	58.37	56.17	55.74	61.27
Q_{sys} (L/min)	2.35 ± 0.02	2.08 ± 0.02	1.72 ± 0.02	1.29 ± 0.02
Q_{LVAD} (L/min)	1.57 ± 0.01	1.82 ± 0.01	1.85 ± 0.01	1.93 ± 0.01
Q_{AV} (L/min) †	0.78	0.26	-0.12	-0.64
Q ratio	0.67	0.88	1.07	1.49
PI	8.34	10.33	12.80	14.88
NF (%)	33.05	10.91	-5.23	-27.23
Forward LVEF (%)	20.73	19.05	15.34	11.62
S/D ratio		2.71	2.72	2.71
A_{dia} (cm/s^2)		10.61	11.73	13.52
EDPS (L/min/sec)		-20.05	-19.05	-19.55
AVO time (sec)	0.19	0.19	0.18	0.15

[A] Low LVAD speed

Table 4.3: (cont.)

5.4k rpm Parameters	Baseline	Mild AI	Moderate AI	Severe AI
LVP (mmHg)	26.01 ± 0.28	25.26 ± 0.24	27.84 ± 0.16	27.91 ± 0.25
AoP (mmHg) †	99.95 ± 0.10	98.96 ± 0.06	99.41 ± 0.05	103.02 ± 0.07
TVP (mmHg)	73.94	73.70	71.57	75.11
Q_{sys} *(L/min)* †	3.46 ± 0.02	3.21 ± 0.01	2.96 ± 0.01	2.20 ± 0.02
Q_{LVAD} *(L/min)*	3.14 ± 0.01	3.46 ± 0.01	3.68 ± 0.01	3.60 ± 0.01
Q_{AV} *(L/min)* †	0.32	-0.25	-0.72	-1.40
Q ratio †	0.91	1.08	1.24	1.64
PI	4.56	4.94	5.85	6.94
NF (%)	9.28	-7.25	-20.85	-40.43
Forward LVEF (%)	31.05	29.41	26.67	20.11
S/D ratio		1.86	1.89	2.02
A_{dia} *(cm/s²)*		7.24	7.26	7.31
EDPS (L/min/sec)		-17.01	-16.74	-17.43
AVO time (sec)	0.16	0.16	0.14	0.10

[B] Medium LVAD speed

6.4k rpm Parameters	Baseline	Mild AI	Moderate AI	Severe AI
LVP (mmHg) †	23.94 ± 0.29	21.49 ± 0.22	26.72 ± 0.16	26.43 ± 0.24
AoP (mmHg) †	109.81 ± 0.07	110.69 ± 0.04	109.65 ± 0.03	108.24 ± 0.04
TVP (mmHg) †	85.87	89.19	82.94	81.81
Q_{sys} *(L/min)* †	4.63 ± 0.01	4.68 ± 0.01	4.15 ± 0.01	3.52 ± 0.01
Q_{LVAD} *(L/min)* †	4.66 ± 0.01	5.04 ± 0.01	5.32 ± 0.01	5.41 ± 0.01
Q_{AV} *(L/min)* †	-0.03	-0.36	-1.18	-1.88
Q ratio †	1.01	1.08	1.28	1.53
PI	2.65	2.46	3.10	3.10
NF (%)	-0.70	-7.72	-25.44	-40.73
Forward LVEF (%)	41.69	42.66	37.17	31.29
S/D ratio		1.58	1.53	1.51
A_{dia} *(cm/s²)*		2.65	4.64	4.69
EDPS (L/min/sec)		-16.25	-14.13	-13.43
AVO time (sec)	0.13	0.13	0.00	0.00

[C] High LVAD speed

LVAD support worsens AI severity

The AV flow of BL and AI conditions at low, medium, and high LVAD support are shown in Figure 4.12. The interaction between the cardiac contraction and the AP produces an interference pattern that repeats approximately every 50s. During low LVAD support, forward flow

occurred in Mild AI conditions at an average of 0.26 L/min, 67% lower than the BL's average, and more than 140% higher than the Moderate and Severe AI conditions. Increasing LVAD speed lowered the fluctuation of AV flow and produced backward flow in all AI conditions.

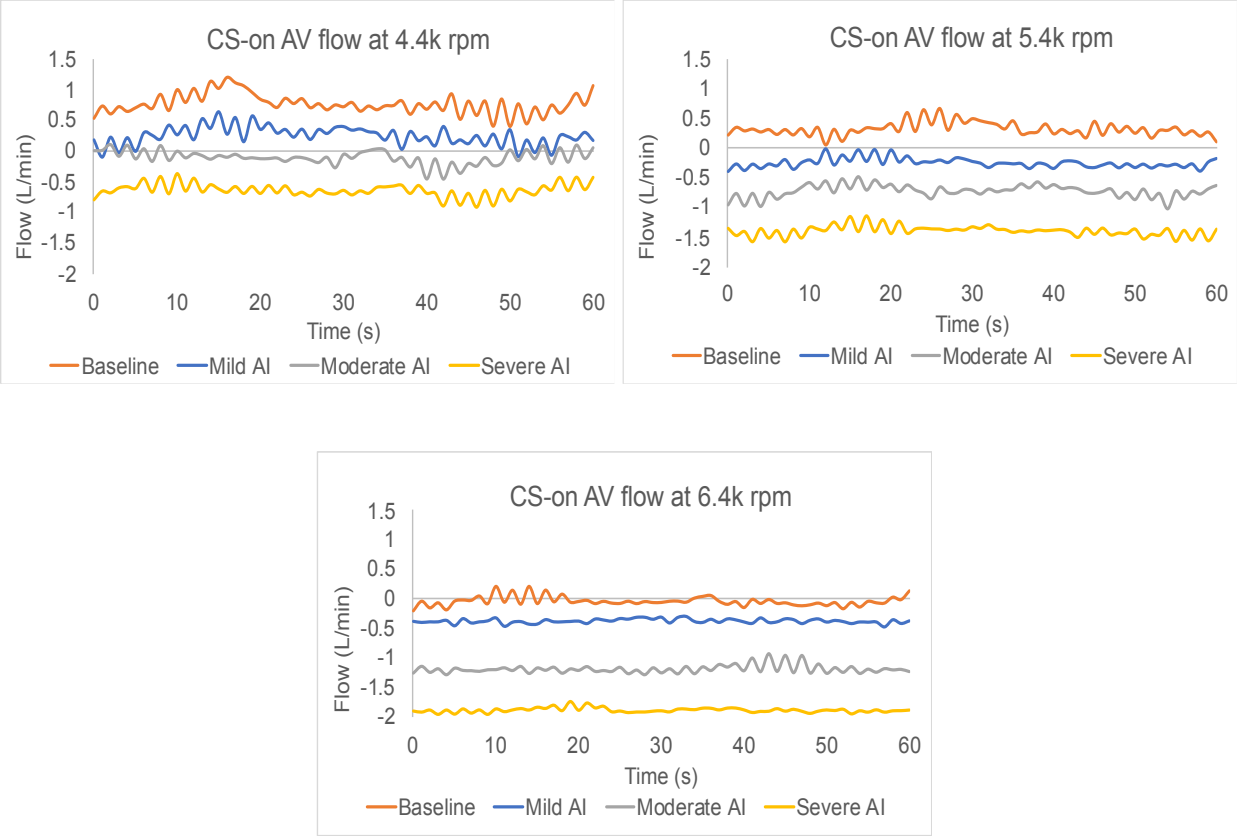

Figure 4.12: Cyclic variations (every 1s) of flow through the aortic valve during low, medium, and high HeartMate 3 support of Baseline, Mild, Moderate, and Severe AI conditions.

At the same LVAD speed, the LVP, AoP, and TVP were similar across all AI groups (Table 4.3). For Moderate and Severe AI, Q_{sys} and forward LVEF reduced by 10-27% and 24-45%, while Q_{LVAD} increased by 14-17% and 14-23% compared to BL at the same speed. Negative Q_{AV} (backward flow) and NF occurred in Mild AI during medium and high LVAD support, and in all LVAD conditions of Moderate and Severe AI. The Q ratio increased at higher LVAD speed and was greater than one when Q_{LVAD} exceeded Q_{sys}. For the same AI severity, the ratio between the systolic and diastolic peak of LVAD velocity (S/D ratio) and the diastolic acceleration (A_{dia})

decreased, while the early diastolic phase slope (EDPS) values increased. Vortex properties of different AI groups are shown in Table 4.4. As AI worsened, vortex circulation and KE increased. For the same AI severity, a higher LVAD speed increased CCW vortex circulation and KE and decreased vortex symmetry compared to a lower speed.

Table 4.4: Intraventricular vortex properties (mean ± standard error) of Baseline (normal valve), Mild, Moderate, and Severe aortic insufficiency (AI) conditions in the presence of native cardiac function (CS on) (Clockwise (CW), and counter-clockwise (CCW)).
(In the case which had multiple CW and CCW vortices occurrences: total CW and CCW vortex circulation and kinetic energy, radius/aspect ratio/vortex symmetry of the primary (largest) CW and CCW vortex were reported). († Statistical significance ($p<0.01$) for different LVAD speeds).

Baseline Parameters		**4.4k**	**5.4k**	**6.4k**
Circulation ($x10^{-3}$ m^2/s)	*CW* †	12.93 ± 1.29	15.32 ± 1.77	21.93 ± 1.94
	CCW †	-5.22 ± 1.27	-7.22 ± 1.43	-10.76 ± 1.74
Total Kinetic Energy (mJ/m) †		1.78 ± 0.42	2.75 ± 0.64	4.34 ± 0.90
Kinetic Energy (mJ/m)	*CW* †	0.98 ± 0.19	1.45 ± 0.29	2.29 ± 0.42
	CCW †	0.80 ± 0.24	1.30 ± 0.36	2.05 ± 0.50
Radius (cm)	*CW* †	0.80 ± 0.05	0.82 ± 0.05	0.95 ± 0.05
	CCW †	0.42 ± 0.03	0.41 ± 0.02	0.48 ± 0.04
Aspect Ratio	*CW* †	1.93 ± 0.10	2.03 ± 0.12	1.86 ± 0.08
	CCW †	1.83 ± 0.23	1.93 ± 0.18	1.89 ± 0.21
Vortex symmetry CW:CCW †		1.82 ± 0.16	2.15 ± 0.24	2.16 ± 0.28

[A] Baseline conditions during different LVAD speeds

Mild AI Parameters		**4.4k**	**5.4k**	**6.4k**
Circulation ($x10^{-3}$ m^2/s)	*CW*	6.49 ± 0.66	8.31 ± 0.81	10.15 ± 1.02
	CCW	-7.58 ± 0.69	-8.12 ± 0.80	-9.19 ± 0.94
Total Kinetic Energy (mJ/m) †		0.76 ± 0.14	1.02 ± 0.19	1.25 ± 0.21
Kinetic Energy (mJ/m)	*CW*	0.36 ± 0.07	0.52 ± 0.10	0.65 ± 0.11
	CCW	0.41 ± 0.07	0.50 ± 0.09	0.60 ± 0.11
Radius (cm)	*CW*	0.42 ± 0.02	0.49 ± 0.04	0.44 ± 0.02
	CCW	0.42 ± 0.02	0.52 ± 0.05	0.45 ± 0.05
Aspect Ratio	*CW*	1.96 ± 0.14	2.54 ± 0.20	2.35 ± 0.18
	CCW	1.90 ± 0.12	1.85 ± 0.17	2.12 ± 0.22
Vortex symmetry CW:CCW		1.07 ± 0.07	0.94 ± 0.10	0.98 ± 0.10

[B] Mild AI conditions during different LVAD speeds

Table 4.4: (cont.)

Moderate AI Parameters		**4.4k**	**5.4k**	**6.4k**
Circulation ($x10^{-3}$ m^2/s)	*CW*	8.65 ± 0.89	10.77 ± 0.96	13.18 ± 1.09
	CCW	-12.35 ± 0.98	-12.30 ± 0.89	-13.07 ± 0.98
Total Kinetic Energy (mJ/m) †		1.06 ± 0.14	1.41 ± 0.16	1.75 ± 0.22
Kinetic Energy (mJ/m)	*CW* †	0.50 ± 0.07	0.74 ± 0.09	0.76 ± 0.12
	CCW	0.56 ± 0.07	0.68 ± 0.08	0.79 ± 0.11
Radius (cm)	*CW*	0.40 ± 0.02	0.41 ± 0.03	0.45 ± 0.04
	CCW	0.63 ± 0.05	0.61 ± 0.03	0.64 ± 0.04
Aspect Ratio	*CW*	2.63 ± 0.18	2.35 ± 0.14	2.20 ± 0.13
	CCW	1.72 ± 0.08	2.17 ± 0.15	2.51 ± 0.18
Vortex symmetry CW:CCW		0.63 ± 0.07	0.67 ± 0.11	0.69 ± 0.10

[C] Moderate AI conditions during different LVAD speeds

Severe AI Parameters		**4.4k**	**5.4k**	**6.4k**
Circulation ($x10^{-3}$ m^2/s)	*CW*	12.74 ± 1.06	11.65 ± 1.15	12.68 ± 1.12
	CCW	-11.75 ± 1.04	-13.13 ± 1.11	-15.34 ± 1.20
Total Kinetic Energy (mJ/m)		1.41 ± 0.16	1.58 ± 0.19	1.96 ± 0.22
Kinetic Energy (mJ/m)	*CW*	0.76 ± 0.08	0.75 ± 0.10	0.95 ± 0.12
	CCW †	0.66 ± 0.09	0.83 ± 0.11	1.00 ± 0.11
Radius (cm)	*CW*	0.65 ± 0.05	0.66 ± 0.06	0.63 ± 0.06
	CCW	0.58 ± 0.04	0.53 ± 0.03	0.64 ± 0.04
Aspect Ratio	*CW*	2.49 ± 0.15	2.38 ± 0.17	2.80 ± 0.21
	CCW	1.79 ± 0.14	2.18 ± 0.15	2.60 ± 0.21
Vortex symmetry CW:CCW		1.27 ± 0.10	1.29 ± 0.09	0.99 ± 0.10

[D] Severe AI conditions during different LVAD speeds

The SV of LVAD, AV, and systemic are shown in Table 4.5 and Figure 4.13 for all conditions. LVAD support increased total SV during BL conditions by increasing flow through the LVAD and reducing flow through the AV. As LVAD speed increased from 4.4k to 6.4k, systemic and LVAD SV increased by 468% and 534% during diastole, and by 6.5% and 62% during systole, respectively. When AI is present, a similar pattern with more dramatic changes in systemic and LVAD diastolic SV were noted. During filling, higher LVAD speed increased the systemic SV but caused backward flow through the AV. The backward flow occurred in all AI groups and increased as AI worsened. During systole, increased LVAD SV was coupled with a decrease in AV SV. Negative AV SV was observed in Moderate and Severe AI during high LVAD support.

Table 4.5: Diastole and systole systemic, aortic valve (AV), and LVAD stroke volume (mean ± standard error)

4.4k Parameters		**Baseline**	**Mild AI**	**Moderate AI**	**Severe AI**
Systemic SV (mL)	Diastole	7.65 ± 0.46	4.48 ± 1.36	-1.32 ± 0.81	-2.79 ± 0.64
	Systole	29.66 ± 0.27	29.81 ± 0.30	28.93 ± 0.21	23.71 ± 0.26
AV SV (mL)	Diastole	0.53 ± 0.35	-5.54 ± 0.15	-12.26 ± 0.34	-14.81 ± 0.21
	Systole	10.76 ± 0.42	9.49 ± 0.33	9.68 ± 0.24	4.07 ± 0.38
LVAD SV (mL)	Diastole	7.12 ± 0.51	25.18 ± 4.36	10.94 ± 0.56	12.02 ± 0.49
	Systole	18.90 ± 0.45	15.68 ± 0.73	19.26 ± 0.07	19.64 ± 0.14
5.4k Parameters					
Systemic SV (mL)	Diastole	26.41 ± 0.33	25.22 ± 1.34	21.13 ± 0.43	14.26 ± 0.76
	Systole	29.47 ± 0.09	27.71 ± 0.38	26.87 ± 0.18	21.94 ± 0.16
AV SV (mL)	Diastole	-0.73 ± 0.17	-5.89 ± 0.20	-14.44 ± 0.15	-20.51 ± 0.18
	Systole	5.45 ± 0.12	1.52 ± 0.13	2.53 ± 0.14	-2.26 ± 0.14
LVAD SV (mL)	Diastole	27.14 ± 0.41	14.66 ± 3.26	35.57 ± 0.35	34.78 ± 0.81
	Systole	24.03 ± 0.10	17.40 ± 0.71	24.34 ± 0.10	24.21 ± 0.17
6.4k Parameters					
Systemic SV (mL)	Diastole	43.45 ± 0.27	45.57 ± 1.19	37.79 ± 0.83	31.17 ± 0.71
	Systole	31.60 ± 0.13	31.22 ± 0.45	29.12 ± 0.60	25.15 ± 0.49
AV SV (mL)	Diastole	-1.67 ± 0.14	-5.59 ± 0.10	-16.67 ± 0.20	-23.79 ± 0.16
	Systole	0.92 ± 0.12	-0.42 ± 0.06	-2.85 ± 0.17	-7.14 ± 0.25
LVAD SV (mL)	Diastole	45.12 ± 0.16	13.17 ± 2.86	54.45 ± 0.78	54.96 ± 0.84
	Systole	30.68 ± 0.03	13.35 ± 1.02	31.97 ± 0.94	32.29 ± 0.74

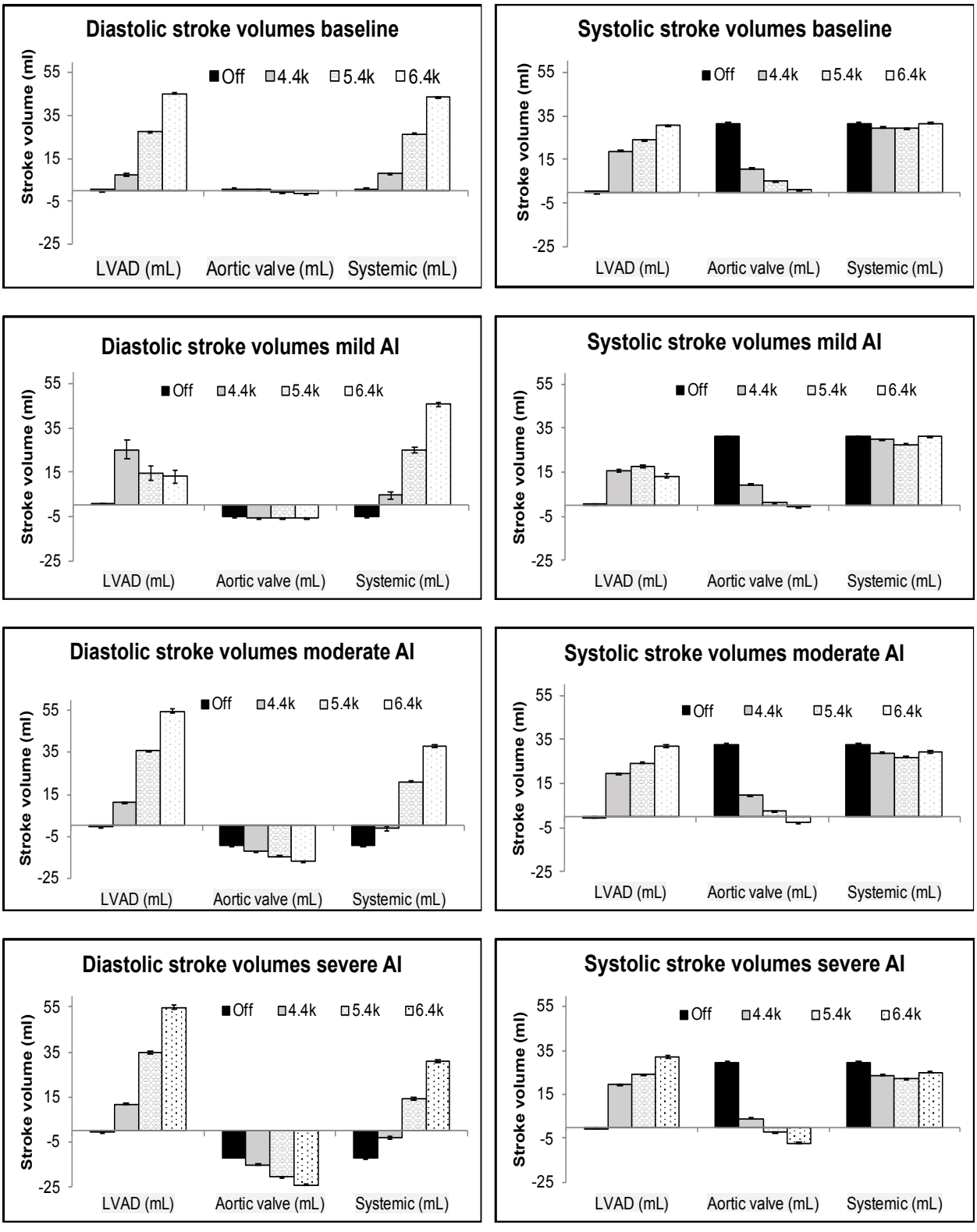

Figure 4.13: Stroke volume during diastolic and systolic for Baseline, Mild, Moderate, and Severe AI conditions.

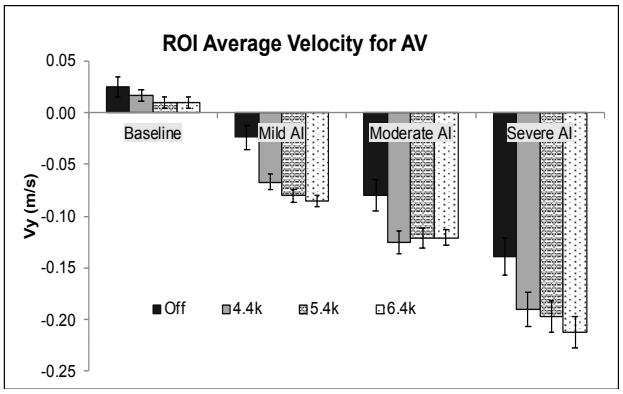

[A]

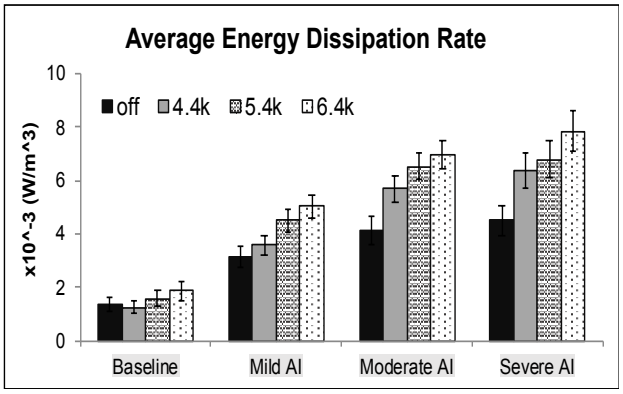

[B]

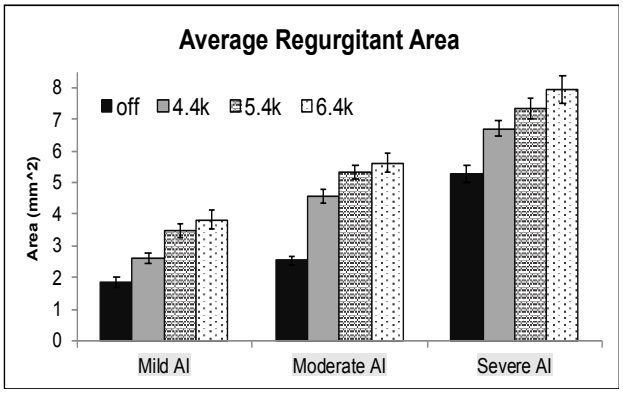

[C]

Figure 4.14: [A] Average velocity in the region of interest at the aortic valve, [B] Average energy dissipation rate, and [C] Average regurgitant area for all conditions (cont.)

Table 4.6: Regurgitant jet properties (mean ± standard error) of Mild, Moderate, and Severe aortic insufficiency (AI) conditions in the presence of native cardiac function (CS on). († Statistical significance ($p<0.01$) for different LVAD speeds).

Mild AI	**4.4k**	**5.4k**	**6.4k**
Area (cm^2) †	2.62 ± 0.18	3.48 ± 0.22	3.82 ± 0.30
Max Diameter (cm) †	0.97 ± 0.05	1.19 ± 0.05	1.22 ± 0.07
Vena Contracta Width (cm) †	0.37 ± 0.01	0.43 ± 0.01	0.44 ± 0.02
Length (cm) †	3.85 ± 0.18	4.51 ± 0.20	4.78 ± 0.25
Velocity (m/s) †	0.24 ± 0.00	0.25 ± 0.00	0.24 ± 0.01
Peak velocity (m/s) †	0.41 ± 0.01	0.44 ± 0.01	0.44 ± 0.02

[A] Mild AI conditions during different LVAD speeds

Moderate AI	**4.4k**	**5.4k**	**6.4k**
Area (cm^2) †	4.56 ± 0.21	5.34 ± 0.23	5.62 ± 0.31
Max Diameter (cm)	1.55 ± 0.04	1.65 ± 0.05	1.67 ± 0.07
Vena Contracta Width (cm) †	0.38 ± 0.01	0.38 ± 0.01	0.41 ± 0.02
Length (cm) †	5.10 ± 0.16	5.63 ± 0.15	5.62 ± 0.22
Velocity (m/s)	0.26 ± 0.00	0.27 ± 0.00	0.27 ± 0.01
Peak velocity (m/s)	0.50 ± 0.01	0.53 ± 0.01	0.52 ± 0.02

[B] Moderate AI conditions during different LVAD speed

Severe AI	**4.4k**	**5.4k**	**6.4k**
Area (cm^2) †	6.69 ± 0.24	7.34 ± 0.35	7.93 ± 0.44
Max Diameter (cm) †	1.87 ± 0.08	2.18 ± 0.09	2.37 ± 0.12
Vena Contracta Width (cm)	0.53 ± 0.01	0.57 ± 0.02	0.61 ± 0.03
Length (cm) †	6.07 ± 0.14	6.09 ± 0.16	5.92 ± 0.22
Velocity (m/s)	0.27 ± 0.00	0.27 ± 0.00	0.28 ± 0.1
Peak velocity (m/s)	0.54 ± 0.01	0.54 ± 0.02	0.56 ± 0.2

[C] Severe AI conditions during different LVAD speeds

Average ROI velocity is shown in Figure 3.14A, in which velocity of flow moved toward the aorta was designated as positive (forward), while the flow toward the LV was designated as negative (backward). Increasing in LVAD speed decreased forward AV velocity in the BL condition, and increased backward AV velocity in AI conditions. Larger average EDR occurred with higher LVAD support and more severe AI (Figure 3.14B). Moreover, higher average area, diameter, and length of the jet occurred when LVAD support increased (Figure 3.14C and Table 4.6). Compared to the pre-LVAD condition, RJ areas increased the least when LVAD speed

changed from 4.4k to 6.4k rpm in Severe AI (Table 4.7). However, in post-LVAD, the jet area increased the most (46%) with pump speed in Mild AI. The maximum diameter, length, and peak velocity of the RJ followed similar patterns. The quantitative clinical parameters increased with worsening AI and higher LVAD support except for the RF (Table 4.8).

Table 4.7: Percentage change of average RJ area in Mild and Severe AI

Average RJ area	*% changes from Pre-LVAD to*		*% changes from 4.4k to 6.4k rpm*
	4.4k rpm	*6.4k rpm*	
Mild AI	41	106	46
Moderate AI	80	121	23
Severe AI	27	50	18

Table 4.8: Quantitative clinical parameters for grading AI

Mild AI	*VC width (cm)*	*Jet width/ LVOT width (%)*	*Jet CSA/ LVOT CSA (%)*	*Regurgitant Volume (mL/beat)*	*Regurgitant fraction (%)*	*EROA (cm^2)*
Off	0.26	31	8	5.23	20	0.34
4.4k	0.27	37	14	5.54	13	0.32
5.4k	0.43	46	21	5.90	8	0.31
6.4k	0.44	47	22	6.01	0	0.29
Moderate AI						
Off	0.33	40	16	9.28	28	0.57
4.4k	0.38	60	26	112.26	36	0.60
5.4k	0.38	63	40	14.44	17	0.69
6.4k	0.41	64	41	19.51	12	0.85
Severe AI						
Off	0.49	61	37	11.91	45	0.72
4.4k	0.53	72	52	14.81	82	0.76
5.4k	0.57	84	70	22.78	58	1.09
6.4k	0.61	91	83	30.93	31	1.34

T_R maps of the LV following 20CC varied notably among the different conditions (Figure 4.15 and Table 4.9). The Pre-LVAD BL case exhibited the lowest T_R and residual region of 21% (T_R > 2 cycles) followed by Moderate, Severe, and Mild AI. The residual region formed underneath the AV base in BL case and was located along the LVOT and LV free-wall in AI cases. After LVAD

implantation, the T_R and residual regions varied depended on LVAD speeds. In BL, Moderate and Severe AI conditions, LVAD support decreased T_R and residual area. Mild AI experienced increasing T_R during LVAD support. Regardless of LVAD support level, Moderate AI had the lowest T_R, followed by BL, Severe, and Mild AI. The distributions of residual regions in post-LVAD were similar to the pre-LVAD conditions.

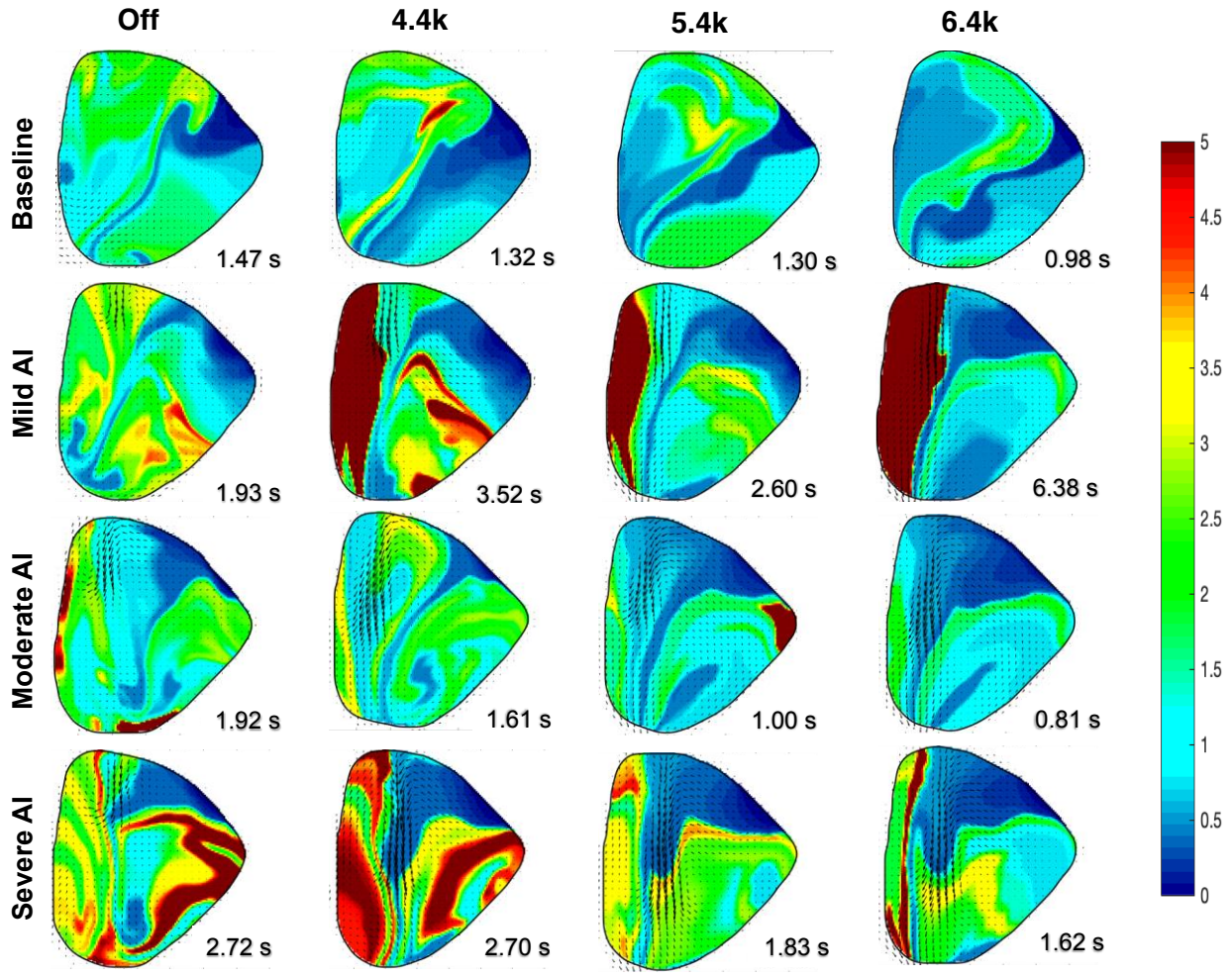

Figure 4.15: Left ventricle maps of residence time calculated for the midplane area over 20 cycles of integration are shown for CS-On conditions.

Table 4.9**:** Residence time (T_R) summary after 20 cardiac cycles of CS-On Baseline (normal valve), Mild, Moderate, and Severe aortic insufficiency (AI) conditions.

Parameter		*Average T_R (s)*	*% T_R area > 2CC (%)*	*Average T_R of area > 2CC (s)*
Baseline	*Off*	1.47	20.79	2.34
	4.4k	1.32	18.47	2.64
	5.4k	1.30	13.59	2.36
	6.4k	0.98	4.44	2.27
Mild AI	*Off*	1.93	47.75	3.00
	4.4k	3.52	47.5	5.58
	5.4k	2.60	34.29	4.51
	6.4k	6.38	30.73	13.91
Moderate AI	*Off*	1.92	29.55	5.01
	4.4k	1.61	37.02	2.48
	5.4k	1.00	6.07	3.37
	6.4k	0.81	5.57	2.05
Severe AI	*Off*	2.72	62.62	3.89
	4.4k	2.70	59.62	3.96
	5.4k	1.83	53.48	2.8
	6.4k	1.62	31.48	2.76

4.4 Discussion

Hemodynamics Parameters to Assess AI Severity During LVAD Support

This study presents a side-by-side comparison of the intraventricular flow dynamics of a dilated heart failure model during normal AV function and graded AI combined with centrifugal continuous flow HM3 support. Characterization of the hemodynamics, intraventricular flow field, and residence time provide insight into the features of valve dysfunction that can be applied to improving early diagnosis and possible interventions. The pre-LVAD AI classifications used in this study agree with clinical guidelines[162,192]. The RF and EROA decreased due to the unloading effect of LVAD, while the jet CSA/LVOT CSA had the highest percentage of changes (Figure 4.16 (left)). For the jet properties, the RJ area changed significantly, up to 36% higher than the VC width (Figure 4.16 (right)). The normalized changes of different echo parameters were shown in Figure 4.17, as AI severity was classified according to the current AHA standard[151]. The RegV

underestimated AI severity, while RF suggested AI improving with high LVAD support, contracting with other parameters (Figure 4.17).

As discussed in Chapter 3, S/D ratio, $A_{dia,}$ and EDPS have been proposed as new indices to assess AI in LVAD patients[195,262]. Our measurements of these variables did not reflect the sensitivity described in previous publications. As the AI model progressed from Mild to Severe, the indices matched with the previous description of worsening AI. For an LVAD speed increase from 4.4k to 6.4k for each of the three AI groups, A_{dia} indicated AI improvement, disagreeing with S/D the ratio and EDPS. The result implied that these indices might not be suitable for evaluating AI severity during HM3 support. Moreover, the AP features incorporated into HM3 speed control caused some cycle-to-cycle flow variations. Indices, calculating from LVAD flow, changed between cycles and must be collected and averaged from 50 or more cycles to ensure their accuracy in characterizing AI. Similar to the HM2 results discussed in Chapter 3, the NF decreased when AI worsened or increased LVAD speed (Table 4.11). Forward LVEF increased with LVAD support for each AI group, following the increase of systemic SV. The results suggest that forward LVEF is not sensitive to LVAD speed change, but NF is and could be used to quantify AI severity during LVAD support.

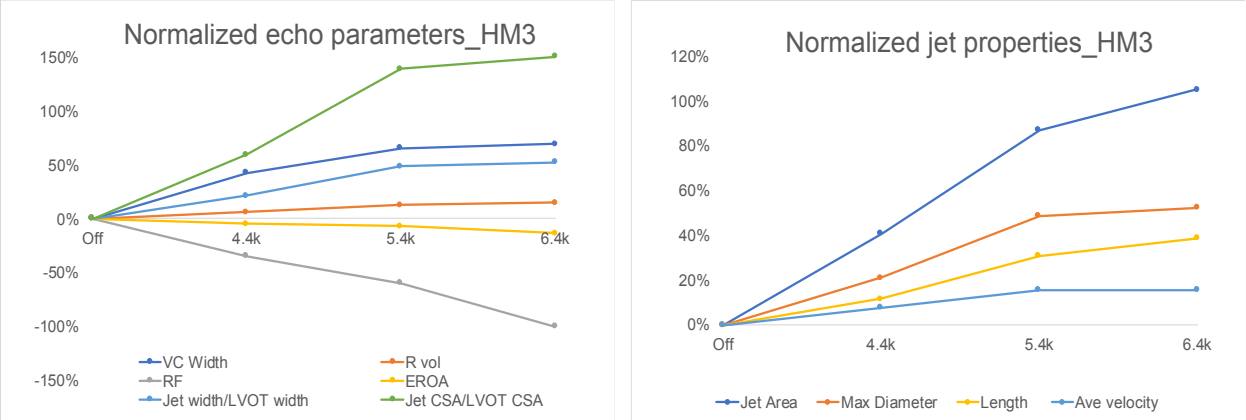

Figure 4.16: Percentage change of different AI indices from pre-LVAD

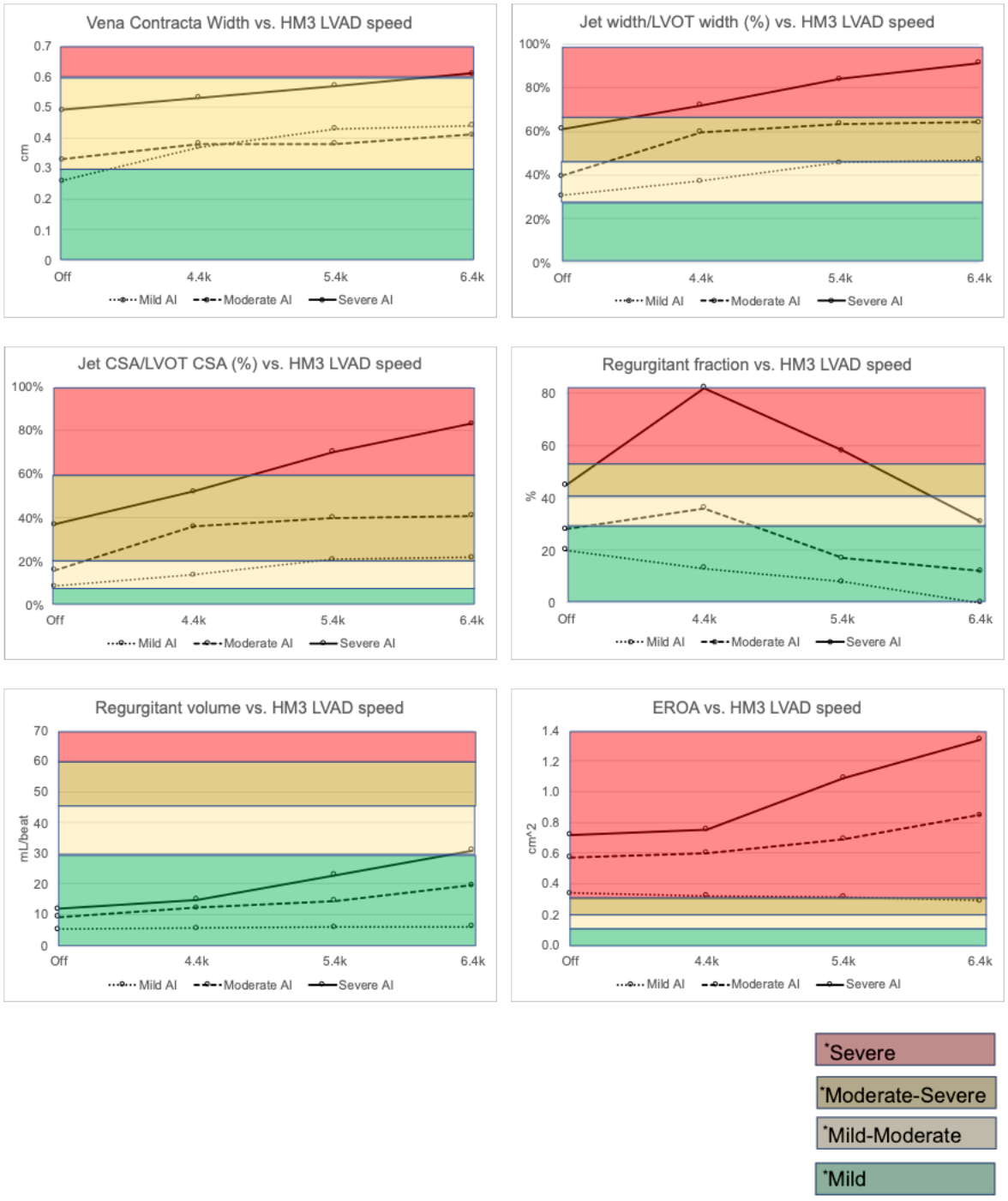

Figure 4.17: Sensitivity of echo quantitative parameters as a function of LVAD speed

Table 4.10: Post-LVAD AI assessment indices characterized base on AI severity and LVAD speed.

Parameters trends	AI severity: Mild→ Severe				LVAD speed: 4.4k → 6.4k rpm		
	4.4k	5.4k	6.4k		Mild AI	Moderate AI	Severe AI
S/D ratio	~	↑ slightly	↓ slightly		↓	↓	↓
A_{dia}	↑	~	↑		↓	↓	↓
EDPS ≥ -17.6	No	Yes	Yes		Yes	Yes	Yes

Table 4.11: Net flow (NF) and forward left ventricle ejection fraction (LVEF) trends during the post-LVAD study.

Parameters trends	AI severity: Mild→ Severe				LVAD speed: 4.4k → 6.4k rpm		
	4.4k	5.4k	6.4k		Mild AI	Moderate AI	Severe AI
NF (%)	↓	↓	↓		↓	↓	↓
Forward LVEF (%)	↓	↓	↓		↑	↑	↑

Effects of AI during HeartMate 3 support

The vortex structure observed in the pre-LVAD BL condition was similar to that described in Chapter 3 and previous publications[245,247,248]. The vortex pattern closely resembled those of dilated cardiomyopathy patients with larger circulation and KE[245,253,254]. During HM3 support, vortex circulation patterns and trajectories were measured that were similar to those measured for HM2 support[59,255]. Pre-LVAD AI increased CCW vortex circulation, especially in Severe cases. Due to the interaction of RJ with septum wall and mitral inflow, multiple vortices were observed[254–256]. AI combined with LVAD support featured a dominant RJ, and the AP perturbation that enabled the primary CW vortex to roll up and move toward the AV even during high LVAD speed. EDR increased with AI and LVAD speed due to the disruption of the normal vortex trajectories.

Aortic Insufficiency in the Absence of Cardiac Contraction: HeartMate II vs. HeartMate 3

Table 4.12 compares the results of different AI conditions with HM2 and HM3 support when pump speed was changed from low to high in the absence of cardiac contraction (CS Off). For all AI conditions, HM3 increased TVP by 20%; Q_{sys} and Q_{LVAD} by 10%; backward Q_{AV} by 5-

20% in comparison to HM2 cases. Vortex symmetry decreased in all conditions (indicating the CCW became more dominant as LVAD speed increased and AI worsened). During HM3 support, CW, CCW vortex circulation, and total KE increased in all AI cases. The area, max diameter, and length of the RJ increased more than with HM2 support. Interestingly, during HM3 support, the VC width increased more dramatically, accompanying with higher TVP increased rate. These results suggest that the AP did contribute to the hemodynamics, flow pattern, and may induce a different RJ structure formation.

Table 4.12: Comparative summary of different parameters in the absence of cardiac contraction when changing LVAD speed from low to high for HeartMate II (8k to 11k rpm) and HeartMate 3 (4.4k to 6.4k rpm) in Mild, Moderate and Severe aortic insufficiency (AI).
(TVP (transaortic pressure), Q_{sys} (total systemic flow), Q_{LVAD} (LVAD flow), Q_{AV} (flow through aortic valve), Q_{ratio} (Flow ratio), clockwise (CW) and counter-clockwise (CCW) vortex circulation, kinetic energy (KE)).

Hemodynamics (% change)	**HM 2: 8k → 11k rpm**				**HM 3: 4.4k → 6.4k rpm**		
	Mild AI	**Moderate AI**	**Severe AI**		**Mild AI**	**Moderate AI**	**Severe AI**
TVP	78%	78%	74%		99%	97%	93%
Q_{sys}	44%	46%	47%		53%	54%	51%
Q_{LVAD}	47%	44%	47%		58%	58%	54%
Backward Q_{AV}	85%	40%	44%		81%	64%	57%
Q ratio	4%	-1%	-1%		3%	2%	2%
Vortex Dynamics (% change)							
CW Circulation	-39%	-70%	82%		69%	29%	45%
CCW Circulation	-34%	59%	120%		69%	104%	63%
Total KE	-26%	42%	200%		144%	130%	124%
Vortex Symmetry	14%	-43%	-38%		-1%	-18%	-17%
Regurgitant Jet Properties (% change)							
Area	410%	67%	39%		81%	64%	44%
Max Diameter	169%	42%	15%		35%	28%	20%
Vena Contracta Width	0%	0%	0%		59%	13%	19%
Length	122%	11%	30%		18%	21%	9%
Average Velocity	12%	10%	16%		19%	15%	17%

Aortic Insufficiency in the Presence of Cardiac Contraction: HeartMate II vs. HeartMate 3

Table 4.13: Comparative summary of different parameters in the presence of cardiac contraction from LVAD off to medium LVAD speed and from changing LVAD speed from low to high for [A] HeartMate II (Pre-LVAD to 9.4k rpm; 8k to 11k rpm) and [B] HeartMate 3 (Pre-LVAD to 5.4k rpm; 4.4k to 6.4k rpm) in Mild, Moderate and Severe aortic insufficiency (AI). (TVP (transaortic pressure), Q_{sys} (total systemic flow), Q_{LVAD} (LVAD flow), Q_{AV} (flow through aortic valve), Q_{ratio} (Flow ratio), clockwise (CW) and counter-clockwise (CCW) vortex circulation, kinetic energy (KE), energy dissipation rate (EDR), residence time (T_R)).

Hemodynamics (% change)	HM 2: Pre-LVAD → 9.4k rpm				HM 2: 8k → 11k rpm		
	Mild AI	Moderate AI	Severe AI		Mild AI	Moderate AI	Severe AI
TVP	98%	97%	76%		30%	36%	15%
Q_{sys}	103%	104%	110%		133%	119%	154%
Q_{LVAD}					158%	139%	141%
Backward Q_{AV}	110%	138%	188%		291%	391%	109%
Q ratio					10%	9%	-5%
Vortex Dynamics (% change)							
CW Circulation	-11%	31%	7%		32%	-12%	-15%
CCW Circulation	32%	24%	49%		-37%	42%	20%
Total KE	21%	71%	72%		20%	34%	24%
Vortex Symmetry	-12%	-13%	-9%		64%	-1%	-15%
Regurgitant Jet Properties (% change)							
Area	87%	84%	28%		16%	11%	41%
Max Diameter	41%	12%	21%		3%	18%	44%
Vena Contracta Width	30%	9%	4%		6%	3%	3%
Length	41%	43%	13%		10%	15%	12%
Average Velocity	5%	14%	14%		-9%	0%	3%
Other (% change)							
EDR	46%	77%	48%		-5%	19%	16%
T_R	-90%	-30%	157%		196%	-50%	-89%

[A] HeartMate II

Table 4.13: (cont.)

Hemodynamics (% change)	HM 3: Pre-LVAD → 5.4k rpm				HM 3: 4.4k → 6.4k rpm		
	Mild AI	Moderate AI	Severe AI		Mild AI	Moderate AI	Severe AI
TVP	94%	112%	93%		59%	49%	34%
Q_{sys}	103%	105%	99%		126%	140%	172%
Q_{LVAD}					177%	188%	180%
Backward Q_{AV}	116%	150%	226%		239%	857%	194%
Q ratio					23%	20%	3%
Vortex Dynamics (% change)							
CW Circulation	31%	41%	5%		56%	52%	0%
CCW Circulation	18%	117%	45%		21%	6%	31%
Total KE	46%	120%	61%		64%	65%	39%
Vortex Symmetry	1%	3%	12%		-8%	10%	-22%
Regurgitant Jet Properties (% change)							
Area	87%	110%	39%		46%	23%	19%
Max Diameter	49%	60%	37%		26%	8%	27%
Vena Contracta Width	65%	15%	16%		19%	8%	15%
Length	31%	40%	16%		24%	10%	-2%
Average Velocity	9%	13%	13%		0%	4%	4%
Other (% change)							
EDR	44%	57%	51%		40%	22%	22%
T_R	35%	-48%	-33%		81%	-50%	-40%

[B] HeartMate 3

Table 4.13 shows the results of different AI conditions combined with HM2 and HM3 support and cardiac function. LVAD support at medium speed (9.4k in HM2 and 5.4k in HM3), increased TVP, Q_{sys}, backward Q_{AV}, CCW circulation, RJ properties, EDR in both HM2 and HM3, and T_R in HM2 Severe AI and HM3 Mild AI conditions. When LVAD speed increased (8k to 11k rpm in HM2, and 4.4k to 6.4k rpm in HM3), in all HM3 conditions, the hemodynamics, vortex circulation, and KE increased more significantly, in comparison to HM2 conditions. Moreover, as LVAD speed increased, the RJ properties and EDR of HM3 Mild AI increased more substantially than HM2 mild AI, while T_R increased in Mild AI and decreased in Moderate and Severe AI conditions for both LVAD types.

As discussed in Chapter 3, the changes in RJ properties suggested that Mild AI conditions worsen immediately after LVAD implant, but did not increase significantly when HM2 speed increased. During HM3 support, Mild AI worsened immediately with LVAD support and progressed with LVAD speed. This observation was made using an *in vitro* bench-test and needed to be validated with clinical studies. However, the result suggests that additional attention is necessary in post-implant management and speed optimization of HM3 patients with pre-existing AI to ensure the AP augments native cardiac contraction under all conditions.

Proposed indices to assess AI during LVAD support

From the previous result, the jet CSA/LVOT CSA and the jet area had the highest percentage changes. Under the assumption that the CSA of the jet and LVOT is circular, the jet/LVOT ratio was estimated using equation 1. This proposed index can be calculated directly from the echo parameters obtaining in the 3-chamber view during an echo color Doppler study. The AHA classification of AI can still be applied since it was an estimation of the currently used clinical index (Figure 4.19). In comparison to HM2, HM3 seemed to worsen AI more, especially with a pre-existing moderate or severe AI presence. The reported data were averaged from 39 times points during the cardiac cycle. In clinical practice, further investigation is required to determine the right time point to perform the measurement.

$$\text{Jet/LVOT ratio} = \frac{\text{jet}_{\text{max diameter}}{}^2}{\text{LVOT}_{\text{width}}{}^2} \qquad \text{(Equation 4.1)}$$

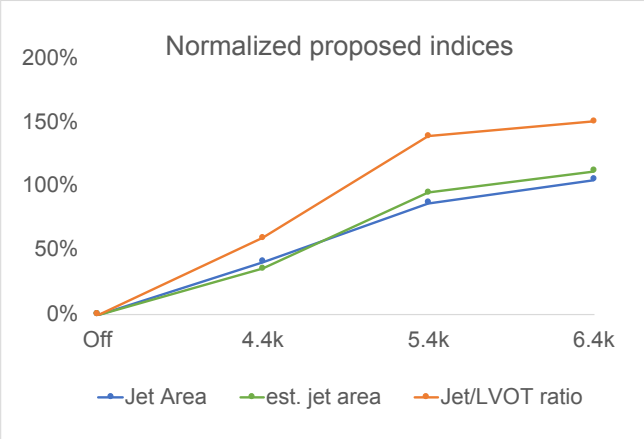

Figure 4.18: Normalized proposed indices

The estimated (est.) jet area is calculated using equation 2 by assuming the jet 2D long-axis view has a triangular shape. The est. area was similar to the actual jet area (Figure 4.18). This proposed index can be calculated directly from the echo parameters obtaining in the 3-chamber view. Further investigation is required to determine the appropriate threshold for different AI classifications. Similar to the previous index, the est. jet area seemed to increase more during HM3 support, especially in moderate and severe AI conditions (Figure 4.20).

$$\text{Est. jet area} = \frac{1}{2} \times \text{jet}_{\text{max diameter}} \times \text{LVOT}_{\text{width}} \qquad \text{(Equation 4.2)}$$

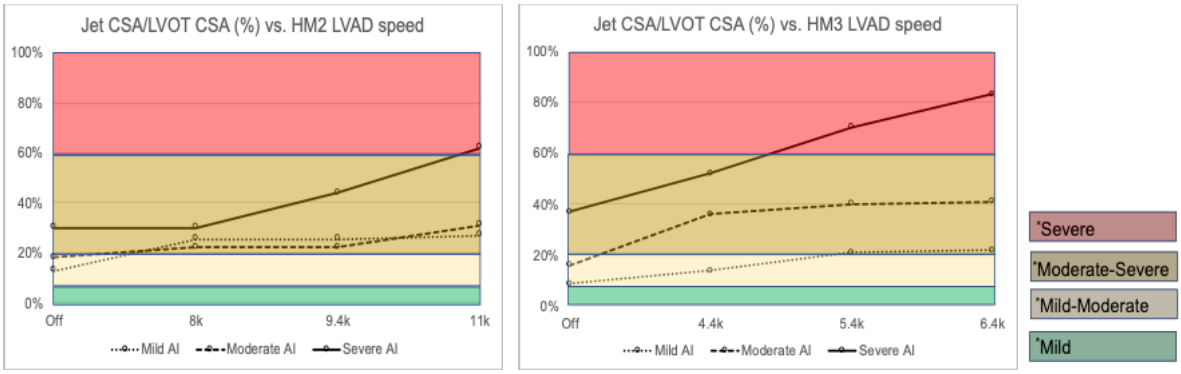

Figure 4.19: Change of jet CSA/LVOT CSA index when HM2 and HM3 presences

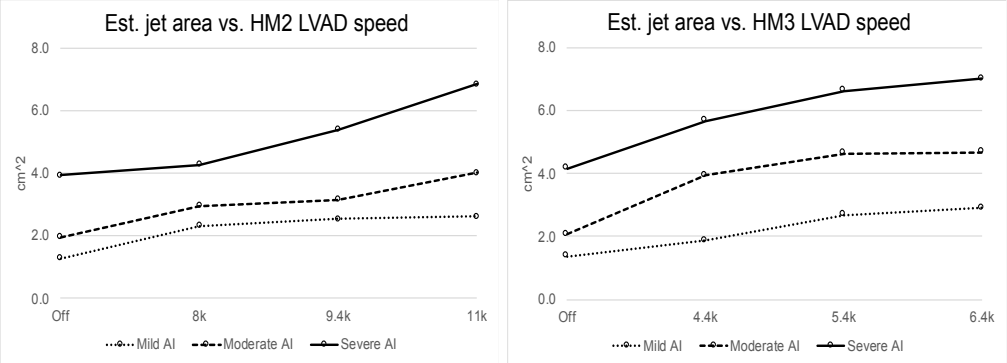

Figure 4.20: Change of est. jet area when HM2 and HM3 presences

4.5 Limitation and Conclusion

The intraventricular flow field indices for Baseline, Mild, Moderate, and Severe AI under matched hemodynamic conditions were measured during three HM3 speed conditions using a cardiac simulator and PIV. Similar system limitations to those discussed in Chapter 3 apply to this study. Overall, HM3 support affects pre-existing, AI similar to HM2. The LVAD worsens AI indices by introducing turbulence, altering the intraventricular flow pattern, increasing energy loss, and prolonging the diastolic phase. Two new indices were proposed to assess AI severity during LVAD support, which seemed to have higher sensitivity than the currently used indices. This study suggests that additional studies are needed to inform post-implant patient management in patients with pre-existing AI, and evaluate the potential benefit of synchronizing the AP with the native heartbeat.

4.6 Acknowledgements

This chapter, in full, is in an early prepared stage for publication. The co-author is Karen May-Newman. The dissertation author is the primary author of this paper.

Chapter 5

The Effect of Mitral Valve Prostheses Design and Orientation on Left Ventricular Flow during LVAD Support

5.1 Introduction

Annually in the US, there are more than 100,000 cases of mitral valve (MV) replacement[130]. Bioprosthesis (BP), bi-leaflet (BL), single-leaflet (tilting-disk (TD)), etc. are different designs of MV prostheses, each interacts distinctly with the incoming flow during diastole[124]. While MV replacements are beneficial, they have drawbacks. Each prosthesis valve type is linked with particular complications, e.g., higher thromboembolic risk in TD, a higher bleeding complication in BL, and a higher rate of deterioration and stenosis in BP[125,126]. Overall, risks of thrombosis are associated with patient's pre-existing conditions (low cardiac function, hypercoagulability, atrial fibrillation/dilation, etc.) and post-surgery care (e.g., anticoagulation management)[263–266]. Typically, anticoagulants, which are required to manage the thromboembolic event (TE) risk, change patients' blood chemistry balance. Moreover, the presence of foreign material, abnormal intraventricular pattern with high shear stress region[124,267–269] further increase the tendency of thrombus formation, according to the classic view of Virchow's triad. Finally, mitral regurgitation can occur post-MV replacement and subsequently increases the risk of HF and arrhythmias[127,128,270].

Previous studies have shown that the shape and orientation of MV prosthesis strongly affect the intraventricular vortex structures[250,271,272]. The impact of MV prostheses design and orientation on intraventricular flow and its associated risk of TE were reported in the recent publication[124]. The BP and the BL valves in the anti-anatomical position produced a similar vortex pattern to the normal heart. The BL valve generated higher shear in the region where it hinges, exhibiting higher platelet shear activation potential. The TD valve in septal orientation produced

a reversed flow and vortex pattern, impairing LV washout and retaining shear activated fluid. The BP valve was found to have the lowest TE risk for patients with progressive heart valve disease[124].

Left ventricular assist device (LVAD) support boosts hemodynamic function in heart failure patients. The LVAD provides intermediate support for Bridge-to-Transplants, and long term support for Destination Therapy (DT) patients[67,229]. The INTERMAC 2018 reported that the concomitant MV procedure (repair or replacement) at the time of LVAD implant did not affect short- and long-term patient mortality rate. Excepted for patients implanted with LVAD as DT, MV procedure is associated with improved long-term survival. Furthermore, MV replacement is associated with less hospital re-admission and higher quality of life in select patients[273].

During LVAD support, the interaction between the MV prosthesis and intraventricular flow, along with its associated TE risks, might change. Several studies reported the outcomes of patients with prostheses MV during pulsatile LVAD support. Schweiger et al. conducted a small clinical study, with one patient with BP and five with mechanical valves in mitral positions who were LVAD candidates. The prostheses valves were left at the time of LVAD implants, while optimal speeds were set to ensure sufficient loading, and periodic AV opening (AVO). During an average of 14 months LVAD support, no valve-related or any thromboembolic events were observed; all patients died due to multiple organ failure. In the BP case, after 3.5 years of LVAD support, the autopsy report found no change in valve tissue, or thrombus formation at the valve leaflet[126]. Similarly, Krishan et al. reported a patient case with long term (20 years) mechanical MV, who received LVAD as BTT. When he received a heart transplant, there was no incidence of MV thrombosis[274]. Similar outcomes were reported in LVAD patients with pre-existing mechanical MV prosthesis[87,129,274–276]. On the other hand, other reported valvular thrombosis incidences in LVAD patients with pre-existing mitral BP[224,277,278]. Additional studies are needed to assess the effects of continuous-flow LVAD in patients with prostheses MV.

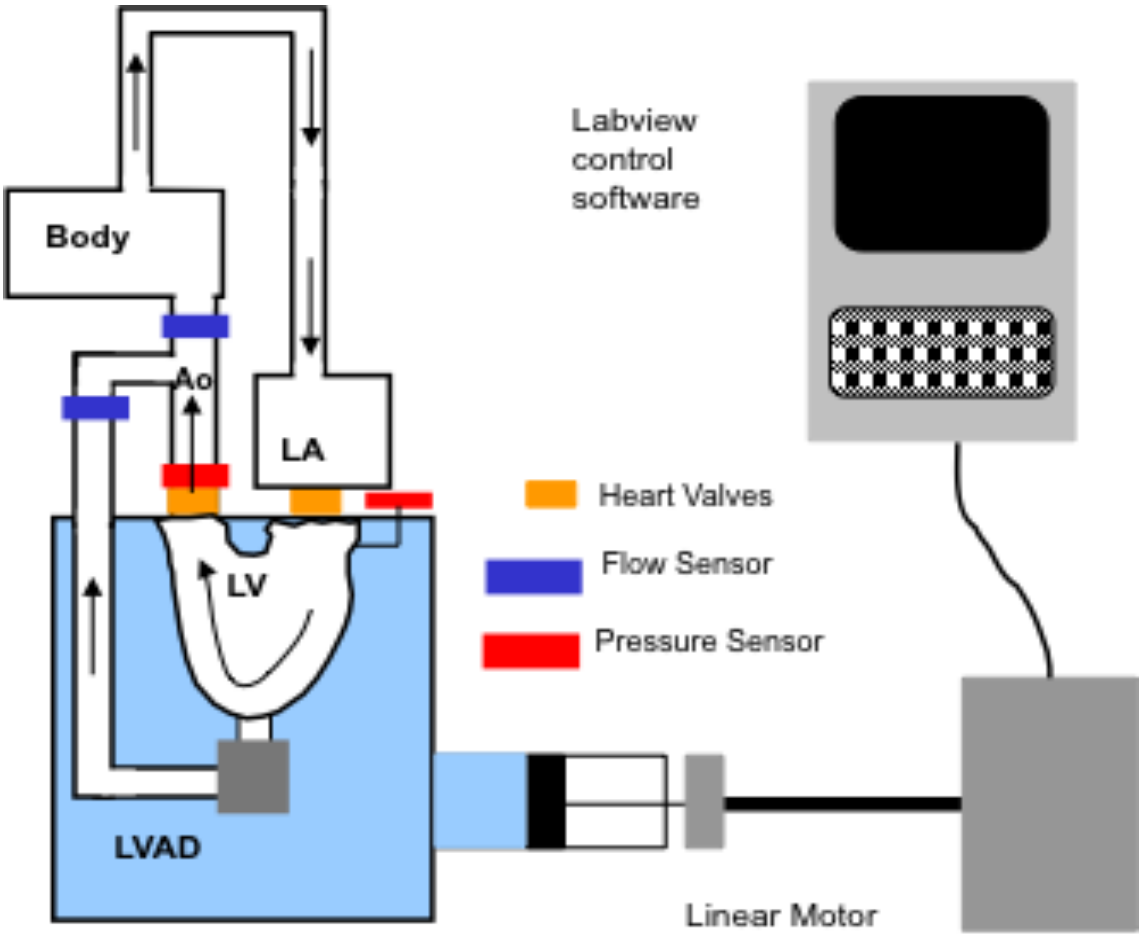

(A)

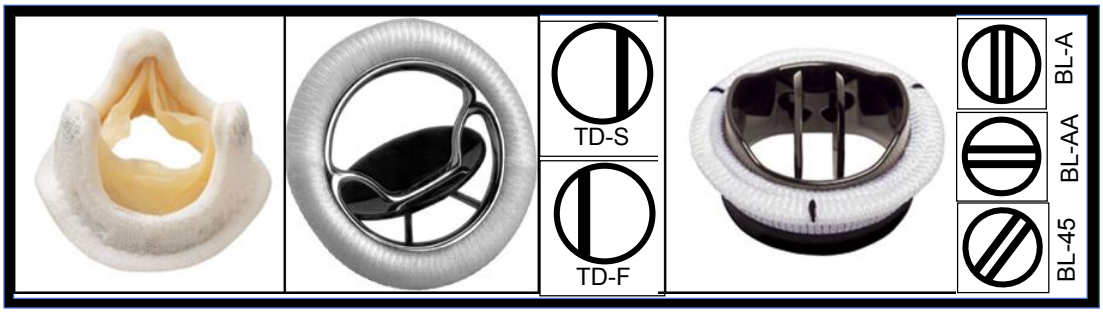

(B)

Figure 5.1: (A) The SDSU cardiac simulator is a mock circulatory loop that reproduces the fluid dynamics of the dilated cardiomyopathy (DCM) heart. The left ventricle is a silicone rubber model positioned with a left ventricular assist device (LVAD) attached inside of a transparent fluid-filled chamber. (B) Three mitral valve prostheses were tested in different orientations under matched hemodynamic conditions (from left to right): porcine bio-prosthesis (BP); tilting disk mechanical heart valve (MHV) in the septal (TD-S) (top), and free wall (TD-F) (bottom) orientations; bileaflet MHV in anatomical (BL-A) (top), anti-anatomical (BL-AA) (middle), and 45° angle (BL-45) (bottom) orientations.

5.2 Methods

The experimental setup is similar to the previous study, and are described in detail in Chapter 3, section 2. Except that the porcine bioprosthetic valves, 26-mm Medtronic Mosaic, and 25-mm Medtronic 305 Cinch were placed in the AoV and MV positions, respectively. A series of MVP was placed in the MV positions: a Medtronic Hall tilting-disk mechanical heart valve (MHV) positioned with the large orifice directing flow toward the free wall (TD-F), or toward the septal (TD-S); a Carbomedics MHV positioned in the 45° angle (BL-45), anatomical (BL-A), and anti-anatomical (BL-AA); and a Medtronic 305 Cinch bio-prosthesis (BP) (Figure 5.1). Two different speeds of HeartMate II (HMII) were tested at two levels of support: 8k (low) and 11k (high) rotations per minute (rpm).

Data Analysis

The Q_{ratio} and Aortic pulsatility index (PI) were calculated from the flow signal:

$$Q_{ratio} = \frac{Q_{LVAD}}{Q_{sys}} \qquad \text{(Equation 5.1)}$$

$$\text{Aortic PI} = \frac{Q_{sys}max - Q_{sys}min}{Q_{sys}mean} \qquad \text{(Equation 5.2)}$$

Where Q_{sys} is the systemic flow rate, and Q_{LVAD} is the LVAD flow rate.

Images Analysis

Velocity profile along the line located 20 mm from the MV annulus was computed at the peak of E- and A- wave for six types of prosthesis valves during 8k and 11k LVAD support, as previously described[124]. The velocity of inflow toward the LV apex was designated as positive, while the flow toward the AV (away from the apex) was designated as negative.

Vortices were identified in the recorded velocity fields, and their dynamical properties tracked as previously described[124,245].

Blood Residence Time

Blood residence time (T_R) was determined using the modified advection equation, as described in detail in previous publications [124,246]. The equation was integrated in time for ten cardiac cycles (CC), which ensured convergence to a periodic solution.

Statistical Analysis

The hemodynamics properties (LVP, AoP, Q_{sys}, Q_{LVAD}, Q_{ratio}, and Aortic PI) for different MVP at 8k and 11k rpm LVAD speed were tested for normality using the Shapiro-Wilk test. A Kruskal-Wallis one-way ANOVA test was used to assess the statistical significance for the 8k and 11k groups, and the Wilcoxon Rank-Sum test with Bonferroni correction used for pairwise comparisons. Significance was achieved for $p \leq 0.01$.

5.3 Results

The hemodynamics were not statistically different for all the valve types and positions in the 8k LVAD group (Table 5.1). The LVP was statistically different during the 11k speed between the BL-AA and BL-A, BL-45, and TD-F conditions. Still, this difference did not impact other hemodynamics values within the same LVAD support level. As LVAD speed increased from 8k to 11k, the AoP, Q_{LVAD}, Q_{sys}, Q_{ratio} were increased approximately by 42%, 80%, 26%, 43%, respectively; while aortic PI decreased by 54%. The $Q_{ratio} < 1$ indicated partial AV opening (AVO), while $Q_{ratio} \approx 1$ indicated no or very minimal AVO. During low to medium LVAD support, the flow got ejected through AV and LVAD conduit during systole, resulting in $Q_{ratio}<1$ and high Aortic PI. While during high support, the flow was mostly by the pump, resulting in $Q_{ratio} \approx 1$ and lower Aortic PI.

Table 5.1: Hemodynamics conditions measured for six orientations of mitral valve prostheses during 8000 and 11000rpm LVAD-supports

Parameter		LVP (mmHg)	AoP (mmHg)	Q_{sys} (L/min)	Q_{LVAD} (L/min)	Q_{ratio}	Aortic PI
LVAD $8x10^3$rpm	BP	23.60 ± 0.14	84.71 ± 0.06	4.14 ± 0.14	2.65 ± 0.01	0.64	3.68
	TD-F	27.11 ± 0.14	86.10 ± 0.07	4.31 ± 0.01	2.54 ± 0.01	0.59	3.75
	TD-S	17.87 ± 0.09	85.39 ± 0.05	4.48 ± 0.01	2.83 ± 0.00	0.63	4.16
	BL-AA	24.99 ± 0.12	81.23 ± 0.05	4.05 ± 0.01	2.95 ± 0.01	0.73	3.25
	BL-A	23.45 ± 0.12	80.20 ± 0.06	4.34 ± 0.01	2.98 ± 0.01	0.69	3.38
	BL-45	25.01 ± 0.13	83.70 ± 0.07	4.24 ± 0.01	2.81 ± 0.01	0.66	3.66
		LVP (mmHg) †	AoP (mmHg)	Q_{sys} (L/min)	Q_{LVAD} (L/min)	Q_{ratio}	Aortic PI
LVAD $11x10^3$rpm	BP	26.77 ± 0.16	118.25 ± 0.02	5.20 ± 0.01	4.89 ± 0.01	0.94	1.49
	TD-F	32.80 ± 0.17	121.18 ± 0.04	5.28 ± 0.01	4.75 ± 0.01	0.90	1.79
	TD-S	22.84 ± 0.11	119.79 ± 0.03	5.62 ± 0.01	5.14 ± 0.00	0.92	1.99
	BL-AA	21.25 ± 0.24	118.83 ± 0.05	5.24 ± 0.01	4.95 ± 0.01	0.95	1.52
	BL-A	28.55 ± 0.14	114.64 ± 0.03	5.50 ± 0.01	5.33 ± 0.01	0.97	1.46
	BL-45	28.77 ± 0.14	118.49 ± 0.03	5.33 ± 0.01	5.07 ± 0.01	0.95	1.71

Average ± standard error for the cardiac cycle of LVP (LV pressure), AoP (Aortic pressure), Q_{sys} (total systemic flow), Q_{LVAD} (LVAD flow), Q_{ratio} (Flow ratio), and Aortic PI (Aortic pulsatility index)
† Statistical significance ($p<0.01$) for mitral valve prosthesis design

Table 5.2: [Top] Intraventricular vortex properties and [Bottom] ANOVA pairwise comparisons summary for six orientations of mitral valve prostheses during 8k and 11k LVAD supports

Vortex Properties 8k LVAD		BP	TD-F	TD-S	BL-AA	BL-A	BL-45
Total Kinetic energy (mJ/m)		3.26 ± 0.72	3.37 ± 0.39	2.86 ± 0.63	3.31 ± 0.65	2.02 ± 0.25	2.04 ± 0.37
Kinetic energy (mJ/m)	CW†	2.54±0.56	2.93±0.31	1.01±0.35	2.43±0.40	1.57±0.17	1.32±0.19
	CCW†	0.72±0.26	0.44±0.11	1.84±0.36	0.89±0.32	0.46±0.09	0.72±0.19
Circulation (x10^{-3} m^2/s)	CW†	21.78±2.57	30.60±2.20	6.24±1.28	22.65±1.80	20.22±0.97	17.78±1.17
	CCW†	-4.70±0.96	-4.17±0.72	-20.25±1.62	-7.21±0.86	-4.66±0.74	-6.54±1.12
Radius (cm)	CW†	0.73±0.04	0.97±0.05	0.40±0.02	0.82±0.05	0.76±0.04	0.73±0.04
	CCW†	0.30±0.01	0.26±0.01	0.74±0.04	0.24±0.01	0.31±0.01	0.35±0.01
Aspect Ratio	CW†	1.62±0.08	1.51±0.06	1.85±0.10	1.65±0.08	1.58±0.06	1.50±0.06
	CCW†	1.62±0.07	1.57±0.09	1.78±0.09	1.84±0.08	1.45±0.07	1.48±0.08
Vortex symmetry CW:CCW†		2.56±0.19	3.77±0.31	0.76±0.09	3.60±0.25	2.20±0.13	2.04±0.18

Vortex Properties 11k LVAD		BP	TD-F	TD-S	BL-AA	BL-A	BL-45
Total Kinetic energy (mJ/m) †		3.09 ± 0.70	3.06 ± 0.40	3.23 ± 0.70	0.66 ± 0.15	2.07 ± 0.25	2.02 ± 0.31
Kinetic energy (mJ/m)	CW†	2.47±0.55	2.56±0.30	1.08±0.42	0.49±0.11	1.58±0.19	1.40±0.17
	CCW†	0.62±0.17	0.19±0.05	2.05±0.37	0.21±0.08	0.54±0.09	0.64±0.15
Circulation (x10^{-3} m^2/s)	CW†	21.29±2.41	27.03±2.06	6.31±1.53	9.00±1.11	19.27±0.94	18.41±0.93
	CCW†	-4.20±0.58	1.86±0.42	-21.12±1.90	-2.83±0.52	-5.10±0.64	-6.31±1.09
Radius (cm)	CW†	0.71±0.04	1.04±0.05	0.46±0.03	1.05±0.05	0.87±0.05	0.85±0.05
	CCW†	0.27±0.01	0.30±0.03	0.90±0.06	0.38±0.06	0.35±0.02	0.40±0.03
Aspect Ratio	CW†	1.60±0.08	1.62±0.05	2.06±0.19	1.68±0.10	1.64±0.06	1.54±0.06
	CCW†	1.76±0.11	1.89±0.24	2.07±0.10	2.54±0.41	1.68±0.08	1.76±0.19
Vortex symmetry CW:CCW†		2.86±0.19	3.58±0.37	0.74±0.11	3.47±0.39	2.55±0.24	2.46±0.25

[Grab your reader's attention with a great quote from the document or use this space to emphasize a key point. To place this text box anywhere on the page, just drag it.]

Table 5.3: ANOVA pairwise comparisons summary for six orientations of mitral valve prostheses during 8k and 11k LVAD support

8k	BP	BL-45	BL-A	BL-AA	TD-F
BL-45	No deviations				
BL-A	No deviations	No deviations			
BL-AA	R_{CW}	R_{CCW}^{*}, S^{**}	R_{CW}^{*}, S^{**}		
TD-F	Γ_{CW}^{**}, R_{CW}^{**}	KE_{CW}^{*}, KE_{CCW}^{**}, Γ_{CW}^{**}, Γ_{CCW}^{*}, R_{CW}^{**}, R_{CCW}^{**}, S^{**}	Γ_{CW}^{*}, Γ_{CCW}^{*}, R_{CW}^{**}, R_{CCW}, S^{**}	No deviations	
TD-S	KE_{CW}^{**},KE_{CCW}^{**}, Γ_{CW}^{**}, Γ_{CCW}^{*}, R_{CW}^{**}, R_{CCW}^{**}, S^{**}	KE_{CW}^{*}, KE_{CCW}^{**}, Γ_{CW}^{**}, Γ_{CCW}^{*}, R_{CW}^{**}, R_{CCW}^{**}, S^{**}	KE_{CW}^{**},KE_{CCW}^{**}, Γ_{CW}^{**}, Γ_{CCW}^{*}, R_{CW}^{**}, R_{CCW}^{**}, aR_{CW}, S^{**}	KE_{CW}^{**},KE_{CCW}^{**}, Γ_{CW}^{**}, Γ_{CCW}^{*}, R_{CW}^{**}, R_{CCW}^{**}, aR_{CW}^{*}, S^{**}	KE_{CW}^{**},KE_{CCW}^{**}, Γ_{CW}^{**}, Γ_{CCW}^{*}, R_{CW}^{**}, R_{CCW}^{**}, aR_{CW}^{*}, S^{**}

11k	BP	BL-45	BL-A	BL-AA	TD-F
BL-45	No deviations				
BL-A	KE_{CW}, Γ_{CCW}^{*}	No deviations			
BL-AA	KE_{T}^{**}, KE_{CW}^{**}, Γ_{CW}^{**}, R_{CW}^{**}	KE_{T}^{**}, KE_{CW}^{**},Γ_{CW}^{**}, R_{CW}^{**}	KE_{T}^{**}, KE_{CW}^{**}, KE_{CCW}^{*}, Γ_{CW}^{**}, Γ_{CCW}		
TD-F	R_{CW}^{**}	KE_{CW}^{**}, Γ_{CW}^{*}, Γ_{CCW}^{*}, R_{CW}^{**}	KE_{CW}^{*}, KE_{CCW}^{*}, Γ_{CCW}^{**}, Γ_{CCW}^{**}	KE_{T}^{**}, KE_{CW}^{**}, Γ_{CW}^{**}	
TD-S	KE_{CW}^{*}, KE_{CCW}^{**}, Γ_{CW}^{**}, Γ_{CCW}, R_{CW}^{*}, R_{CCW}^{**}, S^{**}	KE_{CW}^{**}, KE_{CCW}^{**}, Γ_{CW}^{**}, Γ_{CCW}^{*}, R_{CW}^{**}, R_{CCW}^{*}, S^{**}	KE_{CW}^{**}, KE_{CCW}^{**}, Γ_{CW}^{**}, Γ_{CCW}^{*}, R_{CW}^{**}, R_{CCW}^{**}, S^{**}	KE_{T}^{**}, KE_{CCW}^{**}, Γ_{CCW}^{**}, R_{CW}^{**}, R_{CCW}^{**}, S^{**}	KE_{CW}^{**}, KE_{CCW}^{**}, Γ_{CW}^{**}, Γ_{CCW}^{*}, R_{CW}^{**}, R_{CCW}^{**}, S^{**}

Significance codes: 0 '**' 0.001 '*' 0.01 ' '

KE_T – Total Kinetic Energy, KE_{CW} – CW Kinetic Energy, KE_{CCW} – CCW Kinetic Energy, Γ_{CW} – CW Circulation, Γ_{CCW} – CCW Circulation, R_{CW} – CW Radius, R_{CCW} – CCW Radius,
aR_{CW} – CW Aspect Ratio, aR_{CCW} – CCW Aspect Ratio, S – Symmetry

(In the cases which had multiple CW and CCW vortices occurrences: total CW and CCW vortex circulation and kinetic energy, radius/ aspect ratio/ vortex symmetry of the main (largest) CW and CCW vortex were reported

Velocity Field Visualization and Inflow Profiles

Figure 5.2 displays the velocity fields in the LV mid-plane for selected instants of the CC, illustrating the flow dynamics produced by each valve case at low and high levels of LVAD support. These results showed that during the diastole the BP valve produced a similar flow pattern to that observed for the native valve [247], with an asymmetric vortex ring forming and resulting in a 2D pattern of a large clockwise (CW) anterior core and a small counter-clockwise (CCW) posterior core. During systole, the low LVAD support case induces partial AVO, and the flow was split between the valve and LVAD. At high LVAD support, AV closed and flow continuously exited through the LVAD. The velocity profiles of MV inflow for peak E- and A- waves are shown in Figure 5.3. Consistent with the velocity fields, the inflow profiles were roughly symmetric, with a single parabolic peak that diminished in magnitude during the A-wave. Higher LVAD support slightly increased the incoming E-wave velocity while the A-wave had a similar profile and magnitude to low LVAD support.

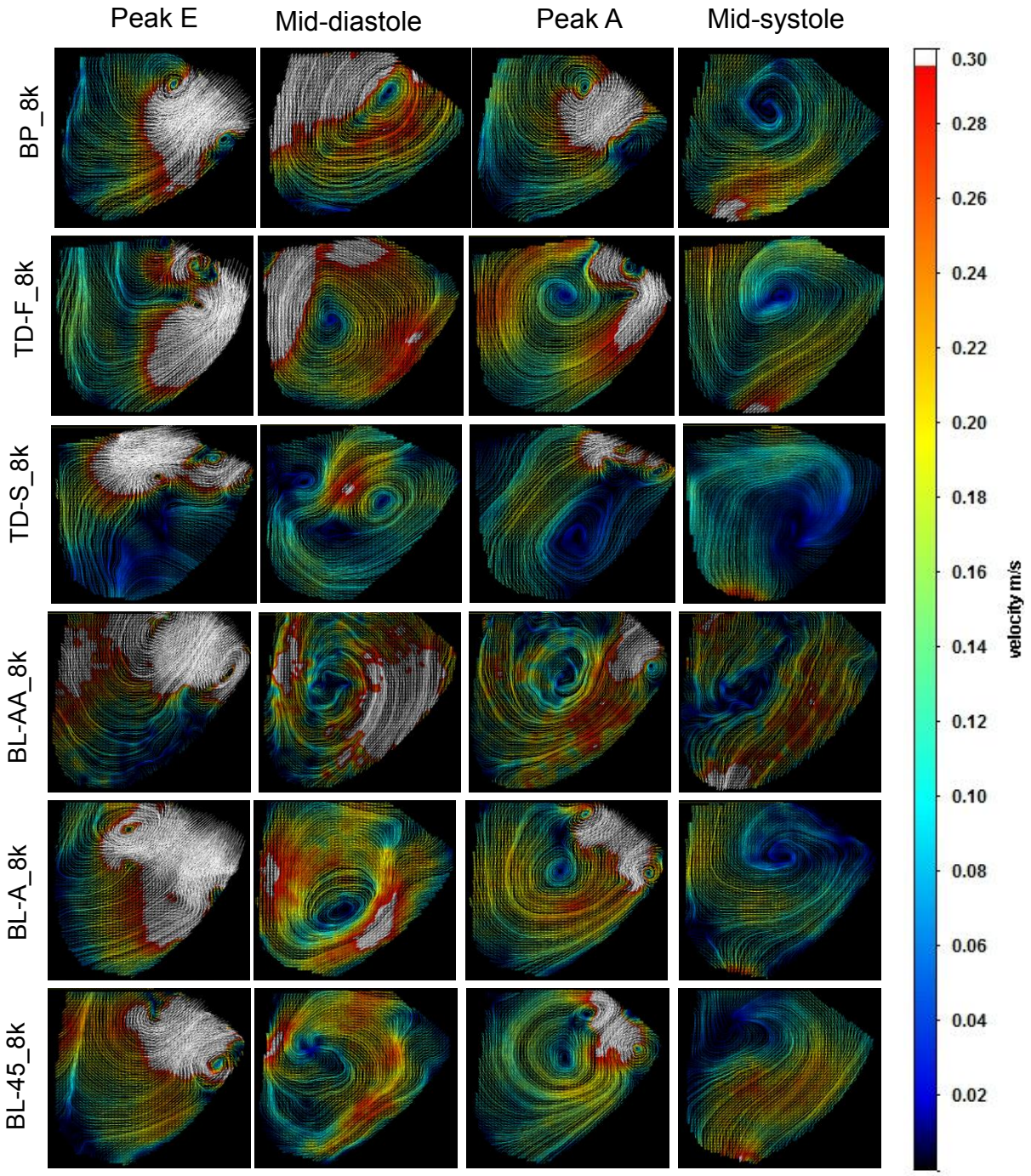

[A] 8k rpm Velocity Field Images

Figure 5.2: Velocity field images at four instants of the cardiac cycle shown for the six prosthesis mitral valve cases during (A) 8 kilo rotations per minute (krpm), and (B) 11 krpm LVAD supports: early diastole (1st left column), mid-diastole (2nd column), late diastole (3rd column), and mid-systole (4th column). In each image, the prosthesis mitral valve is located on the *upper right*, the aortic valve is in the *upper left*.

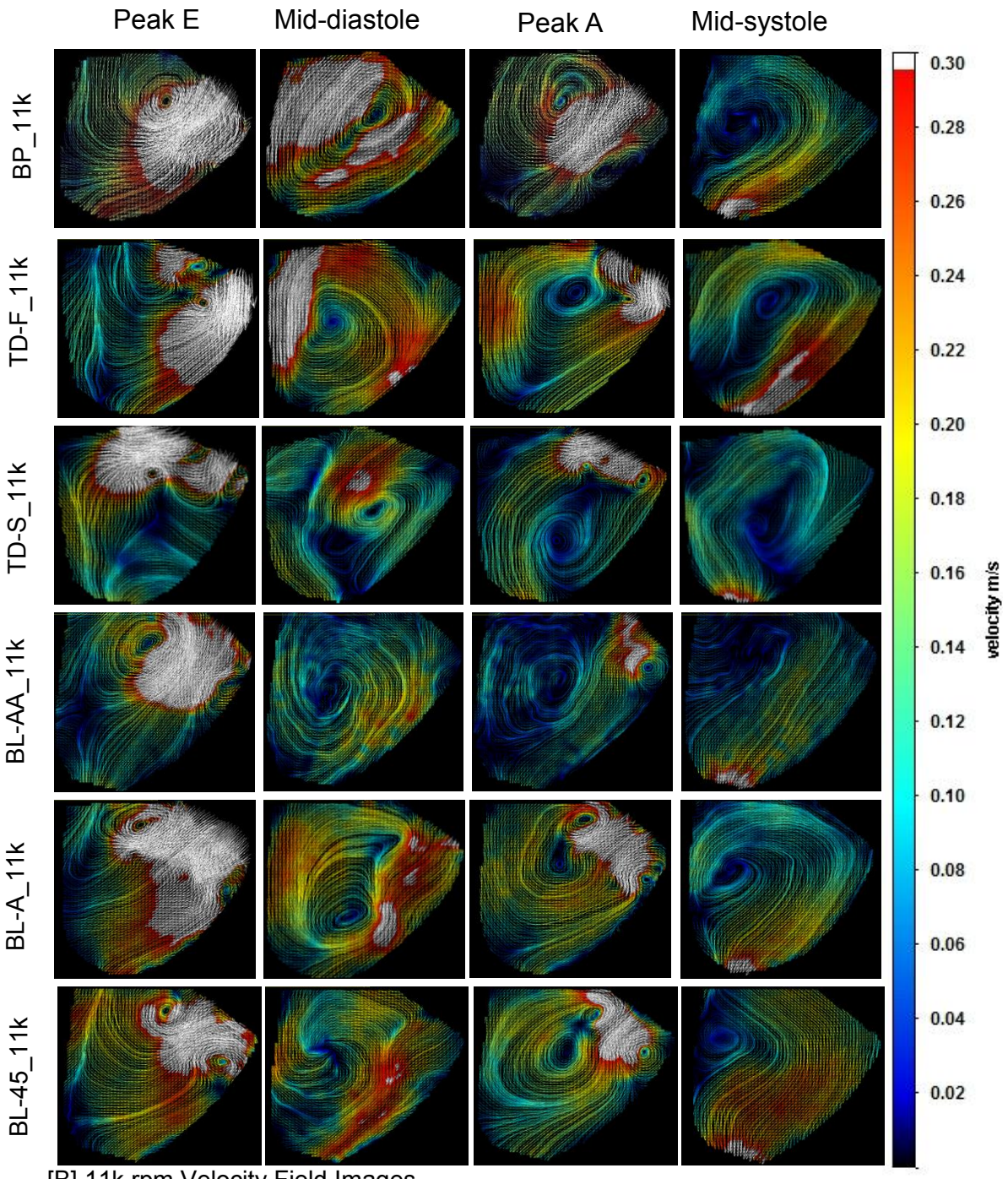

[B] 11k rpm Velocity Field Images

Figure 5.2: Velocity field images for the six prosthesis mitral valve cases (cont.)

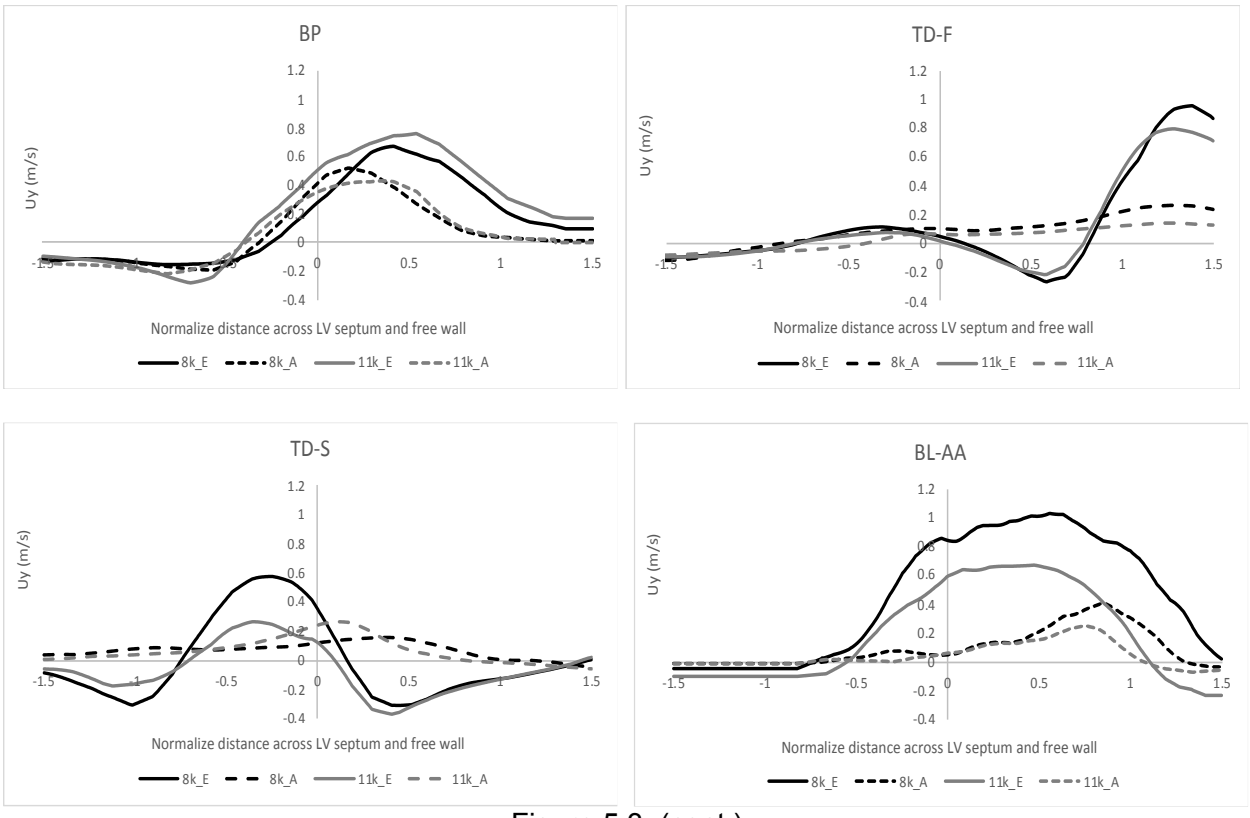

Figure 5.3: (cont.)

Figure 5.3: Vertical velocity profiles along the lines 20 mm from and parallel to the MV annulus, at both peak E and A waves during 8 krpm and 11 krpm LVAD support for the six mitral valve prosthesis cases. Fluid entering through the mitral valve and going toward the line is assigned (+) value, and fluid moving toward the aortic valve is assigned (-) value.

The TD-F valves exhibited a strong inflow jet attached to the lateral wall and a more persistent CW vortex than the BP valves. This was reflected in the velocity profiles, which were not symmetric and peaked toward the free-wall. In contrast, the TD-S valves exhibited a complete reversal of the normal flow pattern, with dominant and more persistent CCW vortices that crossed

the outflow path. By directing the larger jets toward the septum, the inflow profiles were shifted away from the free-wall.

The BL design altered the diastolic flow pattern through the MV, although the overall swirling motion of blood was less affected. The BL-AA and BL-45 displayed similar flow patterns to the BP valve, with wider parabolic inflow profiles. The BL-A exhibited distinct vortex formation during early diastole and two-peaks inflow profiles, clearly reflecting the bileaflet valve geometry. In contrast to the BP valve, low LVAD support produced higher E-wave velocities, especially in BL-AA and TD-S cases, while the A-wave profiles were roughly for both LVAD speeds. Consistent with the Q_{ratio} results, velocity fields during systole of 8k showed partial flow exited through AV, while during 11k, very minimal AVO caused most flows exited at the LV apex.

Vortex Properties: Circulation and Trajectories

The vortex analysis (Table 5.2) indicated that the total KE was comparable among all valve types and orientations during low LVAD support. At higher LVAD speed, the total KE of BL-AA was significantly lower than in other valve types. In all conditions, excepted for the TD-S valves, the CW circulations were dominant, resulting in larger CW circulation and KE.

The circulation and trajectories for CW and CCW vortices during the CC, beginning with the MV opening, following by early and late diastolic filling, and concluding at end-systole, are displayed in Figure 5.4. For the BP valve during low LVAD support, the CW vortex formed and followed a straight trajectory toward the apex during E-wave filling, then moved up toward the base. A weaker A-wave jet joined and strengthened the CW vortex, which moved toward AV, channeling some forward flow through AV during systole. CCW vortices appeared at early E- and A- filling phases and moved toward the apex to exit through the LVAD. At high LVAD support, a similar CW vortex pattern was observed, excepted during late diastole the CW resided near LV center, and the CCW vortex persisted longer

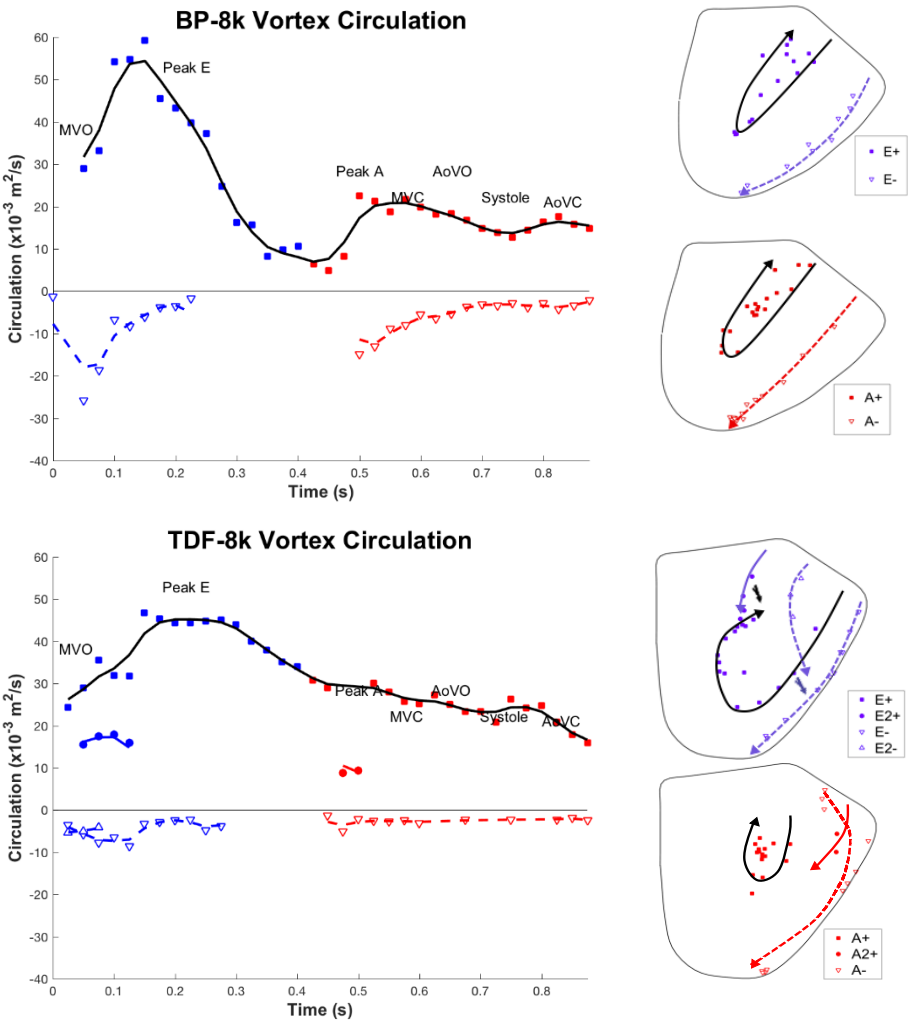

[A] 8k rpm LVAD speed

Figure 5.4: (Left) Time-varying (positive) clockwise (CW) and (negative) counterclockwise (CCW) vortex circulation are shown for six orientations of mitral valve prostheses during [A] 8k rpm and [B] 11 krpm LVAD support: blue symbols denote E wave vortices, red symbols denote A wave and systolic vortices; square symbols denote main CW vortices, circle symbols denote secondary CW vortices, down-triangle symbols denote main CCW vortices, up-triangle symbols denote secondary CCW vortices; blue lines and red lines denote vortices that appear and dissipate during E wave and A wave respectively, black lines denote vortices that perpetuate the entire cardiac cycle (MVO = mitral valve opens, MVC = mitral valve closes, AoVO = aortic valve opens, AoVC = aortic valve closes).
(Middle, Right) Vortex core trajectories as the result of the E-wave and A-wave inflow contributions are shown for six orientations of prosthesis mitral valves: the trajectories' symbols and lines are corresponded to the circulation plot (symbol indicates the merging to vortices).

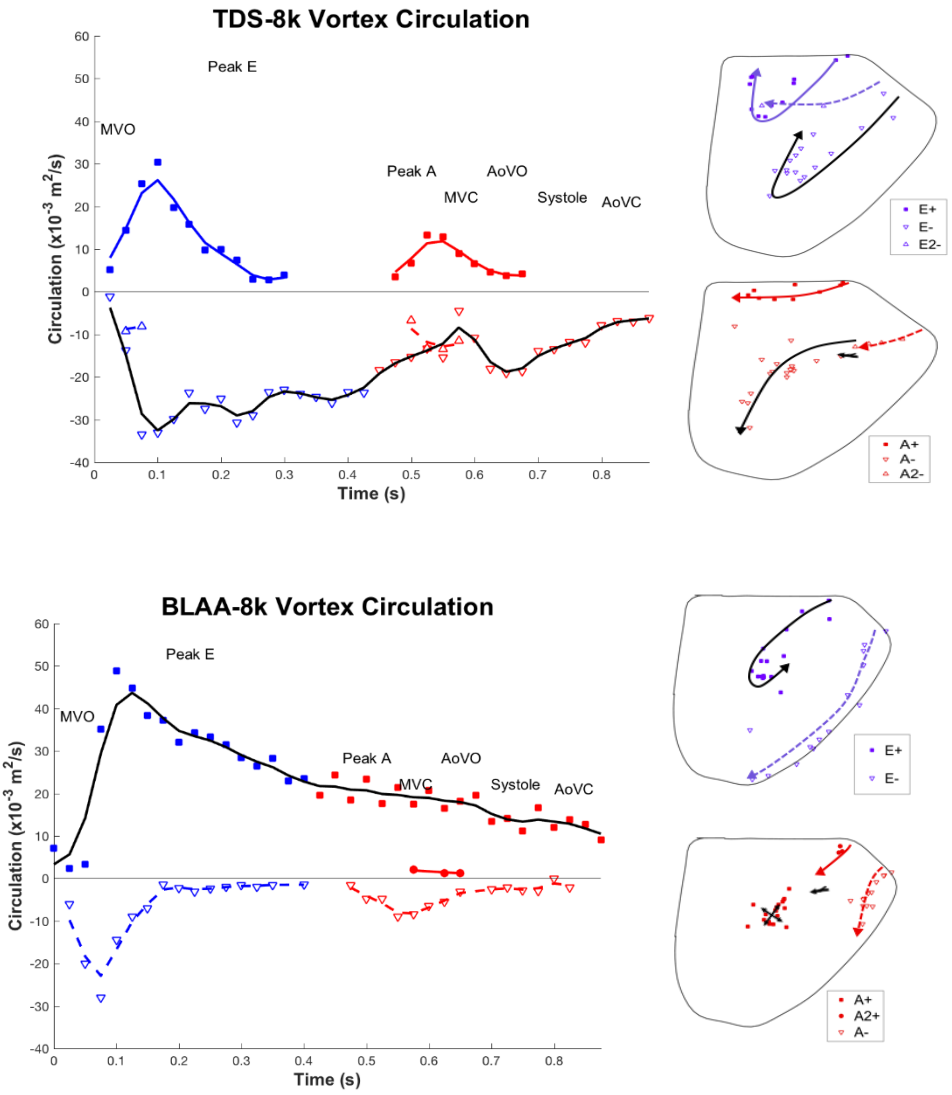

[A] 8k rpm LVAD speed

Figure 5.4: Vortex Circulation and Trajectories (cont.)

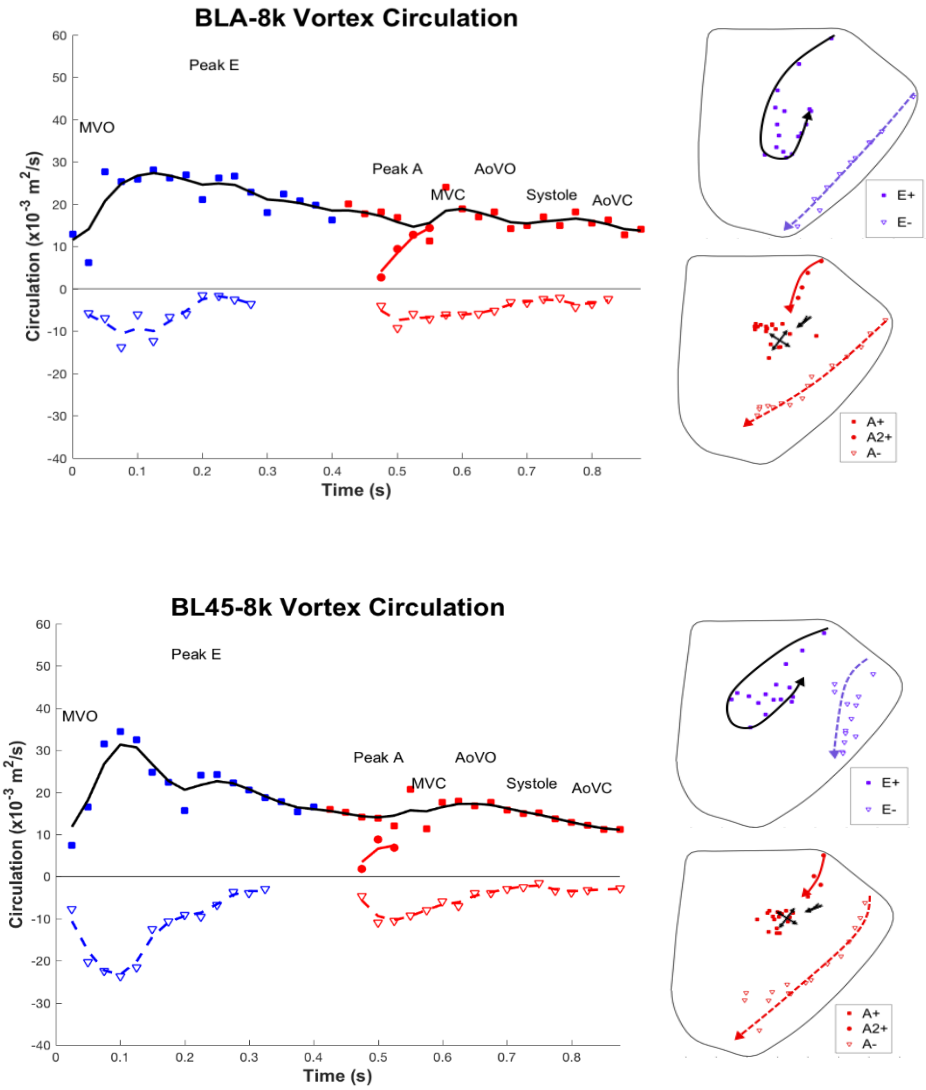

[A] 8k rpm LVAD speed

Figure 5.4: Vortex Circulation and Trajectories (cont.)

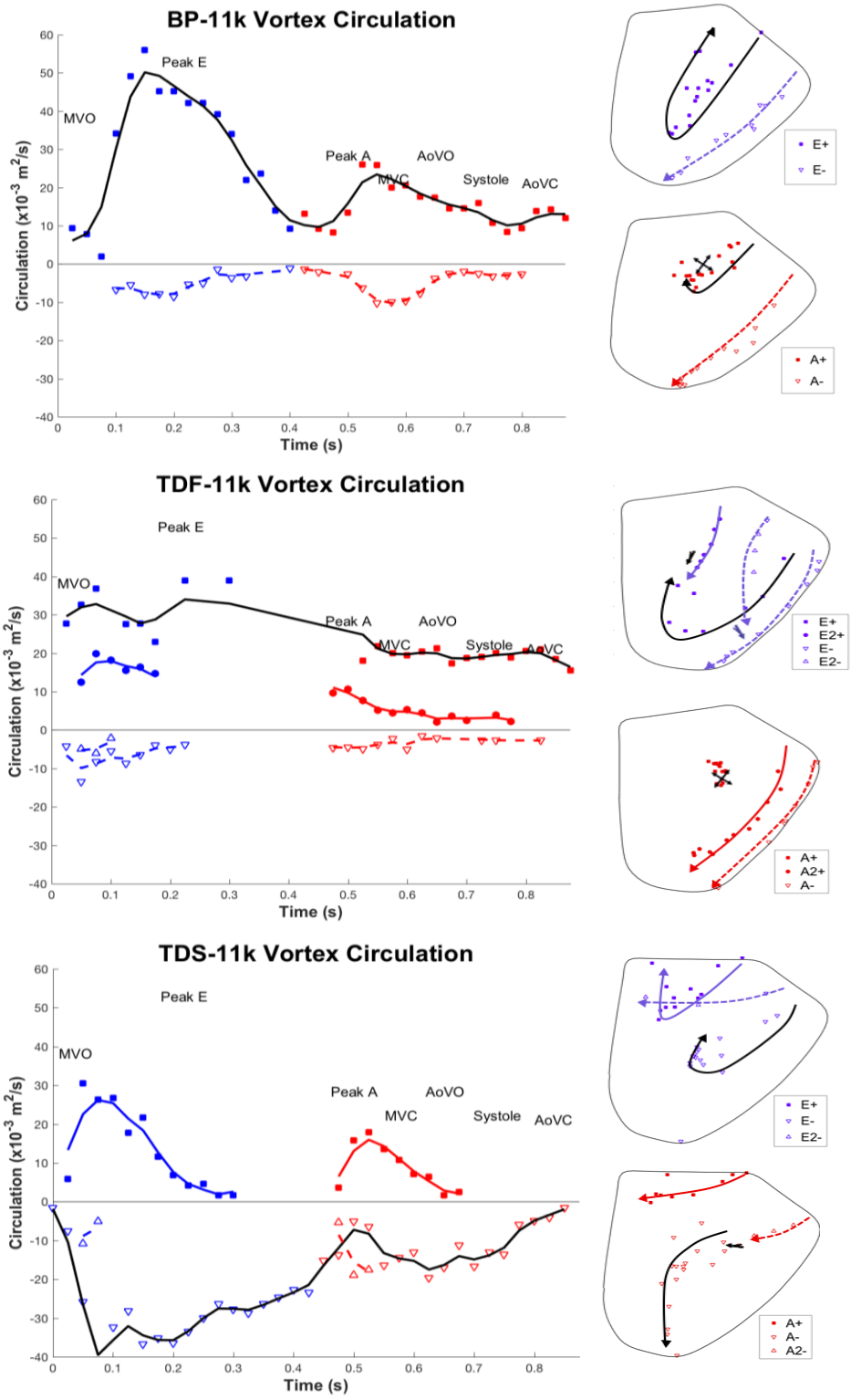

[B] 11k rpm LVAD speed

Figure 5.4: Vortex Circulation and Trajectories (cont.)

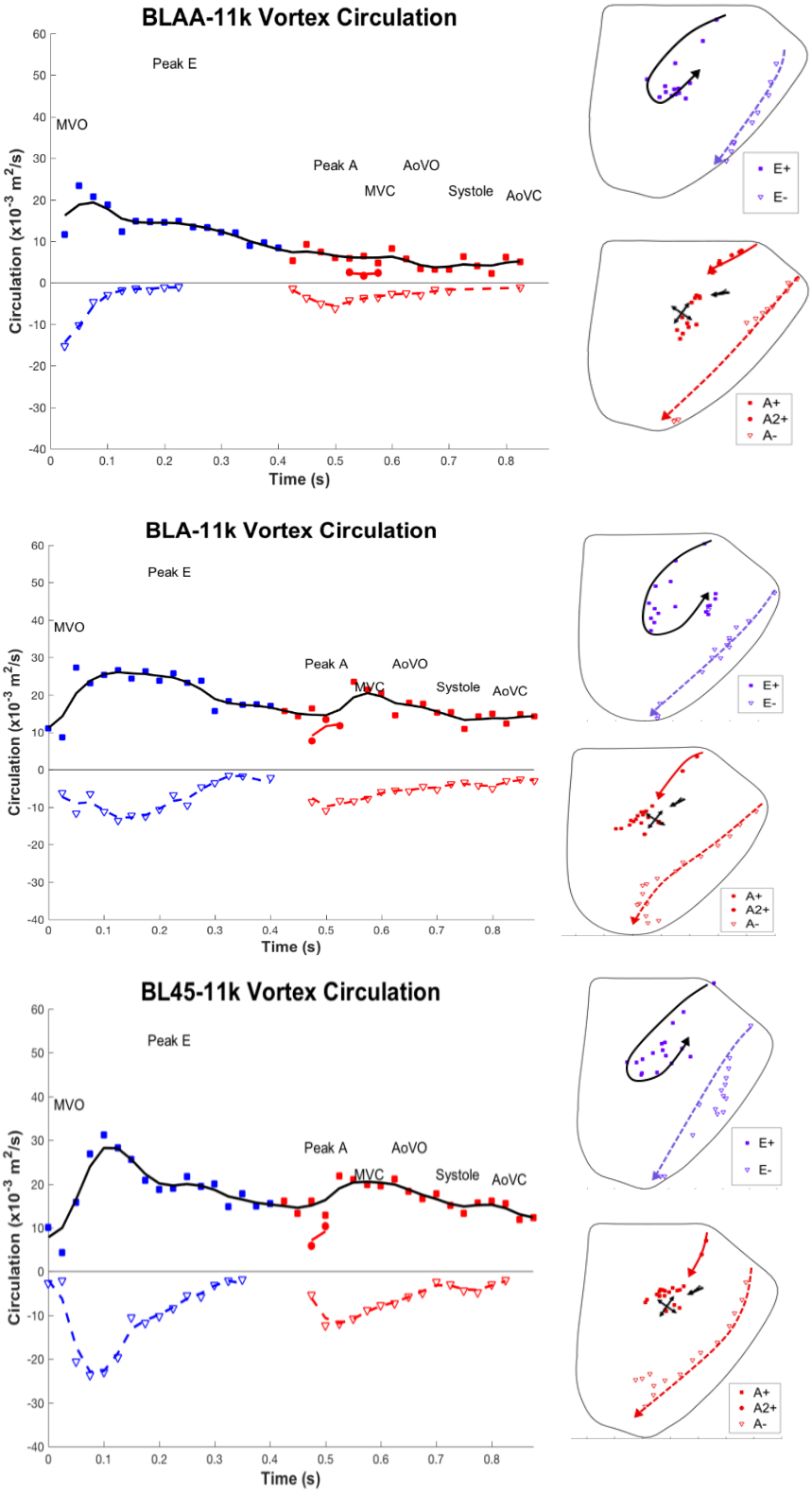

[B] 11k rpm LVAD speed

Figure 5.4: Vortex Circulation and Trajectories (cont.)

For the TD valves, secondary vortices were formed in addition during the early filling phases to the main CW and CCW vortices. The TD-F had the larger orifice area opening toward the free wall, developing a stronger and four times larger elliptical CW vortex. The main CW and CCW vortices traveled a similar path as the BP valve, excepts that the CW vortex lasted longer during diastasis. Secondary CW and CCW vortices formed during early E- and A-wave, traveling toward the LV center to merge with the main vortices. Higher LVAD support increased the persistency of the 2° CW vortices and kept the main CW vortex at the LV center. Alternatively, the TD-S channeled the filling jet towards the septum wall and gave extra space for the CCW vortex to grow, resulting in the reversal of CW and CCW symmetry. The main CCW vortex persisted during diastole, moving toward the LV apex during systole; while the CW vortex mostly circulated the AV base. Secondary CCW vortex generated at the E-wave moved toward the septum and dissipated, while the A-wave structure traveled toward the apex to merge with the main CCW vortex. The higher level of LVAD support yielded similar vortex properties and patterns. The BL designs produced secondary CW vortices during early A-wave, which subsequently merged with the main CW vortices at the LV center. The CCW vortices were also more persistent and traveled toward the LV apex. During 8k support, the BL designs produced comparable KE and circulation to the BP case. Higher LVAD support decreased BL-AA KE and circulation significantly, but not other BL case

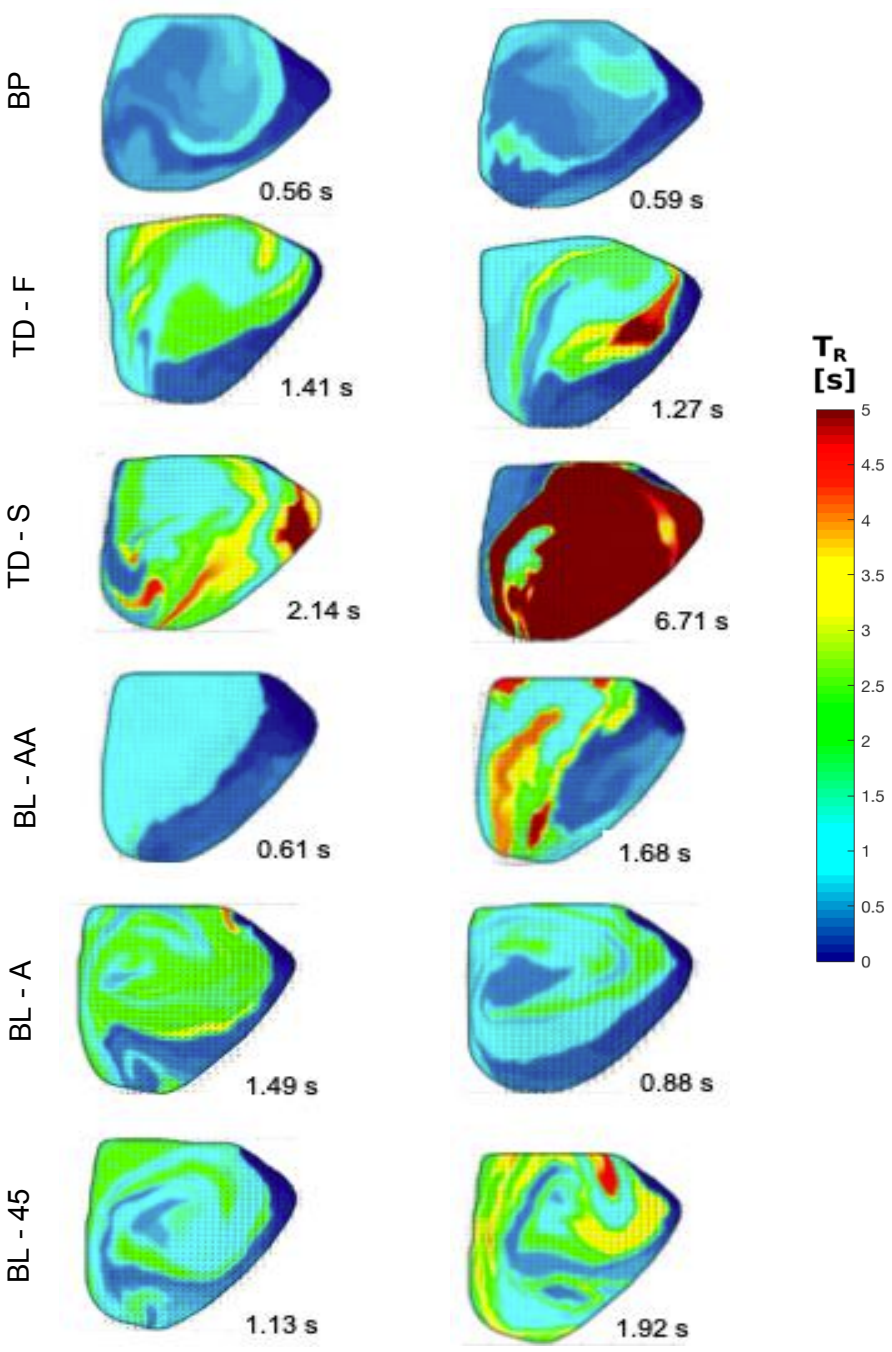

[A] [B]

Figure 5.5: Left ventricle spatial average maps of residence time for the midplane area over 10 cycles of integration during (A) 8k and (B) 11k LVAD supports are shown for each of the six different valve cases

Blood Residence Time

T_R maps of the LV following 10 CC varied among the different valve designs and configurations (Figure 5.5 and Table 5.4). The BP case exhibited the lowest T_R, with no regions with residual blood (T_R > 2 cycles) during different LVAD support levels. At the low LVAD support level, T_R of BL-AA was slightly worse than the BP valve but had no residual blood. The BL-A, BL-45, and TD-F had a relatively similar T_R. The residual area of BL-45 is lowest among those three, spreading along the LV outflow tract. The BL-A has the largest residual area, mostly confined to the LV center, while the TD-F's residual area was localized underneath the AV base and LV center. The reversed swirling pattern impaired LV washout in the TD-S case, leading to the highest T_R and region with $T_R \geq 5$ cycles at the MV base. During high LVAD support, BL-A had a significant reduction in T_R and residual area, followed by the TD-F case. The other BL cases, however, had higher average times and some T_R region ≥ 4 cycles. The TD-F's T_R increased dramatically (more than 3 folds), covering approximately 90% LV area with $T_R \approx 7.56$ s.

Table 5.4**:** Residence Time (T_R) summary after 10 cardiac cycle

Parameter		*Average T_R (s)*	*% T_R area > 2CC (%)*	*Average T_R of area > 2CC (s)*
LVAD 8x10^3 rpm	**BP**	0.56	N/A	N/A
	TD-F	1.41	33.99	2.43
	TD-S	2.14	52.89	3.05
	BL-AA	0.61	N/A	N/A
	BL-A	1.49	66.84	2.32
	BL-45	1.13	16.06	2.08
LVAD 11x10^3 rpm	**BP**	0.59	N/A	N/A
	TD-F	1.27	21.24	3.21
	TD-S	6.71	89.10	7.56
	BL-AA	1.68	35.22	3.17
	BL-A	0.88	9.00	1.92
	BL-45	1.92	47.15	2.82

5.4 Discussion

This study presents a side-by-side comparison of MV prosthesis designs and orientations under in a dilated heart failure model during continuous axial-flow HeartMate II LVAD support. Characterization of the intraventricular flow field, including vortex dynamics, and residence time, provide insight into assessing the risk of TE. Previous publications reported that preexisting prosthesis MV (biological or mechanical) could be left in place upon LVAD implantation without any significant impacts on the pump function or TE risk, while special attention was needed to ensure proper anticoagulation management[126,274,276]. However, due to the small study sample and unspecified valve types/orientation, they failed to fully assess the TE risk on prosthesis MV during LVAD support.

Diastolic vortical flow in the LV was first observed back in 1995 using color Doppler mapping an MRI[247,279,280], in comparison to ejection, ventricular filling remains a complex process and is less understood[281]. For the efficient filling and limited dissipated energy, the LV must draw blood from LA by recoiling and have sufficient room for the asymmetric growth of diastolic vortex[247]. The LV flow pattern is significantly altered in dilated cardiomyopathy (DCM) heart due to the changes in LV geometry and function, affecting blood transit and vortex formation[245,249,282,283]. The vortex dynamics of DCM patients consisted of well-rounded, lingered CW vortex near the MV, causing lower velocity propagation and favoring stasis flow at the LV apex[245,284]. The echocardiographic assessment reported that DCM hearts had larger CW circulation and KE than healthy hearts[245]. There were no *in vivo* data of intraventricular flow during LVAD support in the presence of different MV prosthesis.

The previous publication reported that the presence of continuous flow LVAD did not alter overall vortex dynamics, except for slightly increased the circulation and KE, particularly during systole[59]. The formation and evolution of CW and CCW vortices were similar in the pre-LVAD case, but the CCW vortex was stronger[59]. In most cases, the PIV quantification for all the valve types and orientations agreed with previous publications, following similar vortex patterns with

slightly higher circulation and KE compared to the pre-LVAD cases[59,124]. The BL-AA during 11k LVAD support had significantly decreased in vortex circulation and KE, while its hemodynamics data was in good agreement with other BL cases. This deviation could partially due to the increase of out of plane velocity and LV turbulence, due to the interaction between the mechanical leaflet hinges in anti-anatomical position and incoming flow during high LVAD support. Some errors may be caused by small out-of-plane motions of the LV bag from the laser mid-plane, resulting in a discontinuity of the average velocity and inaccurate vortex and KE results.

Large residual LV volume has been found in DCM patients[282] and linked to thrombosis in acute myocardial infarction[285,286]. There is a poverty of literature available to assess the TE risk for different MV prostheses during LVAD support. Therefore, *in vitro* quantitative efforts such as one presented here are valuable to establish how high residence time relates to high TE risk in LVAD patients with MV prosthesis. Higher LVAD support limited AVO, introducing larger regions of residual flow, especially around the AV base in most cases. The BP had lowest T_R in comparison to other valve types and positions, although the LVAD presence slightly increased the average T_R and introduced some region of high T_R underneath the MV base. For the BL valves, increasing LVAD support improved flow mixing and transport, resulting in lower average T_R in the anatomical position, but increased T_R and introduced residual flow regions along the LV outflow tract (LVOT) in the anti-anatomical and 45° positions. High LVAD support allowed better wash out of LV apex in the TD-F, but amplified the effect of reversal vortex pattern and worsened flow transport in the TD-S case. The residual flow regions were mostly localized near the AV base and LV center during low LVAD support. However, they expanded to spread along the LVOT and underneath the MV, which potentially pose a risk of ventricular and valvular thrombosis.

The BP valve produced the most efficient LV washout, the result of the highest inflow infiltration capacity, and strong CW vortex circulation limiting stasis flow region formation. On the other hand, the TD-S case exhibited reversed CCW flow swirl causing a collision of the inflow and outflow jets, which were previously linked to lower mechanical efficiency and higher TE risk[271,287],

and heavily impacted LV flow transport. These performances are consistent with the previously published result of the pre-LVAD condition[124].

5.5 Limitation and Conclusion

Similar system limitations, as discussed in Chapter 3, are in this study. A small degree of spatial resolution in the image sequences was lacked as the result of only 10 images sets collected and phased average for each time point. The uncertainty of the average velocity fields at each time point was below 5%, except for the 5 frames during the early E-wave. In those frames, maximum uncertainty was 25% and only visible in the mitral inflow region.

Intraventricular flow field indices for six different MV prosthesis designs/orientations under matched low cardiac output conditions during low and high LVAD support were measured in a cardiac simulator. The presence of the LVAD approximately did not substantially alter the overall vortex formation, except for slightly increased circulation and KE. The BP valve provided the best transport at low LVAD speed, which was maintained at higher speed; while the TD-S severely impaired LV washout. This finding suggested that BL has a lower risk of thromboembolism for MHV in the mitral position, particularly DCM patients during HeartMate II support. However, depending on the LVAD support level, different orientations of the BL valve might produce better flow mixing and transport.

5.6 Acknowledgements

This chapter, in full, is in an early prepared stage for publication. The co-authors are Lorenzo Rossini, Pablo Martinez-Legazpi, Juan C. del Álamo, and Karen May-Newman. The dissertation author is the primary author of this paper.

Chapter 6

Summary and Future Direction

6.1 Summary of the Dissertation

Left Ventricular assist device (LVAD) support disrupts the normal blood path by removing blood from the left ventricle (LV) apex and pumping directly into the ascending aorta. During low/medium LVAD support, blood flow occurs through both the aortic valve (AV) and the pump. During high LVAD support, the AV is hemodynamically closed, and blood exits the LV through the pump[63]. The altered intraventricular flow pattern is thought to contribute to the observed increased valvular dysfunction and its associated clinical risks. Upon LVAD implant, pre-existing prosthetic (biological or mechanical) mitral valves(MV) is not a contraindication and often left in patients[87,288]. Some centers prefer to replace mechanical MV with bioprosthesis to minimize the potential valvular thrombosis complication[289]. On the other hand, the current consensus guidelines for the AV advocates repair or replacement for moderate-severe aortic insufficiency (AI), while mild AI is often left uncorrected[162]. Valve dysfunction, whether aortic or mitral, disrupts the intraventricular flow and contributes to declining heart function. When combined with the mechanical alterations imposed by a LVAD, the flow interactions become of great clinical importance for assessing the progression and associated risk of thrombus, stroke, and AI.

This thesis examined the interaction of continuous-flow LVAD support with two forms of valve dysfunction, aortic insufficiency (AI), and MV replacement. A mock circulatory loop served as a testbed to match baseline conditions and measure the hemodynamics and the velocity patterns for a range of conditions. Further analysis evaluated vortex dynamics, pulsatility, and residence time as indices of flow stasis and recirculation. In Chapter 1, a broad introduction to the work is provided, followed by a detailed literature review in Chapter 2.

Chapters 3 and 4 describe the studies of AI during LVAD support with both HeartMate II (HMII) and HeartMate 3 (HM3) designs. In the presence of pre-existing AI, regurgitant AV flow occurred during the diastolic phase, with regurgitant jet parameters (e.g., area, vena contracta width, velocity, etc.) increasing with LVAD severity. LVAD support aggravates AI by increasing the duration and magnitude of regurgitant flow. The HM2 and HM3 both worsen AI indices by introducing turbulence, altering the intraventricular flow pattern, increasing energy loss, and prolonging the diastolic phase. The results also suggested that the current clinical indices underestimate AI severity during LVAD support (either when LVAD is first introduced or over a range of LVAD speed), thus introduced a need for new indices to assess AI in LVAD patients. Other easily acquired indices (jet/LVOT ratio and est. jet area) showed higher sensitivity and area are recommended for further clinical exploration. Furthermore, LVAD support altered the AV flow and biomechanics drastically and driven the worsening of AI. The presence of LVAD increases the tensile stress and decreases the forward shear that the AV tissue is experienced without AI, while introducing oscillating shear when AI presence. From the result, we proposed a new risk prediction and treatment of AI, modifying from the current guidelines[63,138,162,179].

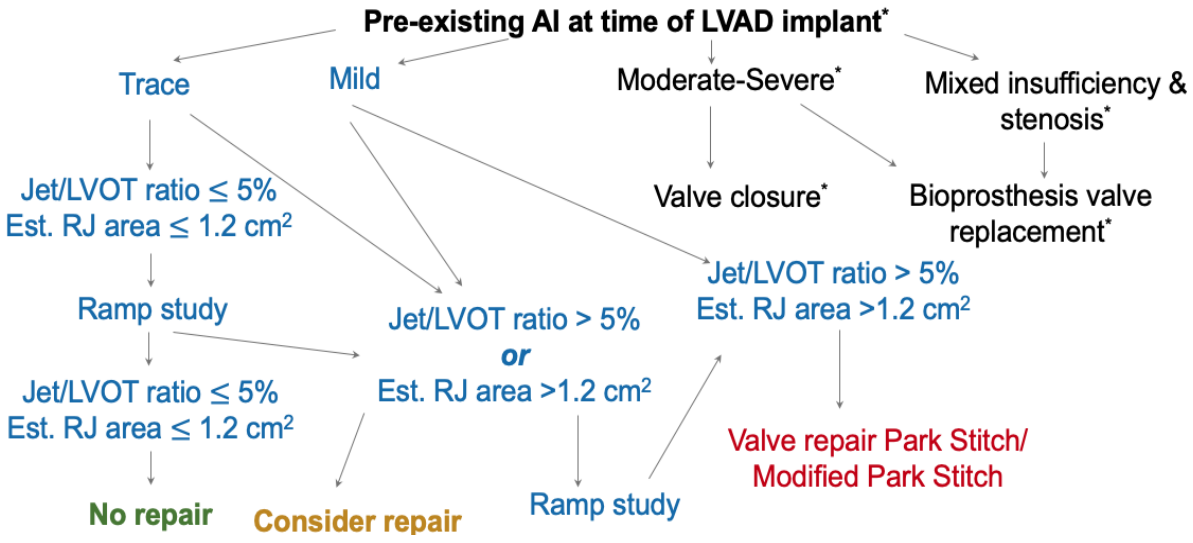

Figure 6.1: Proposed AI risk prediction and treatment (the thresholds were extracted the Chapter 3 and 4 result, *current guidelines[63,138,162,179].).

In Chapter 5, the effect of MV prosthesis design on intraventricular flow during HM2 LVAD support is described for six different MV prosthesis design/orientations. This study follows a previously published work reporting the flow patterns introduced by the MV prostheses without LVAD support. The LVAD did not substantially alter the overall vortex formation but created distinct residual flow regions. The results show that the bioprosthetic valve provided the best transport for all LVAD speeds, while the tilting-disk mechanical valve prosthesis, particularly in septal orientation, severely impaired the LV washout.

6.2 Recommendations for Future Work

6.2.1 Two-dimensional Velocity Vector Field Limitation

A single-camera PIV system was used to measure the two-dimensional (2D) flow patterns at the LV mid-plane[59] (Figure 3.3). The 2D image captured the asymmetric mitral inflow vortex previously identified in MRI and echocardiography studies[290]. However, the velocity field data lacks out-of-plane information when particles leave the imaging plane during the recording cycle. To compensate, in the residence time calculation, it was assumed that any particles entering the plane at a specific location would have the same residence time of the particle currently located at that point[124].

To assess the magnitude of the out-of-plane velocity components, a pilot study was performed with two-camera stereoscopic PIV[291] used to measure velocity in the LV midplane for a small number of conditions. The resulting 3D velocity vector field includes the in-plane (Vx and Vy) and out-of-plane (Vz) components, displayed at early-diastole for the Pre-LVAD condition in Figure 6.2. The average in-plane velocity (V), calculated as the root mean square of the Vx and Vy, is compared to the average Vz for one cardiac cycle and shown in Figure 6.3. During the peak E- and A-wave (at t= 0.1 and 0.6 second (s)), for the Pre-LVAD Baseline and Mild AI conditions, Vz was 12%- 30% of V. This suggests that the in-plane velocity is dominant and sufficient to represent the swirling diastolic flow pattern, in agreement in the previous 2D-flow assumption[290].

However, when AI was present, during diastasis (t=0.2-05 s) and systole (t=0.65-0.95 s), Vz was 58%-90% of V. As LVAD speed increased, the in-plane velocity increased significantly at 25%-102%, while Vz increased only 15%-25%. A similar observation was noted in Moderate and Severe AI conditions. Without accounting for the out-of-plane velocity contribution in the presence of complex flow architectures (such as AI), the residence time calculation might yield inaccurate results.

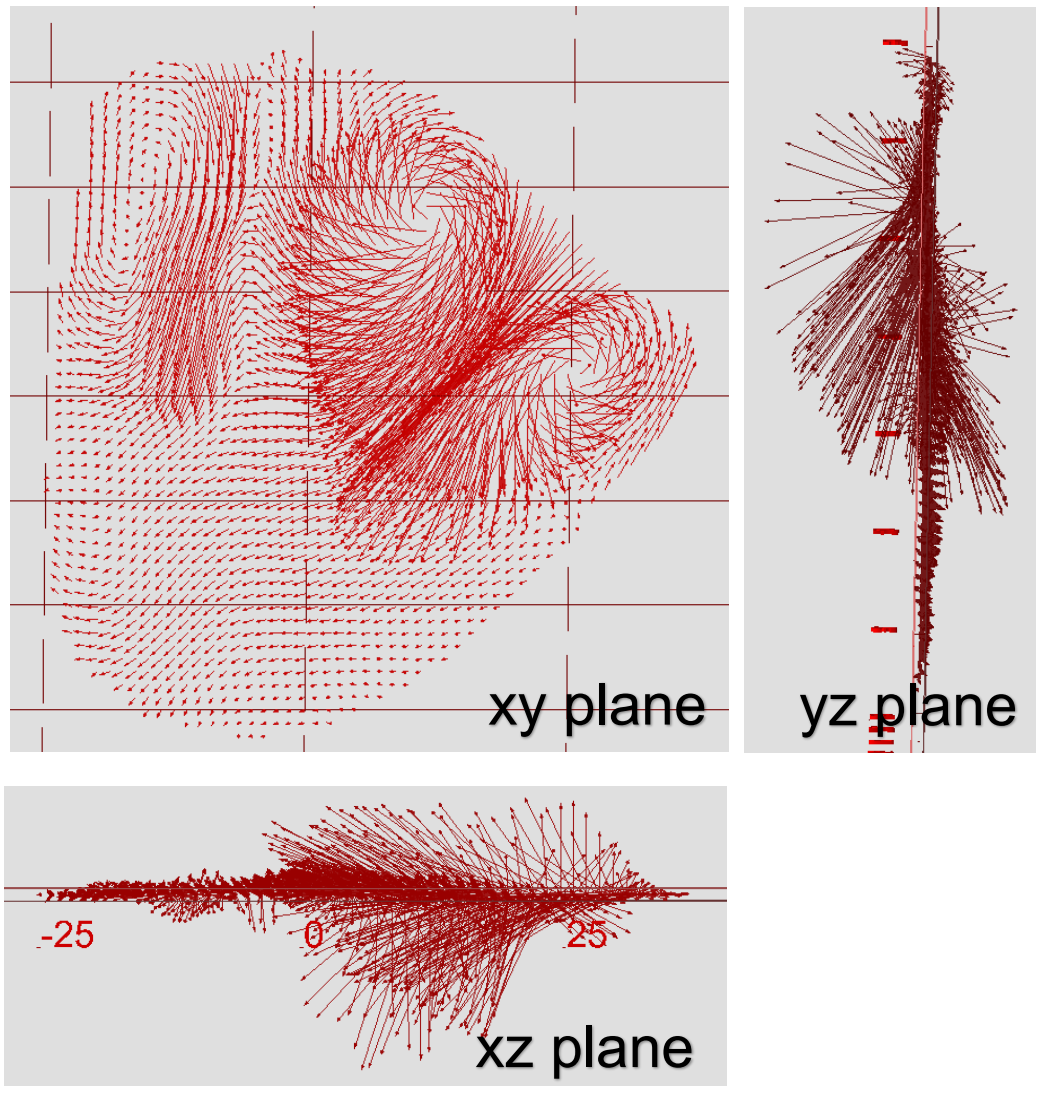

Figure 6.2: Velocity vector fields captured using two-cameras PIV setup in the LV midplane. Out-of-plane (Vz) components were shown in yz and zx planes.

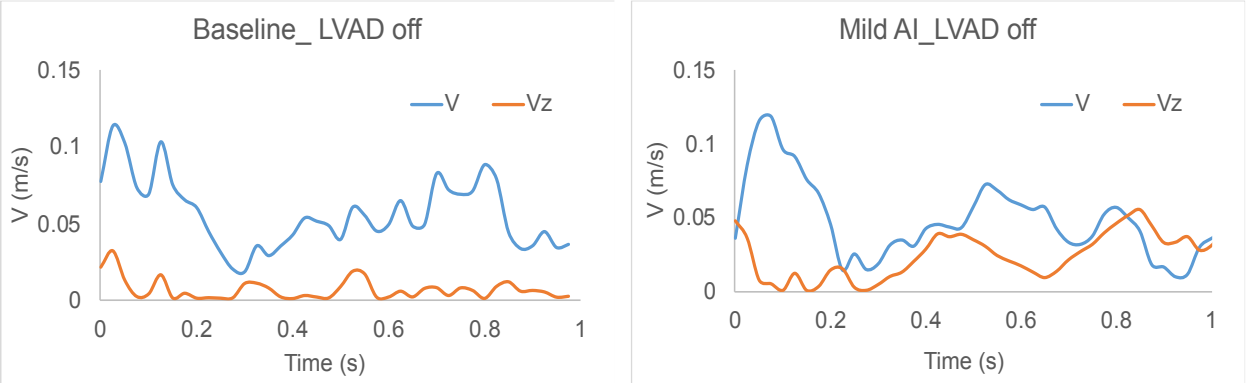

[A]

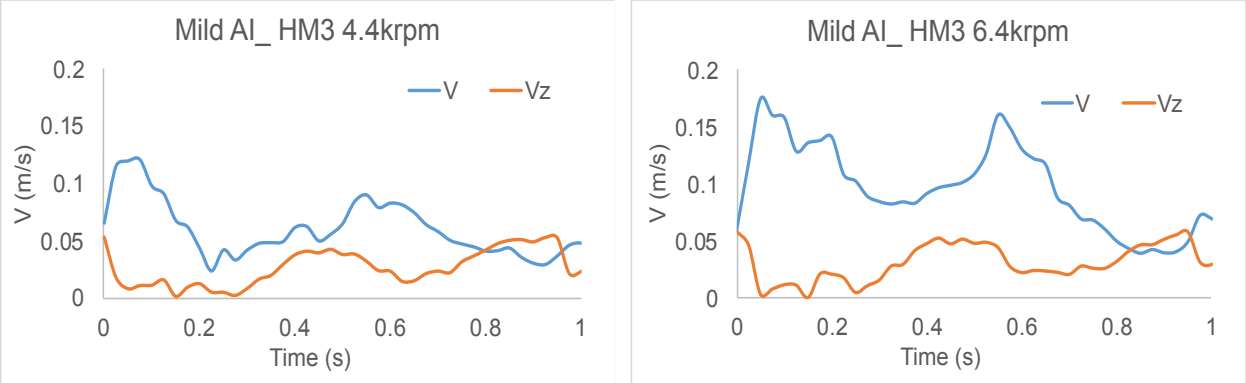

[B]

Figure 6.3: Mid-plane average velocity (V) and out-of-plane velocity (Vz) time-varying during one cardiac cycle of [A] Baseline and Mild AI pre-LVAD conditions and [B] Mild AI during low (4.4 krpm) and high (5.4 krpm) Heartmate 3 (HM3) LVAD support. (Diastole starts at t=0, the 2nd filling phase occurs at t=0.525s, and the systole starts at 0.65s)

6.2.2 Future Works

The mock loop design has several limitations for fully replicating clinical conditions, as discussed in detail in chapter 3.5. The control of cardiac filling and emptying in the mock loop is accomplished by the motion of a piston attached to the fluid-filled chamber surrounding the silicone LV. Downward displacement of the piston expands the LV, which decreases LV pressure and initiates filling. Upward displacement increases the pressure surrounding the LV, increasing pressure until it exceeds aortic pressure, and the aortic valve opens to allow flow. This is a standard mechanism for simulating the cardiac cycle in a mock loop [251,287,292–294], and the

appropriate LV flow pattern is produced. However, in the presence of AI, the additional A-wave expansion may also prolong the regurgitant jet. Moreover, the system's left atrium chamber is open to the atmosphere and provides unlimited preload; thus, the study of suction is not possible. Future studies could modify the cardiac system to reflect a more physiological model of the left atrium.

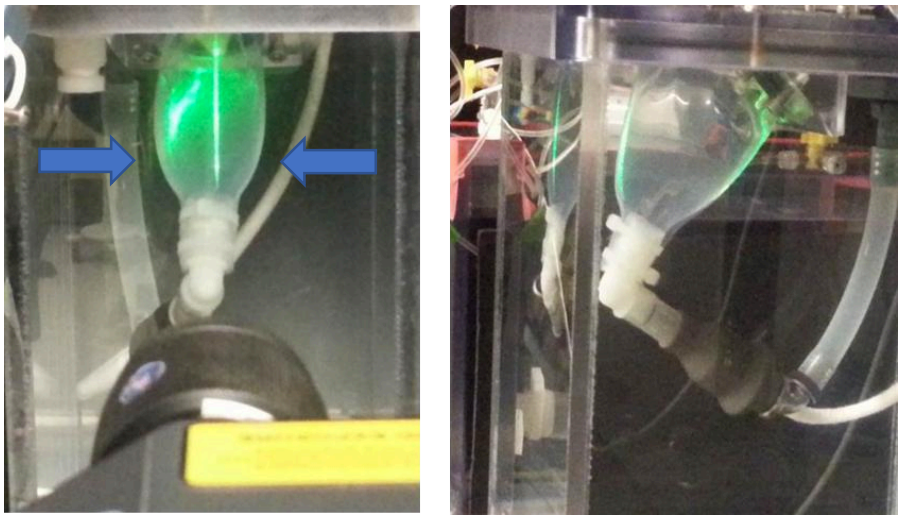

Figure 6.4: (Left) The laser sheet at the silicone LV mid-plane passing through the valves and apex (arrows indicated the orientation where most of the bag compression occurred). (Right) The camera view is perpendicular to the laser sheet.

Furthermore, in the current setup, the LV bag is compressed in the plane perpendicular to the PIV imaging plane (Figure 6.4). Hence, the midplane boundary motion is inadequate for estimating LV volume changes during the cardiac cycle. Future studies will utilize the two-camera stereoscopic PIV setup of multiple parallel and perpendicular planes to capture the 3-D velocity field, reconstruct three-dimensional flow architectures, and quantify LV volume changes. The 3-D PIV will improve the spatial image resolution, and provide the out-of-plane velocity component to accurately determine residence time.

The interaction of valve dysfunction and LVAD support was assessed with measurements of the intraventricular flow in a controlled testbed. The results provide a focus for future clinical

evaluation to use echocardiography and computational modeling, providing additional insight to aid in future patient management and LVAD design.

Bibliography

(1) Benjamin, E. J.; Muntner, P.; Alonso, A.; Bittencourt, M. S.; Callaway, C.; Carson, A.; Chamberlain, A.; Chang, A.; Cheng, S.; Das, S.; Delling, F.; Djousse, L.; Elkind, M.; Ferguson, J.; Fornage, M.; Jordan, L. C.; Khan, S.; Kissela, B. Heart Disease and Stroke Statistics—2019 Update: A Report From the American Heart Association. *Circ. J.* 2019, No. 139, e56–e528.

(2) Young, J. B. Healing the Heart with Ventricular Assist Device Therapy: Mechanisms of Cardiac Recovery. *Ann. Thorac. Surg.* 2001, *71* (3), S210–S219. https://doi.org/10.1016/S0003-4975(00)02633-3.

(3) WRITING GROUP MEMBERS; Lloyd-Jones, D.; Adams, R. J.; Brown, T. M.; Carnethon, M.; Dai, S.; De Simone, G.; Ferguson, T. B.; Ford, E.; Furie, K.; Gillespie, C.; Go, A.; Greenlund, K.; Haase, N.; Hailpern, S.; Ho, P. M.; Howard, V.; Kissela, B.; Kittner, S.; Lackland, D.; Lisabeth, L.; Marelli, A.; McDermott, M. M.; Meigs, J.; Mozaffarian, D.; Mussolino, M.; Nichol, G.; Roger, V. L.; Rosamond, W.; Sacco, R.; Sorlie, P.; Stafford, R.; Thom, T.; Wasserthiel-Smoller, S.; Wong, N. D.; Wylie-Rosett, J. Heart Disease and Stroke Statistics—2010 Update: A Report From the American Heart Association. *Circulation* 2010, *121* (7). https://doi.org/10.1161/CIRCULATIONAHA.109.192667.

(4) Heidenreich, P. A.; Albert, N. M.; Allen, L. A.; Bluemke, D. A.; Butler, J.; Fonarow, G. C.; Ikonomidis, J. S.; Khavjou, O.; Konstam, M. A.; Maddox, T. M.; Nichol, G.; Pham, M.; Piña, I. L.; Trogdon, J. G. Forecasting the Impact of Heart Failure in the United States: A Policy Statement From the American Heart Association. *Circ. Heart Fail.* 2013, *6* (3), 606–619. https://doi.org/10.1161/HHF.0b013e318291329a.

(5) Califf, R. M.; Adams, K. F.; McKenna, W. J.; Gheorghiade, M.; Uretsky, B. F.; McNulty, S. E.; Darius, H.; Schulman, K.; Zannad, F.; Handberg-Thurmond, E.; Harrell, F. E.; Wheeler, W.; Soler-Soler, J.; Swedberg, K. A Randomized Controlled Trial of Epoprostenol Therapy for Severe Congestive Heart Failure: The Flolan International Randomized Survival Trial (FIRST). *Am. Heart J.* 1997, *134* (1), 44–54. https://doi.org/10.1016/S0002-8703(97)70105-4.

(6) Loehr, L. R.; Rosamond, W. D.; Chang, P. P.; Folsom, A. R.; Chambless, L. E. Heart Failure Incidence and Survival (from the Atherosclerosis Risk in Communities Study). *Am. J. Cardiol.* 2008, *101* (7), 1016–1022. https://doi.org/10.1016/j.amjcard.2007.11.061.

(7) Roger, V. L.; Go, A. S.; Lloyd-Jones, D. M.; Benjamin, E. J.; Berry, J. D.; Borden, W. B.; Bravata, D. M.; Dai, S.; Ford, E. S.; Fox, C. S.; Fullerton, H. J.; Gillespie, C.; Hailpern, S. M.; Heit, J. A.; Howard, V. J.; Kissela, B. M.; Kittner, S. J.; Lackland, D. T.; Lichtman, J. H.; Lisabeth, L. D.; Makuc, D. M.; Marcus, G. M.; Marelli, A.; Matchar, D. B.; Moy, C. S.; Mozaffarian, D.; Mussolino, M. E.; Nichol, G.; Paynter, N. P.; Soliman, E. Z.; Sorlie, P. D.; Sotoodehnia, N.; Turan, T. N.; Virani, S. S.; Wong, N. D.; Woo, D.; Turner, M. B. Heart Disease and Stroke Statistics—2012 Update: A Report From the American Heart Association. *Circulation* 2012, *125* (1). https://doi.org/10.1161/CIR.0b013e31823ac046.

(8) Rose, E. A.; Stevenson, L. W.; Tierney, A. R. Long-Term Use of a Left Ventricular Assist Device for End-Stage Heart Failure. *N. Engl. J. Med.* 2001, 9.

(9) Gridelli, B.; Remuzzi, G. Strategies for Making More Organs Available for Transplantation. *N. Engl. J. Med.* 2000, *343* (6), 404–410. https://doi.org/10.1056/NEJM200008103430606.

(10) Slaughter, M. S.; Pagani, F. D.; Rogers, J. G.; Miller, L. W.; Sun, B.; Russell, S. D.; Starling, R. C.; Chen, L.; Boyle, A. J.; Chillcott, S.; Adamson, R. M.; Blood, M. S.; Camacho, M. T.; Idrissi, K. A.; Petty, M.; Sobieski, M.; Wright, S.; Myers, T. J.; Farrar, D. J. Clinical Management of Continuous-Flow Left Ventricular Assist Devices in Advanced Heart Failure. *J. Heart Lung Transplant.* 2010, *29* (4), S1–S39. https://doi.org/10.1016/j.healun.2010.01.011.

(11) Prinzing, A.; Herold, U.; Berkefeld, A.; Krane, M.; Lange, R.; Voss, B. Left Ventricular Assist Devices—Current State and Perspectives. *J. Thorac. Dis.* 2016, *8* (8), E660–E666. https://doi.org/10.21037/jtd.2016.07.13.

(12) Smits, J. M. Actual Situation in Eurotransplant Regarding High Urgent Heart Transplantation. *Eur. J. Cardiothorac. Surg.* 2012, *42* (4), 609–611. https://doi.org/10.1093/ejcts/ezs424.

(13) Cooley, D.; Liotta, D.; Hallman, G.; Bloodwell, R.; Leachman, R.; Milan, J. Orthotopic Cardiac Prosthesis for Two-Staged Cardiac Replacement. *Am J Cardiol* 1969, *24* (5), 723–730.

(14) DeBakey, M. Left Ventricular Bypass Pump for Cardiac Assistance. Clinical Experience. *Am J Cardiol* 1971, *27* (1), 3–11.

(15) Frazier, O. H. First Use of an Untethered, Vented Electric Left Ventricular Assist Device for Long-Term Support. *Circulation* 1994, *89* (6), 2908–2914. https://doi.org/10.1161/01.CIR.89.6.2908.

(16) Oz, M.; Argenziano, M.; Catanese, K.; Gardocki, M.; Goldstein, D.; Ashton, R.; Gelijns, A.; Rose, E.; Levin, H. Bridge Experience with Long-Term Implantable Left Ventricular Assist Devices. Are They an Alternative to Transplantation? *Circulation* 1997, *95* (7), 1844–1852.

(17) Muller, J.; Wallukat, G.; Weng, Y.; Dandel, M.; Spiegelsberger, S.; Semrau, S.; Brandes, K.; Theodoridis, V.; Loebe, M.; Meyer, R.; Hetzer, R. Weaning From Mechanical Cardiac Support in Patients With Idiopathic Dilated Cardiomyopathy. *Circulation* 1997, *96* (2), 542–549.

(18) McCarthy, P. M.; Young, J. B.; Smedira, N. G.; Hobbs, R. E.; Vargo, R. L.; Starling, R. C. Permanent Mechanical Circulatory Support with an Implantable Left Ventricular Assist Device. *Ann. Thorac. Surg.* 1997, *63* (5), 1458–1461. https://doi.org/10.1016/S0003-4975(97)00110-0.

(19) William, M.; Oz, M. Indications and Patient Selection for Mechanical Ventricular Assistance. *Ann Thorac Surg* 2001, *71* (3 Suppl), S86-91.

(20) Fitzpatrick, J. R.; Frederick, J. R.; Hsu, V. M.; Kozin, E. D.; O'Hara, M. L.; Howell, E.; Dougherty, D.; McCormick, R. C.; Laporte, C. A.; Cohen, J. E.; Southerland, K. W.; Howard, J. L.; Jessup, M. L.; Morris, R. J.; Acker, M. A.; Woo, Y. J. Risk Score Derived from Pre-Operative Data Analysis Predicts the Need for Biventricular Mechanical Circulatory Support. *J. Heart Lung Transplant.* 2008, *27* (12), 1286–1292. https://doi.org/10.1016/j.healun.2008.09.006.

(21) Frazier, O. H.; Rose, E. A.; Oz, M. C.; Dembitsky, W.; McCarthy, P.; Radovancevic, B.; Poirier, V. L.; Dasse, K. A. Multicenter Clinical Evaluation of the HeartMate Vented Electric Left Ventricular Assist System in Patients Awaiting Heart Transplantation. *J. Thorac. Cardiovasc. Surg.* 2001, *122* (6), 1186–1195. https://doi.org/10.1067/mtc.2001.118274.

(22) McCarthy, P. M.; Smedira, N. O.; Vargo, R. L.; Goormastic, M.; Hobbs, R. E.; Starling, R. C.; Young, J. B. One Hundred Patients with the HeartMate Left Ventricular Assist Device: Evolving Concepts and Technology. *J. Thorac. Cardiovasc. Surg.* 1998, *115* (4), 904–912. https://doi.org/10.1016/S0022-5223(98)70373-3.

(23) Mueller, J. Predictive Factors for Weaning from a Cardiac Assist Device. An Analysis of Clinical, Gene Expression, and Protein Data. 2001, *20* (2), 202.

(24) Deng, M. C.; Loebe, M.; El-Banayosy, A. Mechanical Circulatory Support for Advanced Heart Failure: Effect of Patient Selection on Outcome. *ACC Curr. J. Rev.* 2001, *10* (4), 55. https://doi.org/10.1016/S1062-1458(01)00315-4.

(25) Hetzer, R.; Müller, J. H.; Weng, Y.; Meyer, R.; Dandel, M. Bridging-to-Recovery. *Ann. Thorac. Surg.* 2001, *71* (3), S109–S113. https://doi.org/10.1016/S0003-4975(00)02638-2.

(26) Rogers, J. G.; Bostic, R. R.; Tong, K. B.; Adamson, R.; Russo, M.; Slaughter, M. S. Cost-Effectiveness Analysis of Continuous-Flow Left Ventricular Assist Devices as Destination Therapy. *Circ. Heart Fail.* 2012, *5* (1), 10–16. https://doi.org/10.1161/CIRCHEARTFAILURE.111.962951.

(27) Khazanie, P.; Hammill, B. G.; Patel, C. B.; Eapen, Z. J.; Peterson, E. D.; Rogers, J. G.; Milano, C. A.; Curtis, L. H.; Hernandez, A. F. Trends in the Use and Outcomes of Ventricular Assist Devices Among Medicare Beneficiaries, 2006 Through 2011. *J. Am. Coll. Cardiol.* 2014, *63* (14), 1395–1404. https://doi.org/10.1016/j.jacc.2013.12.020.

(28) Miller, L. W.; Guglin, M.; Rogers, J. Cost of Ventricular Assist Devices: Can We Afford The Progress? *Circulation* 2013, *127* (6), 743–748. https://doi.org/10.1161/CIRCULATIONAHA.112.139824.

(29) Drakos, S. G. The Odyssey of Chronic Cardiac Mechanical Support∗ . *J. Am. Coll. Cardiol.* 2014, *63* (17), 1758–1760. https://doi.org/10.1016/j.jacc.2014.02.531.

(30) Williams, M. L.; Trivedi, J. R.; McCants, K. C.; Prabhu, S. D.; Birks, E. J.; Oliver, L.; Slaughter, M. S. Heart Transplant vs Left Ventricular Assist Device in Heart Transplant-Eligible Patients. *Ann. Thorac. Surg.* 2011, *91* (5), 1330–1334. https://doi.org/10.1016/j.athoracsur.2011.01.062.

(31) Marasco, S. F.; Summerhayes, R.; Quayle, M.; McGiffin, D.; Luthe, M. Cost Comparison of Heart Transplant vs. Left Ventricular Assist Device Therapy at One Year. *Clin. Transplant.* 2016, *30* (5), 598–605. https://doi.org/10.1111/ctr.12725.

(32) Gemmato, C. J.; Forrester, M. D.; Myers, T. J.; Frazier, O. H.; Cooley, D. A. Thirty-Five Years of Mechanical Circulatory Support at the Texas Heart Institute. *Tex. Heart Inst. J.* 2005, *32* (2), 10.

(33) Frazier, O. H.; Baldwin, R. T.; Eskin, S.; Duncan, M. J. Immunochemical Identification of Human Endothelial Cells on the Lining of a Ventricular Assist Device. *Tex. Heart Inst. J.* 1993, *20*, 78–82.

(34) Levin, H. R.; Oz, M. C.; Chen, J. M.; Packer, M.; Rose, E. A.; Burkhoff, D. Reversal of Chronic Ventricular Dilation in Patients With End-Stage Cardiomyopathy by Prolonged Mechanical Unloading. *Circulation* 1995, *91* (11), 2717–2720. https://doi.org/10.1161/01.CIR.91.11.2717.

(35) Kormos, R. L.; Cowger, J.; Pagani, F. D.; Teuteberg, J. J.; Goldstein, D. J.; Jacobs, J. P.; Higgins, R. S.; Stevenson, L. W.; Stehlik, J.; Atluri, P.; Grady, K. L.; Kirklin, J. K. The Society of Thoracic Surgeons Intermacs Database Annual Report: Evolving Indications, Outcomes, and Scientific Partnerships. *J. Heart Lung Transplant.* 2019, *38* (2), 114–126. https://doi.org/10.1016/j.healun.2018.11.013.

(36) Schmitto, J. D.; Molitoris, U.; Haverich, A.; Strueber, M. Implantation of a Centrifugal Pump as a Left Ventricular Assist Device through a Novel, Minimized Approach: Upper Hemisternotomy Combined with Anterolateral Thoracotomy. *J. Thorac. Cardiovasc. Surg.* 2012, *143* (2), 511–513. https://doi.org/10.1016/j.jtcvs.2011.07.046.

(37) Kuehl, M.; Garbade, J. The Evolution of Left Ventricular Assist Devices—a Moment to Reflect. *J. Thorac. Dis.* 2017, *9* (5), E492–E494. https://doi.org/10.21037/jtd.2017.03.72.

(38) Slaughter, M. S.; Rogers, J. G.; Milano, C. A.; Russell, S. D.; Conte, J. V.; Feldman, D.; Sun, B.; Tatooles, A. J.; Delgado, R. M.; Long, J. W.; Wozniak, T. C.; Ghumman, W.; Farrar, D. J.; Frazier, O. H. Advanced Heart Failure Treated with Continuous-Flow Left Ventricular Assist Device. *N. Engl. J. Med.* 2009, *361* (23), 2241–2251. https://doi.org/10.1056/NEJMoa0909938.

(39) Pagani, F. D.; Miller, L. W.; Russell, S. D.; Aaronson, K. D.; John, R.; Boyle, A. J.; Conte, J. V.; Bogaev, R. C.; MacGillivray, T. E.; Naka, Y.; Mancini, D.; Massey, H. T.; Chen, L.; Klodell, C. T.; Aranda, J. M.; Moazami, N.; Ewald, G. A.; Farrar, D. J.; Frazier, O. H. Extended Mechanical Circulatory Support With a Continuous-Flow Rotary Left Ventricular Assist Device. *J. Am. Coll. Cardiol.* 2009, *54* (4), 312–321. https://doi.org/10.1016/j.jacc.2009.03.055.

(40) Moazami, N.; Fukamachi, K.; Kobayashi, M.; Smedira, N. G.; Hoercher, K. J.; Massiello, A.; Lee, S.; Horvath, D. J.; Starling, R. C. Axial and Centrifugal Continuous-Flow Rotary Pumps: A Translation from Pump Mechanics to Clinical Practice. *J. Heart Lung Transplant.* 2013, *32* (1), 1–11. https://doi.org/10.1016/j.healun.2012.10.001.

(41) Jorde, U. P.; Kushwaha, S. S.; Tatooles, A. J.; Naka, Y.; Bhat, G.; Long, J. W.; Horstmanshof, D. A.; Kormos, R. L.; Teuteberg, J. J.; Slaughter, M. S.; Birks, E. J.; Farrar, D. J.; Park, S. J. Results of the Destination Therapy Post-Food and Drug Administration Approval Study With a Continuous Flow Left Ventricular Assist Device. *J. Am. Coll. Cardiol.* 2014, *63* (17), 1751–1757. https://doi.org/10.1016/j.jacc.2014.01.053.

(42) Starling, R. C.; Moazami, N.; Silvestry, S. C.; Ewald, G.; Rogers, J. G.; Milano, C. A.; Rame, J. E.; Acker, M. A.; Blackstone, E. H.; Ehrlinger, J.; Thuita, L.; Mountis, M. M.; Soltesz, E. G.; Lytle, B. W.; Smedira, N. G. Unexpected Abrupt Increase in Left Ventricular Assist

Device Thrombosis. *N. Engl. J. Med.* 2014, *370* (1), 33–40. https://doi.org/10.1056/NEJMoa1313385.

(43) Kirklin, J. K.; Naftel, D. C.; Pagani, F. D.; Kormos, R. L.; Myers, S.; Acker, M. A.; Rogers, J.; Slaughter, M. S.; Stevenson, L. W. Pump Thrombosis in the Thoratec HeartMate II Device: An Update Analysis of the INTERMACS Registry. *J. Heart Lung Transplant.* 2015, *34* (12), 1515–1526. https://doi.org/10.1016/j.healun.2015.10.024.

(44) Mehra, M. R.; Uriel, N.; Naka, Y.; Cleveland, J. C.; Yuzefpolskaya, M.; Salerno, C. T.; Walsh, M. N.; Milano, C. A.; Patel, C. B.; Hutchins, S. W.; Ransom, J.; Ewald, G. A.; Itoh, A.; Raval, N. Y.; Silvestry, S. C.; Cogswell, R.; John, R.; Bhimaraj, A.; Bruckner, B. A.; Lowes, B. D.; Um, J. Y.; Jeevanandam, V.; Sayer, G.; Mangi, A. A.; Molina, E. J.; Sheikh, F.; Aaronson, K.; Pagani, F. D.; Cotts, W. G.; Tatooles, A. J.; Babu, A.; Chomsky, D.; Katz, J. N.; Tessmann, P. B.; Dean, D.; Krishnamoorthy, A.; Chuang, J.; Topuria, I.; Sood, P.; Goldstein, D. J. A Fully Magnetically Levitated Left Ventricular Assist Device — Final Report. *N. Engl. J. Med.* 2019, *380* (17), 1618–1627. https://doi.org/10.1056/NEJMoa1900486.

(45) Sakaguchi, T.; Matsumiya, G.; Yoshioka, D.; Miyagawa, S.; Nishi, H.; Yoshikawa, Y.; Fukushima, S.; Saito, S.; Ueno, T.; Sawa, Y. DuraHeartTM Magnetically Levitated Left Ventricular Assist Device. *Circ. J.* 2013, *77* (7), 1736–1741. https://doi.org/10.1253/circj.CJ-12-1410.

(46) Farrar, D. J.; Bourque, K.; Dague, C. P.; Cotter, C. J.; Poirier, V. L. Design Features, Developmental Status, and Experimental Results With the Heartmate III Centrifugal Left Ventricular Assist System With a Magnetically Levitated Rotor: *ASAIO J.* 2007, *53* (3), 310–315. https://doi.org/10.1097/MAT.0b013e3180536694.

(47) Bourque, K.; Cotter, C.; Dague, C.; Harjes, D.; Dur, O.; Duhamel, J.; Spink, K.; Walsh, K.; Burke, E. Design Rationale and Preclinical Evaluation of the HeartMate 3 Left Ventricular Assist System for Hemocompatibility: *ASAIO J.* 2016, *62* (4), 375–383. https://doi.org/10.1097/MAT.0000000000000388.

(48) Milano, C. A.; Schroder, J.; Daneshmand, M. Total Artificial Heart Replacement With 2 Centrifugal Blood Pumps. *Oper. Tech. Thorac. Cardiovasc. Surg.* 2015, *20* (3), 306–321. https://doi.org/10.1053/j.optechstcvs.2016.02.001.

(49) Schroder, J. N.; Milano, C. A. A Tale of Two Centrifugal Left Ventricular Assist Devices. *J. Thorac. Cardiovasc. Surg.* 2017, *154* (3), 850–852. https://doi.org/10.1016/j.jtcvs.2017.04.033.

(50) Katz, A. M. Maladaptive Growth in the Failing Heart: The Cardiomyopathy of Overload. 2002, 5.

(51) Pedrizzetti, G.; Martiniello, A. R.; Bianchi, V.; D'Onofrio, A.; Caso, P.; Tonti, G. Cardiac Fluid Dynamics Anticipates Heart Adaptation. *J. Biomech.* 2015, *48* (2), 388–391. https://doi.org/10.1016/j.jbiomech.2014.11.049.

(52) Nakatani, S.; McCarthy, P. M.; Kottke-Marchant, K.; Harasaki, H.; James, K. B.; Savage, R. M.; Thomas, J. D. Left Ventricular Echocardiographic and Histologic Changes: Impact of

Chronic Unloading by an Implantable Ventricular Assist Device. *J. Am. Coll. Cardiol.* 1996, *27* (4), 894–901. https://doi.org/10.1016/0735-1097(95)00555-2.

(53) Zafeiridis, A.; Jeevanandam, V.; Houser, S. R.; Margulies, K. B. Regression of Cellular Hypertrophy After Left Ventricular Assist Device Support. *Circulation* 1998, *98* (7), 656–662. https://doi.org/10.1161/01.CIR.98.7.656.

(54) Frazier, O. H.; Benedict, C. R.; Radovancevic, B.; Bick, R. J.; Capek, P.; Springer, W. E.; Macris, M. P.; Delgado, R.; Buja, L. M. Improved Left Ventricular Function After Chronic Left Ventricular Unloading. *Ann. Thorac. Surg.* 1996, *62* (3), 675–682. https://doi.org/10.1016/S0003-4975(96)00437-7.

(55) Drakos, S. G.; Wever-Pinzon, O.; Kfoury, A. G.; Selzman, C. H.; Reid, B. B.; Alharethi, R.; Budge, D.; Gilbert, E. M.; McKellar, S.; Caine, W.; Verma, D. R.; Saidi, A.; Brunisholz, K.; Stehlik, J. Magnitude and Time Course of Changes Induced by Continuous-Flow Left Ventricular Assist Device Unloading in Chronic Heart Failure: Insights into Cardiac Recovery. *J. Heart Lung Transplant.* 2013, *32* (4), S31–S32. https://doi.org/10.1016/j.healun.2013.01.880.

(56) Nair, N.; Thotakura, S.; Gongora, E. Do Continuous Flow LVADS Improve Diastolic Dysfunction? *Open J. Organ Transpl. Surg.* 2014, *04* (03), 23–28. https://doi.org/10.4236/ojots.2014.43004.

(57) Bartoli, C. R.; Giridharan, G. A.; Litwak, K. N.; Sobieski, M.; Prabhu, S. D.; Slaughter, M. S.; Koenig, S. C. Hemodynamic Responses to Continuous versus Pulsatile Mechanical Unloading of the Failing Left Ventricle: *ASAIO J.* 2010, *56* (5), 410–416. https://doi.org/10.1097/MAT.0b013e3181e7bf3c.

(58) Mahr, C.; Chivukula, V. K.; McGah, P.; Prisco, A. R.; Beckman, J. A.; Mokadam, N. A.; Aliseda, A. Intermittent Aortic Valve Opening and Risk of Thrombosis in Ventricular Assist Device Patients: *ASAIO J.* 2017, *63* (4), 425–432. https://doi.org/10.1097/MAT.0000000000000512.

(59) Wong, K.; Samaroo, G.; Ling, I.; Dembitsky, W.; Adamson, R.; del Álamo, J. C.; May-Newman, K. Intraventricular Flow Patterns and Stasis in the LVAD-Assisted Heart. *J. Biomech.* 2014, *47* (6), 1485–1494. https://doi.org/10.1016/j.jbiomech.2013.12.031.

(60) Meisner, J. S.; McQueen, D. M.; Ishida, Y.; Vetter, H. O.; Bortolotti, U.; Strom, J. A.; Frater, R. W.; Peskin, C. S.; Yellin, E. L. Effects of Timing of Atrial Systole on LV Filling and Mitral Valve Closure: Computer and Dog Studies. *Am. J. Physiol.-Heart Circ. Physiol.* 1985, *249* (3), H604–H619. https://doi.org/10.1152/ajpheart.1985.249.3.H604.

(61) Humphrey, J. D. Review Paper: Continuum Biomechanics of Soft Biological Tissues. *Proc. R. Soc. Lond. Ser. Math. Phys. Eng. Sci.* 2003, *459* (2029), 3–46. https://doi.org/10.1098/rspa.2002.1060.

(62) Butcher, J. T.; Simmons, C.; Warnock, J. N. Mechanobiology of the Aortic Heart Valve. *J Heart Valve Dis* 2007, *17* (1), 62–73.

(63) John, R.; Mantz, K.; Eckman, P.; Rose, A.; May-Newman, K. Aortic Valve Pathophysiology during Left Ventricular Assist Device Support. *J. Heart Lung Transplant.* 2010, *29* (12), 1321–1329. https://doi.org/10.1016/j.healun.2010.06.006.

(64) May-Newman, K.; Enriquez-Almaguer, L.; Posuwattanakul, P.; Dembitsky, W. Biomechanics of the Aortic Valve in the Continuous Flow VAD-Assisted Heart: *ASAIO J.* 2010, *56* (4), 301–308. https://doi.org/10.1097/MAT.0b013e3181e321da.

(65) Klotz, S.; Foronjy, R. F.; Dickstein, M. L.; Gu, A.; Garrelds, I. M.; Jan Danser, A. H.; Oz, M. C.; D'Armiento, J.; Burkhoff, D. Mechanical Unloading During Left Ventricular Assist Device Support Increases Left Ventricular Collagen Cross-Linking and Myocardial Stiffness. *Circulation* 2005, *112* (3), 364–374. https://doi.org/10.1161/CIRCULATIONAHA.104.515106.

(66) Ortiz, S.; Vu, V.; Montes, R.; Sparks, A.; May-Newman, K. The Effect of the LVAD Artificial Pulse Feature on the Intraventricular Flow Field An in Vitro Flow Visualization Study Using the HeartMate3 LVAD. *submitted* 2020.

(67) Park, S. J.; Tector, A.; Piccioni, W.; Raines, E.; Gelijns, A.; Moskowitz, A.; Rose, E.; Holman, W.; Furukawa, S.; Frazier, O. H.; Dembitsky, W. Left Ventricular Assist Devices as Destination Therapy: A New Look at Survival. *J. Thorac. Cardiovasc. Surg.* 2005, *129* (1), 9–17. https://doi.org/10.1016/j.jtcvs.2004.04.044.

(68) Mancini, D. M.; Beniaminovitz, A.; Levin, H.; Catanese, K.; Flannery, M.; DiTullio, M.; Savin, S.; Cordisco, M. E.; Rose, E.; Oz, M. Low Incidence of Myocardial Recovery After Left Ventricular Assist Device Implantation in Patients With Chronic Heart Failure. 1998, 7.

(69) Rogers, J. G.; Pagani, F. D.; Tatooles, A. J.; Bhat, G.; Slaughter, M. S.; Birks, E. J.; Boyce, S. W.; Najjar, S. S.; Jeevanandam, V.; Anderson, A. S.; Gregoric, I. D.; Mallidi, H.; Leadley, K.; Aaronson, K. D.; Frazier, O. H.; Milano, C. A. Intrapericardial Left Ventricular Assist Device for Advanced Heart Failure. *N. Engl. J. Med.* 2017, *376* (5), 451–460. https://doi.org/10.1056/NEJMoa1602954.

(70) Kirklin, J. K.; Naftel, D. C.; Pagani, F. D.; Kormos, R. L.; Stevenson, L. W.; Blume, E. D.; Myers, S. L.; Miller, M. A.; Baldwin, J. T.; Young, J. B. Seventh INTERMACS Annual Report: 15,000 Patients and Counting. *J. Heart Lung Transplant.* 2015, *34* (12), 1495–1504. https://doi.org/10.1016/j.healun.2015.10.003.

(71) Kirklin, J. K.; Pagani, F. D.; Kormos, R. L.; Stevenson, L. W.; Blume, E. D.; Myers, S. L.; Miller, M. A.; Baldwin, J. T.; Young, J. B.; Naftel, D. C. Eighth Annual INTERMACS Report: Special Focus on Framing the Impact of Adverse Events. *J. Heart Lung Transplant.* 2017, *36* (10), 1080–1086. https://doi.org/10.1016/j.healun.2017.07.005.

(72) Sharma, V.; Deo, S. V.; Stulak, J. M.; Durham, L. A.; Daly, R. C.; Park, S. J.; Baddour, L. M.; Mehra, K.; Joyce, L. D. Driveline Infections in Left Ventricular Assist Devices: Implications for Destination Therapy. *Ann. Thorac. Surg.* 2012, *94* (5), 1381–1386. https://doi.org/10.1016/j.athoracsur.2012.05.074.

(73) Slaughter, M. S.; Myers, T. J. Transcutaneous Energy Transmission for Mechanical Circulatory Support Systems: History, Current Status, and Future Prospects. *J. Card. Surg.* 2010, *25* (4), 484–489. https://doi.org/10.1111/j.1540-8191.2010.01074.x.

(74) Stulak, J. M.; Davis, M. E.; Haglund, N.; Dunlay, S.; Cowger, J.; Shah, P.; Pagani, F. D.; Aaronson, K. D.; Maltais, S. Adverse Events in Contemporary Continuous-Flow Left Ventricular Assist Devices: A Multi-Institutional Comparison Shows Significant Differences. *J. Thorac. Cardiovasc. Surg.* 2016, *151* (1), 177–189. https://doi.org/10.1016/j.jtcvs.2015.09.100.

(75) Najjar, S. S.; Slaughter, M. S.; Pagani, F. D.; Starling, R. C.; McGee, E. C.; Eckman, P.; Tatooles, A. J.; Moazami, N.; Kormos, R. L.; Hathaway, D. R.; Najarian, K. B.; Bhat, G.; Aaronson, K. D.; Boyce, S. W. An Analysis of Pump Thrombus Events in Patients in the HeartWare ADVANCE Bridge to Transplant and Continued Access Protocol Trial. *J. Heart Lung Transplant.* 2014, *33* (1), 23–34. https://doi.org/10.1016/j.healun.2013.12.001.

(76) Goldstein, D. J.; Meyns, B.; Xie, R.; Cowger, J.; Pettit, S.; Nakatani, T.; Netuka, I.; Shaw, S.; Yanase, M.; Kirklin, J. K. Third Annual Report From the ISHLT Mechanically Assisted Circulatory Support Registry: A Comparison of Centrifugal and Axial Continuous-Flow Left Ventricular Assist Devices. *J. Heart Lung Transplant.* 2019, *38* (4), 352–363. https://doi.org/10.1016/j.healun.2019.02.004.

(77) Grant, A. D. M.; Smedira, N. G.; Starling, R. C.; Marwick, T. H. Independent and Incremental Role of Quantitative Right Ventricular Evaluation for the Prediction of Right Ventricular Failure After Left Ventricular Assist Device Implantation. *J. Am. Coll. Cardiol.* 2012, *60* (6), 521–528. https://doi.org/10.1016/j.jacc.2012.02.073.

(78) Kavarana, M. N.; Pessin-Minsley, M. S.; Urtecho, J.; Catanese, K. A.; Flannery, M.; Oz, M. C.; Naka, Y. Right Ventricular Dysfunction and Organ Failure in Left Ventricular Assist Device Recipients: A Continuing Problem. *Ann. Thorac. Surg.* 2002, *73* (3), 745–750. https://doi.org/10.1016/S0003-4975(01)03406-3.

(79) Genovese, E. A.; Dew, M. A.; Teuteberg, J. J.; Simon, M. A.; Kay, J.; Siegenthaler, M. P.; Bhama, J. K.; Bermudez, C. A.; Lockard, K. L.; Winowich, S.; Kormos, R. L. Incidence and Patterns of Adverse Event Onset During the First 60 Days After Ventricular Assist Device Implantation. *Ann. Thorac. Surg.* 2009, *88* (4), 1162–1170. https://doi.org/10.1016/j.athoracsur.2009.06.028.

(80) Kormos, R. L.; Teuteberg, J. J.; Pagani, F. D.; Russell, S. D.; John, R.; Miller, L. W.; Massey, T.; Milano, C. A.; Moazami, N.; Sundareswaran, K. S.; Farrar, D. J. Right Ventricular Failure in Patients with the HeartMate II Continuous-Flow Left Ventricular Assist Device: Incidence, Risk Factors, and Effect on Outcomes. *J. Thorac. Cardiovasc. Surg.* 2010, *139* (5), 1316–1324. https://doi.org/10.1016/j.jtcvs.2009.11.020.

(81) Hayek, S.; Sims, D. B.; Markham, D. W.; Butler, J.; Kalogeropoulos, A. P. Assessment of Right Ventricular Function in Left Ventricular Assist Device Candidates. *Circ. Cardiovasc. Imaging* 2014, *7* (2), 379–389. https://doi.org/10.1161/CIRCIMAGING.113.001127.

(82) Letsou, G. V.; Connelly, J. H.; Delgado, R. M.; Myers, T. J.; Gregoric, I. D.; Smart, F. W.; Frazier, O. H. Is Native Aortic Valve Commissural Fusion in Patients With Long-Term Left Ventricular Assist Devices Associated With Clinically Important Aortic Insufficiency? *J. Heart Lung Transplant.* 2006, *25* (4), 395–399. https://doi.org/10.1016/j.healun.2005.11.451.

(83) Cowger, J.; Pagani, F. D.; Haft, J. W.; Romano, M. A.; Aaronson, K. D.; Kolias, T. J. The Development of Aortic Insufficiency in Left Ventricular Assist Device-Supported Patients. *Circ. Heart Fail.* 2010, *3* (6), 668–674. https://doi.org/10.1161/CIRCHEARTFAILURE.109.917765.

(84) Aggarwal, A.; Raghuvir, R.; Eryazici, P.; Macaluso, G.; Sharma, P.; Blair, C.; Tatooles, A. J.; Pappas, P. S.; Bhat, G. The Development of Aortic Insufficiency in Continuous-Flow Left Ventricular Assist Device–Supported Patients. *Ann. Thorac. Surg.* 2013, *95* (2), 493–498. https://doi.org/10.1016/j.athoracsur.2012.09.020.

(85) Bryant, A. S.; Holman, W. L.; Nanda, N. C.; Vengala, S.; Blood, M. S.; Pamboukian, S. V.; Kirklin, J. K. Native Aortic Valve Insufficiency in Patients With Left Ventricular Assist Devices. *Ann. Thorac. Surg.* 2006, *81* (2), e6–e8. https://doi.org/10.1016/j.athoracsur.2005.08.072.

(86) Mudd, J. O.; Cuda, J. D.; Halushka, M.; Soderlund, K. A.; Conte, J. V.; Russell, S. D. Fusion of Aortic Valve Commissures in Patients Supported by a Continuous Axial Flow Left Ventricular Assist Device. *J. Heart Lung Transplant.* 2008, *27* (12), 1269–1274. https://doi.org/10.1016/j.healun.2008.05.029.

(87) Rao, V.; Slater, J. P.; Edwards, N. M.; Naka, Y.; Oz, M. C. Surgical Management of Valvular Disease in Patients Requiring Left Ventricular Assist Device Support. *Ann. Thorac. Surg.* 2001, *71* (5), 1448–1453. https://doi.org/10.1016/S0003-4975(01)02479-1.

(88) Samuels, L. E.; Thomas, M. P.; Holmes, E. C.; Narula, J.; Fitzpatrick, J.; Wood, D.; Fyfe, B.; Wechsler, A. S. Insufficiency of the Native Aortic Valve and Left Ventricular Assist System Inflow Valve after Support with an Implantable Left Ventricular Assist System: Signs, Symptoms, and Concerns. *J. Thorac. Cardiovasc. Surg.* 2001, *122* (2), 380–381. https://doi.org/10.1067/mtc.2001.114770.

(89) Dreger, S. A.; Taylor, P. M.; Allen, S. P.; Yacoub, M. H. Profile and Localization of Matrix Metalloproteinases (MMPs) and Their Tissue Inhibitors (TIMPs) in Human Heart Valves. *J. Heart Valve Dis.* 2002, *11* (6), 875–880; discussion 880.

(90) Sacks, M. S.; Yoganathan, A. P. Heart Valve Function: A Biomechanical Perspective. *Philos. Trans. R. Soc. B Biol. Sci.* 2007, *362* (1484), 1369–1391. https://doi.org/10.1098/rstb.2007.2122.

(91) Sacks, M. S.; David Merryman, W.; Schmidt, D. E. On the Biomechanics of Heart Valve Function. *J. Biomech.* 2009, *42* (12), 1804–1824. https://doi.org/10.1016/j.jbiomech.2009.05.015.

(92) Grande, K. J.; Cochran, R. P.; Reinhall, P. G.; Kunzelman, K. S. Stress Variations in the Human Aortic Root and Valve: The Role of Anatomic Asymmetry. *Ann. Biomed. Eng.* 1998, *26* (4), 534–545. https://doi.org/10.1114/1.122.

(93) De Hart, J.; Peters, G. W. M.; Schreurs, P. J. G.; Baaijens, F. P. T. A Three-Dimensional Computational Analysis of Fluid–Structure Interaction in the Aortic Valve. *J. Biomech.* 2003, *36* (1), 103–112. https://doi.org/10.1016/S0021-9290(02)00244-0.

(94) May-Newman, K.; Mendoza, A.; Abulon, D. J. K.; Joshi, M.; Kunda, A.; Dembitsky, W. Geometry and Fusion of Aortic Valves from Pulsatile Flow Ventriuclar Assist Device Patients. *J Heart Valve Dis* 2011, *20* (2), 149–158.

(95) Otto, C. M. Evaluation and Management of Chronic Mitral Regurgitation. *N. Engl. J. Med.* 2001, *345* (10), 740–746. https://doi.org/10.1056/NEJMcp003331.

(96) Reul, H.; Talukder, N. Heart Valve Mechanics. In *The heart*; MCGraw Hill: New York, NY, 1989.

(97) Lo, D.; Vesely, I. Biaxial Strain Analysis of the Porcine Aortic Valve. *Ann. Thorac. Surg.* 1995, *60*, S374–S378. https://doi.org/10.1016/0003-4975(95)00249-K.

(98) Thubrikar, M. J. *The Aortic Valve*, 1st ed.; CRC Press: Boca Ranton, FL, 1989.

(99) Ku, C.; Johnson, P.; Batten, P.; Sarathchandra, P.; Chambers, R.; Taylor, P.; Yacoub, M.; Chester, A. Collagen Synthesis by Mesenchymal Stem Cells and Aortic Valve Interstitial Cells in Response to Mechanical Stretch. *Cardiovasc. Res.* 2006, *71* (3), 548–556. https://doi.org/10.1016/j.cardiores.2006.03.022.

(100) Balachandran, K.; Konduri, S.; Sucosky, P.; Jo, H.; Yoganathan, A. P. An Ex Vivo Study of the Biological Properties of Porcine Aortic Valves in Response to Circumferential Cyclic Stretch. *Ann. Biomed. Eng.* 2006, *34* (11), 1655–1665. https://doi.org/10.1007/s10439-006-9167-8.

(101) Merryman, W. D.; Lukoff, H. D.; Long, R. A.; Engelmayr, G. C.; Hopkins, R. A.; Sacks, M. S. Synergistic Effects of Cyclic Tension and Transforming Growth Factor-B1 on the Aortic Valve Myofibroblast. *Cardiovasc. Pathol.* 2007, *16* (5), 268–276. https://doi.org/10.1016/j.carpath.2007.03.006.

(102) Yacoub, M. H.; Cohn, L. H. Novel Approaches to Cardiac Valve Repair: From Structure to Function: Part I. *Circulation* 2004, *109* (8), 942–950. https://doi.org/10.1161/01.CIR.0000115633.19829.5E.

(103) Yip, C. Y. Y.; Simmons, C. A. The Aortic Valve Microenvironment and Its Role in Calcific Aortic Valve Disease. *Cardiovasc. Pathol.* 2011, *20* (3), 177–182. https://doi.org/10.1016/j.carpath.2010.12.001.

(104) Butcher, J. T.; Penrod, A. M.; García, A. J.; Nerem, R. M. Unique Morphology and Focal Adhesion Development of Valvular Endothelial Cells in Static and Fluid Flow Environments. *Arterioscler. Thromb. Vasc. Biol.* 2004, *24* (8), 1429–1434. https://doi.org/10.1161/01.ATV.0000130462.50769.5a.

(105) Deck, D. J. Endothelial Cell Orientation on Aortic Valve Leaflets. *Cardiovasc. Res.* 1986, *20* (10), 760–767.

(106) Vesely, I. The Role of Elastin in Aortic Valve Mechanics. *J. Biomech.* 1997, *31* (2), 115–123. https://doi.org/10.1016/S0021-9290(97)00122-X.

(107) De Hart, J.; Peters, G. W. M.; Schreurs, P. J. G.; Baaijens, F. P. T. Collagen Fibers Reduce Stresses and Stabilize Motion of Aortic Valve Leaflets during Systole. *J. Biomech.* 2004, *37* (3), 303–311. https://doi.org/10.1016/S0021-9290(03)00293-8.

(108) El-Hamamsy, I.; Chester, A. H.; Yacoub, M. H. Cellular Regulation of the Structure and Function of Aortic Valves. *J. Adv. Res.* 2010, *1* (1), 5–12. https://doi.org/10.1016/j.jare.2010.02.007.

(109) Tilea, I.; Suciu, H.; Tilea, B.; Maria, C.; Ispas, M.; Constantin, R. Anatomy and Function of Normal Aortic Valvular Complex. In *Calcific Aortic Valve Disease*; Aikawa, E., Ed.; InTech, 2013. https://doi.org/10.5772/53403.

(110) Leask, R. L.; Jain, N.; Butany, J. Endothelium and Valvular Diseases of the Heart. *Microsc. Res. Tech.* 2003, *60* (2), 129–137. https://doi.org/10.1002/jemt.10251.

(111) Taylor, P. M.; Batten, P.; Brand, N. J.; Thomas, P. S.; Yacoub, M. H. The Cardiac Valve Interstitial Cell. *Int. J. Biochem. Cell Biol.* 2003, *35* (2), 113–118. https://doi.org/10.1016/S1357-2725(02)00100-0.

(112) Liu, A. C.; Joag, V. R.; Gotlieb, A. I. The Emerging Role of Valve Interstitial Cell Phenotypes in Regulating Heart Valve Pathobiology. *Am. J. Pathol.* 2007, *171* (5), 1407–1418. https://doi.org/10.2353/ajpath.2007.070251.

(113) Rajamannan, N. M.; Evans, F. J.; Aikawa, E.; Grande-Allen, K. J.; Demer, L. L.; Heistad, D. D.; Simmons, C. A.; Masters, K. S.; Mathieu, P.; O'Brien, K. D.; Schoen, F. J.; Towler, D. A.; Yoganathan, A. P.; Otto, C. M. Calcific Aortic Valve Disease: Not Simply a Degenerative Process: A Review and Agenda for Research From the National Heart and Lung and Blood Institute Aortic Stenosis Working Group *Executive Summary: Calcific Aortic Valve Disease – 2011 Update*. *Circulation* 2011, *124* (16), 1783–1791. https://doi.org/10.1161/CIRCULATIONAHA.110.006767.

(114) Merryman, W. D.; Liao, J.; Parekh, A.; Candiello, J.; Lin, H.; Sacks, M. Differences in Tissue-Remodeling Potential of Aortic and Pulmonary Heart Valve Interstitial Cells. *Tissue engineering* 2007, *13*.

(115) Tuzun, E.; Pennings, K.; van Tuijl, S.; de Hart, J.; Stijnen, M.; van de Vosse, F.; de Mol, B.; Rutten, M. Assessment of Aortic Valve Pressure Overload and Leaflet Functions in an Ex Vivo Beating Heart Loaded with a Continuous Flow Cardiac Assist Device. *Eur. J. Cardiothorac. Surg.* 2014, *45* (2), 377–383. https://doi.org/10.1093/ejcts/ezt355.

(116) May-Newman, K.; Lam, C.; Yin, F. C. P. A Hyperelastic Constitutive Law for Aortic Valve Tissue. *J. Biomech. Eng.* 2009, *131* (8), 081009. https://doi.org/10.1115/1.3127261.

(117) Lee, A. A.; Delhaas, T.; McCulloch, A. D.; Villarreal, F. J. Differential Responses of Adult Cardiac Fibroblasts to in Vitro Biaxial Strain Patterns. *J. Mol. Cell. Cardiol.* 1999, *31* (10), 1833–1843. https://doi.org/10.1006/jmcc.1999.1017.

(118) Fung, Y. *Biomechanics: Mechanical Properties of Living Tissues*, 2nd ed.; Springer-Verlag: New York, NY, 1993.

(119) Weyman, A. E. *Principles and Practices of Echocardiography*; Lea & Febiger: Philadelphia, PA, 1994.

(120) Acker, M. A.; Jessup, M.; Bolling, S. F.; Oh, J.; Starling, R. C.; Mann, D. L.; Sabbah, H. N.; Shemin, R.; Kirklin, J.; Kubo, S. H. Mitral Valve Repair in Heart Failure: Five-Year Follow-up from the Mitral Valve Replacement Stratum of the Acorn Randomized Trial. *J. Thorac. Cardiovasc. Surg.* 2011, *142* (3), 569-574.e1. https://doi.org/10.1016/j.jtcvs.2010.10.051.

(121) Patel, J. B.; Borgeson, D. D.; Barnes, M. E.; Rihal, C. S.; Daly, R. C.; Redfield, M. M. Mitral Regurgitation in Patients with Advanced Systolic Heart Failure. *J. Card. Fail.* 2004, *10* (4), 285–291. https://doi.org/10.1016/j.cardfail.2003.12.006.

(122) Urban, M.; Pirk, J.; Szarszoi, O.; Skalsky, I.; Maly, J.; Netuka, I. Mitral Valve Repair versus Replacement in Simultaneous Aortic and Mitral Valve Surgery. 2013, *18* (1), 5.

(123) Shuhaiber, J.; Anderson, R. J. Meta-Analysis of Clinical Outcomes Following Surgical Mitral Valve Repair or Replacement. *Eur. J. Cardiothorac. Surg.* 2007, *31* (2), 267–275. https://doi.org/10.1016/j.ejcts.2006.11.014.

(124) Vu, V.; Rossini, L.; Montes, R.; Campos, J.; Moon, J.; Martinez-Legazpi, P.; Bermejo, J.; del Álamo, J. C.; May-Newman, K. Mitral Valve Prosthesis Design Affects Hemodynamic Stasis and Shear In The Dilated Left Ventricle. *Ann. Biomed. Eng.* 2019, *47* (5), 1265–1280. https://doi.org/10.1007/s10439-019-02218-z.

(125) Campos, N. L. K. L. de. Comparison of the Occurrence of Thromboembolic and Bleeding Complications in Patients with Mechanical Heart Valve Prosthesis with One and Two Leaflets in the Mitral Position. *Rev. Bras. Cir. Cardiovasc.* 2014, *29* (1), 59–68. https://doi.org/10.5935/1678-9741.20140012.

(126) Schweiger, M.; Stepanenko, A.; Vierecke, J.; Drews, T.; Potapov, E.; Hetzer, R.; Krabatsch, T. Preexisting Mitral Valve Prosthesis in Patients Undergoing Left Ventricular Assist Device Implantation: MITRAL VALVE PROSTHESIS AND LVAD SUPPORT. *Artif. Organs* 2012, *36* (1), 49–53. https://doi.org/10.1111/j.1525-1594.2011.01304.x.

(127) Hammermeister, K.; Sethi, G. K.; Henderson, W. G.; Grover, F. L.; Oprian, C.; Rahimtoola, S. H. Outcomes 15 Years after Valve Replacement with a Mechanical versus a Bioprosthetic Valve: Final Report of the Veterans Affairs Randomized Trial. *J. Am. Coll. Cardiol.* 2000, *36* (4), 1152–1158. https://doi.org/10.1016/S0735-1097(00)00834-2.

(128) Kulik, A.; Bedard, P.; Lam, B.; Rubens, F.; Hendry, P.; Masters, R.; Mesana, T.; Ruel, M. Mechanical versus Bioprosthetic Valve Replacement in Middle-Aged Patients. *Eur. J. Cardiothorac. Surg.* 2006, *30* (3), 485–491. https://doi.org/10.1016/j.ejcts.2006.06.013.

(129) Liu, T.; Jessup, M.; Acker, M.; Morris, R. Management of Prosthetic Valves during Ventricular Assist Device Implantation. *J. Card. Surg.* 2010, *25* (5), 601–605. https://doi.org/10.1111/j.1540-8191.2010.01098.x.

(130) Nkomo, V. T.; Gardin, J. M.; Skelton, T. N.; Gottdiener, J. S.; Scott, C. G.; Enriquez-Sarano, M. Burden of Valvular Heart Diseases: A Population-Based Study. *The Lancet* 2006, *368* (9540), 1005–1011. https://doi.org/10.1016/S0140-6736(06)69208-8.

(131) Coffey, S.; Cox, B.; Williams, M. J. A. Lack of Progress in Valvular Heart Disease in the Pre–Transcatheter Aortic Valve Replacement Era: Increasing Deaths and Minimal

Change in Mortality Rate over the Past Three Decades. *Am. Heart J.* 2014, *167* (4), 562-567.e2. https://doi.org/10.1016/j.ahj.2013.12.030.

(132) Boudoulas, B.; Stefanadis, C. *The Aorta: Structure, Function, Dysfunction and Diseases*, 1st ed.; Informa Healthcare USA, Inc.: New York, NY, 2009.

(133) Pal, J. D.; Klodell, C. T.; John, R.; Pagani, F. D.; Rogers, J. G.; Farrar, D. J.; Milano, C. A.; for the HeartMate II Clinical Investigators. Low Operative Mortality With Implantation of a Continuous-Flow Left Ventricular Assist Device and Impact of Concurrent Cardiac Procedures. *Circulation* 2009, *120* (11_suppl_1), S215–S219. https://doi.org/10.1161/CIRCULATIONAHA.108.844274.

(134) Rose, A. G.; Park, S. J.; Bank, A. J.; Miller, L. W. Partial Aortic Valve Fusion Induced by Left Ventricular Assist Device. *Ann. Thorac. Surg.* 2000, *70* (4), 1270–1274. https://doi.org/10.1016/S0003-4975(00)01929-9.

(135) Connelly, J. Acquired Commissural Fusion of Aortic Valves in Patients with Left Ventricular Assist Devices. *J. Heart Lung Transplant.* 2003, *22* (12), 1291–1295. https://doi.org/10.1016/S1053-2498(03)00028-7.

(136) Pak, S.-W.; Uriel, N.; Takayama, H.; Cappleman, S.; Song, R.; Colombo, P. C.; Charles, S.; Mancini, D.; Gillam, L.; Naka, Y.; Jorde, U. P. Prevalence of de Novo Aortic Insufficiency during Long-Term Support with Left Ventricular Assist Devices. *J. Heart Lung Transplant.* 2010, *29* (10), 1172–1176. https://doi.org/10.1016/j.healun.2010.05.018.

(137) Cowger, J. A.; Aaronson, K. D.; Romano, M. A.; Haft, J.; Pagani, F. D. Consequences of Aortic Insufficiency during Long-Term Axial Continuous-Flow Left Ventricular Assist Device Support. *J. Heart Lung Transplant.* 2014, *33* (12), 1233–1240. https://doi.org/10.1016/j.healun.2014.06.008.

(138) Jorde, U. P.; Uriel, N.; Nahumi, N.; Bejar, D.; Gonzalez-Costello, J.; Thomas, S. S.; Han, J.; Morrison, K. A.; Jones, S.; Kodali, S.; Hahn, R. T.; Shames, S.; Yuzefpolskaya, M.; Colombo, P.; Takayama, H.; Naka, Y. Prevalence, Significance, and Management of Aortic Insufficiency in Continuous Flow Left Ventricular Assist Device Recipients. *Circ. Heart Fail.* 2014, *7* (2), 310–319. https://doi.org/10.1161/CIRCHEARTFAILURE.113.000878.

(139) Hatano, M.; Kinugawa, K.; Shiga, T.; Kato, N.; Endo, M.; Hisagi, M.; Nishimura, T.; Yao, A.; Hirata, Y.; Kyo, S.; Ono, M.; Nagai, R. Less Frequent Opening of the Aortic Valve and a Continuous Flow Pump Are Risk Factors for Postoperative Onset of Aortic Insufficiency in Patients With a Left Ventricular Assist Device. *Circ. J.* 2011, *75* (5), 1147–1155. https://doi.org/10.1253/circj.CJ-10-1106.

(140) Toda, K.; Fujita, T.; Domae, K.; Shimahara, Y.; Kobayashi, J.; Nakatani, T. Late Aortic Insufficiency Related to Poor Prognosis During Left Ventricular Assist Device Support. *Ann. Thorac. Surg.* 2011, *92* (3), 929–934. https://doi.org/10.1016/j.athoracsur.2011.04.115.

(141) Mano, A.; Gorcsan, J.; Teuteberg, J. J.; Bermudez, C. A.; Bhama, J. K.; McNamara, D. M.; Ramani, R.; Simon, M. A.; Kormos, R. L. Incidence and Impact of De Novo Aortic

Insufficiency Following Continuous Flow LVADs Implantation. *J. Heart Lung Transplant.* 2012, *31* (4), S22. https://doi.org/10.1016/j.healun.2012.01.041.

(142) Atkins, B. Z.; Hashmi, Z. A.; Ganapathi, A. M.; Harrison, J. K.; Hughes, G. C.; Rogers, J. G.; Milano, C. A. Surgical Correction of Aortic Valve Insufficiency after Left Ventricular Assist Device Implantation. *J. Thorac. Cardiovasc. Surg.* 2013, *146* (5), 1247–1252. https://doi.org/10.1016/j.jtcvs.2013.05.019.

(143) Martina, J.; de Jonge, N.; Sukkel, E.; Lahpor, J. Left Ventricular Assist Device-Related Systolic Aortic Regurgitation. *Circulation* 2011, *124* (4), 487–488. https://doi.org/10.1161/CIRCULATIONAHA.111.020891.

(144) Hayes, H.; Barber, J.; Dembo, L.; Lam, K.; Shah, A.; Dias, P.; Lambert, J.; Larbalestier, R.; Baumwol., J. The World's Longest-Supported HeartWare TM Ventricular Assist Device Patient 10 Years & Counting: The Western Australian Experience. *J. Heart Lung Transplant.* 2018, *37* (4), S272. https://doi.org/10.1016/j.healun.2018.01.682.

(145) Adamson, R. M.; Dembitsky, W. P.; Baradarian, S.; Chammas, J.; May-Newman, K.; Chillcott, S.; Stahovich, M.; McCalmont, V.; Ortiz, K.; Hoagland, P.; Jaski, B. Aortic Valve Closure Associated with HeartMate Left Ventricular Device Support: Technical Considerations and Long-Term Results. *J. Heart Lung Transplant.* 2011, *30* (5), 576–582. https://doi.org/10.1016/j.healun.2010.11.007.

(146) Bluestein, D. Research Approaches for Studying Flow-Induced Thromboembolic Complications in Blood Recirculating Devices. *Expert Rev. Med. Devices* 2004, *1* (1), 65–80. https://doi.org/10.1586/17434440.1.1.65.

(147) Jung, M. H.; Hansen, P. B.; Sander, K.; Olsen, P. S.; Rossing, K.; Boesgaard, S.; Russell, S. D.; Gustafsson, F. Effect of Increasing Pump Speed during Exercise on Peak Oxygen Uptake in Heart Failure Patients Supported with a Continuous-Flow Left Ventricular Assist Device. A Double-Blind Randomized Study: Effect of Increasing Pump Speed during Exercise. *Eur. J. Heart Fail.* 2014, *16* (4), 403–408. https://doi.org/10.1002/ejhf.52.

(148) Noor, M. R.; Bowles, C.; Banner, N. R. Relationship between Pump Speed and Exercise Capacity during HeartMate II Left Ventricular Assist Device Support: Influence of Residual Left Ventricular Function. *Eur. J. Heart Fail.* 2012, *14* (6), 613–620. https://doi.org/10.1093/eurjhf/hfs042.

(149) Ben-ali, W.; Bouhout, I.; Lambert, J.; Bouchard, D.; Carrier, M. PREVALENCE AND IMPACT OF DE NOVO AORTIC INSUFFICIENCY DURING LONG-TERM SUPPORT ON A LEFT VENTRICULAR ASSIST DEVICE: A SYSTEMATIC REVIEW AND META-ANALYSIS. *Can. J. Cardiol.* 2017, *33* (10), S68–S69. https://doi.org/10.1016/j.cjca.2017.07.141.

(150) Deo, S. V.; Sharma, V.; Cho, Y. H.; Shah, I. K.; Park, S. J. De Novo Aortic Insufficiency During Long-Term Support on a Left Ventricular Assist Device: A Systematic Review and Meta-Analysis. *ASAIO J.* 2014, *60* (2), 183–188. https://doi.org/10.1097/MAT.0000000000000042.

(151) Zoghbi, W. A.; Adams, D.; Bonow, R. O.; Enriquez-Sarano, M.; Foster, E.; Grayburn, P. A.; Hahn, R. T.; Han, Y.; Hung, J.; Lang, R. M.; Little, S. H.; Shah, D. J.; Shernan, S.;

Thavendiranathan, P.; Thomas, J. D.; Weissman, N. J. Recommendations for Noninvasive Evaluation of Native Valvular Regurgitation. *J. Am. Soc. Echocardiogr.* 2017, *30* (4), 303–371. https://doi.org/10.1016/j.echo.2017.01.007.

(152) Maurer, G. Aortic Regurgitation. *Heart* 2006, *92* (7), 994–1000. https://doi.org/10.1136/hrt.2004.042614.

(153) Chaliki, H. P.; Mohty, D.; Avierinos, J.-F.; Scott, C. G.; Schaff, H. V.; Tajik, A. J.; Enriquez-Sarano, M. Outcomes After Aortic Valve Replacement in Patients With Severe Aortic Regurgitation and Markedly Reduced Left Ventricular Function. *Circulation* 2002, *106* (21), 2687–2693. https://doi.org/10.1161/01.CIR.0000038498.59829.38.

(154) Klodas, E.; Enriquez-Sarano, M.; Tajik, A. J.; Mullany, C. J.; Bailey, K. R.; Seward, J. B. Aortic Regurgitation Complicated by Extreme Left Ventricular Dilation: Long-Term Outcome after Surgical Correction. *J. Am. Coll. Cardiol.* 1996, *27* (3), 670–677. https://doi.org/10.1016/0735-1097(95)00525-0.

(155) Evangelista, A.; Tornos, P.; Sambola, A.; Permanyer-Miralda, G.; Soler-Soler, J. Long-Term Vasodilator Therapy in Patients with Severe Aortic Regurgitation. *N. Engl. J. Med.* 2005, *353* (13), 1342–1349. https://doi.org/10.1056/NEJMoa050666.

(156) Carabello, B. A. Vasodilators in Aortic Regurgitation — Where Is the Evidence of Their Effectiveness? *N. Engl. J. Med.* 2005, *353* (13), 1400–1402. https://doi.org/10.1056/NEJMe058213.

(157) Nishimura, R. A.; Otto, C. M.; Bonow, R. O.; Carabello, B. A.; Erwin, J. P.; Guyton, R. A.; O'Gara, P. T.; Ruiz, C. E.; Skubas, N. J.; Sorajja, P.; Sundt, T. M.; Thomas, J. D. 2014 AHA/ACC Guideline for the Management of Patients With Valvular Heart Disease. *J. Am. Coll. Cardiol.* 2014, *63* (22), e57–e185. https://doi.org/10.1016/j.jacc.2014.02.536.

(158) Al-Atassi, T.; Boodhwani, M. Aortic Valve Insufficiency in Aortic Root Aneurysms: Consider Every Valve for Repair. *J. Vis. Surg.* 2018, *4*, 60–60. https://doi.org/10.21037/jovs.2018.01.13.

(159) Nash, P. J.; Vitvitsky, E.; Li, J.; Cosgrove, D. M.; Pettersson, G.; Grimm, R. A. Feasibility of Valve Repair for Regurgitant Bicuspid Aortic Valves—An Echocardiographic Study. *Ann. Thorac. Surg.* 2005, *79* (5), 1473–1479. https://doi.org/10.1016/j.athoracsur.2004.09.053.

(160) Robertson, J. O.; Naftel, D. C.; Meyers, S. L.; Kirklin, J. K.; Mertz, G. D.; Prasad, S.; Itoh, A.; Silvestry, S. C. Concomitant Aortic Valve Procedures in Patients Undergoing Implantation of Continuous-Flow LVADs: An INTERMACS Database Analysis. *J. Heart Lung Transplant.* 2015, *34* (6), 797–805. https://doi.org/10.1016/j.healun.2014.01.051.

(161) Fukuhara, S.; Ikegami, H.; Polanco, A. R.; Song, J. J.; Han, J.; Takeda, K.; Kurlansky, P. A.; Takayama, H.; Naka, Y. Concomitant Repair for Mild Aortic Insufficiency and Continuous-Flow Left Ventricular Assist Devices. *Eur. J. Cardiothorac. Surg.* 2017, *52* (6), 1062–1068. https://doi.org/10.1093/ejcts/ezx150.

(162) Cowger, J.; Rao, V.; Massey, T.; Sun, B.; May-Newman, K.; Jorde, U.; Estep, J. D. Comprehensive Review and Suggested Strategies for the Detection and Management of

Aortic Insufficiency in Patients with a Continuous-Flow Left Ventricular Assist Device. *J. Heart Lung Transplant.* 2015, *34* (2), 149–157. https://doi.org/10.1016/j.healun.2014.09.045.

(163) Braunberger, E.; Deloche, A.; Berrebi, A.; Abdallah, F.; Celestin, J. A.; Meimoun, P.; Chatellier, G.; Chauvaud, S.; Fabiani, J. N.; Carpentier, A. Very Long-Term Results (More Than 20 Years) of Valve Repair With Carpentier's Techniques in Nonrheumatic Mitral Valve Insufficiency. *Circulation* 2001, No. 104, I-8-I11.

(164) Beck, A.; Thubrikar, M. J.; Robicsek, F. Stress Analysis of the Aortic Valve with and without the Sinuses of Valsalva. *J. Heart Valve Dis.* 2001, *10* (1), 1–11.

(165) El Khoury, G.; de Kerchove, L. Principles of Aortic Valve Repair. *J. Thorac. Cardiovasc. Surg.* 2013, *145* (3), S26–S29. https://doi.org/10.1016/j.jtcvs.2012.11.071.

(166) Bonow, R. O.; Lakatos, E.; Maron, B. J.; Epstein, S. E. Serial Long-Term Assessment of the Natural History of Asymptomatic Patients with Chronic Aortic Regurgitation and Normal Left Ventricular Systolic Function. *Circulation* 1991, *84* (4), 1625–1635. https://doi.org/10.1161/01.CIR.84.4.1625.

(167) Xing, Y.; Warnock, J. N.; He, Z.; Hilbert, S. L.; Yoganathan, A. P. Cyclic Pressure Affects the Biological Properties of Porcine Aortic Valve Leaflets in a Magnitude and Frequency Dependent Manner. *Ann. Biomed. Eng.* 2004, *32* (11), 1461–1470. https://doi.org/10.1114/B:ABME.0000049031.07512.11.

(168) Balachandran, K.; Sucosky, P.; Jo, H.; Yoganathan, A. P. Elevated Cyclic Stretch Alters Matrix Remodeling in Aortic Valve Cusps: Implications for Degenerative Aortic Valve Disease. *Am. J. Physiol.-Heart Circ. Physiol.* 2009, *296* (3), H756–H764. https://doi.org/10.1152/ajpheart.00900.2008.

(169) Boodhwani, M.; de Kerchove, L.; Glineur, D.; Poncelet, A.; Rubay, J.; Astarci, P.; Verhelst, R.; Noirhomme, P.; El Khoury, G. Repair-Oriented Classification of Aortic Insufficiency: Impact on Surgical Techniques and Clinical Outcomes. *J. Thorac. Cardiovasc. Surg.* 2009, *137* (2), 286–294. https://doi.org/10.1016/j.jtcvs.2008.08.054.

(170) Maurer, M. M.; Burkhoff, D.; Maybaum, S.; Franco, V.; Vittorio, T. J.; Williams, P.; White, L.; Kamalakkannan, G.; Myers, J.; Mancini, D. M. A Multicenter Study of Noninvasive Cardiac Output by Bioreactance During Symptom-Limited Exercise. *J. Card. Fail.* 2009, *15* (8), 689–699. https://doi.org/10.1016/j.cardfail.2009.04.005.

(171) Goliasch, G.; Goscinska-Bis, K.; Caracciolo, G.; Nakabo, A.; Smolka, G.; Pedrizzetti, G.; Narula, J.; Sengupta, P. P. CRT Improves LV Filling Dynamics. *JACC Cardiovasc. Imaging* 2013, *6* (6), 704–713. https://doi.org/10.1016/j.jcmg.2013.04.004.

(172) Pedrizzetti, G.; La Canna, G.; Alfieri, O.; Tonti, G. The Vortex—an Early Predictor of Cardiovascular Outcome? *Nat. Rev. Cardiol.* 2014, *11* (9), 545–553. https://doi.org/10.1038/nrcardio.2014.75.

(173) Dujardin, K. S.; Enriquez-Sarano, M.; Schaff, H. V.; Bailey, K. R.; Seward, J. B.; Tajik, A. J. Mortality and Morbidity of Aortic Regurgitation in Clinical Practice. *Circulation* 1999, 1851–1857.

(174) Garcia, M. A. Z.; Enriquez, L. A.; Dembitsky, W.; May-Newman, K. The Effect of Aortic Valve Incompetence on the Hemodynamics of a Continuous Flow Ventricular Assist Device in a Mock Circulation: *ASAIO J.* 2008, *54* (3), 237–244. https://doi.org/10.1097/MAT.0b013e31816a309b.

(175) Iizuka, K.; Nishinaka, T.; Takewa, Y.; Yamazaki, K.; Tatsumi, E. The Influence of Pump Rotation Speed on Hemodynamics and Myocardial Oxygen Metabolism in Left Ventricular Assist Device Support with Aortic Valve Regurgitation. *J. Artif. Organs* 2017, *20* (3), 194–199. https://doi.org/10.1007/s10047-017-0960-y.

(176) Imamura, T.; Kinugawa, K.; Fujino, T.; Inaba, T.; Maki, H.; Hatano, M.; Kinoshita, O.; Nawata, K.; Kyo, S.; Ono, M. Aortic Insufficiency in Patients With Sustained Left Ventricular Systolic Dysfunction After Axial Flow Assist Device Implantation. *Circ. J.* 2014, *79* (1), 104–111. https://doi.org/10.1253/circj.CJ-14-0944.

(177) Soleimani, B.; Haouzi, A.; Manoskey, A.; Stephenson, E. R.; El-Banayosy, A.; Pae, W. E. Development of Aortic Insufficiency in Patients Supported With Continuous Flow Left Ventricular Assist Devices: *ASAIO J.* 2012, *58* (4), 326–329. https://doi.org/10.1097/MAT.0b013e318251cfff.

(178) Gregory, S. D.; Stevens, M. C.; Wu, E.; Fraser, J. F.; Timms, D. In Vitro Evaluation of Aortic Insufficiency With a Rotary Left Ventricular Assist Device: Aortic Insufficiency With a Rotary LVAD. *Artif. Organs* 2013, n/a-n/a. https://doi.org/10.1111/aor.12143.

(179) Holtz, J.; Teuteberg, J. Management of Aortic Insufficiency in the Continuous Flow Left Ventricular Assist Device Population. *Curr. Heart Fail. Rep.* 2014, *11* (1), 103–110. https://doi.org/10.1007/s11897-013-0172-6.

(180) Tanaka, Y.; Nakajima, T.; Fisher, I.; Kotfar, K.; Moon, M. R.; Damiano Jr., R. J.; Masood, M. F.; Itoh, A. The Impact of Uncorrected Mild Aortic Insufficiency at the Time of Left Ventricular Assist Device Implantation. *J Thorac Cardiovasc Surg* 2020.

(181) Rajagopal, K.; Daneshmand, M. A.; Patel, C. B.; Ganapathi, A. M.; Schechter, M. A.; Rogers, J. G.; Milano, C. A. Natural History and Clinical Effect of Aortic Valve Regurgitation after Left Ventricular Assist Device Implantation. *J. Thorac. Cardiovasc. Surg.* 2013, *145* (5), 1373–1379. https://doi.org/10.1016/j.jtcvs.2012.11.066.

(182) Holley, C. T.; Fitzpatrick, M.; Roy, S. S.; Alraies, M. C.; Cogswell, R.; Souslian, L.; Eckman, P.; John, R. Aortic Insufficiency in Continuous-Flow Left Ventricular Assist Device Support Patients Is Common but Does Not Impact Long-Term Mortality. *J. Heart Lung Transplant.* 2017, *36* (1), 91–96. https://doi.org/10.1016/j.healun.2016.07.018.

(183) Imamura, T.; Kinugawa, K. Preoperative Prediction of Aortic Insufficiency During Ventricular Assist Device Treatment. *Int. Heart. J.* 2016, *57* (1), 3–10. https://doi.org/10.1536/ihj.15-250.

(184) Westaby, S.; Bertoni, G. B.; Clelland, C.; Nishinaka, T.; Frazier, O. H. Circulatory Support with Attenuated Pulse Pressure Alters Human Aortic Wall Morphology. *J. Thorac. Cardiovasc. Surg.* 2007, *133* (2), 575–576. https://doi.org/10.1016/j.jtcvs.2006.10.014.

(185) Benedik, J.; Pilarzcyk, K.; Wendt, D.; Price, V.; Tsagakis, K.; Perrey, M.; Baba, H. A.; Jakob, H. Is There Any Difference in Aortic Wall Quality between Patients with Aortic Stenosis and Those with Regurgitation?†. *Eur. J. Cardiothorac. Surg.* 2013, *44* (4), 754–759. https://doi.org/10.1093/ejcts/ezt123.

(186) Akasaka, T.; Okumachi, F.; Takao, S. Age-Related Valvular Regurgitation: A Study by Pulsed Doppler Echocardiography. *VALVULAR HEART Dis.* 1987, *76* (2), 4.

(187) Singh, J. P.; Evans, J. C.; Levy, D.; Larson, M. G.; Freed, L. A.; Fuller, D. L.; Lehman, B.; Benjamin, E. J. Prevalence and Clinical Determinants of Mitral, Tricuspid, and Aortic Regurgitation (the Framingham Heart Study). *Am. J. Cardiol.* 1999, *83* (6), 897–902. https://doi.org/10.1016/S0002-9149(98)01064-9.

(188) Stanfield, J. R.; Selzman, C. H. In Vitro Pulsatility Analysis of Axial-Flow and Centrifugal-Flow Left Ventricular Assist Devices. *J. Biomech. Eng.* 2013, *135* (3), 034505. https://doi.org/10.1115/1.4023525.

(189) Soucy, K. G.; Koenig, S. C.; Giridharan, G. A.; Sobieski, M. A.; Slaughter, M. S. Defining Pulsatility during Continuous-Flow Ventricular Assist Device Support. *J. Heart Lung Transplant.* 2013, *32* (6), 581–587. https://doi.org/10.1016/j.healun.2013.02.010.

(190) Grinstein, J.; Kruse, E.; Sayer, G.; Fedson, S.; Kim, G. H.; Jorde, U. P.; Juricek, C.; Ota, T.; Jeevanandam, V.; Lang, R. M.; Uriel, N. Accurate Quantification Methods for Aortic Insufficiency Severity in Patients With LVAD. *JACC Cardiovasc. Imaging* 2016, *9* (6), 641–651. https://doi.org/10.1016/j.jcmg.2015.06.020.

(191) Lang, R.; Bierig, M.; Devereux, R.; Flachskampf, F.; Foster, E.; Pellikka, P.; Picard, M.; Roman, M.; Seward, J.; Shanewise, J. Recommendations for Chamber Quantification☆. *Eur. J. Echocardiogr.* 2006, *7* (2), 79–108. https://doi.org/10.1016/j.euje.2005.12.014.

(192) Zoghbi, W. Recommendations for Evaluation of the Severity of Native Valvular Regurgitation with Two-Dimensional and Doppler Echocardiography. *J. Am. Soc. Echocardiogr.* 2003, *16* (7), 777–802. https://doi.org/10.1016/S0894-7317(03)00335-3.

(193) Estep, J. D.; Chang, S. M.; Bhimaraj, A.; Torre-Amione, G.; Zoghbi, W. A.; Nagueh, S. F. Imaging for Ventricular Function and Myocardial Recovery on Nonpulsatile Ventricular Assist Devices. *Circulation* 2012, *125* (18), 2265–2277. https://doi.org/10.1161/CIRCULATIONAHA.111.040238.

(194) Stainback, R. F.; Estep, J. D.; Agler, D. A.; Birks, E. J.; Bremer, M.; Hung, J.; Kirkpatrick, J. N.; Rogers, J. G.; Shah, N. R. Echocardiography in the Management of Patients with Left Ventricular Assist Devices: Recommendations from the American Society of Echocardiography. *J. Am. Soc. Echocardiogr.* 2015, *28* (8), 853–909. https://doi.org/10.1016/j.echo.2015.05.008.

(195) Grinstein, J.; Kruse, E.; Sayer, G.; Fedson, S.; Kim, G. H.; Sarswat, N.; Adatya, S.; Ota, T.; Jeevanandam, V.; Mor-Avi, V.; Lang, R. M.; Uriel, N. Novel Echocardiographic Parameters of Aortic Insufficiency in Continuous-Flow Left Ventricular Assist Devices and Clinical Outcome. *J. Heart Lung Transplant.* 2016, *35* (8), 976–985. https://doi.org/10.1016/j.healun.2016.05.009.

(196) Imamura, T.; Narang, N.; Rodgers, D.; Nitta, D.; Fujino, T.; Kalantari, S.; Smith, B.; Kim, G.; Nguyen, A.; Chung, B.; Holzhauser, L.; Song, T.; Ota, T.; Jeevanandam, V.; Sayer, G.; Uriel, N. Estimation of the Severity of Aortic Insufficiency by HVAD Flow Waveform. *Ann. Thorac. Surg.* 2019, S0003497519317072. https://doi.org/10.1016/j.athoracsur.2019.09.077.

(197) Okafor, I.; Raghav, V.; Condado, J. F.; Midha, P. A.; Kumar, G.; Yoganathan, A. P. Aortic Regurgitation Generates a Kinematic Obstruction Which Hinders Left Ventricular Filling. *Ann. Biomed. Eng.* 2017, *45* (5), 1305–1314. https://doi.org/10.1007/s10439-017-1790-z.

(198) Travis, A. R.; Giridharan, G. A.; Pantalos, G. M.; Dowling, R. D.; Prabhu, S. D.; Slaughter, M. S.; Sobieski, M.; Undar, A.; Farrar, D. J.; Koenig, S. C. Vascular Pulsatility in Patients with a Pulsatile- or Continuous-Flow Ventricular Assist Device. *J. Thorac. Cardiovasc. Surg.* 2007, *133* (2), 517–524. https://doi.org/10.1016/j.jtcvs.2006.09.057.

(199) May-Newman, K.; Hillen, B.; Dembitsky, W. Effect of Left Ventricular Assist Device Outflow Conduit Anastomosis Location on Flow Patterns in the Native Aorta: *ASAIO J.* 2006, *52* (2), 132–139. https://doi.org/10.1097/01.mat.0000201961.97981.e9.

(200) Martina, J. R.; Schipper, M. E. I.; de Jonge, N.; Ramjankhan, F.; de Weger, R. A.; Lahpor, J. R.; Vink, A. Analysis of Aortic Valve Commissural Fusion after Support with Continuous-Flow Left Ventricular Assist Device. *Interact. Cardiovasc. Thorac. Surg.* 2013, *17* (4), 616–624. https://doi.org/10.1093/icvts/ivt263.

(201) Arjunon, S.; Rathan, S.; Jo, H.; Yoganathan, A. P. Aortic Valve: Mechanical Environment and Mechanobiology. *Ann. Biomed. Eng.* 2013, *41* (7), 1331–1346. https://doi.org/10.1007/s10439-013-0785-7.

(202) White, C. R.; Frangos, J. A. The Shear Stress of It All: The Cell Membrane and Mechanochemical Transduction. *Philos. Trans. R. Soc. B Biol. Sci.* 2007, *362* (1484), 1459–1467. https://doi.org/10.1098/rstb.2007.2128.

(203) Simmons, C. A.; Grant, G. R.; Manduchi, E.; Davies, P. F. Spatial Heterogeneity of Endothelial Phenotypes Correlates With Side-Specific Vulnerability to Calcification in Normal Porcine Aortic Valves. *Circ. Res.* 2005, *96* (7), 792–799. https://doi.org/10.1161/01.RES.0000161998.92009.64.

(204) Otto, C. M.; Kuusisto, J.; Reichenbach, D. D.; Gown, A. M.; O'Brien, K. D. Characterization of the Early Lesion of "degenerative" Valvular Aortic Stenosis. Histological and Immunohistochemical Studies. *Circulation* 1994, *90* (2), 844–853. https://doi.org/10.1161/01.CIR.90.2.844.

(205) Moraes, C.; Likhitpanichkul, M.; Lam, C. J.; Beca, B. M.; Sun, Y.; Simmons, C. A. Microdevice Array-Based Identification of Distinct Mechanobiological Response Profiles in Layer-Specific Valve Interstitial Cells. *Integr. Biol.* 2013, *5* (4), 673. https://doi.org/10.1039/c3ib20254b.

(206) Sucosky, P.; Balachandran, K.; Elhammali, A.; Jo, H.; Yoganathan, A. P. Altered Shear Stress Stimulates Upregulation of Endothelial VCAM-1 and ICAM-1 in a BMP-4– and TGF-B1–Dependent Pathway. *Arterioscler. Thromb. Vasc. Biol.* 2009, *29* (2), 254–260. https://doi.org/10.1161/ATVBAHA.108.176347.

(207) Balachandran, K.; Sucosky, P.; Jo, H.; Yoganathan, A. P. Elevated Cyclic Stretch Induces Aortic Valve Calcification in a Bone Morphogenic Protein-Dependent Manner. *Am. J. Pathol.* 2010, *177* (1), 49–57. https://doi.org/10.2353/ajpath.2010.090631.

(208) Smith, K. E.; Metzler, S. A.; Warnock, J. N. Cyclic Strain Inhibits Acute Pro-Inflammatory Gene Expression in Aortic Valve Interstitial Cells. *Biomech. Model. Mechanobiol.* 2010, *9* (1), 117–125. https://doi.org/10.1007/s10237-009-0165-2.

(209) Huang, H.-Y. S.; Liao, J.; Sacks, M. S. In-Situ Deformation of the Aortic Valve Interstitial Cell Nucleus Under Diastolic Loading. *J. Biomech. Eng.* 2007, *129* (6), 880–889. https://doi.org/10.1115/1.2801670.

(210) Fondard, O.; Detaint, D.; Iung, B.; Choqueux, C.; Adle-Biassette, H.; Jarraya, M.; Hvass, U.; Couetil, J.-P.; Henin, D.; Michel, J.-B.; Vahanian, A.; Jacob, M.-P. Extracellular Matrix Remodelling in Human Aortic Valve Disease: The Role of Matrix Metalloproteinases and Their Tissue Inhibitors. *Eur. Heart J.* 2005, *26* (13), 1333–1341. https://doi.org/10.1093/eurheartj/ehi248.

(211) Rathan, S.; Yap, C. H.; Morris, E.; Arjunon, S.; Jo, H.; Yoganathan, A. P. Low and Unsteady Shear Stresses Upregulate Calcification Response of the Aortic Valve Leaflets. In *ASME 2011 Summer Bioengineering Conference, Parts A and B*; American Society of Mechanical Engineers: Farmington, Pennsylvania, USA, 2011; pp 245–246. https://doi.org/10.1115/SBC2011-53946.

(212) Yip, C. Y. Y.; Blaser, M. C.; Mirzaei, Z.; Zhong, X.; Simmons, C. A. Inhibition of Pathological Differentiation of Valvular Interstitial Cells by C-Type Natriuretic Peptide. *Arterioscler. Thromb. Vasc. Biol.* 2011, *31* (8), 1881–1889. https://doi.org/10.1161/ATVBAHA.111.223974.

(213) Walker, G. A.; Masters, K. S.; Shah, D. N.; Anseth, K. S.; Leinwand, L. A. Valvular Myofibroblast Activation by Transforming Growth Factor-β: Implications for Pathological Extracellular Matrix Remodeling in Heart Valve Disease. *Circ. Res.* 2004, *95* (3), 253–260. https://doi.org/10.1161/01.RES.0000136520.07995.aa.

(214) Wyss, K.; Yip, C. Y. Y.; Mirzaei, Z.; Jin, X.; Chen, J.-H.; Simmons, C. A. The Elastic Properties of Valve Interstitial Cells Undergoing Pathological Differentiation. *J. Biomech.* 2012, *45* (5), 882–887. https://doi.org/10.1016/j.jbiomech.2011.11.030.

(215) Fisher, C. I.; Chen, J.; Merryman, W. D. Calcific Nodule Morphogenesis by Heart Valve Interstitial Cells Is Strain Dependent. *Biomech. Model. Mechanobiol.* 2013, *12* (1), 5–17. https://doi.org/10.1007/s10237-012-0377-8.

(216) Mendoza_Annamarie Thesis 2011.

(217) Naka, Y.; Edwards, N. M.; Oz, M. C. Novel Technique to Repair Type A Acute Aortic Dissection in Patients with a Left Ventricular Assist Device. *Ann. Thorac. Surg.* 2001, *72* (4), 1403–1404. https://doi.org/10.1016/S0003-4975(01)02889-2.

(218) Savage, E. B. Aortic Valve Patch Closure: An Alternative to Replacement with HeartMatew LVAS Insertion. *Thorac. Surg.* 1999, 3.

(219) Park, S. J.; Liao, K. K.; Segurola, R.; Madhu, K. P.; Miller, L. W. Management of Aortic Insufficiency in Patients with Left Ventricular Assist Devices: A Simple Coaptation Stitch Method (Park's Stitch). *J. Thorac. Cardiovasc. Surg.* 2004, *127* (1), 264–266. https://doi.org/10.1016/S0022-5223(03)01301-1.

(220) Morgan, J. A.; Brewer, R. J. Modified Central Closure Technique for Treatment of Aortic Insufficiency in Patients on Left Ventricular Assist Device Support: *ASAIO J.* 2012, *58* (6), 626–628. https://doi.org/10.1097/MAT.0b013e318271bc49.

(221) McKellar, S. H.; Deo, S.; Daly, R. C.; Durham, L. A.; Joyce, L. D.; Stulak, J. M.; Park, S. J. Durability of Central Aortic Valve Closure in Patients with Continuous Flow Left Ventricular Assist Devices. *J. Thorac. Cardiovasc. Surg.* 2014, *147* (1), 344–348. https://doi.org/10.1016/j.jtcvs.2012.09.098.

(222) Goda, A.; Takayama, H.; Pak, S.-W.; Uriel, N.; Mancini, D.; Naka, Y.; Jorde, U. P. Aortic Valve Procedures at the Time of Ventricular Assist Device Placement. *Ann. Thorac. Surg.* 2011, *91* (3), 750–754. https://doi.org/10.1016/j.athoracsur.2010.11.012.

(223) Rose, A. G.; Connelly, J. H.; Park, S. J.; Frazier, O. H.; Miller, L. W.; Ormaza, S. Total Left Ventricular Outflow Tract Obstruction Due to Left Ventricular Assist Device–Induced Sub-Aortic Thrombosis in 2 Patients with Aortic Valve Bioprosthesis. *J. Heart Lung Transplant.* 2003, *22* (5), 594–599. https://doi.org/10.1016/S1053-2498(02)01180-4.

(224) Barbone, A.; Rao, V.; Oz, M. C.; Naka, Y. LVAD Support in Patients with Bioprosthetic Valves. *Ann. Thorac. Surg.* 2002, *74* (1), 232–234. https://doi.org/10.1016/S0003-4975(01)03514-7.

(225) Jaski, B. E.; Miller, D. A.; Hoagland, P. M.; Gordon, J. B.; Chillcott, S. R.; Stahovich, M. J.; Adamson, R. M.; Baradarian, S.; Dembitsky, W. P. Assessment of Recurrent Heart Failure Associated with Left Ventricular Assist Device Dysfunction. *J. Heart Lung Transplant.* 2005, *24* (12), 2060–2067. https://doi.org/10.1016/j.healun.2005.05.016.

(226) Feldman, C.; Silver, M.; Sobieski, M.; Slaughter, M. Management of Aortic Insufficiency With Continuous Flow Left Ventricular Assist Devices: Bioprosthetic Valve Replacement. *J. Heart Lung Transplant.* 2006, *25* (12), 1410–1412. https://doi.org/10.1016/j.healun.2006.10.004.

(227) Butany, J.; Leong, S. W.; Rao, V.; Borger, M. A.; David, T. E.; Cunningham, K. S.; Daniel, L. Early Changes in Bioprosthetic Heart Valves Following Ventricular Assist Device Implantation. *Int. J. Cardiol.* 2007, *117* (1), e20–e23. https://doi.org/10.1016/j.ijcard.2006.08.041.

(228) Estep, J. D.; Stainback, R. F.; Little, S. H.; Torre, G.; Zoghbi, W. A. The Role of Echocardiography and Other Imaging Modalities in Patients With Left Ventricular Assist Devices. *JACC Cardiovasc. Imaging* 2010, *3* (10), 1049–1064. https://doi.org/10.1016/j.jcmg.2010.07.012.

(229) Miller, L. W.; Pagani, F. D.; Russell, S. D.; John, R.; Boyle, A. J.; Aaronson, K. D.; Conte, J. V.; Naka, Y.; Mancini, D.; Delgado, R. M.; MacGillivray, T. E.; Farrar, D. J.; Frazier, O.

H. Use of a Continuous-Flow Device in Patients Awaiting Heart Transplantation. *N. Engl. J. Med.* 2007, *357* (9), 885–896. https://doi.org/10.1056/NEJMoa067758.

(230) Rose, E.; Gelijns, A.; Moskowitz, A.; Heitjan, D.; Steveson, L.; Dembitsky, W.; Long, J.; Ascheim, D.; Tierney, A.; Levitan, R.; Watson, J.; Meier, P. Long-Term Use of a Left Ventricular Assist Device for End-Stage Heart Failure. *N. Engl. J. Med.* 2001, *345* (20), 1435–1443.

(231) Frazier, O. H.; Rose, E. a; Oz, M. C.; Dembitsky, W.; McCarthy, P.; Radovancevic, B.; Poirier, V. L.; Dasse, K. a. Multicenter Clinical Evaluation of the HeartMate Vented Electric Left Ventricular Assist System in Patients Awaiting Heart Transplantation. *J. Thorac. Cardiovasc. Surg.* 2001, *122* (6), 1186–1195. https://doi.org/10.1067/mtc.2001.118274.

(232) Russell, S. D.; Miller, L. W.; Pagani, F. D. Advanced Heart Failure : A Call to Action. *Congest. Heart Fail.* 2008, No. december. https://doi.org/10.1111/j.1751-7133.2008.00022.x.

(233) Farrar, D. J.; Holman, W. R.; McBride, L.; Kormos, R. L.; Icenogle, T. B.; Hendry, P. J.; Moore, C. H.; Loisance, D. Y.; El-banayosy, A.; Frazier, H. Long-Term Follow-up of Thoratec Ventricular Assist Device Bridge-to-Recovery Patients Successfully Removed From Support After Recovery of Ventricular Function. *J. Heart Lung Transplant.* 2002, *21* (5), 516–521.

(234) Hetzer, R.; Muller, J. H.; Weng, Y.; Meyer, R.; Dandel, M. Bridging-to-Recovery. *Ann Thorac Surg* 2001, *71*, S109–S113.

(235) Kumpati, G. S.; Mccarthy, P. M.; Hoercher, K. J. Left Ventricular Assist Device Bridge to Recovery : A Review of the Current Status. *Ann Thorac Surg* 2001, *71*, S103–S108.

(236) Mancini, D. M.; Beniaminovitz, A.; Levin, H.; Catanese, K.; Flannery, M.; Ditullio, M.; Savin, S.; Cordisco, M. E.; Rose, E.; Oz, M. Low Incidence of Myocardial Recovery After Left Ventricular Assist Device Implantation in Patients With Chronic Heart Failure. *Circulation* 1998, *98*, 2383–2389.

(237) Young, J. B. Healing the Heart With Ventricular Assist Device Therapy : Mechanisms of Cardiac Recovery. *Ann Thorac Surg* 2001, *71*, S210–S219.

(238) Mueller, J.; Wallukat, G.; Weng, Y.; Dandel, M.; Ellinghaus, P.; Huetter, J.; Hetzer, R. Predictive Factors for Weaning from a Cardiac Assist Device. An Analysis of Clinical, Gene Expression, and Protein Data. *J. Heart Lung Transplant.* 2001, No. February.

(239) Billiar, K. L.; Sacks, M. S. Biaxial Mechanical Properties of the Native and Glutaraldehyde-Treated Aortic Valve Cusp: Part II—A Structural Constitutive Model. *J. Biomech. Eng.* 2000, *122* (4), 327–335. https://doi.org/10.1115/1.1287158.

(240) Sengupta, P. P.; Pedrizzetti, G.; Kilner, P. J.; Kheradvar, A.; Ebbers, T.; Tonti, G.; Fraser, A. G.; Narula, J. Emerging Trends in CV Flow Visualization. *JACC Cardiovasc. Imaging* 2012, *5* (3), 305–316. https://doi.org/10.1016/j.jcmg.2012.01.003.

(241) Rodriguez Munoz, D.; Markl, M.; Moya Mur, J. L.; Barker, A.; Fernandez-Golfin, C.; Lancellotti, P.; Zamorano Gomez, J. L. Intracardiac Flow Visualization: Current Status and

Future Directions. *Eur. Heart J. - Cardiovasc. Imaging* 2013, *14* (11), 1029–1038. https://doi.org/10.1093/ehjci/jet086.

(242) John, R.; Mantz, K.; Eckman, P.; Rose, A.; May-Newman, K. Aortic Valve Pathophysiology during Left Ventricular Assist Device Support. *J. Heart Lung Transplant. Off. Publ. Int. Soc. Heart Transplant.* 2010, *29* (12), 1321–1329. https://doi.org/10.1016/j.healun.2010.06.006.

(243) Willert, C. E.; Gharib, M. Digital Particle Image Velocimetry. *Exp. Fluids* 1991, 13.

(244) Dupuis, M.; Mahjoub, H.; Clavel, M.; Côté, N.; Toubal, O.; Tastet, L.; Dumesnil, J. G.; O'Connor, K.; Dahou, A.; Thébault, C.; Bélanger, C.; Beaudoin, J.; Arsenault, M.; Bernier, M.; Pibarot, P. Forward Left Ventricular Ejection Fraction: A Simple Risk Marker in Patients With Primary Mitral Regurgitation. *J. Am. Heart Assoc.* 2017, *6* (11). https://doi.org/10.1161/JAHA.117.006309.

(245) Bermejo, J.; Benito, Y.; Alhama, M.; Yotti, R.; Martínez-Legazpi, P.; del Villar, C. P.; Pérez-David, E.; González-Mansilla, A.; Santa-Marta, C.; Barrio, A.; Fernández-Avilés, F.; del Álamo, J. C. Intraventricular Vortex Properties in Nonischemic Dilated Cardiomyopathy. *Am. J. Physiol.-Heart Circ. Physiol.* 2014, *306* (5), H718–H729. https://doi.org/10.1152/ajpheart.00697.2013.

(246) Rossini, L.; Martinez-Legazpi, P.; Vu, V.; Fernández-Friera, L.; Pérez del Villar, C.; Rodríguez-López, S.; Benito, Y.; Borja, M.-G.; Pastor-Escuredo, D.; Yotti, R.; Ledesma-Carbayo, M. J.; Kahn, A. M.; Ibáñez, B.; Fernández-Avilés, F.; May-Newman, K.; Bermejo, J.; del Álamo, J. C. A Clinical Method for Mapping and Quantifying Blood Stasis in the Left Ventricle. *J. Biomech.* 2016, *49* (11), 2152–2161. https://doi.org/10.1016/j.jbiomech.2015.11.049.

(247) Kilner, P. J.; Yang, G.-Z.; Wilkes, A. J.; Mohiaddin, R. H.; Firmin, D. N.; Yacoub, M. H. Asymmetric Redirection of Flow through the Heart. 2000, *404*, 3.

(248) Pedrizzetti, G.; Domenichini, F. Nature Optimizes the Swirling Flow in the Human Left Ventricle. *Phys. Rev. Lett.* 2005, *95* (10), 108101. https://doi.org/10.1103/PhysRevLett.95.108101.

(249) Hendabadi, S.; Bermejo, J.; Benito, Y.; Yotti, R.; Fernández-Avilés, F.; del Álamo, J. C.; Shadden, S. C. Topology of Blood Transport in the Human Left Ventricle by Novel Processing of Doppler Echocardiography. *Ann. Biomed. Eng.* 2013, *41* (12), 2603–2616. https://doi.org/10.1007/s10439-013-0853-z.

(250) Faludi, R.; Szulik, M.; D'hooge, J.; Herijgers, P.; Rademakers, F.; Pedrizzetti, G.; Voigt, J.-U. Left Ventricular Flow Patterns in Healthy Subjects and Patients with Prosthetic Mitral Valves: An in Vivo Study Using Echocardiographic Particle Image Velocimetry. *J. Thorac. Cardiovasc. Surg.* 2010, *139* (6), 1501–1510. https://doi.org/10.1016/j.jtcvs.2009.07.060.

(251) Pierrakos, O.; Vlachos, P. P. The Effect of Vortex Formation on Left Ventricular Filling and Mitral Valve Efficiency. *J. Biomech. Eng.* 2006, *128* (4), 527. https://doi.org/10.1115/1.2205863.

(252) Watanabe, H.; Sugiura, S.; Hisada, T. The Looped Heart Does Not Save Energy by Maintaining the Momentum of Blood Flowing in the Ventricle. *Am. J. Physiol.-Heart Circ. Physiol.* 2008, *294* (5), H2191–H2196. https://doi.org/10.1152/ajpheart.00041.2008.

(253) Kanski, M.; Arvidsson, P. M.; Töger, J.; Borgquist, R.; Heiberg, E.; Carlsson, M.; Arheden, H. Left Ventricular Fluid Kinetic Energy Time Curves in Heart Failure from Cardiovascular Magnetic Resonance 4D Flow Data. *J. Cardiovasc. Magn. Reson.* 2015, *17* (1), 111. https://doi.org/10.1186/s12968-015-0211-4.

(254) Morisawa, D.; Falahatpisheh, A.; Avenatti, E.; Little, S. H.; Kheradvar, A. Intraventricular Vortex Interaction between Transmitral Flow and Paravalvular Leak. *Sci. Rep.* 2018, *8* (1), 15657. https://doi.org/10.1038/s41598-018-33648-9.

(255) Rossini, L.; Braun, O.; Brambatti, M.; Benito, Y.; Mizeracki, A.; Miramontes, M.; Nguyen, C.; Martinez-Legazpi, P.; Almeida, S.; Vu, V.; May-Newman, K.; Bermejo, J.; Adler, E.; Kahn, A.; del Alamo, J. C. Intraventricular Flow Patterns in Patients Treated with Left Ventricular Assist Devices. *ASAIO J.* 2020.

(256) Di Labbio, G.; Kadem, L. Jet Collisions and Vortex Reversal in the Human Left Ventricle. *J. Biomech.* 2018, *78*, 155–160. https://doi.org/10.1016/j.jbiomech.2018.07.023.

(257) Stugaard, M.; Koriyama, H.; Katsuki, K.; Masuda, K.; Asanuma, T.; Takeda, Y.; Sakata, Y.; Itatani, K.; Nakatani, S. Energy Loss in the Left Ventricle Obtained by Vector Flow Mapping as a New Quantitative Measure of Severity of Aortic Regurgitation: A Combined Experimental and Clinical Study. *Eur. Heart J. - Cardiovasc. Imaging* 2015, *16* (7), 723–730. https://doi.org/10.1093/ehjci/jev035.

(258) Pedrizzetti, G.; Sengupta, P. P. Vortex Imaging: New Information Gain from Tracking Cardiac Energy Loss. *Eur. Heart J. - Cardiovasc. Imaging* 2015, *16* (7), 719–720. https://doi.org/10.1093/ehjci/jev070.

(259) Tanaka, Y.; Vu, V.; Fischer, I.; Nakajima, T.; May-Newman, K.; Itoh, A. Is the Severity of Aortic Insufficiency with Left Ventricular Assist Device Underestimated in Traditional Echocardiographic Evaluation? A Mock Loop Study. *submitted* 2020.

(260) Cowger, J.; Rao, V.; Massey, T.; Sun, B.; May-Newman, K.; Jorde, U.; Estep, J. D. Comprehensive Review and Suggested Strategies for the Detection and Management of Aortic Insufficiency in Patients with a Continuous-Flow Left Ventricular Assist Device. *J. Heart Lung Transplant.* 2015, *34* (2). https://doi.org/10.1016/j.healun.2014.09.045.

(261) Reider, C.; Moon, J.; Ramesh, V.; Montes, R.; Campos, J.; Herold, B.; Martinez-Legazpi, P.; Rossini, L.; del Alamo, J. C.; Dembitsky, W.; May-Newman, K. Intraventricular Thrombus Formation in the LVAD-Assisted Heart Studied in a Mock Circulatory Loop. *Meccanica* 2017, *52* (3), 515–528. https://doi.org/10.1007/s11012-016-0433-z.

(262) Imamura, T.; Nguyen, A.; Chung, B.; Rodgers, D.; Sarswat, N.; Kim, G.; Raikhelkar, J.; Adatya, S.; Ota, T.; Song, T.; Juricek, C.; Estep, J. D.; Burkhoff, D.; Jeevanandam, V.; Sayer, G.; Uriel, N. Association of Inflow Cannula Position with Left Ventricular Unloading and Clinical Outcomes in Patients with HeartMate II Left Ventricular Assist Device: *ASAIO J.* 2019, *65* (4), 331–335. https://doi.org/10.1097/MAT.0000000000000823.

(263) Kagiyama, N.; Okura, H.; Nezuo, S.; Kawamoto, T.; Murakami, T.; Hashimoto, Y.; Tanemoto, K.; Yoshida, K. Two Cases of Acute Bioprosthetic Mitral Valve Thrombosis Immediately After Mitral Valve Replacement. *Circulation* 2014, *129* (6). https://doi.org/10.1161/CIRCULATIONAHA.113.005583.

(264) Zlotnick, A. Y.; Shehadeh, J.; Flugelman, M. Y.; Bursztein-De Myttenaere, S. A.; Gaspar, T.; Shiran, A. Acute Reversible Bioprosthetic Mitral Valve Stenosis Caused by Heparin-Induced Thrombocytopenia. *Circulation* 2008, *118* (4). https://doi.org/10.1161/CIRCULATIONAHA.107.759498.

(265) Gottfried, R.; Paluszkiewicz, L.; Kizner, L.; Morshuis, M.; Koertke, H.; Gummert, J. Thrombosis of a Bioprosthetic Mitral Valve Under Extracorporeal Membrane Oxygenation: Thrombus Formation in the Left Heart. *Ann. Thorac. Surg.* 2012, *94* (2), 657. https://doi.org/10.1016/j.athoracsur.2012.02.021.

(266) Tsiouris, A.; Nemeh, H.; Borgi, J. Early Acute Thrombosis of Bioprosthetic Mitral Valve Presenting with Cardiogenic Shock. *Gen. Thorac. Cardiovasc. Surg.* 2013, *61* (3), 152–154. https://doi.org/10.1007/s11748-012-0121-4.

(267) Le Tourneau, T.; Lim, V.; Inamo, J.; Miller, F. A.; Mahoney, D. W.; Schaff, H. V.; Enriquez-Sarano, M. Achieved Anticoagulation vs Prosthesis Selection for Mitral Mechanical Valve Replacement. *Chest* 2009, *136* (6), 1503–1513. https://doi.org/10.1378/chest.08-1233.

(268) Prasongsukarn, K.; Jamieson, W.; Lichtenstein, S. Performance of Bioprostheses and Mechanical Prostheses in Age Group 61- 70 Years. *J Heart Valve Dis* 2005, *14* (4), 501-8,510-1.

(269) Ribeiro, A. H. S.; Wender, O. C. B.; de Almeida, A. S.; Soares, L. E.; Picon, P. D. Comparison of Clinical Outcomes in Patients Undergoing Mitral Valve Replacement with Mechanical or Biological Substitutes: A 20 Years Cohort. *BMC Cardiovasc. Disord.* 2014, *14* (1), 146. https://doi.org/10.1186/1471-2261-14-146.

(270) Simprini, L. A.; Afroz, A.; Klem, I.; Jensen, C.; Kim, R.; Heitner, J.; Sood, M.; Chandy, E.; Shah, D.; Lopez-Mattei, J.; Biederman, R.; Srichai, M. B.; Grizzard, J.; Fuisz, A.; Ghafourian, K.; Farzaneh-Far, A.; Weinsaft, J. ROUTINE CINE-CMR FOR PROSTHESIS ASSOCIATED MITRAL REGURGITATION: A MULTICENTER COMPARISON TO ECHOCARDIOGRAPHY. *J. Am. Coll. Cardiol.* 2013, *61* (10), E942. https://doi.org/10.1016/S0735-1097(13)60942-0.

(271) Pedrizzetti, G.; Domenichini, F.; Tonti, G. On the Left Ventricular Vortex Reversal after Mitral Valve Replacement. *Ann. Biomed. Eng.* 2010, *38* (3), 769–773. https://doi.org/10.1007/s10439-010-9928-2.

(272) Gadhinglajkar, S.; Namboodiri, N.; Pillai, V.; Sreedhar, R. Double-Envelope Continuous-Wave Doppler Flow Profile Across a Tilting-Disc Mitral Prosthesis: Intraoperative Significance. *J. Cardiothorac. Vasc. Anesth.* 2011, *25* (3), 491–494. https://doi.org/10.1053/j.jvca.2010.03.008.

(273) Robertson, J. O.; Naftel, D. C.; Myers, S. L.; Tedford, R. J.; Joseph, S. M.; Kirklin, J. K.; Silvestry, S. C. Concomitant Mitral Valve Procedures in Patients Undergoing Implantation of Continuous-Flow Left Ventricular Assist Devices: An INTERMACS Database Analysis.

J. Heart Lung Transplant. 2018, *37* (1), 79–88. https://doi.org/10.1016/j.healun.2017.09.016.

(274) Krishan, K.; Pinney, S.; Anyanwu, A. C. Successful Use of Continuous Flow Ventricular Assist Device in a Patient with Mechanical Mitral and Aortic Valve Prosthesis without Replacement or Exclusion of Valves. *Interact. Cardiovasc. Thorac. Surg.* 2010, *10* (2), 325–327. https://doi.org/10.1510/icvts.2009.221036.

(275) Mussa, S.; Large, S.; Tsui, S.; van Doorn, C.; Jenkins, D. Mechanical Mitral Prosthesis With a Short-Term Left Ventricular Assist Device: *ASAIO J.* 2008, *54* (4), 439–441. https://doi.org/10.1097/MAT.0b013e31817c921b.

(276) Mokashi, S. A.; Schmitto, J. D.; Lee, L. S.; Rawn, J. D.; Bolman III, R. M.; Shekar, P. S.; Couper, G. S.; Chen, F. Y. Ventricular Assist Device in Patients With Prosthetic Heart Valves: THOUGHTS AND PROGRESS. *Artif. Organs* 2010, *34* (11), 1030–1034. https://doi.org/10.1111/j.1525-1594.2010.01102.x.

(277) Hagley, M. T.; Lopez-Candales, A.; Phillips, K. J.; Daily, B. B.; Kouchoukos, N. T. Thrombosis of Mitral Valve Bioprostheses in Patients Requiring Circulatory Assistance. *Ann. Thorac. Surg.* 1995, *60* (6), 1814–1816. https://doi.org/10.1016/0003-4975(95)00627-3.

(278) Schubmehl, H. B.; Saric, M.; Vainrib, A. F.; Williams, M.; Balsam, L. B. Rapid Bioprosthetic Mitral Valve Failure after Temporary Left Ventricular Assist Device Support. *Heart Surg. Forum* 2017, *20* (6), 256. https://doi.org/10.1532/hsf.1861.

(279) Bellhouse, B. J. Fluid Mechanics of a Model Mitral Valve and Left Ventricle. *Cardiovasc. Res.* 1972, *6* (2), 199–210. https://doi.org/10.1093/cvr/6.2.199.

(280) Reul, H.; Talukder, N.; Mu¨ller, E. W. Fluid Mechanics of the Natural Mitral Valve. *J. Biomech.* 1981, *14* (5), 361–372. https://doi.org/10.1016/0021-9290(81)90046-4.

(281) Pasipoularides, A.; Vlachos, P. P.; Little, W. C. Vortex Formation Time Is Not an Index of Ventricular Function. *J Cardiovasc. Transl. Res.* 2015, *8* (1), 54–58. https://doi.org/10.1007/s12265-015-9607-7.

(282) Eriksson, J.; Carlhäll, C. J.; Dyverfeldt, P.; Engvall, J.; Bolger, A. F.; Ebbers, T. Semi-Automatic Quantification of 4D Left Ventricular Blood Flow. *J. Cardiovasc. Magn. Reson.* 2010, *12* (1), 9. https://doi.org/10.1186/1532-429X-12-9.

(283) Arvidsson, P. M.; Kovács, S. J.; Töger, J.; Borgquist, R.; Heiberg, E.; Carlsson, M.; Arheden, H. Vortex Ring Behavior Provides the Epigenetic Blueprint for the Human Heart. *Sci. Rep.* 2016, *6* (1), 22021. https://doi.org/10.1038/srep22021.

(284) Baccani, B.; Domenichini, F.; Pedrizzetti, G.; Tonti, G. Fluid Dynamics of the Left Ventricular Filling in Dilated Cardiomyopathy. *J. Biomech.* 2002, *35* (5), 665–671. https://doi.org/10.1016/S0021-9290(02)00005-2.

(285) Rossini, L.; Martinez-Legazpi, P.; Benito, Y.; Pérez del Villar, C.; Gonzalez-Mansilla, A.; Barrio, A.; Borja, M.-G.; Yotti, R.; Kahn, A. M.; Shadden, S. C.; Fernández-Avilés, F.; Bermejo, J.; del Álamo, J. C. Clinical Assessment of Intraventricular Blood Transport in

Patients Undergoing Cardiac Resynchronization Therapy. *Meccanica* 2017, *52* (3), 563–576. https://doi.org/10.1007/s11012-015-0322-x.

(286) Martinez-Legazpi, P.; Rossini, L.; Pérez del Villar, C.; Benito, Y.; Devesa-Cordero, C.; Yotti, R.; Delgado-Montero, A.; Gonzalez-Mansilla, A.; Kahn, A. M.; Fernandez-Avilés, F.; del Álamo, J. C.; Bermejo, J. Stasis Mapping Using Ultrasound. *JACC Cardiovasc. Imaging* 2018, *11* (3), 514–515. https://doi.org/10.1016/j.jcmg.2017.06.012.

(287) Querzoli, G.; Fortini, S.; Cenedese, A. Effect of the Prosthetic Mitral Valve on Vortex Dynamics and Turbulence of the Left Ventricular Flow. *Phys. Fluids* 2010, *22* (4), 041901. https://doi.org/10.1063/1.3371720.

(288) Peura, J. L.; Colvin-Adams, M.; Francis, G. S.; Grady, K. L.; Hoffman, T. M.; Jessup, M.; John, R.; Kiernan, M. S.; Mitchell, J. E.; O'Connell, J. B.; Pagani, F. D.; Petty, M.; Ravichandran, P.; Rogers, J. G.; Semigran, M. J.; Toole, J. M. Recommendations for the Use of Mechanical Circulatory Support: Device Strategies and Patient Selection: A Scientific Statement From the American Heart Association. *Circulation* 2012, *126* (22), 2648–2667. https://doi.org/10.1161/CIR.0b013e3182769a54.

(289) Smith, L. A.; Yarboro, L. T.; Kennedy, J. L. W. Left Ventricular Assist Device Implantation Strategies and Outcomes. *J. Thorac. Dis.* 2015, *7* (12), 9.

(290) Garcia, D.; del Álamo, J. C.; Tanné, D.; Yotti, R.; Cortina, C.; Bertrand, É.; Antoranz, J. C.; Pérez-David, E.; Rieu, R.; Fernández-Avilés, F.; Bermejo, J. Two-Dimensional Intraventricular Flow Mapping by Digital Processing Conventional Color-Doppler Echocardiography Images. *IEEE Trans. Med. Imaging* 2010, *29* (10), 1701–1713. https://doi.org/10.1109/TMI.2010.2049656.

(291) Saaid, H.; Segers, P.; Novara, M.; Claessens, T.; Verdonck, P. Single Calibration Multiplane Stereo-PIV: The Effect of Mitral Valve Orientation on Three-Dimensional Flow in a Left Ventricle Model. *Exp. Fluids* 2018, *59* (3), 49. https://doi.org/10.1007/s00348-018-2504-5.

(292) Domenichini, F.; Querzoli, G.; Cenedese, A.; Pedrizzetti, G. Combined Experimental and Numerical Analysis of the Flow Structure into the Left Ventricle. *J. Biomech.* 2007, *40* (9), 1988–1994. https://doi.org/10.1016/j.jbiomech.2006.09.024.

(293) Falahatpisheh, A.; Kheradvar, A. High-Speed Particle Image Velocimetry to Assess Cardiac Fluid Dynamics in Vitro: From Performance to Validation. *Eur. J. Mech. - BFluids* 2012, *35*, 2–8. https://doi.org/10.1016/j.euromechflu.2012.01.019.

(294) Meschini, V.; de Tullio, M. D.; Querzoli, G.; Verzicco, R. Flow Structure in Healthy and Pathological Left Ventricles with Natural and Prosthetic Mitral Valves. *J. Fluid Mech.* 2018, *834*, 271–307. https://doi.org/10.1017/jfm.2017.725.